8-2021

Phytochrome Physiology and Plant Perception of Far-Red Photons

Paul Kusuma
Utah State University

PHYTOCHROME PHYSIOLOGY AND PLANT PERCEPTION OF FAR-RED PHOTONS

by

Paul Kusuma

A dissertation submitted in partial fulfillment
of the requirements for the degree

of

DOCTOR OF PHILOSOPHY

in

Plant Science

Approved:

_____	_____
Bruce Bugbee, Ph.D. Crop Physiology Major Professor	Lawrence Hipps, Ph.D. Biometeorology & Atmospheric Science Committee Member
_____	_____
Marc van Iersel, Ph.D. Plant Physiology Committee Member	Lance Seefeldt, Ph.D. Biochemistry Committee Member
_____	_____
Raymond Wheeler, Ph.D. Plant Physiology Committee Member	D. Richard Cutler, Ph.D. Interim Vice Provost for Graduate Studies

UTAH STATE UNIVERSITY
Logan, Utah

2021

ABSTRACT

Phytochrome Physiology and Plant Perception of Far-red Photons

by

Paul Kusuma, Doctor of Philosophy

Utah State University, 2021

Major Professor: Dr. Bruce Bugbee
Department: Plant, Soils and Climate

Plants evolved in the natural environment where resources are often scarce. Photons within the range of photosynthetically active radiation (PAR) are a critical resource that can be blocked by neighboring vegetation. As plants are shaded, they adjust their shape (stem length and leaf area) to either reach for the light and/or maximize photon capture. These responses are modulated through an array of photoreceptors that have evolved to perceive the photon flux from 280 to 800 nm.

One spectral region with significant impacts on plant shape is far-red (FR), which is barely visible to the human eye. Photons in this range are minimally absorbed by chlorophyll, and are therefore transmitted through leaves and relatively enriched in canopy shade. Plants sense this enrichment through the photoreceptor phytochrome, which has two primary states: Pfr, which inhibits elongation in sunlight; and Pr, which cannot inhibit elongation and is abundant in the shade. The dynamic relationship between Pfr and Pr has been described by the phytochrome photoequilibrium (PPE), which is the ratio of Pfr/(Pr+Pfr). PPE is often predicted with photoconversion coefficients that are

used to estimate the rates of Pr and Pfr conversion under a given spectral photon distribution. I describe shortcomings of this technique and provide a modified approach that incorporates spectral distortions in leaves.

Due to the complexity of PPE, environmental metrics may be preferable for predicting morphology. The R:FR ratio is often used as an environmental metric, but it has shortcomings. Instead, the FR fraction [FR/(PAR+FR)] integrates plant responses to blue, green, red and far-red photons. Blue photons reduce plant size through cryptochrome, while green photons are hypothesized to induce shade avoidance responses by reversing this blue photon response. However, I show that green photons have minimal effects on morphology. The FR fraction is an intuitive metric and appears to be well correlated with morphology.

Total photon intensity interacts with the FR fraction to predict morphology, especially leaf area – a crucial component of plant development that determines how many photons can be captured for photosynthesis. Under high photon intensities, FR increased lettuce leaf area, but under low intensities, FR decreases leaf area.

(318 pages)

PUBLIC ABSTRACT

Phytochrome Physiology and Plant Perception of Far-red Photons

Paul Kusuma

Photons are the primary energy source for most life on Earth, as they drive photosynthesis, a process that turns the CO_2 in air into food. One crucial parameters for the optimization of growth is leaf area, which determines the ability of a plant to capture photons for photosynthesis. In order to gain access to photons in shaded environments, plants have evolved unique sensors, called photoreceptors, which respond to changes in the color and intensity of light.

Far-red photons (photons at the edge of human vision that appear as dim red light) hold particular promise in regulating plant shape and photon capture. These photons are minimally absorbed by chlorophyll, and are thus enriched in the shade – making them a potent signal of the presence of shade. These photons have been shown to increase leaf area and stem elongation, which increase access to photons, and thus increase plant growth. Additionally, the lower energy of far-red photons make them particularly useful for reducing the massive requirement for electrical power in indoor agriculture.

Here, I describes how far-red interacts with blue, green, and red photons to affect plant morphology. I compare traditional and newly developed models/metrics that predict the action of far-red through a photoreceptor called phytochrome. Additionally, I discuss their interactions with total photon intensity.

ACKNOWLEDGMENTS

I would have not made it nearly this far without the love from my family: my parents Lynda and David, as well as my siblings Sarah, Thomas and Timothy. I would also like to thank Drs. William Wheeler and Shuyang Zhen who had the misfortune of sharing an office with me over the course of my PhD program.

I have received much assistance from members of the Crop Physiology Laboratory over the past five years, namely from Mitchell Westmoreland, Matthew Hardy, Wyatt Johnson, Jakob Johnson, Boston Swan, Erik Sargent, Kahlin Wacker, Logan Banner, Terri Manwaring, Alec Hay and other unnamed laboratory members. I am grateful for all of their help.

Thanks to Dr. Morgan Pattison for his insight in writing manuscripts, and thanks to Dr. Kevin Folta who initially led me down this road. I thank my committee members, Dr. Lance Seefeldt, Dr. Raymond Wheeler, Dr. Marc van Iersel, Dr. Lawrence Hipps and Dr. Keith Mott, whose assistance and discussion in specific areas helped guide my understanding across various topics.

Finally, I thank my major advisor, Dr. Bruce Bugbee who has been a guiding mentor throughout my program. I have spent many hours in his office talking through data, refining manuscripts and generally scheming. It has been a wild five years.

Paul Kusuma

CONTENTS

LIST OF TABLES

LIST OF FIGURES

Figure Page

Figure Page

Figure Page

Figure Page

CHAPTER 1

INTRODUCTION AND LITERATURE REVIEW

1.1 Introduction

Photons are both an energy source for plant growth and a signal for plant development. Through photosynthesis, plants convert photon energy into chemical energy, which drives most life of Earth. However, in the natural environment, availability of photons can be highly limited, as they are absorbed by overhead vegetation. Plants have thus evolved photoreceptors that sense the changes in the photon environment and guide plant development to maximize fitness.

In plant photobiology, the photo-biologically active region of radiation (280 to 800 nm) can be divided into six useful categories. These include ultraviolet-B (UV-B; 280 to 320 nm), UV-A (320 to 400 nm), blue (400 to 500 nm), green (500 to 600 nm), red (600 to 700 nm) and far-red (700 to 800 nm). In shaded environments, UV-B, UV-A, blue and red are selectively filtered, while green and far-red are relatively enriched – a phenomenon driven by both the preferential absorption of blue and red photons by chlorophyll for photosynthesis and absorption of UV-B, UV-A and blue photons by photoprotective pigments (e.g. anthocyanin). Photoreceptors have therefore evolved to be sensitive to the relative enrichment of green and far-red photons and the relative depletion of UV-B, UV-A, blue and red photons. In response to shade, some plant species bend their leaves upward (hyponasty) and elongate their stems (which occurs in concert with an increase in biomass partitioning to stems); these responses are commonly referred to as shade avoidance. Other plant species will not elongate stems in response to shade, and instead they reduce chlorophyll a:b ratios,

increase PSII:PSI ratios, and increase specific leaf area (SLA, which is the leaf area divided by leaf mass); these responses are commonly referred to as shade tolerance. Notably however, these shade tolerance responses can occur in both shade tolerant and shade avoidant species (Gommers et al., 2013).

Light-emitting diode (LED) technology has improved rapidly over the past two decades and is now far more efficient than other electric lighting technologies (Appendix A to C). In addition to this improved efficiency, LED technology provides a high degree of control over spectral output, which can be utilized to manipulate plant photoreceptors in order to optimize growth. But, manipulation requires a comprehensive understanding of the photoreceptor activity and resulting whole-plant responses.

1.2 Literature review

1.2.1 General Effect of Specific Wavelengths

1.2.1.1 Blue Photons

Blue photons are well absorbed by pigments within leaves and are thus filtered out in the shaded environments. Plants modulate their shape in response to the total flux of photosynthetically active radiation (PAR), and this response to the intensity of PAR has long been suspected to be sensed through the blue photon receptors (Smith, 1982). This does appear to partially be the case (de Wit et al., 2016), but there are likely other contributing factors (Millenaar et al., 2009).

In general, studies conducted in controlled environments have shown that increasing the fraction of blue photons in the spectrum, especially when the percent blue (percent of

PPFD) is increased between 10% to 50%, causes leaf area and stem length to decrease, thus leading to decreases in photon capture and yield (Hernández and Kubota, 2016; Kang et al., 2016; Meng et al., 2019, 2020; Snowden et al., 2016; Son and Oh, 2013, 2015; Wang et al., 2016). Less commonly, studies have found no effect on yield from increasing the fraction of blue photons (Li and Kubota, 2009; Snowden et al., 2016).

1.2.1.2 Green Photons

The green color of leaves is caused by a slightly lower absorptance (higher reflectance) of green photons relative to blue and red photons. In canopy shade the B:G ratio decreases (Smith et al., 2017), and therefore it has been suspected that an increase in green photons (especially relative to blue) is perceived as a shade signal in plants. Studies over the past two decades have revealed that shade avoidance occurs in response to green photons in the model plant species *Arabidopsis thaliana* (Bouly et al., 2007; Zhang et al., 2011). This has led to the suggestion that green photons may be a beneficial addition to controlled environment plant growth (Smith et al., 2017). In an early study, leaf area and fresh/dry mass of lettuce was observed to increase in response to an increase in green photons (Kim et al. 2004), but subsequent studies in horticultural species have shown minimal responses to green photons (Hernández and Kubota, 2016; Kang et al., 2016; Snowden et al., 2016; Son and Oh, 2015), and in some cases, plant diameter/leaf area actually decrease (Meng et al., 2020; Snowden et al., 2016). Overall, increasing the fraction of green photons has been observed to minimally affect leaf area and stem/petiole elongation in horticultural species.

1.2.1.3 Red Photons

Red photons are highly absorbed by leaves for photosynthesis, causing their relative depletion in canopy-shade light. Studies investigating plant responses to red photons led to the discovery of the photoreceptor phytochrome (Bothwick et al., 1952; Borthwick, 1972; Sage, 1992), the most studied plant photoreceptor. The effect of red photons is often discussed in tandem with far-red, either through the R:FR ratio (the flux of red photons divided by the flux of far-red photons), or phytochrome photoequilibrium (PPE), which is an estimated ratio of active phytochrome (P_{FR}) to total phytochrome (P_R+P_{FR}).

1.2.1.4 Far-red Photons

Far-red is a plant specific categorization of photon wavelengths that was created due to absorbance of the phytochrome photoreceptor. Far-red is at the very edge of human vision and these photons appear as dim red light to the human eye.

Despite minimal effects on human vision, these photons have large effects on plant morphogenesis through the photoreceptor phytochrome (Casal, 2012). In species that are adapted to high photon fluxes like tomato and cucumber, far-red tends to increase stem and/or petiole elongation (Kalaitzoglou et al., 2019; Meng et al., 2019; Park and Runkle, 2017).

Despite these increases in stem elongation, which are often considered undesirable in agriculture, far-red photons have promise in sole-source lighting environments because these photon are low energy and have been shown to increase fresh and dry mass of lettuce by increasing leaf area (Lee et al., 2016; Meng and Runkle, 2019). However, the ability of far-

red photons to induce photosynthesis, and thus increase growth rates, must be considered when assessing the effect of far-red on leaf expansion. Studies that substitute far-red rather than supplement far-red have still shown an increase in leaf expansion and dry mass (Zhen and Bugbee, 2020). In contrast, ornamental species geranium and snapdragon were shown to increase leaf area with far-red substitution but without an increase in dry mass (Park and Runkle, 2017). Although lettuce has been shown to increase leaf area in response to far-red, a decrease in leaf area is often reported in shade-avoiding species (Casal, 2012).

In addition to these effects on morphology, one recent study found that supplemental far-red increased fruit yield of tomatoes; possibly through increased fruit sink strength and dry mass partitioning to the fruits (Ji et al., 2020).

Far-red can be applied near the end of the day to mimic the relative increase in far-red under natural conditions (Kasperbauer, 1971). These end-of-day far-red treatments are still used to this day as an energy saving method to alter development in greenhouse and indoor crop production, but it tends to be less effective than far-red applied over the entire photoperiod (Kalaitzoglou et al., 2019; Morgan and Smith, 1978).

1.2.2 Photoreceptors

There are three well-studied classes of photoreceptors that modulate development. These are 1) the phytochromes, which have peak absorbance in the red and far-red regions, although they can absorb from 300 to 800 nm; 2) the cryptochromes, which primarily absorb in the UV-A, blue, and green regions; and 3) the phototropins, which primarily absorb in the UV-A and blue regions (Fig. 1-1). Plants also contain other photoreceptors including UV RESISTANCE LOCUS8 (UVR8), which responds to UV-B photons; and zeitlupes, which

respond to blue and UV-A photons, but these are less well studied (Folta and Carvalho, 2015; Galvão and Fankhauser, 2015).

1.2.2.1 Phototropins and Zeitlupes

Phototropins control plant development through association with cell membranes, while zeitlupes act through modulation of gene expression (Galvão and Fankhauser, 2015; Lin, 2000). Responses mediated by phototropins include phototropism, stomatal opening, chloroplast reorientation and leaf movement (Christie, 2007). Zeitlupes play a role in flowering and the circadian clock (Galvão and Fankhauser, 2015). Both of these photoreceptors contain flavin mononucleotide chromophores (FMN), and thus have similar absorbance (Fig. 1-1a)

1.2.2.2 Cryptochromes

The chromophore within cryptochrome is a flavin adenine dinucleotide (FAD), which has three states: FAD_{ox}, the oxidized state; $FADH^{o}$, the semi-reduced neutral radical state; and $FADH^{-}$, the fully reduced state. Of these three states, $FADH^{o}$ is the active form, while FAD_{ox} and $FADH^{-}$ are both inactive (Ahmad, 2016). FAD_{ox} absorbs most prominently in the blue region, converting it into active $FADH^{o}$ (Fig. 1-1b). As the active form, $FADH^{o}$ inhibits stem extension. The absorption spectrum of $FADH^{o}$ shows a high absorbance of green photons, which leads to the inactivation of cryptochrome (to $FADH^{-}$). Green photons induce shade avoidance responses (reversing blue photon responses) by this mechanism (Bouly et al., 2007). Both $FADH^{o}$ and $FADH^{-}$ can only revert back to FAD_{ox} by thermal reversion.

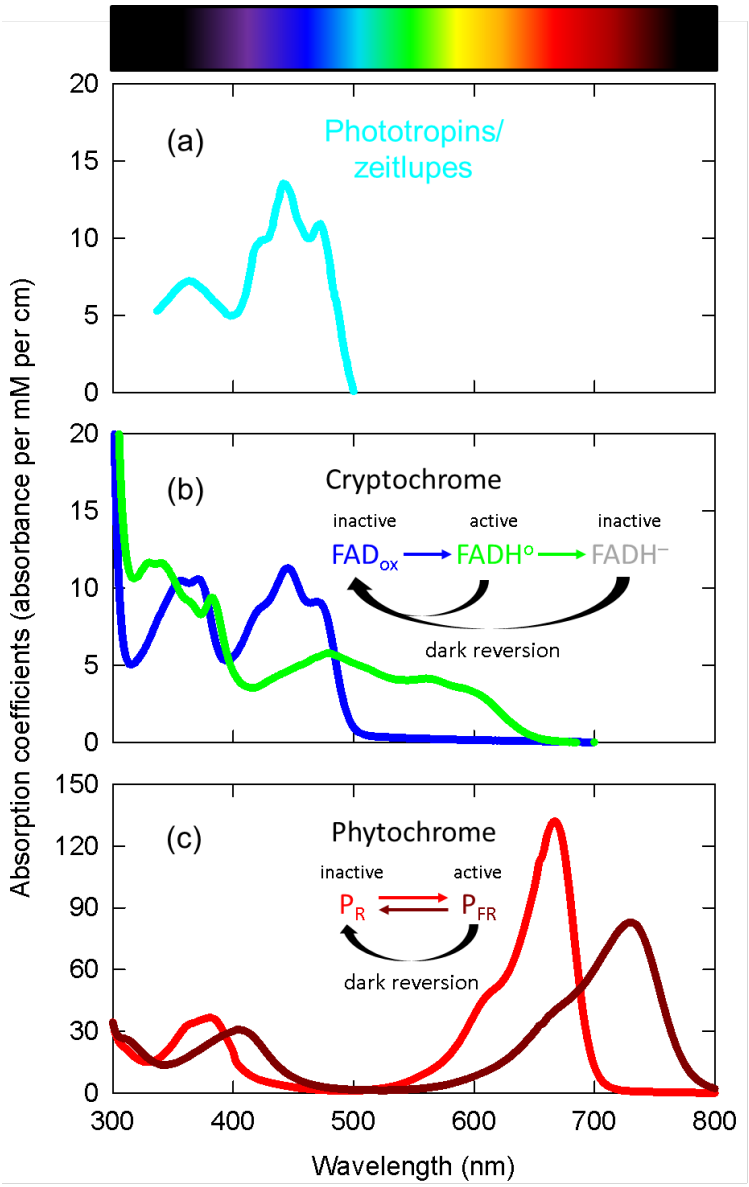

Fig. 1-1. Absorption coefficients of three major families of photoreceptors that modulate plant development. (a) Phototropins and zeitlupes (data from Ahmad et al., 2002 and Salomon et al., 2000). (b) Absorption coefficients for the cytochrome chromophore (FAD) in the oxidized (FAD_{ox}) and neutral radical ($FADH^{o}$) states [data was kindly provided by Dr. Pavel Müller, see Müller et al. (2014) for more detail]. (c) Absorption coefficients for the P_R and P_{FR} forms of phytochrome (curves redrawn from data by Kelly and Lagarias, 1985 and Lagarias et al., 1987). Straight colored arrows indicate photoreceptor activation or deactivation upon photon absorption and curved black arrows indicate dark (meaning light-independent) reversion; Dark reversion rate in cryptochrome is dependent on the

concentration of oxygen (Müller and Ahmad, 2011) and that of phytochrome on temperature (Klose et al., 2020).

1.2.2.3 Phytochromes

Phytochromes primarily exist in two photoreversible states: phytochrome-red (P_R), which is most sensitive to red photons and phytochrome-far-red (P_{FR}), which is most sensitive to far-red photons (Fig. 1-1c). P_R accumulates in the cytosol in the dark and is activated into P_{FR} upon photon absorbance. P_{FR} is then transported into the nucleus where it modulates gene expression, but it is converted back into inactive P_R both upon photon absorbance and by dark reversion (Legris et al., 2019). In addition to these nuclear roles of phytochrome, it may also have cytoplasmic roles (Hughes, 2013), but this is poorly studied by comparison. In the natural environment, reflection from neighboring vegetation can increase the flux of far-red before a decrease in PAR is detected. In severe shade, the flux of far-red and PAR are both decreased, but far-red remains enriched relative to PAR (Casal, 2012). In this way, far-red perception thorough phytochrome is the primary signal of shade.

Plant responses to far-red interact with temperature, as reversion of active P_{FR} back to inactive form of P_R can occur independent of light in a temperature-dependent manner, with faster reversion rate at higher temperature. This is known as thermal reversion of phytochromes, and the effect is more pronounced under lower fluxes of PAR (Sellaro et al., 2019; Klose et al., 2020). This effect means that plant responses to far-red (elongation) are expected to be more significant at both higher temperatures and lower fluxes of PAR.

Both phytochrome and cryptochrome exist as dimers within plant cells, but the importance of this is still being elucidated (Klose et al., 2015; Liu et al., 2016; Sellaro et al., 2019; Legris et al., 2019).

1.2.2.4 Signaling Partners

Both phytochromes and cryptochromes interact with a family of transcription factors called PHYTOCHROME INTERACTING FACTORS (PIFs). PIFs control the expression of genes related to cell wall expansion and the hormones auxin, gibberellin and brassinosteroids (de Lucas and Prat, 2014; Leivar and Monte, 2014). Photon-activated phytochromes (P_{FR}) and cryptochromes both inhibit the activity of PIFs, leading to an inhibition of genes and hormones that induce elongation. Therefore, relative enrichment of far-red and depletion of blue photons inactivate the phytochrome and cryptochrome photoreceptors lifting this inhibition of PIFs and allowing elongation to progress.

In addition to PIFs, photomorphogenesis is regulated by the E3 ubiquitin ligase formed by CONSTITUTIVELY PHOTOMORPHOGENIC 1 (COP1) and SUPRESSOR OF PHYA-105 (SPA) proteins. This COP1/SPA complex inhibits the activity of transcription factors that promote photomorphogenesis (Legris et al., 2019; Podolec and Ulm, 2018), such as LONG HYPOCOTYL IN FAR-RED 1 (HFR1). Because HFR1 and related transcription factors promote the expression of genes that inhibit elongation, they act antagonistically to PIFs. Photon-activated phytochromes and cryptochromes inhibit the activity of the COP1/SPA complex, allowing the accumulation of HFR1 and related transcriptions factors.

These downstream signaling components have primarily been studied in the species *Arabidopsis thaliana*, and many of the signaling pathways appear to be generally conserved across species, but this is not always the case (Legris et al., 2019).

This gene-eye view of photoreceptor control of plant growth and development only begins to explain the complex interaction between these proteins, as there are many complex feedback loops (Legris et al., 2019).

1.2.3 Photoconversion Coefficients

Photoconversion coefficients are probability functions for photoreceptors that estimate the likelihood of photon absorbance at a given wavelength and subsequent conversion of the photoreceptor into a different form (Holmes and Fukshansky, 1979). These coefficients are usually referred to as photoconversion/photochemical cross-sections, but cross-section is an obscure term, so I use the term coefficient, which has historically had a different meaning (see below). It is common to use photoconversion coefficients to predict the dynamics of the plant photoreceptor phytochrome, specifically the ratio of active to total phytochrome. The active form of phytochrome is often considered to be P_{FR}, thus this ratio is equal to $P_{FR}/(P_R+P_{FR})$, where P_{FR} is the active, far-red (FR) absorbing form of phytochrome and P_R is the inactive red (R) absorbing form of phytochrome. But, active to total phytochrome has been more recently considered to be $D_2/(D_0+D_1+D_2)$, where D_2 is the fully active homodimer (P_{FR}-P_{FR}), D_0 is the fully inactive homodimer (P_R-P_R) and D_1 is the half activated heterodimer (P_R-P_{FR}). This ratio is commonly called phytochrome photoequilibrium (PPE) or the photostationary state (PSS) of phytochrome. These terms (PPE and PSS) are

regularly used interchangeably, especially in horticulture, but distinctions have been made; PPE refers to equilibrium assuming only photoconversions, while PSS refers to photoconversions and thermal reversions (Mancinelli, 1994; Sage, 1992).

1.2.3.1 Derivation of Photoconversion Coefficients

Phytochrome photoconversion coefficients were first determined by Butler et al. (1964) soon after the discovery of the photoreceptor. The 1980s saw improvements in the methodology for determining the photochemical properties of phytochrome (absorbance spectra [$A_{R,\lambda}$ and$A_{\lambda}^{m,R}$], PPE^{R}, $\varepsilon_{R,\lambda max}$, ϕ_{R} and ϕ_{FR} – described below) required to calculate the photoconversion coefficients. Here I describe the step-by-step process for deriving the photoconversion coefficients, primarily using data from Kelly and Lagarias (1985).

Extraction/purification is the first step in determining the photochemical properties of phytochrome in vitro because it eliminates other absorbing molecules within a sample. Inadequate extraction can lead to partial degradation, which will result in inaccurate values. From the 1960s through the 1980s the reports of the molecular weight of phytochrome increased from 60 kDa to 118/114 kDa to 120 kDa to finally 124 kDa as purification techniques improved. In the literature, these different purifications were referred to as small, large and native phytochrome (Sage, 1992). It was for this reason that Mancinelli (1986) suggested avoiding using the original photoconversion coefficients from Butler et al. (1964), instead it is most appropriate to use values that report on 124 kDa phytochrome.

Absorbance spectra are determined for both forms of phytochrome. Saturating doses of either red or far-red photons are applied to the extracted phytochrome sample within a spectrophotometer and the absorbance spectrum is measured following Eq. [1.1].

$$A_\lambda = -\log_{10}(T_\lambda) \quad [1.1]$$

Where T_λ is equal to the fractional transmission of photons at wavelength, λ. It is important to note that A_λ is calculated with a base 10 logarithm.

Absorbance measurements under saturating doses of red and far-red photons provide $A_\lambda^{m,R}$ and $A_{R,\lambda}$, respectively, where $A_{R,\lambda}$ is the absorbance spectrum of P_R, while $A_\lambda^{m,R}$ is the absorbance spectrum of a mixture of both P_R and P_{FR}. This is because only PFR absorbs in the far-red regions while both forms absorb in the red region (see below). Here, a superscripted 'R' indicates a parameter determined under saturating red photons.

Solvents can affect the absorption spectra of molecules (Harris and Zscheile, 1943), but Lagarias et al. (1987) saw no difference between the absorbance spectra of phytochrome between two solvents used in their study. This provides confidence that the solvent did not alter these spectra.

The saturating doses of red and far-red used by Kelly and Lagarias (1985) were at 648 and 738 nm. From the absorbance data (Fig. 1-2), it can be seen that at 738 nm P_R has minimal absorbance. Thus, under the saturating dose of far-red (738 nm) the spectrophotometer will output the absorbance spectrum of P_R (A_R).

By contrast, a saturating dose of 648 nm photons is absorbed by both forms of phytochrome. Thus, when the saturating dose of R (648 nm) is applied, the spectrophotometer provides the absorbance spectrum of a mix of P_R and P_{FR} ($A_\lambda^{m,R}$). Therefore, to obtain the absorbance spectrum of just P_{FR} (A_{FR}) the solid dark red line in Fig. 1-2 must be corrected.

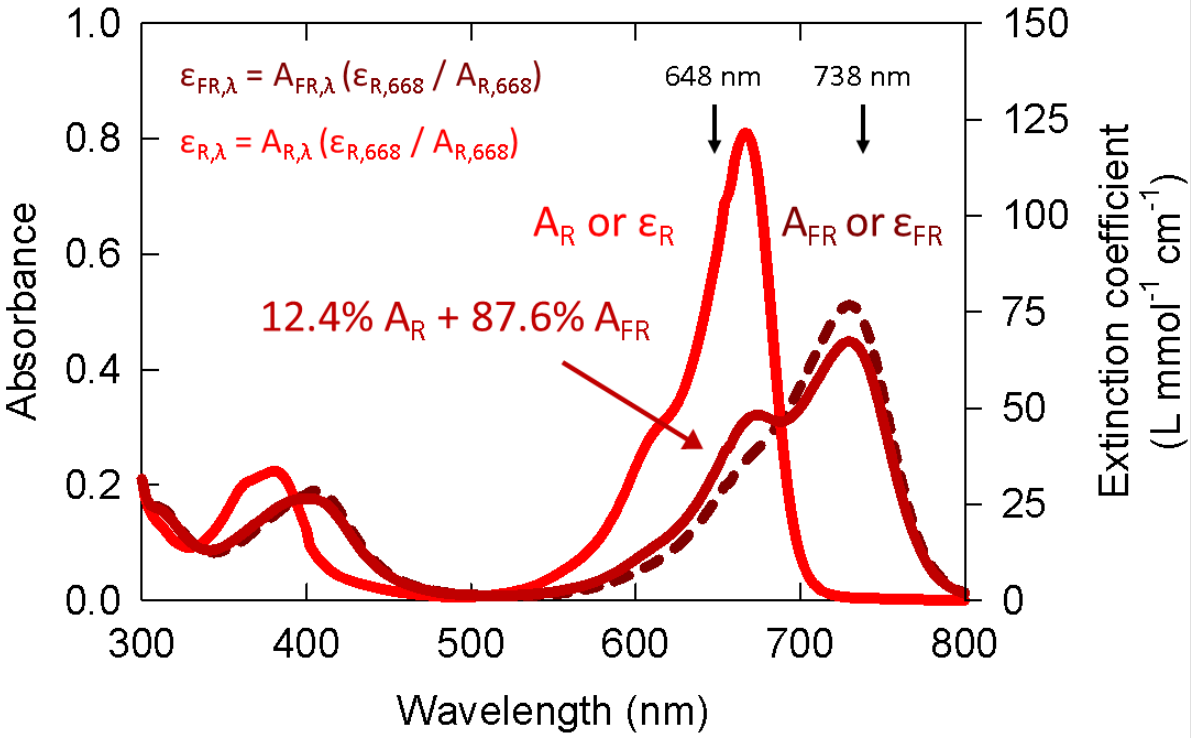

Fig. 1-2. Absorbance spectra and extinction coefficients of P_R and P_{FR}. Left axis, Absorbance spectra are provided in Kelly and Lagarias (1985), but because these values depend on the concentration of the sample, they are arbitrary. The arrows point to the wavelength of saturating red (648 nm) and far-red (738 nm) used to measure the absorbance spectrum of $A_\lambda^{m,R}$ and $A_{R,\lambda}$, respectively. $A_\lambda^{m,R}$ is then corrected to provide A_{FR} assuming that 87.6% of the total phytochrome is in the P_{FR} form under a saturating dose of 648 nm photons (dashed dark red line). The right axis shows the extinction coefficients. These values use a $\varepsilon_{R,668}$ nm of 121 L mmol^{-1} cm^{-1}.

This correction uses a calculated value of PPE^R, which is the estimate of PPE under the saturating dose of 648 nm photons. The theory and equation used to calculate PPE^R are

thoroughly described in Butler (1972). One of the parameters required to calculate PPE^R is the quantum yield ratio (ϕ_R/ϕ_{FR}), which can be calculated following two approaches:

1) *Initial rate analysis*. This method is also thoroughly described in Butler (1972). It uses the initial rates of change in the absorbance at 730 nm (representative of the P_{FR} concentration) given a dose (intensity) of either red or far-red photons.
2) *Approach to equilibrium analysis*. This method is described in Kelly and Lagarias (1985), who modify equations/methods from Johns (1969). Kelly and Lagarias (1985) point out that initial rate analysis extrapolates the rate of change from a tangent line using little data. Furthermore, initial rate analysis does not account for the impact of forward and reverse cycling between the two pools of phytochrome (P_R and P_{FR}). Instead, it assumes that the reaction goes to completion without a reverse reaction. Approach to equilibrium analysis accounts for both of these shortcomings by measuring absorbance across a full range of applied photons, and considering the reverse reactions in their calculations. Although not part of approach to equilibrium technique specifically, Kelly and Lagarias (1985) performed careful actinometry and instrument calibrations to obtain more exact absorbance values than previous studies.

Values for PPE^R have been reported as low as 0.75 (Pratt 1975), but most publications in the 1980s working with native phytochrome determined that PPE^R is between 0.86 and 0.89 (Vierstra and Quail 1983a; Kelly and Lagarias 1985; Mancinelli 1986; Lagarias et al. 1987; Holdsworth and Whitelam 1987). Most of the variation between earlier and later studies is due to the altered photochemistry in partially degraded phytochrome caused by impure extraction. However, even using similar purification methods, PPE^R can

vary depending on the species. Lagarias et al. (1987) reported a PPE^R value of 0.875 for *Avena* (oat) phytochrome, but a value of 0.887 for *Secale* (rye) phytochrome (these values are the average of two buffers/solvents reported in this study). The differences between species are small.

A PPE^R value of 0.876 (Kelly and Lagarias, 1985) indicates that the solid dark red line is a mixture of 87.6% P_{FR} and 12.4% P_R. Therefore the $A_\lambda^{m,R}$spectrum can be correct A_{FR} with the following equation:

$$A_\lambda^{m,R} = (1 - PPE^R)\, A_{R,\lambda} + PPE^R A_{FR,\lambda} \quad [1.2]$$

Therefore,

$$A_{FR,\lambda} = \frac{A_\lambda^{m,R} - (1 - PPE^R)\, A_{R,\lambda}}{PPE^R} \quad [1.3]$$

$A_{FR,\lambda}$, calculated following this equation, is shown in Fig. 1-2 as a dashed dark-red line.

Extinction coefficients (ε), also called molar absorption coefficients, provide absorbance values at a fixed concentration of the pigment (ε_R and ε_{FR} for phytochrome). Absorbance is dependent on the concentration, thus extinction coefficients are normalized absorbance. This means that an extinction coefficient spectrum will have the same shape as an absorbance spectrum with different absolute values. Converting between absorbance measurements and concentrations follows:

$$A_\lambda = \varepsilon_\lambda\, c\, \ell \quad [1.4]$$

Where c is the molar concentration (M) of the absorbing molecule and ℓ is the path-length through which the photons pass. ℓ is usually equal to 1 cm (although in some cases path-length is corrected to apparent path-length due to the non-ideal geometry of absorbance measurements). Therefore, extinction coefficients have units of L mol^{-1} cm^{-1} or M^{-1} cm^{-1}.

Converting an absorbance spectrum to an extinction coefficient spectrum only requires knowledge of the extinction coefficient at a single wavelength, which can be calculated from absorbance data of a known sample concentration. For the derivation of photoconversion coefficients, this is usually accomplished with a value of $\varepsilon_{R,\lambda max}$ which is the extinction coefficient of P_R at the absorbance peak, which has generally been measured to be 666 or 668 nm. Values of $\varepsilon_{R,\lambda max}$ vary significantly, with some reported values approximately double others. This is in part due to differences in the methods of determining the concentration of the sample. Total protein assays via colorimetric methods were reported to overestimate concentrations, leading to underestimates of $\varepsilon_{R,\lambda max}$ (Roux et al. 1982). Thus, amino acid analysis was suggested as a superior method (amino acid analysis counts the amino acids regardless of proteolysis). Vierstra and Quail (1983a) appear to agree with this conclusion, although they used a total protein assay.

Using amino acid analysis in a sample with (mostly) native phytochrome, Litts et al. (1983) determined that a sample of phytochrome with an $A_{R,668}$ of 0.385 had a concentration of 3.19×10^{-6} M. $\varepsilon_{R,668}$ can then be calculated from Eq. [1.4] to result in 120,690 M^{-1} cm^{-1} or roughly 121 mM^{-1} cm^{-1} (L per mmol per cm) as used by Kelly and Lagarias (1985).

The absorbance values are converted to extinction coefficients following Eq. [1.5] and [1.6]:

$$\varepsilon_{R,\lambda} = A_{R,\lambda} \times \frac{\varepsilon_{R,\lambda max}}{A_{R,\lambda max}} \quad [1.5]$$

$$\varepsilon_{FR,\lambda} = A_{FR,\lambda} \times \frac{\varepsilon_{R,\lambda max}}{A_{R,\lambda max}} \quad [1.6]$$

Where $A_{R,\lambda max}$ is the value of absorbance at the same wavelength as $\varepsilon_{R,\lambda max}$. This is shown in the right y-axis in Fig. 1-2. In addition to raw absorbance spectra, $\varepsilon_{R,\lambda}$ and $\varepsilon_{FR,\lambda}$ are also provided in the supplementary material in Kelly and Lagarias (1985), but it is important to note that these values are calculated (and rounded) using the same photochemical properties discussed here. Different values of PPE^R and/or $\varepsilon_{R,668}$ would result in different calculated values for $\varepsilon_{R,\lambda}$ and $\varepsilon_{FR,\lambda}$.

Using amino acid analysis, $\varepsilon_{R,\lambda max}$ has been calculated to equal 121, 128 and 132 L per mmol per cm in three different studies (Kelly and Lagarias, 1985; Lagarias et al., 1987; Mancinelli, 1986). Lagarias et al. (1987) suggests that these discrepancies may be caused by impurities within a sample. In addition to accurately measuring the concentration of a sample, $\varepsilon_{R,\lambda max}$ requires accurate measurements of the absorbance of a sample. Partially degraded phytochrome (118/114 kDa) shows differences in its spectral properties compared to 124 kDa (native) phytochrome including shifts in the absorbance maxima to shorter wavelengths and a decrease in the ratio of P_{FR}/P_R peaks (Vierstra and Quail 1983b). These changes in the spectral properties of phytochrome as it degrades indicates that partial degradation of phytochrome can lead to inaccurate absorbance measurements for a given concentration of phytochrome. The sample of extracted phytochrome that provided an $\varepsilon_{R,\lambda max}$ of 121 mM^{-1} cm^{-1} had a significantly greater amount of 118 kDa phytochrome compared to

the sample used to provide 132 mM^{-1} cm^{-1}. It seems likely that the proteolysis of the 124 kDa to the 118 kDa species led to a decrease in absorbance within the sample, but measurements of the concentration still remain accurate (due to "counting" the amino acids). This leads to an underestimation of $\varepsilon_{R,\lambda max}$ (Eq. [1.4]). Additionally, because the same value (132 mM^{-1} cm^{-1}) was obtained for both oat and rye phytochrome in Lagarias et al. (1987) there is a higher degree of confidence in an $\varepsilon_{R,\lambda max}$ of 132 mM^{-1} cm^{-1} compared to other values.

Quantum yields of P_R to P_{FR} conversion (ϕ_R) and P_{FR} to P_R conversion (ϕ_{FR}) are the final parameters required to calculate the photoconversion coefficients (σ_R and σ_{FR}). Quantum yields values must be back-calculated from other measurements. The quantum yield ratio (ϕ_R/ϕ_{FR}) is calculated following the initial rate or approach to equilibrium analysis described above. The first photoconversion coefficients (Butler et al. 1964) back-calculated ϕ_R and ϕ_{FR} from measured rates of change in absorbance for a given dose of photons at a specific wavelength. This analysis resulted in values of $\varepsilon_{R,\lambda}\phi_R$ and $\varepsilon_{FR,\lambda}\phi_{FR}$, from which ϕ_R and ϕ_{FR} could be calculated for a given value of $\varepsilon_{R,\lambda}$ or $\varepsilon_{FR,\lambda}$ (Equations in Butler et al. 1964). This is also the method used by Vierstra and Quail (1983a).

Kelly and Lagarias (1985) back-calculate values of ϕ_R and ϕ_{FR} from their approach to equilibrium analysis, obtaining $\phi_R = 0.152$ and $\phi_{FR} = 0.069$. Unsurprisingly, like with PPE^R and $\varepsilon_{R,\lambda max}$, ϕ_R and ϕ_{FR} can vary. Initial rate analysis predicts higher values than approach to equilibrium analysis. Furthermore, Lagarias et al. (1987) determined that these values were both greater in rye compared to oat under the same conditions and analysis.

Finally, the photoconversion coefficients are calculated as follows (Mancinelli, 1986, 1988, 1994):

$$\sigma_{R,\lambda} = \ln(10)\ \varepsilon_{R,\lambda}\ \phi_R$$

[1.7]

$$\sigma_{FR,\lambda} = \ln(10)\ \varepsilon_{FR,\lambda}\ \phi_{FR}$$

[1.8]

The reason to include the natural logarithm of ten, about 2.303, in this equation is because spectrophotometers provide absorbance values using a base 10 logarithm, but photons are attenuated naturally, thus ln(10) converts the base 10 logarithm into a natural logarithm. Eq. [1.7] and [1.8] without the ln(10) term is what has historically been called photoconversion coefficients, while these equations with the ln(10) term has been called the photoconversion cross-section. As mentioned previously, I have changed the nomenclature by calling σ_R and σ_{FR} coefficients and not cross-sections.

Applying Eq. [1.7] and [1.8] (using $\phi_R = 0.152$ and $\phi_{FR} = 0.069$ from Kelly and Lagarias, 1985) to the extinction coefficients in Fig. 1-2 yield the curves in Fig. 1-3. The standard units of σ_R and σ_{FR} are $m^2\ mol^{-1}$, but I provide final units of $m^2\ \mu mol^{-1}$. This is because photon flux densities usually have units of $\mu mol\ m^{-2}\ s^{-1}$. Multiplying the photon flux density by the photoconversion coefficients yields the first-order rate constants of phytochrome conversion, k_1 and k_2, with units of s^{-1}.

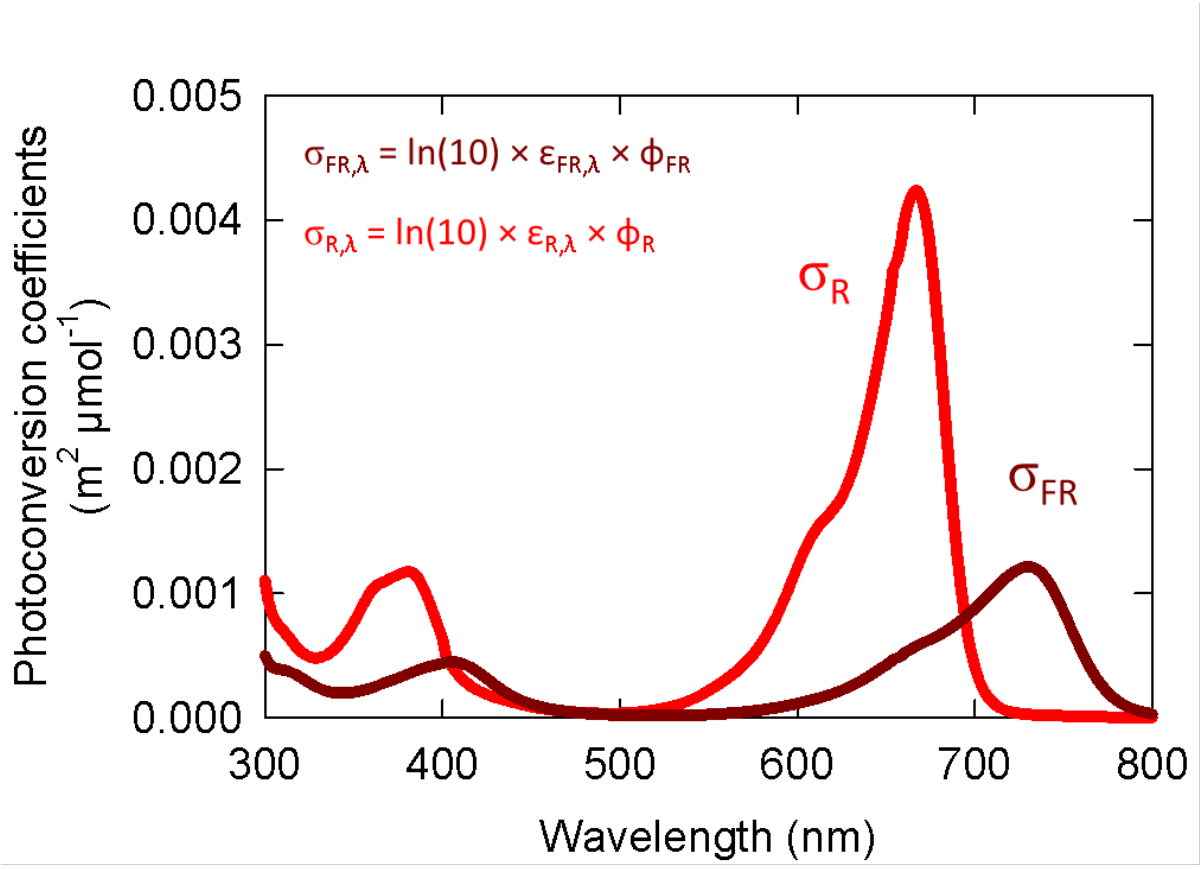

Fig. 1-3. Photoconversion coefficients of P_R and P_{FR} using approach to equilibrium analysis in Kelly and Lagarias (1985).

Caution should be taken to convert units carefully. Notice the values for the extinction coefficients in Fig. 1-2 have units of mM^{-1} cm^{-1} (L per mmol per cm). These can be divided by 10,000 to yield units of m^2 μmol^{-1}.

1.2.3.2 Use of Photoconversion Coefficients

Phytochrome photoconversion is a first-order reaction, which means that the instantaneous rate of change is dependent on the instantaneous concentration. The following equations calculate the rate constants (k_1 and k_2) for phytochrome photoconversions.

$$k_1 = \sum_{\lambda=300\ nm}^{\lambda=800\ nm} I_\lambda\, \sigma_{R,\lambda} \qquad [1.9]$$

$$k_2 = \sum_{\lambda=300\ nm}^{\lambda=800\ nm} I_\lambda\, \sigma_{FR,\lambda} \qquad [1.10]$$

Where I_λ is the photon flux at wavelength, λ. As mentioned previously, multiplying the photoconversion coefficient with the photon flux density yields units of s^{-1} for k_1 and k_2. These rate constants are multiplied by the concentrations of P_R and P_{FR} to yield rates of change (i.e. $\Delta[P_{FR}]$ per second), but because the concentration of P_R, P_{FR} and P_{total} are unknown, only relative changes in P_{FR} per second ($\Delta[P_{FR}/P_{total}]$ per second) are known. At equilibrium, the rates of P_R and P_{FR} interconversion are equal to each other, thus PPE (assuming *the two-state model*) is calculated as

$$PPE = \frac{k_1}{k_1 + k_2} \qquad [1.11]$$

This estimation of PPE has been widely used in horticulture for 40 years (see Kusuma and Bugbee 2021 [and references therein]). Following the recent evidence that the fully active dimer (D_2) is the active form (Klose et al. 2015), PPE (assuming *the three-state model*) is calculated as

$$\mathrm{PPE} = \left(\frac{k_1}{k_1 + k_2}\right)^2 \quad [1.12]$$

Eq. [1.11] and [1.12] are described in Mancinelli (1994), but more recent modelling of phytochrome dynamics has shown that these simple equations may fail to fully predict the state of phytochrome (Rausenberger et al., 2010; Klose et al., 2015). Smith and Fleck (2019) provided a program that incorporates components of this more complex modeling (e.g. thermal reversion of phytochrome, nuclear stabilization, and nuclear import) and calculates different pools of phytochrome including nuclear localized phytochrome (P_{FR} or D_2), called *the cellular model*.

1.3 Objectives & Hypotheses

Plant responses to shade light (relative increases in far-red and green, and reductions in blue, red and total photon intensity) have been well studied, but results can be inconsistent. Compared to plant responses to changes in the fluxes of far-red photon, shade responses to relative increases in green are poorly studied. Responses of horticultural species to relative increases in green are notably inconsistent and often differ in direction from studies performed in *Arabidopsis thaliana* (Appendix D). The photoconversion coefficients described previously are well developed and PPE has been utilized to predict parameters like stem elongation for nearly 50 years (Morgan and Smith, 1976; Park and Runkle, 2017), but this metric has significant issues (Kusuma and Bugbee, 2021). One of the primary issues is that these photoconversion coefficients are developed from extracted phytochrome and therefore predict PPE in vitro (above a leaf) rather than within a leaf where the phytochrome

is located. This means that photoconversion coefficients must incorporate distortion functions that account for absorption by other pigments (e.g. chlorophyll). Interactions between far-red and photon intensity have been studied, but results, especially those on leaf expansion, have been inconsistent and results often fail to align with theory (i.e. increased elongation at lower intensities). Finally, the response of phytochrome to longer wavelength photons, especially beyond 750 nm is poorly studied, and therefore, plant responses to photons from near-infrared LEDs are unknown.

1) The first objective was to determine the effect and interactions of blue and green photons fluxes on plant morphology

   Hypotheses:

   a. Increasing the fraction of blue photons would reduce plant size (e.g., leaf area, dry mass and stem length), while increasing the fraction of green photons would increase plant size.
   b. The effect of blue photons would be more significant at lower intensities (as this would cause photoreceptors to be under-saturated).
   c. The effect of green photons would be more significant at a lower fraction of blue photons.

2) The second objective was to investigate metrics that are commonly used to predict morphological responses to far-red

   Hypotheses:

   a. Environmental metrics would be better predictors of plant morphology than molecular models
   b. Metrics that range from 0 to 1 will be superior to metrics than can approach infinity

3) The third objective was to improve the phytochrome photoequilibrium (PPE) model by accounting for spectral distortions within leaves.

   Hypotheses:

   a. Estimating PPE from spectral photon distributions that have been modified with functions that account for optical distortions within leaves would improve its predictive value
   b. Using distortion functions that assume phytochrome is active within all tissues will be superior to distortions that assume phytochrome is only in the epidermis

4) The fourth objective was to investigate how plant responses to far-red interacted with intensity

   Hypotheses:

   a. Shade avoidance responses to far-red would be more pronounced at lower intensities
   b. Responses of leaf area to far-red will depend on intensity

5) Determine if photons from NIR LEDs can affect plant growth and development

   Hypotheses:

   a. Photons from an NIR LED, when applied during the dark period, will delay flowering in short-day plants.

b. Photons from NIR LEDs will increase stem elongation.

1.4 Literature Cited

Ahmad, M. 2016. Photocycle and signaling mechanisms of plant cryptochromes. Curr. Opin. Plant Biol. 33:108-115. doi: 10.1016/j.pbi.2016.06.013

Ahmad, M., N. Grancher, M. Heil, R.C. Black, B. Giovani, P. Galland, and D. Lardemer. 2002. Action spectrum for cryptochrome-dependent hypocotyl growth inhibition in Arabidopsis. Plant Physiol. 129:774-785. doi: 10.1104/pp.010969

Borthwick, H.A., S.B. Hendricks, M.W. Parker, E.H. Toole, and V.K. Toole. 1952. A reversible photoreaction controlling seed germination. Proc. Natl. Acad. Sci. USA 38:662-666. doi: 10.1073/pnas.38.8.662

Borthwick, H.A. 1972. History of phytochrome, p. 3-23. In: K. Mirakos and W. Shropshire (eds.). Phytochrome. Academic Press, New York.

Bouly, J.P., E. Schleicher, M. Dionisio-Sese, F. Vandenbussche, D. Van Der Straeten, N. Bakrim, S. Meier, A. Batschauer, P. Galland, R. Bittl, and M. Ahmad. 2007. Cryptochrome blue light photoreceptors are activated through interconversion of flavin redox states. J. Biol. Chem. 282:9383-9391. doi: 10.1074/jbc.M609842200

Butler, W.L., S.B. Hendricks, and H.W. Siegelman. 1964. Action spectra of phytochrome *in vitro*. Photochem. Photobiol. 3:521-528. doi: 10.1111/j.1751-1097.1964.tb08171.x

Butler, W.L. 1972. Photochemical properties of phytochrome in vitro, p. 187-192. In: K. Mirakos and W. Shropshire (eds.). Phytochrome. Academic Press, New York.

Casal, J.J. 2012. Shade avoidance. Arabidopsis Book 10:e0157. doi: 10.1199/tab.0157

Christie, J.M. 2007. Phototropin blue-light receptors. Ann. Rev. Plant Biol. 58:21-45. doi: 10.1146/annurev.arplant.58.032806.103951

de Lucas, M., and S. Prat. 2014. PIF s get BR right: PHYTOCHROME INTERACTING FACTORs as integrators of light and hormonal signals. New Phytol. 202:1126-1141. doi: 10.1111/nph.12725

de Wit, M., D.H. Keuskamp, F.J. Bongers, P. Hornitschek, C.M. Gommers, E. Reinen, C. Martínez-Cerón, C. Fankhauser, and R. Pierik. 2016. Integration of phytochrome and cryptochrome signals determines plant growth during competition for light. Current Biol. 26:3320-3326. doi: 10.1016/j.cub.2016.10.031

Folta, K.M., and S.D. Carvalho. 2015. Photoreceptors and control of horticultural plant traits. HortScience 50:1274-1280. doi: 10.21273/HORTSCI.50.9.1274

Galvão, V.C., and C. Fankhauser. 2015. Sensing the light environment in plants: photoreceptors and early signaling steps. Curr. Opin. Neurobiol. 34:46-53. doi: 10.1016/j.conb.2015.01.013

Gommers, C.M., E.J. Visser, K.R. St Onge, L.A. Voesenek, and R. Pierik. 2013. Shade tolerance: when growing tall is not an option. Trends Plant Sci. 18:65-71. doi: 10.1016/j.tplants.2012.09.008

Harris, D.G., and F.P. Zscheile. 1943. Effects of solvent upon absorption spectra of chlorophylls a and b; their ultraviolet absorption spectra in ether solution. Bot. Gaz. 104:515-527. doi: 10.1086/335166

Hernández, R., and C. Kubota. 2016. Physiological responses of cucumber seedlings under different blue and red photon flux ratios using LEDs. Environ. Expt. Bot. 12:66-74. doi: 10.1016/j.envexpbot.2015.04.001

Holdsworth, M.L., and G.C. Whitelam. 1987. A monoclonal antibody specific for the red-absorbing form of phytochrome. Planta 172:539-547. doi: 10.1007/BF00393872

Holmes, M.G., and L. Fukshansky. 1979. Phytochrome photoequilibria in green leaves under polychromatic radiation: a theoretical approach. Plant Cell Environ. 2:59-65. doi: 10.1111/j.1365-3040.1979.tb00774.x

Hughes, J. 2013. Phytochrome cytoplasmic signaling. Ann. Rev. Plant Biol. 64:377-402. doi: 10.1146/annurev-arplant-050312-120045

Ji, Y., D. Nuñez Ocaña, D. Choe, D.H. Larsen, L.F. Marcelis, and E. Heuvelink. 2020. Far-red radiation stimulates dry mass partitioning to fruits by increasing fruit sink strength in tomato. New Phytol. 228:1914-1925. doi: 10.1111/nph.16805

Johns, H.E. 1969. Photochemical reactions in nucleic acids. Methods Enzymol. 16: 253-316. doi: 10.1016/S0076-6879(69)16011-5

Kalaitzoglou, P., W. van Ierpen, J. Harbinson, M. van der Meer, S. Martinakos, K. Weerheim, C.C.S. Nicole, and L.F.M. Marcelis. 2019. Effects of continuous or end-of-day far-red light on tomato plant growth, morphology, light absorption, and fruit production. Front. Plant Sci. 10:322. doi: 10.3389/fpls.2019.00322

Kang, W.H., J.S. Park, K.S. Park, and J.E. Son. 2016. Leaf photosynthetic rate, growth, and morphology of lettuce under different fractions of red, blue, and green light from light-emitting diodes (LEDs). Hort. Environ. Biotechnol. 57 :573-579. doi: 10.1007/s13580-016-0093-x

Kasperbauer, M.J. 1971. Spectral distribution of light in a tobacco canopy and effects of end-of-day light quality on growth and development. Plant Physiol. 47:775-778. doi: 10.1104/pp.47.6.775

Kelly, J.M., and J.C. Lagarias. 1985. Photochemistry of 124-kilodalton *Avena* phytochrome under constant illumination in vitro. Biochemistry 24:6003-6010. doi: 10.1021/bi00342a047

Kim, H.H., G.D. Goins, R.M. Wheeler, and J.C. Sager. 2004. Green-light supplementation for enhanced lettuce growth under red-and blue-light-emitting diodes. HortScience 39:1617-1622. doi: 10.21273/HORTSCI.39.7.1617

Klose, C., F. Venezia, A. Hussong, S. Kircher, E. Schäfer, and C. Fleck. 2015. Systematic analysis of how phytochrome B dimerization determines its specificity. Nature Plants 1:1-9. doi: 10.1038/nplants.2015.90

Klose, C., F. Nagy, and E. Schäfer. 2020. Thermal reversion of plant phytochromes. Mol. Plant 13:386-397. doi: 10.1016/j.molp.2019.12.004

Kusuma, P., and B. Bugbee. 2021. Far-red Fraction: An Improved Metric for Characterizing Phytochrome Effects on Morphology. J. Am. Soc. Hort. Sci. 146:3-13. doi: 10.21273/JASHS05002-20

Lagarias, J.C., J.M. Kelly, K.L. Cyr, and W.O. Smith, Jr. 1987. Comparative photochemical

analysis of highly purified 124 kilodalton oat and rye phytochromes *in vitro*. Photochem. Photobiol. 46:5-13. doi: 10.1111/j.1751-1097.1987.tb04729.x

Lee, M.J., K.H. Son, and M.M. Oh. 2016. Increase in biomass and bioactive compounds in lettuce under various ratios of red to far-red LED light supplemented with blue LED light. Hort. Environ. Biotechnol. 57:139-147. doi: 10.1007/s13580-016-0133-6

Legris, M., C. Klose, E.S. Burgie, C.C. Rojas, M. Neme, A. Hiltbrunner, P.A. Wigge, E. Schäfer, R.D. Vierstra, and J.J. Casal. 2016. Phytochrome B integrates light and temperature signals in *Arabidopsis*. Science 354:897-900. doi: 10.1126/science.aaf5656

Leivar, P., and E. Monte. 2014. PIFs: systems integrators in plant development. Plant Cell 26:56-78. doi: 10.1105/tpc.113.120857

Li, Q., and C. Kubota. 2009. Effects of supplemental light quality on growth and phytochemicals of baby leaf lettuce. Environ. Expt. Bot. 67:59-64. doi: 10.1016/j.envexpbot.2009.06.011

Lin, C. 2000. Plant blue-light receptors. Trends Plant Sci. 5:337-342. doi: 10.1016/S1360-1385(00)01687-3

Litts, J.C., J.M. Kelly, and J.C. Lagarias. 1983. Structure-function studies on phytochrome. Preliminary characterization of highly purified phytochrome from *Avena sativa* enriched in the 124-kilodalton species. J. Biol. Chem. 258:11025–11031. doi: 10.1016/S0021-9258(17)44381-X

Liu, B., Z. Yang, A. Gomez, B. Liu, C. Lin, and Y. Oka. 2016. Signaling mechanisms of plant cryptochromes in *Arabidopsis thaliana*. J. Plant Res. 129:137-148. doi: 10.1007/s10265-015-0782-z

Mancinelli, A.L. 1986. Comparison of spectral properties of phytochromes from different preparations. Plant Physiol. 82:956-961. doi: 10.1104/pp.82.4.956

Mancinelli, A.L. 1988. Some thoughts about the use of predicted values of the state of phytochrome in plant photomorphogenesis research. Plant Cell Environ. 11:429-439. doi: 10.1111/j.1365-3040.1988.tb01780.x

Mancinelli, A.L. 1994. The physiology of phytochrome action, p. 221-296. In: R.E. Kendrick and G.H.M. Kronenberg (eds.). Photomorphogenesis in plants. Springer, Dordrecht, The Netherlands. doi: 10.1007/978-94-011-1884-2_10

Meng, Q., J. Boldt, and E.S. Runkle. 2020. Blue radiation interacts with green radiation to influence growth and predominantly controls quality attributes of lettuce. J. Am. Soc. Hort. Sci. 145:75-87. doi: 10.21273/JASHS04759-19

Meng, Q., N. Kelly, and E.S. Runkle. 2019. Substituting green or far-red radiation for blue radiation induces shade avoidance and promotes growth in lettuce and kale. Environ. Expt. Bot. 162:383-391. doi: 10.1016/j.envexpbot.2019.03.016

Meng, Q., and E.S. Runkle. 2019. Far-red radiation interacts with relative and absolute blue and red photon flux densities to regulate growth, morphology, and pigmentation of lettuce and basil seedlings. Scientia Hort. 255:269-280. doi: 10.1016/j.scienta.2019.05.030

Millenaar, F.F., M. Van Zanten, M.C. Cox, R. Pierik, L.A. Voesenek, and A.J. Peeters. 2009. Differential petiole growth in *Arabidopsis thaliana*: photocontrol and hormonal regulation. New Phytol. 184:141-152. doi: 10.1111/j.1469-8137.2009.02921.x

Morgan, D.C., and H. Smith. 1976. Linear relationship between phytochrome

photoequilibrium and growth in plants under simulated natural radiation. Nature 262:210-212. doi: 10.1038/262210a0

Morgan, D.C., and H. Smith. 1978. The relationship between phytochrome-photoequilibrium and Development in light grown *Chenopodium album* L.. Planta 142:187-193. doi: 10.1007/BF00388211

Müller, P., and M. Ahmad. 2011. Light-activated cryptochrome reacts with molecular oxygen to form a flavin–superoxide radical pair consistent with magnetoreception. J. Biol. Chem. 286:21033-21040. doi: 10.1074/jbc.M111.228940

Müller, P., J.P. Bouly, K. Hitomi, V. Balland, E.D. Getzoff, T. Ritz, and K. Brettel. 2014. ATP binding turns plant cryptochrome into an efficient natural photoswitch. Sci. Rep. 4:1-11. doi: 10.1038/srep05175

Park, Y., and E.S. Runkle. 2017. Far-red radiation promotes growth of seedlings by increasing leaf expansion and whole-plant net assimilation. Environ. Expt. Bot. 136:41-49. doi: 10.1016/j.envexpbot.2016.12.013

Podolec, R., R. Ulm. 2018. Photoreceptor-mediated regulation of the COP1/SPA E3 ubiquitin ligase. Curr. Opin. Plant Biol. 45:18-25. doi: 10.1016/j.pbi.2018.04.018

Pratt, L.H. 1975. Photochemistry of high molecular weight phytochrome *in vitro*. Photochem. Photobiol. 22:33-36. doi: 10.1111/j.1751-1097.1975.tb06717.x

Rausenberger, J., A. Hussong, S. Kircher, D. Kirchenbauer, J. Timmer, F. Nagy, E. Schäfer, and C. Fleck. 2010. An integrative model for phytochrome B mediated photomorphogenesis: from protein dynamics to physiology. PLoS One 5:e10721. doi: 10.1371/journal.pone.0010721

Roux, S.J., K. McEntire, and W.E. Brown. 1982. Determination of extinction coefficients of oat phytochrome by quantitative amino acid analyses. Photochem. Photobiol. 35:537-543. doi: 10.1111/j.1751-1097.1982.tb02606.x

Sage, L.C. 1992. Pigment of the imagination: a history of phytochrome research. Academic Press, San Diego.

Salomon, M., J.M. Christie, E. Knieb, U. Lempert, and W.R. Briggs. 2000. Photochemical and mutational analysis of the FMN-binding domains of the plant blue light receptor, phototropin. Biochemistry 39:9401-9410. doi: 10.1021/bi000585+

Sellaro, R., R.W. Smith, M. Legris, C. Fleck, and J.J. Casal. 2019. Phytochrome B dynamics departs from photoequilibrium in the field. Plant Cell Environ. 42:606-617. doi: 10.1111/pce.13445

Smith, H. 1982. Light quality, photoperception, and plant strategy. Ann. Rev. Plant Physiol. 33:481-518. doi: 10.1146/annurev.pp.33.060182.002405

Smith, H.L., L. McAusland, and E.H. Murchie. 2017. Don't ignore the green light: exploring diverse roles in plant processes. J. Exp. Bot. 68:2099-2110. doi: 10.1093/jxb/erx098

Smith, R.W., and C. Fleck. 2019. Basic Phytochrome B Calculations, p. 121-133. In: H. Hiltbrunner (ed.). Phytochromes. Humana, New York.

Snowden, M.C., K.R. Cope, and B. Bugbee. 2016. Sensitivity of seven diverse species to blue and green light: interactions with photon flux. PLoS One 11:e0163121. doi: 10.1371/journal.pone.0163121

Son, K.H., and M.M. Oh. 2013. Leaf shape, growth, and antioxidant phenolic compounds of two lettuce cultivars grown under various combinations of blue and red light-emitting diodes. HortScience 48:988-995. doi: 10.21273/HORTSCI.48.8.988

Son, K.H., and M.M. Oh. 2015. Growth, photosynthetic and antioxidant parameters of two lettuce cultivars as affected by red, green, and blue light-emitting diodes. Hort. Environ. Biotechnol. 56:639-653. doi: 10.1007/s13580-015-1064-3

Vierstra, R.D., and P.H. Quail. 1983a. Photochemistry of 124 kilodalton *Avena* phytochrome *in vitro*. Plant Physiol. 72:264-267. doi: 10.1104/pp.72.1.264

Vierstra, R.D., and P.H. Quail. 1983b. Purification and initial characterization of 124 kdalton phytochrome from *Avena*. Biochemistry 22:2498-2505. doi: 10.1021/bi00279a029

Wang, J., W. Lu, Y. Tong, and Q. Yang. 2016. Leaf morphology, photosynthetic performance, chlorophyll fluorescence, stomatal development of lettuce (*Lactuca sativa* L.) exposed to different ratios of red light to blue light. Front. Plant Sci. 7:250. doi: 10.3389/fpls.2016.00250

Zhang, T., S.A. Maruhnich, and K.M. Folta. 2011. Green light induces shade avoidance symptoms. Plant Physiol. 157:1528-1536. doi: 10.1104/pp.111.180661

Zhen, S., and B. Bugbee. 2020. Substituting far-red for traditionally defined photosynthetic photons results in equal canopy quantum yield for CO_2 fixation and increased photon capture during long-term studies: Implications for re-defining PAR. Front. Plant Sci. 11:1433. doi: 10.3389/fpls.2020.581156

CHAPTER 2

DOES GREEN REALLY MEAN GO? INCREASING THE FRACTION OF GREEN PHOTONS PROMOTES GROWTH OF TOMATO BUT NOT LETTUCE OR CUCUMBER[A]

2.1 Abstract

The photon flux in the green wavelength region is relatively enriched in shade and the photon flux in the blue region is selectively filtered. In sole source lighting environments, increasing the fraction of blue typically decreases stem elongation and leaf expansion, and smaller leaves reduce photon capture and yield. Photons in the green region reverse these blue reductions through the photoreceptor cryptochrome in *Arabidopsis thaliana*, but studies in other species have not consistently shown the benefits of photons in the green region on leaf expansion and growth. Spectral effects can interact with total photon flux. Here, we report the effect of the fraction of photons in the blue (10 to 30%) and green (0 to 50%) regions at photosynthetic photon flux densities of 200 and 500 μmol m^{-2} s^{-1} in lettuce, cucumber and tomato. As expected, increasing the fraction of photons in the blue region consistently decreased leaf area and dry mass. By contrast, large changes in the fraction of photons in the green region had minimal effects on leaf area and dry mass in lettuce and cucumber. Photons in the green region were more potent at a lower fraction of photons in the blue region. Photons in the green region increased stem and petiole length in cucumber and

[A] Kusuma, P., B. Swan, and B. Bugbee. Published in Plants

tomato, which is a classic shade avoidance response. These results suggest that high-light crop species might respond to the fraction of photons in the green region with either shade tolerance (leaf expansion) or shade avoidance (stem elongation).

2.2 Introduction

In naturally shaded environments, irradiance/photon fluxes in the blue (400 to 500 nm) and red (600 to 700 nm) regions are relatively reduced while the fluxes of photons in the green (500 to 600 nm) and far-red (700 to 750 nm) regions are relatively enriched. In the photobiology literature, the term light is often used to refer to the photon flux, as in blue light, but this terminology does not describe the discrete nature of photons, which drive photobiological reactions. Additionally, light is closely connected to brightness in human perception of photons, thus photon is a preferable term. Here, the terms blue, green, red and far-red photons refer to photons in the regions that induce blue, green, red or far-red color perception.

Plant developmental responses to a relative increase in far-red have been well studied [1,2], with species-specific increases in leaf area or stem length empirically described as shade tolerance or shade avoidance. It should be noted that shade tolerance does not often specify an increase in leaf area; instead, morphological changes are discussed in terms of an increase in specific leaf area, which is leaf area divided by leaf mass [3].

Elevated far-red commonly increases leaf area in controlled environments and this response is beneficial because it increases photon capture [4]. Increases in stem length in controlled environments are typically considered detrimental. In contrast to the well-characterized responses to far-red, shade-responses to green photons are less well studied.

Early light-emitting diode (LED) fixtures for horticultural applications supplied only blue and red photons. One of the first studies that investigated the effects of adding green to this type of spectrum found that increasing the fraction of green photons from zero to 24% increased leaf area in *Lactuca sativa* cv. "Waldmann's Green" by 31% and increased shoot dry mass by 47% [5]. This early finding created a sustained interest in considering green photons to horticultural fixtures in order to promote growth [6,7]. However, more recent studies have shown contradictory results to Kim et al. [5] (e.g., [8]), suggesting the need for a reanalysis of the beneficial effects of green photons on plant growth – especially with continued emerging evidence that green photons act antagonistically against blue photons through the photoreceptor cryptochrome.

Cryptochromes are one of the two most well-studied families of blue photon receptors, and they primarily modulate plant growth through the control of gene expression. The other well-studied family of blue photon receptors are phototropins, which primarily modulate plant growth through interactions with membranes [9,10]. The high flux of blue photons in sunlight cause reduced stem and leaf elongation. Studies investigating hypocotyl elongation in *Arabidopsis thaliana* mutants have indicated that cryptochromes are the primary photoreceptor influencing the decrease in stem length [11,12]. Longer-term studies in pea have corroborated this finding as greenhouse grown plants lacking cryptochrome were 20 to 40% longer than the wild-type plants [13]. Phototropins play a role in reducing hypocotyl elongation when seedlings are moved from darkness to blue light [14], but this rapid response does not appear to have a prolonged effect [12]. The role of these photoreceptors in leaf expansion in mature plants is less well studied.

Studies have typically found that increasing the fraction of blue photons decreases leaf area/plant diameter in the horticultural crops lettuce [8,15–24], cucumber [25–28] and tomato [26,29], but these effects are not always statistically significant [17,18,26,28,30–34] and occasionally go in the opposite direction [18]. Leaf area is generally highly correlated with dry mass (yield). Thus, increasing the fraction of blue photons also typically result in decreased dry mass [8,15,16,20–22,24–26,28,35,36], although this is not always the case [17–19,25–32,34,36–42]. In addition to reducing leaf area and yield, blue photons have also been shown to reduce stem and petiole length in cucumber and tomato [25,26,28,32,33], indicating that the effects of blue photons on manipulating cryptochrome activity in *Arabidopsis* extend to these horticultural species. We review 29 studies spanning 19 years on the effects of blue photon fraction in lettuce, cucumber and tomato in Table D.1. Comparisons are complex because the studies were conducted at multiple temperatures, study durations, photon fluxes, photoperiods and cultivars.

Unlike spectral distributions that lack either blue or red photons [25,26,43], growing plants in the absence of green photons does not necessarily induce abnormal morphology [25,26]. Studies from the past two decades have suggested that green photons act antagonistically against blue photons to modulate the action of the photoreceptor cryptochrome in a similar manner to the red and far-red antagonism in the photoreceptor phytochrome. In cryptochrome, the flavin adenine dinucleotide (FAD) chromophore has three potential states. The oxidized form, FADox, is abundant in the dark, and upon photon absorbance it converts into the semi-reduced radical state (flavosemiquinone, $FADH^{o}$), which is the active form. Photon absorbance by $FADH^{o}$ induces conversion into the fully reduced ($FADH^{-}$) state, which is inactive [44,45]. The absorbance spectra of FADox shows a

sensitivity to blue photons at about 450 nm, with little absorbance beyond 500 nm, while comparatively the absorbance spectrum of $FADH^{o}$ shows relative lower absorbance in the blue region and higher absorbance in the green region [46]. The fully reduced form has a unique absorbance spectrum [47,48], but there are no models of cryptochrome activity that suggest a molecular change in $FADH^{-}$ by photon absorbance [44,49]. This model indicates that green photons ought to partially inhibit/reverse blue induced decreases in stem elongation. If cryptochrome affects leaf expansion, then green photons may increase leaf area and yield.

This hypothesis has been evaluated in multiple studies. Although increasing the green photon flux can induce shade morphology (e.g., increased petiole / total leaf length and decreased leaf angle) in *Arabidopsis thaliana* [50,51], the effect of green photons in horticultural crops is inconsistent. For example, although some studies in cucumber and tomato showed an increase in stem elongation in response to increasing green fraction [26] many others have shown no response of stem or petiole length to increasing the fraction of green photons [25–27,29,33], and occasionally studies show a decrease in stem length [28], which is in the opposite direction than expected.

Additionally, replacing red photons with green photons under a constant fraction of blue has increased leaf area and dry mass in some studies [5,20,22,26,39,41,52], but most studies show no response, and several show an opposite response [8,20,23,25–29,33,36, 38,40] (also see Table D.2). Overall, the expected morphological (and subsequent growth) responses to blue and green photons do not always occur in the horticultural crops lettuce, cucumber and tomato.

The photosynthetic photon flux density (PPFD), or intensity, affects morphology. One notable example is that leaf thickness typically increases with increasing photon flux. Thick and thin leaves are referred to as sun and shade leaves. This response has recently been partially explained by the involvement of both cryptochromes and phototropins [53]. In some studies, the blue fraction has been found to be better a predictor of stem elongation and leaf expansion, while in other species and other studies, absolute blue intensity has been found to be a better predictor of morphological responses [26,30,54,55]. The extent of interactions between photon quality and quantity is not well studied.

Previous studies have investigated some of the following interactions: 1) the effect of blue photons between 10 and 30% blue [8,26], 2) interactions with green photons at multiple levels of blue [8,20], and 3) interactions with intensity [26]. We sought to investigate all three parameters and their interactions. We hypothesized that 1) increasing the fraction of blue photons would reduce plant size (e.g., leaf area, dry mass and stem length), while increasing the fraction of green photons would increase plant size; 2) the effect of blue photons would be more significant at lower intensities (as this would cause photoreceptors to be under-saturated); and 3) the effect of green photons would be more significant at a lower fraction of blue photons.

2.3 Material and Methods

2.3.1 Plant Material and Cultural Conditions

Lettuce (*Lactuca sativa*, var. Red Salad Bowl), tomato (*Solanum lycopersicum*, cv. Early Girl) and cucumber (*Cucumis sativa*, var. Boston Pickling) seeds were direct seeded

then thinned for uniformity after emergence leaving four plants per module. Planted root modules were randomly placed into the 16 treatment chambers. Each chamber had dimensions of 20 × 23 × 30 (L × W × H, 13800 cm^3) with gloss white walls. Fans provided an air velocity of 0.5 m s^{-1} at the top of the canopy. The root modules measured 20 × 18 × 13 (4680 cm^3) and contained a 1:1 ratio of peat and vermiculite by volume with five grams of uniformly mixed Nutricote® slow-release fertilizer (16-2.6-11.2, N-P-K, type 100). Root modules were watered to 10% excess as needed with dilute fertilizer solution (0.1N-0.01P-0.08K; Scotts® Peat-lite, 21-5-20; EC = 1 mS cm^{-1}), and were allowed to passively drain. Type-E Thermocouples connected to a data logger (CR1000, Campbell Scientific, Logan UT, USA) continuously monitored ambient air temperature at the top of the plant canopy. Day/night temperature was 23/20 °C, with less than 1 °C variation over time and 1 °C variation among chambers. CO_2 concentration was continuously monitored and was identical for all treatments and varied over time between 450 and 500 ppm.

2.3.2 Treatments

The system included 16 chambers with eight unique spectral outputs at two intensities for a 16 h photoperiod (PPFD: 200 µmol m^{-2} s^{-1}, DLI: 11.5 mol m^{-2} d^{-1}; and PPFD: 500 µmol m^{-2} s^{-1} DLI: 28.8 mol m^{-2} d^{-1}). Treatments were developed using LEDs (Luxeon Rebel Tri-Star LEDs; Quadica Developments Inc., Ontario, Canada) to output three white (cool, neutral and warm), three red/blue (RB) combinations, and two red/blue/green (RBG) combinations. The RB combination had about 10, 20 and 30% blue, and the RBG treatments contained about 10 and 20% B with 20 or 10% G, respectively. The spectral distributions of

the treatments were measured before each replicate study with a spectroradiometer (model PS-200; Apogee Instruments, Logan UT, USA) and are shown in Figure 2-1. Blue, green and red as a percentage of the PPFD were calculated for each species at the higher and lower PPFD. These are averaged together in Table 2-1. PPFD was measured with a full-spectrum quantum sensor (MQ-200, Apogee Instruments, Logan UT, USA) at the top of the plant canopy, and each chamber was adjusted to maintain PPFD at ± 5%.

Table 2.1. Representative ratios of blue, green and red fluxes as a percentage of photosynthetic photon flux density (PPFD). Values from the three species and two intensities deviated less than 10% from the average and thus we present average values. RB refers to treatments comprised of red and blue LEDs and RBG refers to treatments comprised of red, blue and green LEDs.

	White			RB			RBG	
	Warm	Neutral	Cool	RB10	RB20	RB30	RBG10	RBG20
% Blue (400 to 499)	9	18	23	11	21	32	22	11
% Green (500 to 599)	42	47	51	1	1	1	11	20
% Red (600 to 699)	49	35	26	88	78	67	67	69

2.3.3 Plant Measurements

All species were harvested after canopy closure – when the leaves of the four plants in one of the treatments began to touch. This occurred 21 days after emergence in lettuce, 12, 13 and 20 days after emergence in tomato, and 11 or 13 days after emergence in cucumber. At harvest, stem and longest petiole length of the each of the four plants per chamber were measured in tomato and cucumber. Leaf area was measured using a leaf area meter (LI-3000; LI-COR, Lincoln NE, USA). Leaf area index (LAI, $m^2_{leaf}\, m^{-2}_{ground}$) was calculated by dividing total leaf area per chamber by the ground area of the chamber. Shoot dry mass (DM)

was measured after the tissue was dried at 80 °C for 48 h. Dry mass per unit area (g DM m^{-2}_{ground}) was calculated by dividing total dry mass by the chamber area. Specific leaf mass

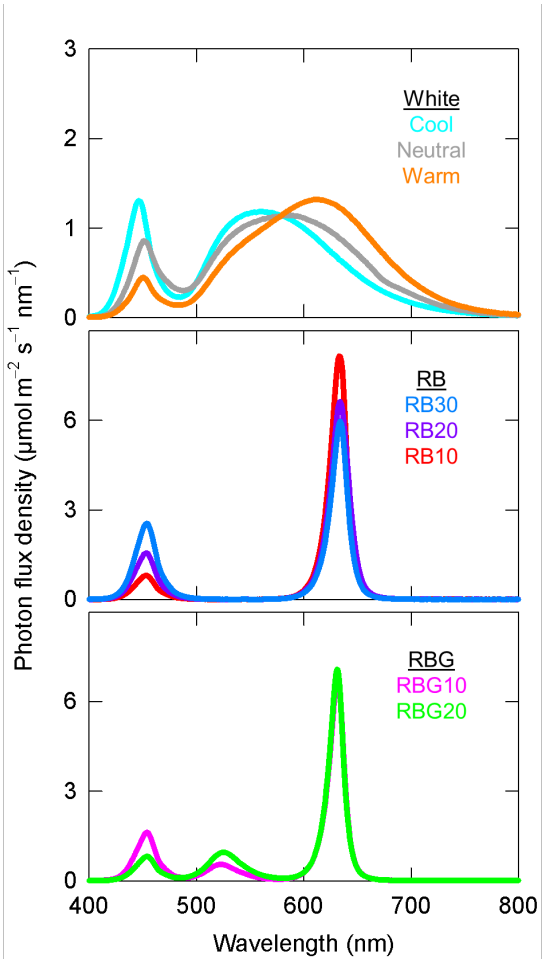

Figure 2-1. Representative spectral output of each of the eight treatments at a PPFD of 200 µmol m^{-2} s^{-1}. (Top) the three white LEDs, (middle) the three RB (red/blue) combinations, (bottom) the two RBG (red/blue/green) treatments.

(SLM, kg DM_{leaf} m^{-2}_{leaf}) was calculated by dividing the total leaf dry mass of the four plants by the total leaf area of the four plants. The average stem and longest petiole length from each chamber were used for statistical analysis (four measurements averaged together).

2.3.4 Statistical Analysis

The study was replicated three times (each with four plants per replicate in time). All data were analyzed using R statistical software (R Foundation for Statistical Computing; Vienna, Austria). Blue, green and PPFD effects on the growth parameters in lettuce, cucumber and tomato were determined using lmer and Anova functions with an F statistic. We present significance at $p < 0.05$ (marked with a *). In a mixed effects linear model, percent blue and percent green were treated as continuous variables while intensity was treated as a fixed effect. Replicates were treated as random factors. Interaction terms between these three factors were included in the linear model. The three-way interaction was insignificant for all parameters and was therefore pooled into the error term.

In order to understand the interactions, the effect of blue photons was also analyzed by separating the data by intensity (200 and 500 μmol m^{-2} s^{-1}). This separation was also done in the analysis of the effects of green photons, and because green photons have been implicated in the reversal of blue photon effects, the data were further separated for 10 or 20% blue photons. The RB30 treatment was not included in this analysis, and both the cool and neutral white LEDs were considered about 20% blue.

2.4 Results

(a)

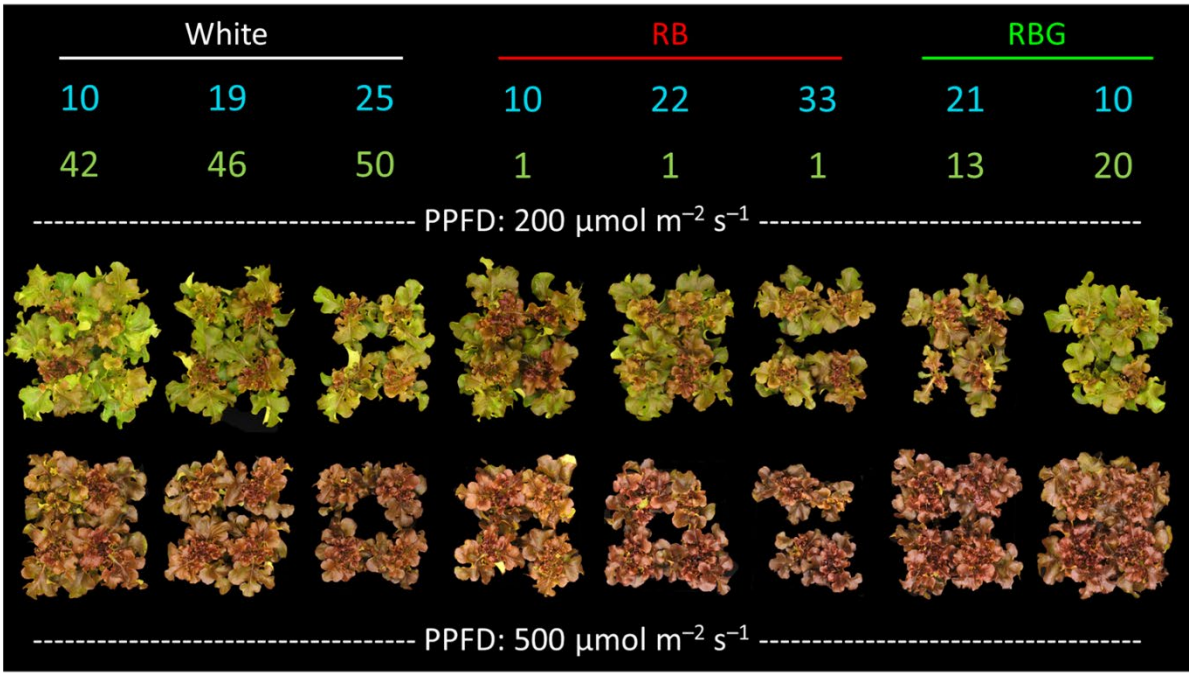

(b)

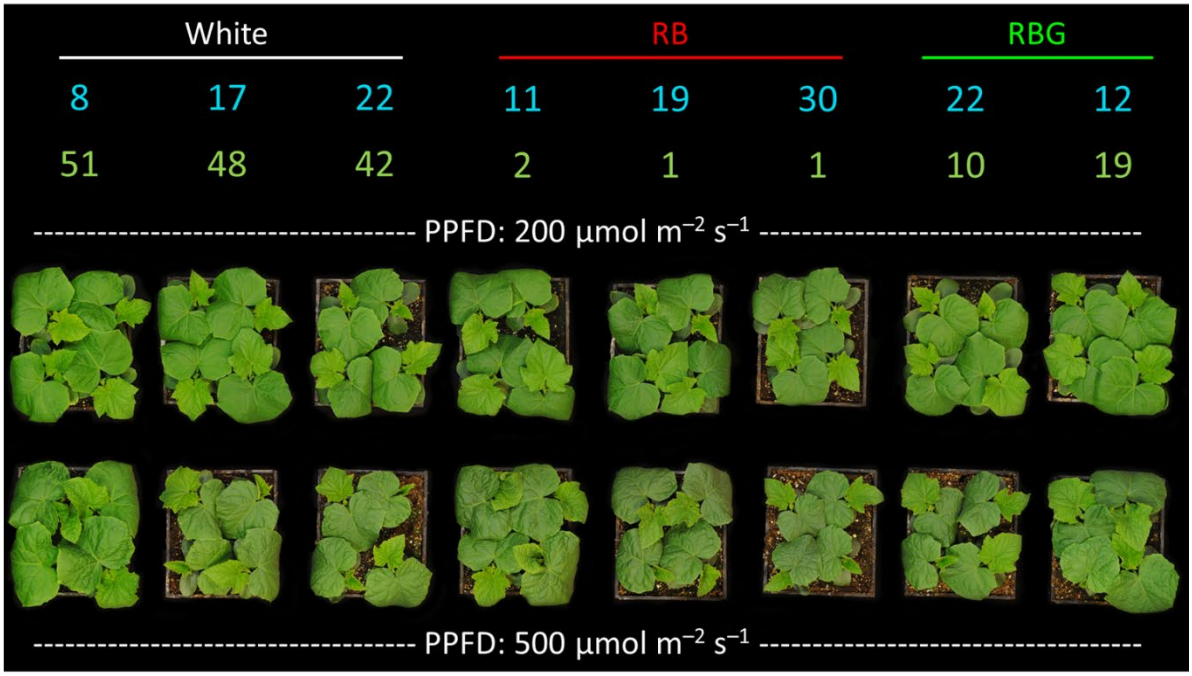

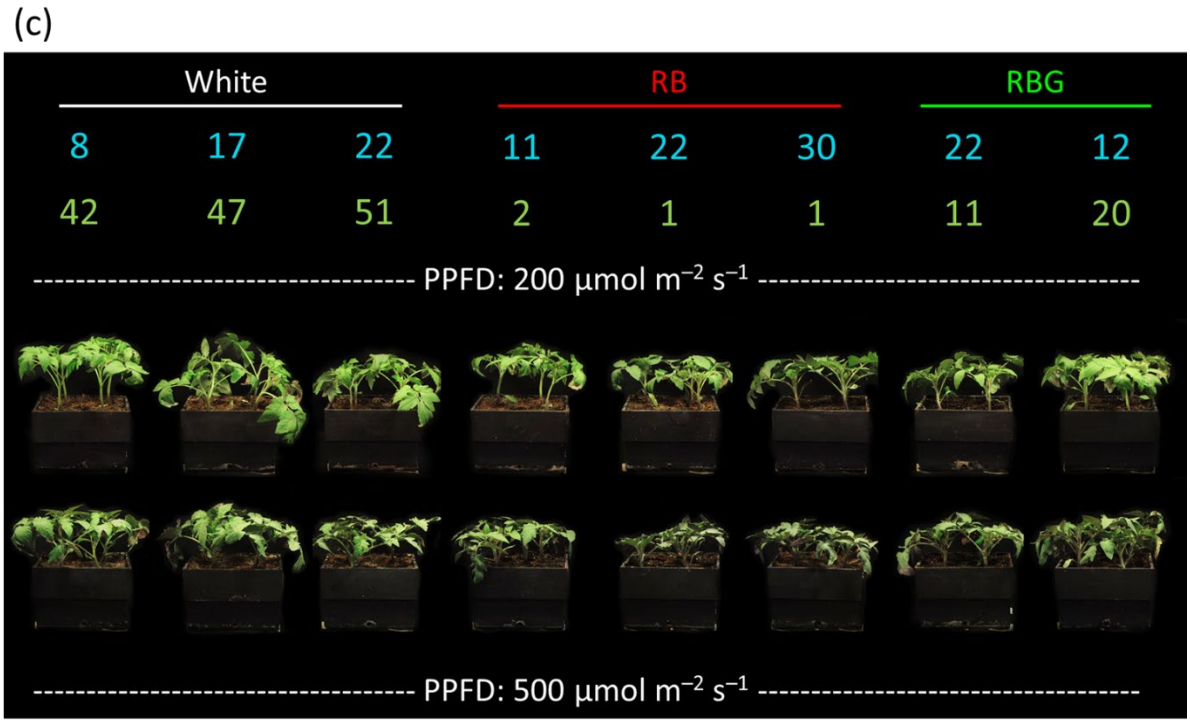

Figure 2-2. Representative photos from a single replicate of each treatment for **(a)** lettuce, **(b)** cucumber and **(c)** tomato. The average percentages of blue and green are shown above the plants in their respective color. RB: red/blue; RBG: red/blue/green; PPFD: photosynthetic photon flux density.

Representative photos of the three species in each treatment are shown with the percentages of blue and green in Figure 2-2.

Significant effects from the mixed effects linear model are presented in Table 2-2. In Figures 2-3 through 2-7, data for dry mass, LAI, SLM, plant height and longest petiole length for each replicate were normalized to the grand mean of the three replicates and standard error bars represent the normalized error. The resulting percent change between 10 and 30% blue or zero and 50% green is shown. These graphs show the significance of the separated data (e.g., the effect of increasing green photons at 10% blue and a PPFD of 200 µmol m^{-2} s^{-1}).

Table 2.2. Significant effects of percent blue (%B), percent green (%G) and PPFD, along with interaction terms on the parameters of dry mass, leaf area index, specific leaf mass, height and longest petiole. * represents a significant effect at $p < 0.05$. NS, not significant. Let: lettuce; Cuc: cucumber; Tom: tomato.

	Dry Mass			Leaf Area			Specific Leaf Mass			Height		Petiole	
	Let	Cuc	Tom	Let	Cuc	Tom	Let	Cuc	Tom	Cuc	Tom	Cuc	Tom
%B	*	*	*	*	*	*	NS	*	*	*	*	*	*
%G	NS	NS	*	NS	NS	*	*	NS	*	*	*	*	*
PPFD	*	*	*	NS	*	NS	*	*	*	*	*	NS	*
%B*%G	*	NS	NS	*	*	NS	NS	NS	NS	NS	*	*	NS
%B*PPFD	NS	*	NS	NS	*	NS	NS	NS	*	NS	*	NS	NS
%G*PPFD	NS	NS	NS	NS	*	NS	*	NS	NS	NS	NS	NS	NS

2.4.1 Dry Mass

The higher PPFD (500 µmol m^{-2} s^{-1}) resulted in an increased dry mass in all three species (Table 2-2, Figure 2-3). Dry mass significantly decreased with increasing percent blue in all three species (Table 2-2, Figure 2-3a–c). In cucumber, percent blue interacted with intensity, indicating that the slope of the linear model was significantly different at both intensities (Table 2-2). Following this interaction, increasing the percent blue from 10 to 30% decreased cucumber dry mass by 32% at the higher PPFD, but only decreased it by 19% at the lower PPFD (Figure 2-3b).

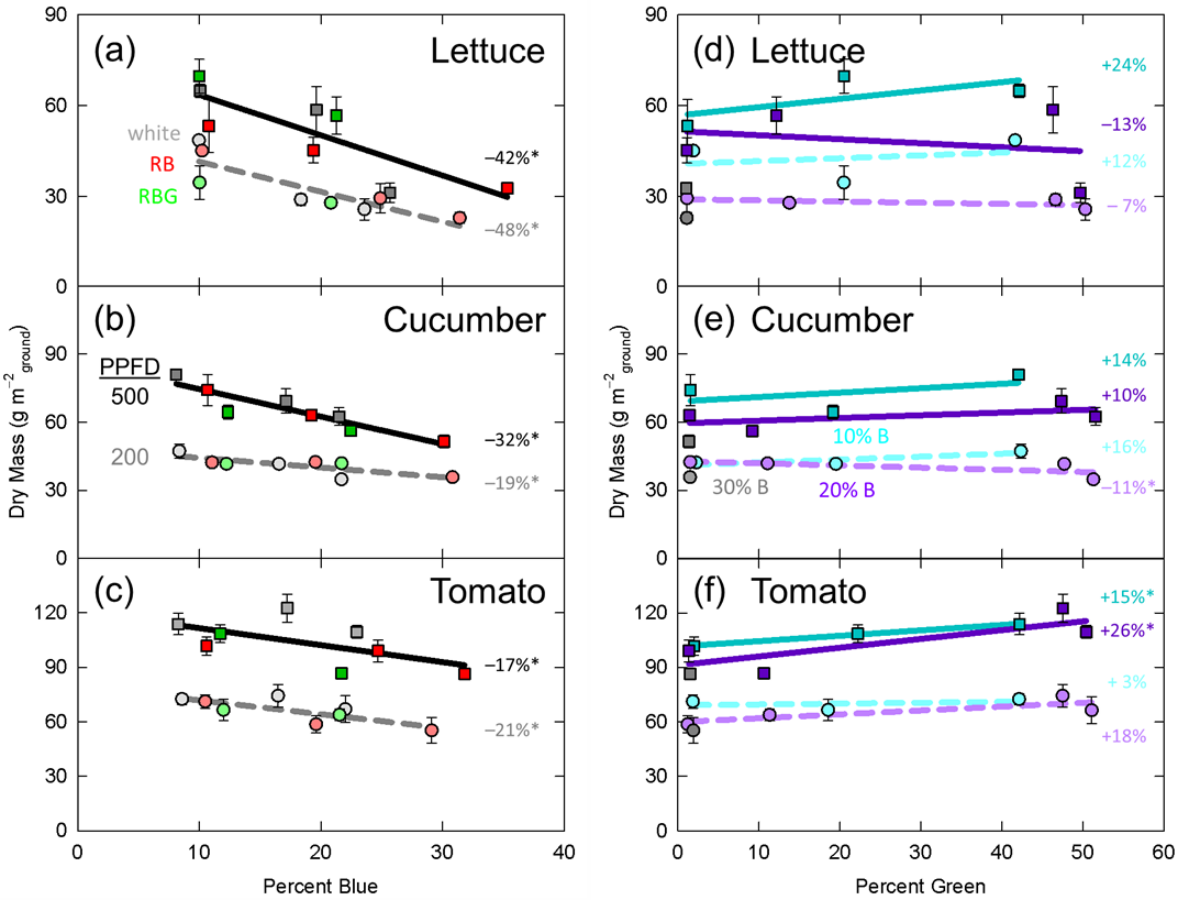

Figure 2-3. Effect of percent blue on dry mass in **(a)** lettuce, **(b)** cucumber, and **(c)** tomato; and effect of percent green on dry mass in **(d)** lettuce, **(e)** cucumber, and **(f)** tomato. In **(a-c)** squares and the solid black line represent the high intensity treatments (PPFD = 500 µmol m^{-2} s^{-1}) and circles and the dashed grey line represent the low intensity treatments (PPFD = 200 µmol m^{-2} s^{-1}). Red data points represent RB treatments, green points are RBG treatments and grey points are white LED treatments. The values in percent indicate the change from 10 to 30% blue. In **(d–f)** solid lines and squares represent the high intensity treatments while the dashed lines and circles represent the low intensity treatment. The cyan data represent treatments with about 10% blue (10% B) and the purple data represent treatments with about 20% blue (20% B). The values in percent indicate the change from zero to 50% green. * represents a significant effect of percent blue or percent green at the $p <$ 0.05 level. Error bars represent normalized standard error of n=3 replicates. RB: red/blue; RBG: red/blue/green. PPFD: photosynthetic photon flux density.

Percent green significant increased dry mass in tomato, but had no effect in lettuce or cucumber (Table 2-2, Figure 2-3d–f) and there was no interaction with PPFD for any species. There was an interaction between percent blue and percent green photons in lettuce, where dry mass trended upward with an increasing fraction of green photons with 10% blue, but trended downward at 20% blue (Figure 2-3d).

2.4.2 Leaf Area Index

Increasing the fraction of blue photons decreased LAI in all three species (Table 2-2, Figure 2-4a–c). PPFD had a significant effect on LAI in cucumber, but not lettuce or tomato. On average, LAI in cucumber was 7% higher in the high PPFD treatment compared to the low PPFD treatment, indicating that this significant effect is not biologically important. Similar to dry mass, there was a significant interaction between percent blue and PPFD in cucumber (Table 2-2). At the higher PPFD, increasing percent blue from 10 to 30% decreased LAI by 48%, but at the lower PPFD LAI was only decreased by 32% (Figure 2-4e).

Increasing the fraction of green photons increased LAI in tomato, with no significant effects in lettuce or cucumber (Table 2-2, Figure 2-4d–f). There was an interaction between percent blue and percent green in lettuce and cucumber but not tomato. This interaction can be observed in the separated data, where percent green appears to have an effect at 10% blue, but not 20%, although in lettuce this was only statistically significant at the higher intensity (Figure 2-4d,e). In cucumber, there was a significant interaction between percent green and

PPFD. The separated cucumber data show that LAI trended upward more at the higher PPFD than the lower PPFD (Figure 2-4e).

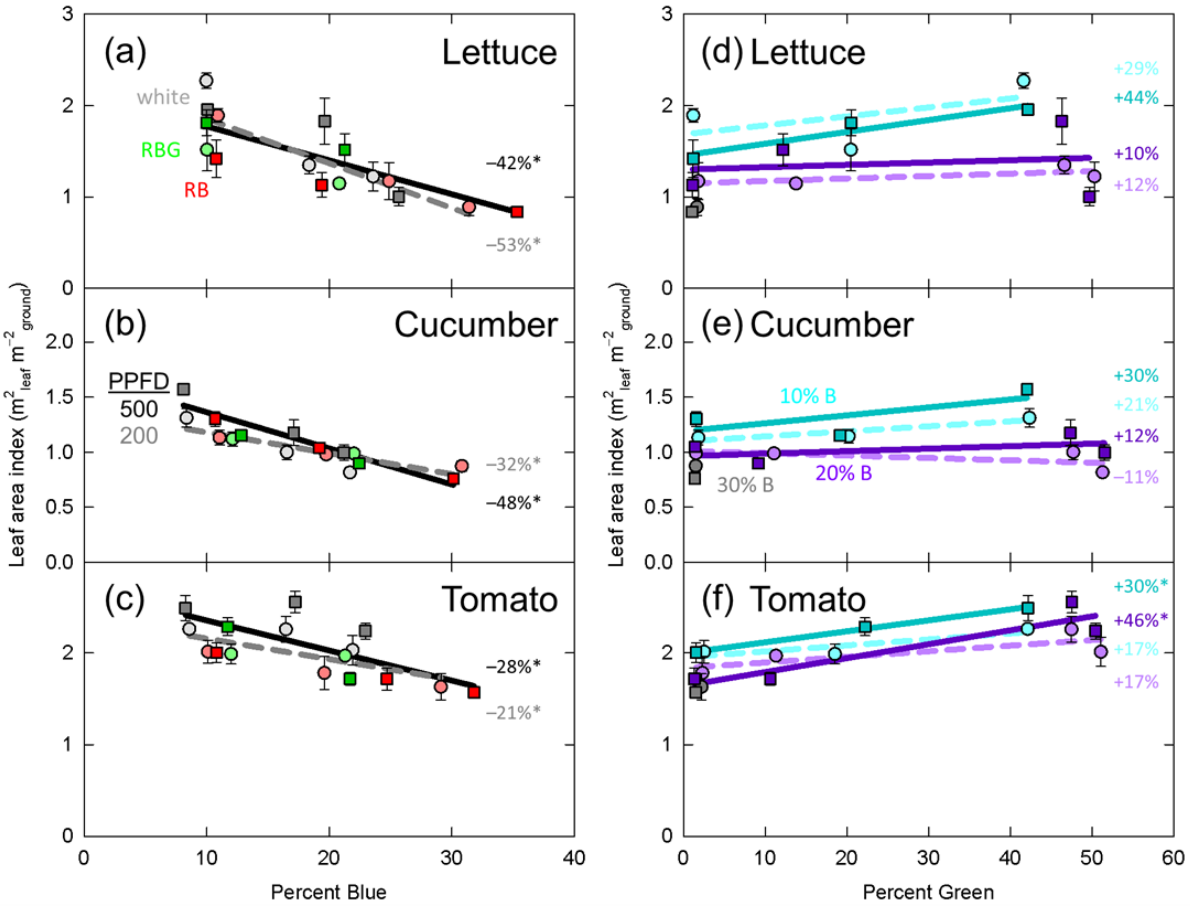

Figure 2-4. Effect of percent blue on leaf area index in **(a)** lettuce, **(b)** cucumber, and **(c)** tomato; and effect of percent green on leaf area index in **(d)** lettuce, **(e)** cucumber, and **(f)** tomato. * represents a significant effect of percent blue or percent green at the $p < 0.05$ level. See Figure 2-3 for the meaning of specific labels. Error bars represent normalized standard error of n=3 replicates.

2.4.3 Specific Leaf Mass

Specific leaf mass is an indicator of leaf thickness; as SLM increases, leaf thickness typically increases. Increasing the percent blue photons increased SLM in cucumber and tomato, but had no effect on SLM in lettuce (Table 2-2, Figure 2-5b,d). Additionally, there was a significant interaction between PPFD and percent blue in tomato (Table 2-2). When the data were separated for intensity this interaction in tomato appeared to be explained by a

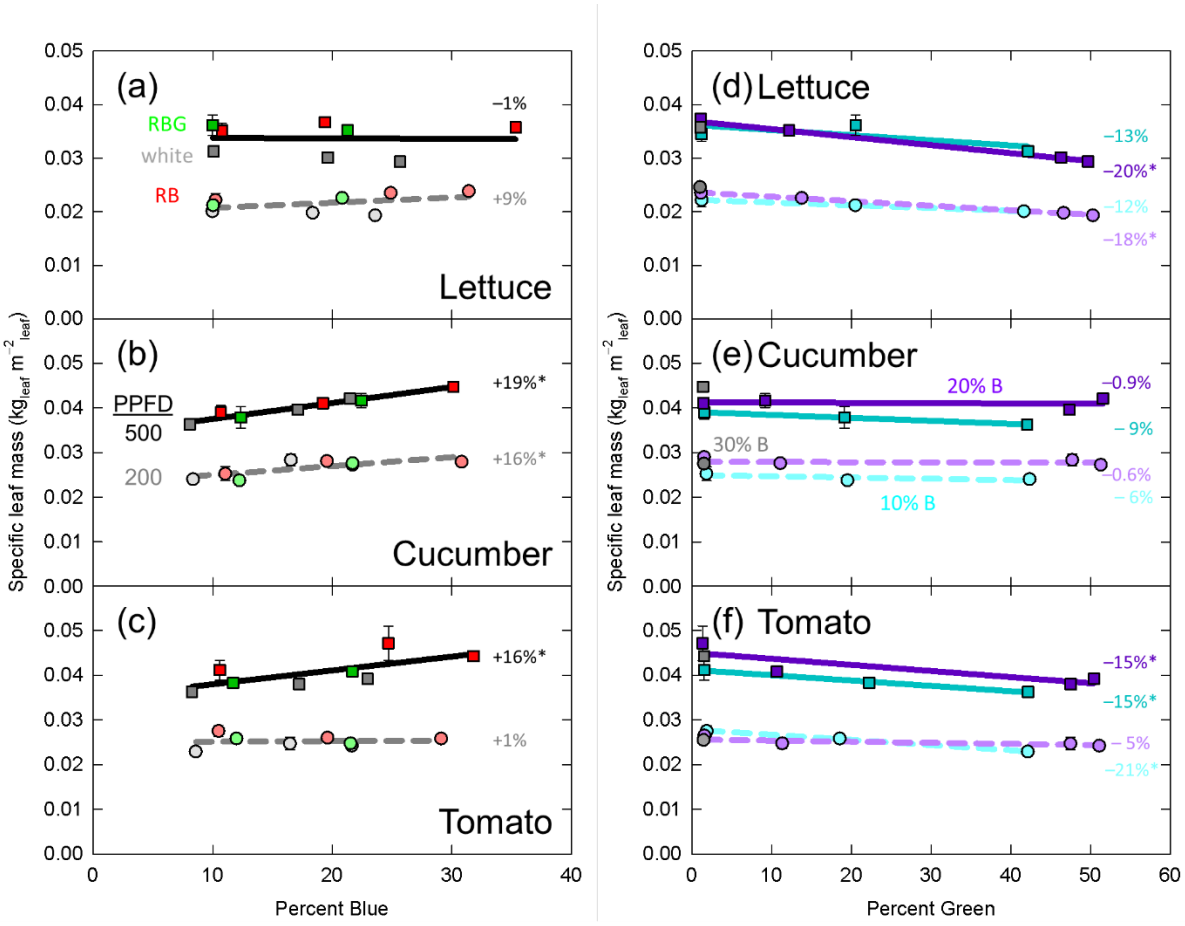

Figure 2-5. Effect of percent blue on specific leaf mass in **(a)** lettuce, **(b)** cucumber, and **(c)** tomato; and effect of percent green on specific leaf mass in **(d)** lettuce, **(e)** cucumber, and **(f)** tomato. * represents a significant effect of percent blue or percent green at the $p < 0.05$ level. See Figure 2-3 for the meaning of specific labels. Error bars represent normalized standard error of n=3 replicates.

significant effect of percent blue at the higher PPFD, but no effect at the low PPFD (Figure 2-5c). In all cases, SLM was higher at a PPFD of 500 μmol m^{-2} s^{-1} compared to a PPFD of 200 μmol m^{-2} s^{-1}.

Increasing the fraction of green photons decreased SLM in lettuce and tomato, but had no effect on cucumber (Table 2-2, Figure 2-5d,f). In lettuce, percent green interacted with PPFD to predict SLM, but this effect does not appear biologically important (Figure 2-5d).

2.4.4 Plant Height

Increasing the fraction of blue photons significantly decreased plant height in both cucumber and tomato (Table 2-2, Figure 2-6a,b). The higher PPFD resulted in reduced plant height in both species. Additionally, there was an interaction between percent blue and PPFD in tomato (Table 2-2). This interaction is apparent in Figure 2-6b, where plant height decreased by 48% at the lower PPFD, but only decreased by 30% at the higher PPFD.

Plant height significantly increased with increasing green photon fraction in both tomato and cucumber (Table 2-2, Figure 2-6c,d). These effects were more dramatic in tomato compared to cucumber, with a 50% increase in stem length as percent green increased from zero to 50% in tomato, but only about 20% increase in height in cucumber. Additionally, in tomato, there was a significant interaction between percent green and percent blue (Figure 2-6d).

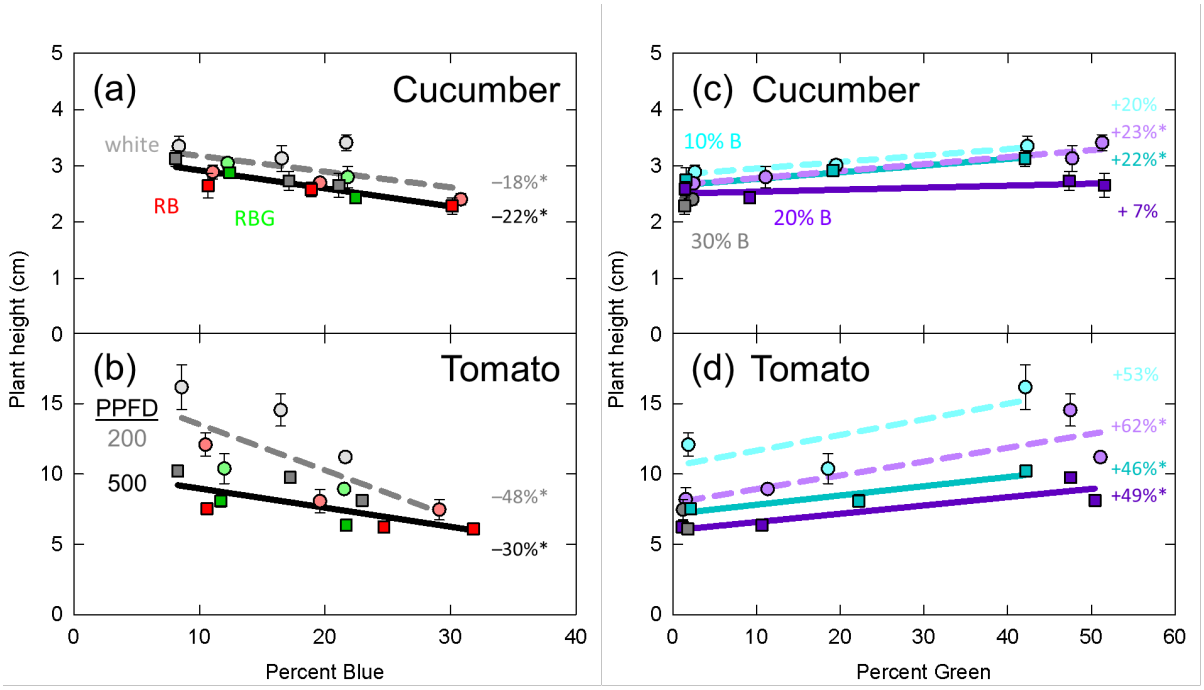

Figure 2-6. Effect of percent blue on plant height in **(a)** cucumber and **(b)** tomato; and effect of green photons on plant height in **(c)** cucumber and **(d)** tomato. * represents a significant effect of percent blue or percent green at the $p < 0.05$ level. See Figure 2-3 for the meaning of specific labels. Error bars represent normalized standard error of n=3 replicates.

2.4.5 Longest Petiole Length

The results for longest petiole length in cucumber and tomato followed a similar trend to plant height with significant decreases as percent blue increased (Table 2-2, Figure 2-7a,b). Additionally, there was a significant effect of PPFD in tomato.

Similar to plant height, increasing the fraction of green photons significantly increased the petiole length in both cucumber and tomato (Table 2-2, Figure 2-7c,d), and there was a significant interaction between blue and green fraction in cucumber. This interaction can be seen in Figure 2-7c where increasing percent green increased petiole length by 26 and 42% at 10% blue, but had no effect at 20% blue.

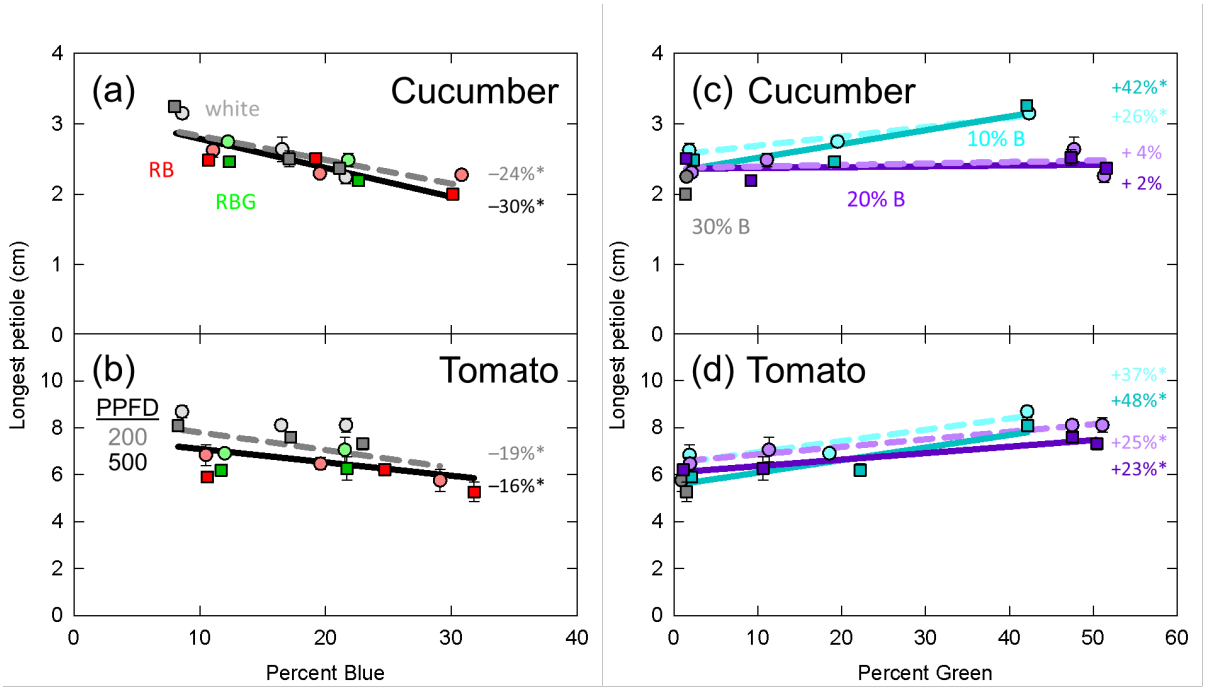

Figure 2-7. Effect of percent blue on longest petiole length in **(a)** cucumber and **(b)** tomato; and effect of percent green on longest petiole length in **(c)** cucumber and **(d)** tomato. * represents a significant effect of percent blue or percent green at the $p < 0.05$ level. See Figure 2-3 for the meaning of specific labels. Error bars represent normalized standard error of n=3 replicates.

2.5 Discussion

2.5.1 Mechanism Underlying Specific Leaf Mass

At high light intensity, leaf thickness increases due to an increase in both cell elongation and cell division along the abaxial to adaxial axis. This has led to the categorizations of sun and shade leaves [56]. It is therefore unsurprising that SLM was significantly increased at the higher intensity (PPFD = 500 µmol m^{-2} s^{-1}) compared to the lower intensity (PPFD = 200 µmol m^{-2} s^{-1}) in all three species (Table 2-2, Figure 2-5). Previous studies using *Arabidopsis thaliana* mutants deficient in the blue photoreceptors

cryptochromes [57] or phototropins [58] showed no difference in leaf thickness from the wild-type when exposed to high or low photon intensity. This led to confusion regarding the mechanism controlling this response, which had long been suspected to be tied to these photoreceptors [59]. Hoshio et al. [53] showed that the increased cell elongation along the abaxial to adaxial axis was absent in the *cry1cry2phot1phot2* quadruple mutant, indicating that all four photoreceptors work together to induce this response at a specific stage of leaf development. They also showed that this quadruple mutant growing under pure blue photons had fewer cell layers than the wild-type, possibly implicating these photoreceptors in the cell division response. They concluded that the photoreceptors only partially explained the response to high intensity, and that other unknown mechanisms remain.

Previous studies have shown that increasing the fraction of blue photons increased SLM, indicating an increase in leaf thickness [20,25,26], but other studies have showed no response [21,22,26]. In this study, increasing the fraction of blue photons increased SLM in both cucumber and tomato (Table 2-2, Figure 2-5b,c).

The chromophore in cryptochrome is FAD and the chromophore in phototropin is a flavin mononucleotide (FMN). These two chromophores (FAD and FMN) are structurally very similar, and as such they have similar absorbance properties for each of their oxidized, semi-reduced and fully reduced states [60]. For cryptochrome, $FADH^{o}$ has been implicated as the active state, and absorbance of green photons by this state can convert it into the fully reduced, inactive state [44,45,61]. Despite the similar absorbance properties of FMN compared to FAD, no inhibition of phototropin action by green photons has been described, and intermediate forms of FMN are extremely transient [62]. In a similar manner, although phototropins have been implicated in stomatal opening [63], the reversal of blue photon

induced stomatal opening by green photons does not appear to be under the control of phototropins [64]. Nonetheless, SLM appears to be modulated by both of these photoreceptors [53], and thus green photons could reverse the blue induced increase in SLM through cryptochrome.

In this study, both lettuce and tomato showed a significant decrease in SLM with an increasing fraction of green photons (Table 2-2, Figure 2-5d,f). This response is in the expected direction if green photons reverse blue-photon-induced increases in SLM.

Photoreceptors may be saturated at higher photon fluxes, meaning that spectral shifts at higher intensity may have a smaller impact on plant morphology than at lower intensities. By contrast, preferential absorption of blue photons by pigments other than the blue photon receptors may minimize plant responses to lower intensities of blue photons. The latter scenario may be the case for the interaction between percent blue and PPFD in tomato SLM, as increasing percent blue at the higher PPFD increased SLM by 16%, but appeared to have no effect at the lower PPFD (Figure 2-5c). The interaction between percent green and PPFD in predicting SLM in lettuce is more difficult to explain as the separated data do not show large differences between the intensities (Figure 2-5d).

Despite these perplexing interactions, the overall response of SLM to an increase in the fraction of blue and green photons is generally consistent with the role of cryptochromes and phototropins.

2.5.2 Leaf Expansion

Mechanisms underlying leaf area are complex due to interactions with photosynthesis. Here, we review the potential role of phototropins and cryptochromes on the control of leaf expansion under blue and green photons.

In a young seedling, blue photons contribute to early cotyledon expansion, and both cryptochromes and phototropins are involved in this response [11,12]. Mature *Arabidopsis thaliana* mutants lacking phototropins have smaller curled leaves compared to wild-type plants [65–67]. This is a puzzling considering observed decreases in leaf area as the fraction of blue photons increases (Table D.1, Table 2-2, Figure 2-4a–c). It is possible that phototropins simply increase cell expansion in all directions, and thus do not contribute to the blue photon induced decreases in leaf expansion.

Cryptochromes have been implicated in low blue shade avoidance responses like hyponasty [68], but the role of cryptochromes in leaf expansion of mature plants is less well determined. Fig. 1a in Wu and Yang [69] showed overexpressing cryptochrome visually decreased plant diameter (leaf expansion and petiole elongation), while mutants lacking cryptochrome looked stretched compared to the wild-type. Overexpression of cryptochrome in rice led to a significant reduction in the expansion of the secondary leaf blade [70]. These results provide some evidence for the role of cryptochrome in reducing leaf expansion upon blue photon perception.

Considering the potential role of cryptochrome and phototropin in SLM, it follows that increasing leaf thickness through cell elongation in the abaxial to adaxial direction may decrease leaf expansion. Dougher and Bugbee [71] found that the blue induced a decrease in soybean leaf area was partially caused by a decrease in epidermal cell area. They also

determined that the observed decrease in leaf area was influenced by a decrease in epidermal (anticlinal) cell division (as measured by dividing leaf area by cell area). Yano and Terashima [72] concluded that high intensity photon flux did not change the rate of total cell division, but increased periclinal cell division at the expense of anticlinal cell division. Hoshino et al. [53] also showed that under monochromatic blue photons, periclinal cell division was reduced in the quadruple mutant (*cry1cry2phot1phot2*). Altogether, increasing the fraction of blue photons (perceived by cryptochromes) may both increase periclinal cell division at the expense of anticlinal cell division, and increase cell expansion along the abaxial to adaxial axis at the expense of elongation along the perpendicular axis.

Although the mechanisms underlying the effect of blue photons on leaf expansion are not clear, cryptochromes appear to modulate the response. It is difficult to determine the role of phototropins in leaf expansion. Further research is warranted.

2.5.3 Potential Contribution of Photosynthesis to Dry Mass Accumulation

The decreases in dry mass as the fraction of blue photons increased were likely caused in part by the lower quantum yield of blue photons compared to green and red photons. McCree [73] showed that in lettuce (cv. Great Lakes and Big Boston), cucumber (cv. Ohio MR-17) and tomato (cv. Floradel) blue photons had a 24, 33 and 30% lower quantum yield than red photons. Green photons had a 16% lower quantum yield than red photons in all three species. As the blue percentage increased from 10 to 30%, dry mass decreased by 42 and 48% in lettuce, 32 and 19% in cucumber, and 17 and 21% in tomato

(Figure 2-3a–c). Although decreased photosynthesis likely contributed to these decreases in dry mass, the effects were also likely caused by reduction in photon capture (decreased LAI).

2.5.4. Comparison to Previous Studies in Horticultural Species

Increasing the fraction of blue photons decreased LAI in all three species, while increasing the fraction of green photons only increased LAI in tomato (Table 2-2, Figure 2-4f). As dry mass is highly correlated with leaf area [74], the decreases in LAI likely contributed to the decreases in dry mass. In lettuce, increasing the fraction of blue photons has often been shown to decrease leaf area and dry mass [8,15,16,20–22,24,35], although some studies show no response [26,28,37–42] (also see Table D.1). Our data showed that increasing the blue photon fraction decreased leaf area and dry mass in lettuce. In cucumber, data from previous publications have generally shown a decrease in leaf area and dry mass [25,26,28], and our data confirm these findings. In tomato, the literature has largely shown no response to increasing the fraction of blue [26,31–33], but our data show a significant decrease in LAI and dry mass. The interaction between percent blue and PPFD for both dry mass and LAI in cucumber resulted in a greater response at the higher intensity, suggesting that blue photons were preferentially absorbed by other pigments at the lower intensity.

Despite the early findings of Kim et al. [5], who showed beneficial effects of adding green photons to the growth spectrum, subsequent studies have rarely shown beneficial effects [8,16,23,25–29,33,36,38,40] (also see Table D.2). Likewise, we found no beneficial effect (increase in dry mass) of adding green photons to lettuce or cucumber, but we did see a beneficial effect for both leaf area and dry mass in tomato (Table 2-2, Figure 2-3d–f, Figure

2-4d–f). Based on our definition of shade tolerance as an increase in leaf area under shade-light, tomato appeared to exhibit shade tolerance in response to green photons, but lettuce and cucumber did not.

Green photons have been shown to induce shade avoidance responses in *Arabidopsis thaliana*, but the shade avoidance responses of stem and petiole elongation in horticultural species are often absent [25–27,29,33]. By contrast, increasing the fraction of blue photons is regularly observed to decreases stem and petiole length in cucumber and tomato [25,26,28,33]. In this study, despite previous findings, we showed that green photons induced shade avoidance responses in the horticultural species cucumber and tomato (Table 2-2, Figure 2-6c,d, Figure 2-7c,d). We also observed the common response of decreased stem and petiole lengths with increasing blue photon fraction. Unlike the interactions discussed previously, the interaction between percent blue and PPFD in predicting tomato plant height may be explained by saturating photoreceptors at higher intensities.

2.5.5 Interaction between Percent Blue and Percent Green

The interactions between blue photons and green photons in predicting leaf area of lettuce and cucumber, and petiole length in cucumber can be explained by the sensitivity of cryptochrome to blue and green photons. Bouly et al. [44] measured cry2 activation and de-activation by its rate of breakdown (cry2 breaks down in its active form). Compared to applying blue photons alone, green photons provided at three times the rate of blue photons, resulted in minimal differences in the concentration of cry2, but when green photons were applied at ten times the rate, there was a significant increase in the concentration of cry2.

This indicates that green photons de-activated cry2 (as measured by a decrease in its degradation) only when applied at ten times, and not three times, the rate of blue photons. More recent studies have estimated the photoconversion coefficients (photoconversion weighting factors) for FAD state changes in vivo are 480 m^2 mol^{-1} for the activation of cry2 by 450 nm blue photons and 30 m^2 mol^{-1} for de-activation by 560 nm green photons [61]. Photoconversion coefficients are probability functions that estimate the likelihood of photon absorbance by a pigment and subsequent conversion to another form; they are regularly used in phytochrome research (e.g., [75]). The results of Procopio et al. [61] indicate that blue photons have a 16-fold greater ability to change the state of cryptochrome compared to green photons. Therefore, increasing the flux of green at a higher fraction of blue would be expected to have a reduced response compared to a lower fraction of blue. Although this is complicated by the fact that the cryptochrome photocycle involves three states rather than two, and the more reduced states are only converted back to the oxidized state via dark reversion. A better understanding of this photocycle may provide better models for the action of blue and green photons in future studies. Nonetheless, green photons were more potent at increasing leaf expansion in lettuce and cucumber (Figure 2-4d,e), and the petiole length in cucumber (Figure 2-7c) at a lower fraction of blue. The response in tomato plant height is more difficult to explain (Figure 2-6d).

2.6 Conclusions

Green photons only benefitted tomatoes. These data are contrary to the early findings of Kim et al. [5], who found that increased green fraction from fluorescent lamps increased

the growth of lettuce compared to LEDs without green. Higher fractions of green photons in horticultural LED fixtures may benefit tomato production, but not lettuce or cucumber production (although responses are likely cultivar dependent). White LEDs, which provide a high fraction of green photons, are the most cost-effective type of LED due to their use in general lighting [76]. Thus, their use in horticultural LED fixtures will likely continue for economic reasons.

We define shade tolerance as an increase in leaf area in response to shade-like light (assuming only photon quality and not photon quantity has been adjusted), and shade avoidance as an increase in stem elongation. Based on these definitions, tomatoes expressed both shade avoidance and shade tolerance in response to an increased fraction of green photons, while cucumber only exhibited shade avoidance.

Blue photons typically decrease leaf area and dry mass. It therefore seems advantageous to include a low fraction of blue photons in a fixture. From our data, the lowest percentage of blue (10%) produced the highest dry mass. We are now studying the minimal amount of blue needed for normal plant growth.

2.7 Literature Cited

1. Demotes-Mainard, S.; Péron, T.; Corot, A.; Bertheloot, J.; Le Gourrierec, J.; Pelleschi-Travier, S.; Crespel, L.; Morel, P.; Huche-Thelier, L.; Boumaza, R.; et al. Plant responses to red and far-red lights, applications in horticulture. *Environ. Exp. Bot.* **2016**, *121*, 4–21, doi:10.1016/j.envexpbot.2015.05.010.
2. Kusuma, P.; Bugbee, B. Far-red rraction: An improved metric for characterizing phytochrome effects on morphology. *J. Am. Soc. Hort. Sci.* **2021**, *146*, 3–13, doi:10.21273/JASHS05002-20.
3. Gommers, C.M.; Visser, E.J.; St Onge, K.R.; Voesenek, L.A.; Pierik, R. Shade tolerance: When growing tall is not an option. *Trends Plant. Sci.* **2013**, *18*, 65–71, doi:10.1016/j.tplants.2012.09.008.

4. Zhen, S.; Bugbee, B. Substituting far-red for traditionally defined photosynthetic photons results in equal canopy quantum yield for CO_2 fixation and increased photon capture during long-term studies: Implications for re-defining PAR. *Front. Plant Sci.* **2020**, *11*, 1433, doi:10.3389/fpls.2020.581156.
5. Kim, H.H.; Goins, G.D.; Wheeler, R.M.; Sager, J.C. Green-light supplementation for enhanced lettuce growth under red-and blue-light-emitting diodes. *HortScience* **2004**, *39*, 1617–1622, doi:10.21273/HORTSCI.39.7.1617.
6. Smith, H.L.; McAusland, L.; Murchie, E.H. Don't ignore the green light: Exploring diverse roles in plant processes. *J. Exp. Bot.* **2017**, *68*, 2099–2110, doi:10.1093/jxb/erx098.
7. Battle, M.W.; Vegliani, F.; Jones, M.A. Shades of green: Untying the knots of green photoperception. *J. Exp. Bot.* **2020**, *71*, 5764–5770, doi:10.1093/jxb/eraa312.
8. Meng, Q.; Boldt, J.; Runkle, E.S. Blue radiation interacts with green radiation to influence growth and predominantly controls quality attributes of lettuce. *J. Am. Soc. Hortic. Sci.* **2020**, *145*, 75–87, doi:10.21273/JASHS04759-19.
9. Lin, C. Plant blue-light receptors. *Trends Plant Sci.* **2000**, *5*, 337–342, doi:10.1016/S1360-1385(00)01687-3.
10. Galvão, V.C.; Fankhauser, C. Sensing the light environment in plants: Photoreceptors and early signaling steps. *Curr. Opin. Neurobiol*. **2015**, *34*, 46–53, doi:10.1016/j.conb.2015.01.013.
11. Lin, C.; Yang, H.; Guo, H.; Mockler, T.; Chen, J.; Cashmore, A.R. Enhancement of blue-light sensitivity of Arabidopsis seedlings by a blue light receptor cryptochrome 2. *Proc. Natl. Acad. Sci. USA* **1998**, *95*, 2686–2690, doi:10.1073/pnas.95.5.2686.
12. Ohgishi, M.; Saji, K.; Okada, K.; Sakai, T. Functional analysis of each blue light receptor, cry1, cry2, phot1, and phot2, by using combinatorial multiple mutants in Arabidopsis. *Proc. Natl. Acad. Sci. USA* **2004**, *101*, 2223–2228, doi:10.1073/pnas.0305984101.
13. Platten, J.D.; Foo, E.; Elliott, R.C.; Hecht, V.; Reid, J.B.; Weller, J.L. Cryptochrome 1 contributes to blue-light sensing in pea. *Plant. Physiol*. **2005**, *139*, 1472–1482, doi:10.1104/pp.105.067462.
14. Folta, K.M.; Spalding, E.P. Unexpected roles for cryptochrome 2 and phototropin revealed by high-resolution analysis of blue light-mediated hypocotyl growth inhibition. *Plant. J.* **2001**, *26*, 471–478, doi:10.1046/j.1365-313x.2001.01038.x.
15. Ohashi-Kaneko, K.; Takase, M.; Kon, N.; Fujiwara, K.; Kurata, K. Effect of light quality on growth and vegetable quality in leaf lettuce, spinach and komatsuna. *Environ. Control Biol.* **2007**, *45*, 189–198, doi:10.2525/ecb.45.189.
16. Son, K.H.; Oh, M.M. Leaf shape, growth, and antioxidant phenolic compounds of two lettuce cultivars grown under various combinations of blue and red light-emitting diodes. *HortScience* **2013**, *48*, 988–995, doi:10.21273/HORTSCI.48.8.988.
17. Cope, K.R.; Snowden, M.C.; Bugbee, B. Photobiological interactions of blue light and photosynthetic photon flux: Effects of monochromatic and broad-spectrum light sources. *Photochem. Photobiol.* **2014**, *90*, 574–584, doi:10.1111/php.12233.
18. Furuyama, S.; Ishigami, Y.; Hikosaka, S.; Goto, E. Effects of blue/red ratio and light intensity on photomorphogenesis and photosynthesis of red leaf lettuce. *Acta Hortic.* **2013**, *1037*, 317–322, doi:10.17660/ActaHortic.2014.1037.38.
19. Lee, J.S.; Lim, T.G.; Yong, H.K. Growth and phytochemicals in lettuce as affected by different ratios of blue to red LED radiation. *Acta Hortic.* **2014**, *1037*, 843–848, doi:10.17660/ActaHortic.2014.1037.112.

20. Son, K.H.; Oh, M.M. Growth, photosynthetic and antioxidant parameters of two lettuce cultivars as affected by red, green, and blue light-emitting diodes. *Hortic. Environ. Biotechnol*. **2015**, *56*, 639–653, doi:10.1007/s13580-015-1064-3.
21. Wang, J.; Lu, W.; Tong, Y.; Yang, Q. Leaf morphology, photosynthetic performance, chlorophyll fluorescence, stomatal development of lettuce (*Lactuca sativa* L.) exposed to different ratios of red light to blue light. *Front. Plant Sci.* **2016**, *7*, 250, doi:10.3389/fpls.2016.00250.
22. Son, K.H.; Jeon, Y.M.; Oh, M.M. Application of supplementary white and pulsed light-emitting diodes to lettuce grown in a plant factory with artificial lighting. *Hortic. Environ. Biotechnol.* **2016**, *57*, 560–572, doi:10.1007/s13580-016-0068-y.
23. Kang, W.H.; Park, J.S.; Park, K.S.; Son, J.E. Leaf photosynthetic rate, growth, and morphology of lettuce under different fractions of red, blue, and green light from light-emitting diodes (LEDs). *Hortic. Environ. Biotechnol*. **2016**, *57*, 573–579, doi:10.1007/s13580-016-0093-x.
24. Meng, Q.; Kelly, N.; Runkle, E.S. Substituting green or far-red radiation for blue radiation induces shade avoidance and promotes growth in lettuce and kale. *Environ. Exp. Bot.* **2019**, *162*, 383–391, doi:10.1016/j.envexpbot.2019.03.016.
25. Hernández, R.; Kubota, C. Physiological responses of cucumber seedlings under different blue and red photon flux ratios using LEDs. *Environ. Exp. Bot.* **2016**, *121*, 66–74, doi:10.1016/j.envexpbot.2015.04.001.
26. Snowden, M.C.; Cope, K.R.; Bugbee, B. Sensitivity of seven diverse species to blue and green light: Interactions with photon flux. *PLoS ONE* **2016**, *11*, e0163121, doi:10.1371/journal.pone.0163121.
27. Song, J.; Meng, Q.; Du, W.; He, D. Effects of light quality on growth and development of cucumber seedlings in controlled environment. *Int. J. Agric. Biol. Eng.* **2017**, *10*, 312–318, doi:10.3965/j.ijabe.20171003.2299.
28. Zou, J.; Zhou, C.B.; Xu, H.; Cheng, R.F.; Yang, Q.C.; Li, T. The effect of artificial solar spectrum on growth of cucumber and lettuce under controlled environment. *J. Integr. Agric.* **2020**, *19*, 2027–2034, doi:10.1016/S2095-3119(20)63209-9.
29. Wollaeger, H.M.; Runkle, E.S. Growth of impatiens, petunia, salvia, and tomato seedlings under blue, green, and red light-emitting diodes. *HortScience* **2014**, *49*, 734–740, doi:10.21273/HORTSCI.49.6.734.
30. Dougher, T.A.; Bugbee, B. Differences in the response of wheat, soybean and lettuce to reduced blue radiation. *Photochem. Photobiol*. **2001**, *73*, 199–207, doi:10.1562/0031-8655(2001)0730199DITROW2.0.CO2.
31. Hernández, R.; Kubota, C. Tomato seedling growth and morphological responses to supplemental LED lighting red: Blue ratios under varied daily solar light integrals. *Acta Hortic.* **2012**, *956*, 187–194, doi:10.17660/ActaHortic.2012.956.19.
32. Wollaeger, H.M.; Runkle, E.S. Growth and acclimation of impatiens, salvia, petunia, and tomato seedlings to blue and red light. *HortScience* **2015**, *50*, 522–529, doi:10.21273/HORTSCI.50.4.522.
33. Hernández, R.; Eguchi, T.; Deveci, M.; Kubota, C. Tomato seedling physiological responses under different percentages of blue and red photon flux ratios using LEDs and cool white fluorescent lamps. *Sci. Hortic.* **2016**, *213*, 270–280, doi:10.1016/j.scienta.2016.11.005.
34. Liu, X.Y.; Jiao, X.L.; Chang, T.T.; Guo, S.R.; Xu, Z.G. Photosynthesis and leaf development of cherry tomato seedlings under different LED-based blue and red photon flux ratios. *Photosynthetica* **2018**, *56*, 1212–1217, doi:10.1007/s11099-018-0814-8.

35. Meng, Q.; Runkle, E.S. Far-red radiation interacts with relative and absolute blue and red photon flux densities to regulate growth, morphology, and pigmentation of lettuce and basil seedlings. *Sci. Hortic.* **2019**, *255*, 269–280, doi:10.1016/j.scienta.2019.05.030.
36. Yan, Z.; He, D.; Niu, G.; Zhou, Q.; Qu, Y. Growth, nutritional quality, and energy use efficiency of hydroponic lettuce as influenced by daily light integrals exposed to white versus white plus red light-emitting diodes. *HortScience* **2019**, *54*, 1737–1744, doi:10.21273/HORTSCI14236-19.
37. Yorio, N.C.; Goins, G.D.; Kagie, H.R.; Wheeler, R.M.; Sager, J.C. Improving spinach, radish, and lettuce growth under red light-emitting diodes (LEDs) with blue light supplementation. *HortScience* **2001**, *36*, 380–383, doi:10.21273/HORTSCI.36.2.380.
38. Li, Q.; Kubota, C. Effects of supplemental light quality on growth and phytochemicals of baby leaf lettuce. *Environ. Exp. Bot.* **2009**, *67*, 59–64, doi:10.1016/j.envexpbot.2009.06.011.
39. Kong, S.W.; Chung, H.Y.; Chang, M.Y.; Fang, W. The contribution of different spectral sections to increase fresh weight of boston lettuce. *HortScience* **2015**, *50*, 1006–1010, doi:10.21273/HORTSCI.50.7.1006.
40. Chen, X.L.; Xue, X.Z.; Guo, W.Z.; Wang, L.C.; Qiao, X.J. Growth and nutritional properties of lettuce affected by mixed irradiation of white and supplemental light provided by light-emitting diode. *Sci. Hortic.* **2016**, *200*, 111–118, doi:10.1016/j.scienta.2016.01.007.
41. Yan, Z.; He, D.; Niu, G.; Zhai, H. Evaluation of growth and quality of hydroponic lettuce at harvest as affected by the light intensity, photoperiod and light quality at seedling stage. *Sci. Hortic*. **2019**, *248*, 138–144, doi:10.1016/j.scienta.2019.01.002.
42. Spalholz, H.; Perkins-Veazie, P.; Hernández, R. Impact of sun-simulated white light and varied blue: Red spectrums on the growth, morphology, development, and phytochemical content of green-and red-leaf lettuce at different growth stages. *Sci. Hortic.* **2020**, *264*, 109195, doi:10.1016/j.scienta.2020.109195.
43. Kong, Y.; Schiestel, K.; Zheng, Y. Maximum elongation growth promoted as a shade-avoidance response by blue light is related to deactivated phytochrome: A comparison with red light in four microgreen species. *Canad. J. Plant Sci.* **2019**, *100*, 314–326, doi:10.1139/cjps-2019-0082.
44. Bouly, J.P.; Schleicher, E.; Dionisio-Sese, M.; Vandenbussche, F.; Van Der Straeten, D.; Bakrim, N.; Meier, S.; Batschauer, A.; Galland, P.; Bittl, R.; et al. Cryptochrome blue light photoreceptors are activated through interconversion of flavin redox states. *J. Biol. Chem.* **2007**, *282*, 9383–9391, doi:10.1074/jbc.M609842200.
45. Banerjee, R.; Schleicher, E.; Meier, S.; Viana, R.M.; Pokorny, R.; Ahmad, M.; Bittl, R.; Batschauer, A. The signaling state of Arabidopsis cryptochrome 2 contains flavin semiquinone. *J. Biol. Chem.* **2007**, *282*, 14916–14922, doi:10.1074/jbc.M700616200.
46. Müller, P.; Bouly, J.P.; Hitomi, K.; Balland, V.; Getzoff, E.D.; Ritz, T.; Brettel, K. ATP binding turns plant cryptochrome into an efficient natural photoswitch. *Sci. Rep.* **2014**, *4*, 1–11, doi:10.1038/srep05175.
47. Kao, Y.T.; Saxena, C.; He, T.F.; Guo, L.; Wang, L.; Sancar, A.; Zhong, D. Ultrafast dynamics of flavins in five redox states. *J. Am. Chem. Soc.* **2008**, *130*, 13132–13139, doi:10.1021/ja8045469.
48. Liu, B.; Liu, H.; Zhong, D.; Lin, C. Searching for a photocycle of the cryptochrome photoreceptors. *Curr. Opin. Plant Biol.* **2010**, *13*, 578–586, doi:10.1016/j.pbi.2010.09.005.

49. Ahmad, M. Photocycle and signaling mechanisms of plant cryptochromes. *Curr. Opin. Plant Biol.* **2016**, *33*, 108–115, doi:10.1016/j.pbi.2016.06.013.
50. Zhang, T.; Maruhnich, S.A.; Folta, K.M. Green light induces shade avoidance symptoms. *Plant Physiol.* **2011**, *157*, 1528–1536, doi:10.1104/pp.111.180661.
51. Wang, Y.; Zhang, T.; Folta, K.M. Green light augments far-red-light-induced shade response. *Plant Growth Regul.* **2015**, *77*, 147–155, doi:10.1007/s10725-015-0046-x.
52. Li, L.; Tong, Y.X.; Lu, J.L.; Li, Y.M.; Yang, Q.C. Lettuce growth, nutritional quality, and energy use efficiency as affected by red–blue light combined with different monochromatic wavelengths. *HortScience* **2020**, *55*, 613–620, doi:10.21273/HORTSCI14671-19.
53. Hoshino, R.; Yoshida, Y.; Tsukaya, H. Multiple steps of leaf thickening during sun-leaf formation in Arabidopsis. *Plant J.* **2019**, *100*, 738–753, doi:10.1111/tpj.14467.
54. Wheeler, R.M.; Mackowiak, C.L.; Sager, J.C. Soybean stem growth under high-pressure sodium with supplemental blue lighting. *Agron. J.* **1991**, *83*, 903–906, doi:10.2134/agronj1991.00021962008300050024x.
55. Cope, K.R.; Bugbee, B. Spectral effects of three types of white light-emitting diodes on plant growth and development: Absolute versus relative amounts of blue light. *HortScience* **2013**, *48*, 504–509, doi:10.21273/HORTSCI.48.4.504.
56. Kim, G.T.; Yano, S.; Kozuka, T.; Tsukaya, H. Photomorphogenesis of leaves: Shade-avoidance and differentiation of sun and shade leaves. *Photochem. Photobiol. Sci.* **2005**, *4*, 770–774, doi:10.1039/B418440H.
57. Weston, E.; Thorogood, K.; Vinti, G.; López-Juez, E. Light quantity controls leaf-cell and chloroplast development in Arabidopsis thaliana wild type and blue-light-perception mutants. *Planta* **2000**, *211*, 807–815, doi:10.1007/s004250000392.
58. López-Juez, E.; Bowyer, J.R.; Sakai, T. Distinct leaf developmental and gene expression responses to light quantity depend on blue-photoreceptor or plastid-derived signals, and can occur in the absence of phototropins. *Planta* **2007**, *227*, 113–123, doi:10.1007/s00425-007-0599-7.
59. Smith, H. Light quality, photoperception, and plant strategy. *Ann. Rev. Plant Physiol.* **1982**, *33*, 481–518, doi:10.1146/annurev.pp.33.060182.002405.
60. Oprian, D.D.; Coon, M.J. Oxidation-reduction states of FMN and FAD in NADPH-cytochrome P-450 reductase during reduction by NADPH. *J. Biol. Chem.* **1982**, *257*, 8935–8944, doi:10.1016/S0021-9258(18)34223-6.
61. Procopio, M.; Link, J.; Engle, D.; Witczak, J.; Ritz, T.; Ahmad, M. Kinetic modeling of the Arabidopsis cryptochrome photocycle: FADH accumulation correlates with biological activity. *Front. Plant Sci.* **2016**, *7*, 888, doi:10.3389/fpls.2016.00888.
62. Folta, K.M.; Maruhnich, S.A. Green light: A signal to slow down or stop. *J. Exp. Bot.* **2007**, *58*, 3099–3111, doi:10.1093/jxb/erm130.
63. Christie, J.M. Phototropin blue-light receptors. *Annu. Rev. Plant Biol.* **2007**, *58*, 21–45, doi:10.1146/annurev.arplant.58.032806.103951.
64. Talbott, L.D.; Hammad, J.W.; Harn, L.C.; Nguyen, V.H.; Patel, J.; Zeiger, E. Reversal by green light of blue light-stimulated stomatal opening in intact, attached leaves of Arabidopsis operates only in the potassium-dependent, morning phase of movement. *Plant Cell Physiol.* **2006**, *47*, 332–339, doi:10.1093/pcp/pci249.
65. Sakamoto, K.; Briggs, W.R. Cellular and subcellular localization of phototropin 1. *Plant Cell* **2002**, *14*, 1723–1735, doi:10.1105/tpc.003293.

66. Takemiya, A.; Inoue, S.I.; Doi, M.; Kinoshita, T.; Shimazaki, K.I. Phototropins promote plant growth in response to blue light in low light environments. *Plant Cell* **2005**, *17*, 1120–1127, doi:10.1105/tpc.104.030049.
67. Kong, Y.; Zheng, Y. Phototropin is partly involved in blue-light-mediated stem elongation, flower initiation, and leaf expansion: A comparison of phenotypic responses between wild Arabidopsis and its phototropin mutants. *Environ. Exp. Bot.* **2020**, *171*, 103967, doi:10.1016/j.envexpbot.2019.103967.
68. Keller, M.M.; Jaillais, Y.; Pedmale, U.V.; Moreno, J.E.; Chory, J.; Ballaré, C.L. Cryptochrome 1 and phytochrome B control shade-avoidance responses in Arabidopsis via partially independent hormonal cascades. *Plant J.* **2011**, *67*, 195–207, doi:10.1111/j.1365-313X.2011.04598.x.
69. Wu, L.; Yang, H.Q. CRYPTOCHROME 1 is implicated in promoting R protein-mediated plant resistance to *Pseudomonas syringae* in Arabidopsis. *Mol. Plant* **2010**, *3*, 539–548, doi:10.1093/mp/ssp107.
70. Zhang, Y.C.; Gong, S.F.; Li, Q.H.; Sang, Y.; Yang, H.Q. Functional and signaling mechanism analysis of rice CRYPTOCHROME 1. *Plant J.* **2006**, *46*, 971–983, doi:10.1111/j.1365-313X.2006.02753.x.
71. Dougher, T.A.; Bugbee, B. Long-term blue light effects on the histology of lettuce and soybean leaves and stems. *J. Am. Soc. Hortic. Sci.* **2004**, *129*, 467–472, doi:10.21273/JASHS.129.4.0467.
72. Yano, S.; Terashima, I. Developmental process of sun and shade leaves in *Chenopodium album* L. *Plant Cell Environ.* **2004**, *27*, 781–793, doi:10.1111/j.1365-3040.2004.01182.x.
73. McCree, K.J. The action spectrum, absorptance and quantum yield of photosynthesis in crop plants. *Agric. Meteorol.* **1971**, *9*, 191–216, doi:10.1016/0002-1571(71)90022-7.
74. Klassen, S.P.; Ritchie, G.; Frantz, J.M.; Pinnock, D.; Bugbee, B. Real-time imaging of ground cover: Relationships with radiation capture, canopy photosynthesis, and daily growth rate. In *Digital Imaging and Spectral Techniques: Applications to Precision Agriculture and Crop Physiology*; American Society of Agronomy, Inc., WI, USA, 2004; Volume 66, pp. 1–14, doi:10.2134/asaspecpub66.c1.
75. Sager, J.C.; Smith, W.O.; Edwards, J.L.; Cyr, K.L. Photosynthetic efficiency and phytochrome photoequilibria determination using spectral data. *Trans. Am. Soc. Agric. Eng.* **1988**, *31*, 1882–1889, doi:10.13031/2013.30952.
76. Kusuma, P.; Pattison, P.M.; Bugbee, B. From physics to fixtures to food: Current and potential LED efficacy. *Hortic. Res.* **2020**, *7*, 1–9, doi:10.1038/s41438-020-0283-7.

CHAPTER 3

FAR-RED FRACTION: AN IMPROVED METRIC FOR CHARACTERIZING PHYTOCHROME EFFECTS ON MORPHOLOGY[B]

3.1 Abstract

Phytochrome, a well-studied photoreceptor in plants, primarily absorbs in the red (R) and far-red (FR) regions and is responsible for the perception of shade (from neighboring or overhanging plants) and subsequent morphological responses. Experiments performed in controlled environments have widely used the red to far-red ratio (R:FR ratio) to simulate the natural environment and used phytochrome photoequilibrium (PPE) to simulate the activity of phytochrome. We review why PPE may be an unreliable metric including differences in weighting factors, multiple phytochromes, non-photochemical reversions, intermediates, variations in the total pool of phytochrome, and screening by other pigments. We suggest that environmental signals based on red and far-red photon fluxes are a better predictor of plant shape than the more complex PPE model. However, the R:FR ratio is non-intuitive and can approach infinity under electric lights, which make it difficult to extrapolate from studies in controlled environments to the field. Here we describe an improved metric: the FR fraction [FR/(R+FR)] with a range from 0 to 1. This is a more intuitive metric both under electric lights and in the field compared to other ratios because it is positively correlated with

[B] Kusuma, P., and B. Bugbee. Published in the Journal of the American Society for Horticultural Science.

phytochrome-mediated morphological responses. We demonstrate the reliability of this new metric by reanalyzing previously published data.

3.2 Introduction

Many photobiological studies are conducted under electric lights to better understand basic plant responses. In this review we discuss the history, derivation and limitations of two of the common metrics that are used to interpret photobiological responses: phytochrome photoequilibrium (PPE) and the red (R) to far-red (FR) ratio (R:FR ratio, R/FR). Issues with these metrics are exacerbated under light-emitting diodes (LEDs), which are important to photobiology because of their narrow bandwidth. Furthermore, the high efficiency output of LEDs has made them a prominent addition to controlled environment agriculture (Kusuma et al., 2020). In these plant factories, plant morphology can be manipulated by the specific choice of LEDs, but first it is vital to develop proper metrics to predict responses.

In this review we describe an improved metric called the FR fraction [FR/(R+FR)], which ranges from 0 to 1. This is a more intuitive metric both under electric and natural conditions compared to other ratios because it is positively correlated with phytochrome-mediated morphological responses like stem elongation. We demonstrate the reliability of this new metric by reanalyzing previously published data.

3.3 Early Phytochrome Research

Seventy years ago, the discovery of phytochrome by Borthwick et al. (1952) and initial extraction by Butler et al. (1959) led to a photobiological focus on the R and FR

regions of the electromagnetic spectrum. Early studies were more focused on *how* phytochrome-mediated responses occurred like wavelength sensitivity, signaling partners and time dependencies; but there was little focus on understanding *why* these responses happened (evolutionary and ecological perspectives). Researchers eventually began considering the ecological implications realizing,

> "*Beneath the forest canopy the intensity of radiation is decreased but the region of 730 nm is enhanced relative to 660 nm because of the filtering action of chlorophyll* (Hendricks and Borthwick, 1963)."

This led to studies in the natural environment (Kasperbauer, 1971; Taylorson and Borthwick, 1969) as opposed to laboratory settings with electric lighting experiments including pulses, flip-flops (following red pulses with far-red pulses to reverse the response) and monochromatic light. The focus remained on R and FR because the two forms of phytochrome, P_r and P_{fr}, had absorbance peaks in these regions (Butler et al., 1964), and the R:FR ratio became well established as an indicator of the degree of shade (Cumming, 1963; Holmes and Smith, 1975, 1977a, 1977b).

Phytochrome responses, especially stem-extension rate and stem length, are often shown to be log-linearly or linearly correlated with the ratio of active phytochrome (P_{fr}) to total phytochrome (P_{total}), where $P_{total} = P_r + P_{fr}$ (Kalaitzoglou et al., 2019; Morgan and Smith, 1976, 1978, 1979; Park and Runkle, 2017, 2018, 2019). This ratio is referred to as phytochrome photoequilibrium (PPE, also called the phytochrome photostationary state; PSS) and was popularized by H. Smith for predicting shade avoidance responses. Smith credits K. M. Hartmann for the model of active to total phytochrome as the appropriate method for predicting phytochrome action (Hartmann, 1966; Smith, 1973).

Therefore, two metrics for predicting phytochrome responses have evolved: PPE and the R:FR ratio. Here we discuss problems with both metrics and propose a new metric.

3.4 Measurement of the Two Forms of Phytochrome

PPE can be estimated with a model (PPE_e) or measured directly in chlorophyll-deficient tissue (PPE_m). In chlorophyll-deficient tissue the relative amounts of the two forms of phytochrome can be measured directly in vivo using a specialized dual-wavelength spectrophotometer. There are two methods for measuring PPE_m with this technique (Dooskin and Mancinelli, 1968; Klose, 2019; Lamparter et al., 1994), but the method utilized by Smith and Holmes (1977) is described by Klein et al. (1967) and more recently, Klose (2019). Briefly, both methods measure the change in the difference in absorbance between two wavelengths upon exposure to R or FR, and the two techniques differ in the wavelengths that they measure. One measures the difference in absorbance between 660 and 730 nm, while the other (Smith and Holmes, 1977) measures the difference between 730 and 800 nm. The former provides a larger signal while the latter reduces error caused by chlorophyll. We describe the theory behind the more commonly used technique in Appendix E. It is important to note that although we call this a measurement of P_{fr}/P_{total}, it is still an estimate.

3.5 Estimating the Equilibrium between the Two Forms (PPE_e)

PPE_e is calculated from the spectral photon distribution (SPD) and weighting factors for both P_r and P_{fr} across the biologically active wavelengths (300 to 800 nm). These weighting factors, called photochemical/photoconversion cross-sections, quantum

efficiencies or photoconversion coefficients can be derived from absorbance spectra, extinction coefficients and quantum yields of P_r to P_{fr} or P_{fr} to P_r conversion. These values are presented in at least ten studies (Butler et al., 1964; Gardner and Graceffo, 1982; Kelly and Lagarias, 1985; Lagarias et al., 1987; Mancinelli, 1986, 1988a, 1994; Pratt and Briggs, 1966; Sager et al., 1988; Seyfried and Schafer, 1985; Vierstra and Quail, 1983a, 1983b). The weighting factors from Sager et al. (1988) have been the most widely used in horticulture, but are not necessarily a reference standard. PPE_e has been widely adopted.

3.6 Differences in Estimated and Measured PPE

Gardner and Graceffo (1982), Sager et al. (1988) and Mancinelli (1988b) all report comparisons between PPE_m and PPE_e. Figure 3-1 shows this comparison. Gardner and Graceffo measured and estimated P_{fr}/P_{total} in vivo, Sager et al. (1988) measured and estimated P_{fr}/P_{total} in vitro, and Mancinelli (1988b) measured P_{fr}/P_{total} in vivo, but used estimations from in vitro data. Additionally, Gardner and Graceffo (1982) assumed a P_{fr}/P_{total} under red actinic photons to be 0.8, Sager et al. (1988) assumes it to be 0.89 and Mancinelli (1988b) assumed it to be 0.876. Mancinelli (1988b) used the approach to equilibrium analysis data from Kelly and Lagarias (1985). Notice that data does not perfectly fall on the 1:1 line.

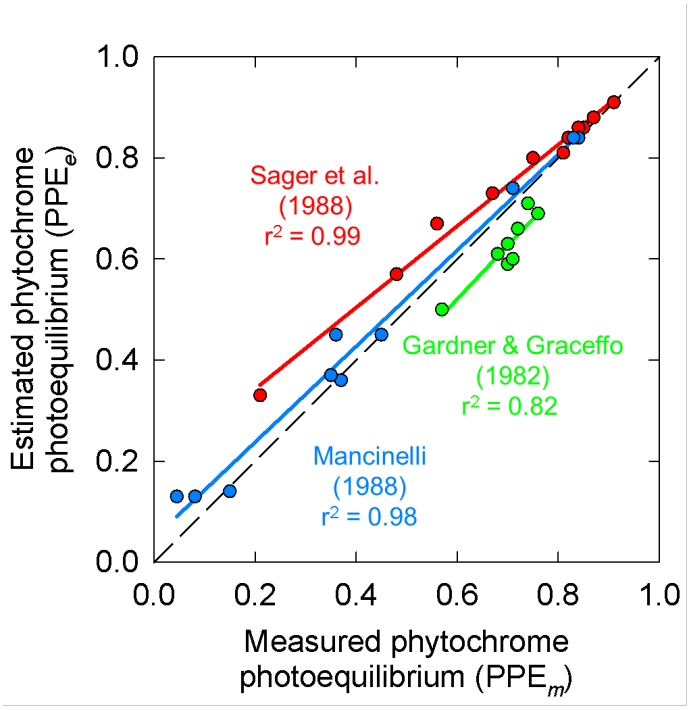

Fig. 3-1. Comparison of measured and estimated phytochrome photoequilibrium (PPE_m and PPE_e) from Gardner and Graceffo [1982 (green)], Sager et al. [1988 (red)] and Mancinelli [1988b (blue)].

3.7 Issues with P_{fr}/P_{total} as a Model to Predict Morphology

Studies on the structure of phytochrome, nuclear localization, and genetic regulating partners have strongly indicated that P_{fr} is the active form of phytochrome (Chen and Chory, 2011; Legris et al., 2019), although some studies have specifically implicated that the P_{fr}-P_{fr} homodimer is the active form while both the P_r-P_r homodimer and the P_r-P_{fr} heterodimer are both inactive (Klose et al., 2015). It is often assumed that P_{fr}/P_{total} is a proxy for the concentration of P_{fr} because it is assumed that the total pool of phytochrome is relatively constant (Casal, 2012; Kilsby and Johnson, 1982; Kozma-Bognar et al., 1999; Park and Runkle, 2017). Many studies have found that P_{fr}/P_{total} is correlated with morphological responses (Kalaitzoglou et al., 2019; Morgan and Smith, 1976, 1978, 1979; Park and Runkle,

2017, 2018, 2019), and it has become common to report PPE_e in photobiology studies even if they are not investigating the effects of R and FR (Hernandez and Kubota, 2016; Johnson et al., 2020; Kim et al., 2019; Meng et al., 2019; Poel and Runkle, 2017). These correlations between P_{fr}/P_{total} and morphology strongly imply the role of phytochrome in these responses, but the correlations in these studies would be equally predicted by a relationship using R and FR because these are the only wavelengths that varied in the studies. In cases where other wavelengths vary, the results have been graphed separately (Park and Runkle, 2019).

The ratio of P_{fr}/P_{total} is often thought to fully explain phytochrome activity and subsequent developmental responses, but there are multiple problems with its use.

1. ***Differences in weighting factors*** are discussed by Mancinelli (1986, 1988a). Up to the mid-1980s it was common to use weighting factors from Butler et al. (1964), but these weighting factors were obtained from less pure and more degraded phytochrome extractions compared to Kelly and Lagarias (1985), Lagarias et al. (1987), Sager et al. (1988) and Vierstra and Quail (1983a, 1983b). Beyond suggesting using newer versus older data, Mancinelli (1986, 1988a) was unable to recommend a superior set of weighting factors, and only mentioned that the choice should be open to revision.

   The weighting factors from these studies can have substantial differences on an absolute scale, and there are further differences when using weighting factors determined in vitro versus in vivo (Gardner and Graceffo, 1982; Pratt and Briggs, 1966; Seyfried and Schafer, 1985), where in vivo data shows a marked decrease in the response to blue and ultra-violet photons. Rajapakse and Kelly (1994)

demonstrated some of the potential differences in PPE_e under a single light source, and furthermore PPE_e and PPE_m do not perfectly match (Fig. 3-1). Fortunately, the most commonly used weighting factors from Kelly and Lagarias (1985), Lagarias et al. (1987) and Sager et al. (1988) are similar on a normalized scale. Despite this similarity, weighting factors primarily come from the monocots oat (*Avena sativa*) and rye (*Secale cereale*), which differ on an absolute scale (Lagarias et al., 1987), and their universal utility is uncertain.

2. ***Multiple phytochromes*** are present in dark-grown and etiolated tissue, but only phytochrome-B (phyB) appears to be primarily responsible for altering plant morphology in response to shade in adult, light grown plants. This conclusion is primarily due to the fact that only monogenic mutants of *Arabidopsis thaliana* without phyB appear to have severe shade-avoidance symptoms in white light (Aukerman et al., 1997; Devlin et al., 1998, 1999; Franklin et al., 2003), while phyA- (Franklin and Quail, 2010; Whitelam et al., 1993), phyC- (Franklin et al., 2003), phyD- (Aukerman et al., 1997; Devin et al., 1999) and phyE-deficient (Devlin et al., 1998) mutants appear indistinguishable from the wild type in the same conditions. The supporting role of these other phytochromes emerge in a phyB-deficient background (Aukerman et al., 1997; Devlin et al., 1998, 1999; Franklin et al., 2003), in which cases the double mutant shows more pronounced shade avoidance symptoms in white light compared to the phyB-deficient monogenic mutant.

In etiolated *Arabidopsis*, the percentages of the different pools of phytochrome protein are 85% phyA, 10% phyB and 5% other (phyC, phyD and

phyE), but on transition into the light the total pool of phytochrome drops by 23-fold and the ratios are readjusted to 5% phyA, 40% phyB and 55% other (Sharrock and Clack, 2002). Both PPE_m and PPE_e use dark-grown etiolated tissue, meaning that P_{fr}/P_{total} is based on a mix of all the phytochromes, but primarily phyA. This may create issues when using PPE_m or PPE_e to estimate the state of phyB in response to shade. Some limited evidence suggests that the photochemical properties of phyA and phyB are similar (Ruddat et al., 1997), but they differ from the photochemical properties of phyC and phyE (Eichenberg et al., 2000).

3. ***Non-photochemical reversions*** of P_{fr} to P_r are independent of light intensity and duration, but dependent on temperature (Jung et al., 2016; Legris et al., 2016). This thermal relaxation of the phytochrome molecule occurs in both in the dark and in the light. This leads to a potential lower value for P_{fr}/P_{total} at warmer temperatures under a single SPD. This effect is increased at lower light intensities where the rates of photoconversion are slower (Sellaro et al., 2019). In addition, nuclear body formation and dimerization of phytochrome may alter the thermal stability of P_{fr} (Klose et al., 2015; Rausenberger et al., 2010).

4. ***Intermediates*** between P_r and P_{fr}, and between P_{fr} and P_r have been studied with flash photolysis, low temperature spectroscopy, dehydration studies, and kinetics of absorbance changes (Kendrick and Spruit, 1977). The conversions between P_r and P_{fr} are not instantaneous processes. Instead, the conversions involve a number of short-lived intermediate forms. When transferred into the dark, P_{fr} (measured by a technique similar to that described in Appendix E) immediately increases to a level higher than the equilibrium level established in the light. This increase above

photoequilibrium indicates that there is a rate limiting chemical conversion between P_r and P_{fr}, leading to an accumulation of an intermediate under high light intensities. Kendrick et al. (1985) suggest that over 50% of total phytochrome may be in intermediate forms in sunlight. Smith and Fork (1992) found similar results, indicating that the concentration of P_{fr} would decrease at high light intensities even if P_{fr}/P_{total} remained the same. Smith (1990) saw no long-term change in stem extension rate at constant R:FR ratios under rapidly increasing or decreasing intensities, an effect that should have decreased or increased, respectively, the total concentration of P_{fr}. This is one of several experiments conducted by H. Smith that attempted to show that P_{fr}/P_{total} could predict responses better than the total amount of P_{fr}, suggesting that both P_{fr} and P_r may be active (Smith, 1981, 1982, 1983, 1990, 1994, 1995). His analysis was largely ignored in the literature, although Schmidt and Mohr (1982) suggested that P_{fr} was the better indicator.

5. ***P_{total} is not constant, as plant physiology textbooks often imply***. Smith (1981) measured P_{total} in adult *Zea mays* tissue bleached with norflurazon and showed that P_{total} could change depending on the background SPD. Similarly, Schafer (1978) showed that the synthesis and degradation rates of P_{total} in *Cucubita pepo* could change with plant age, and suggested that these rates may be under circadian control. The mRNA expression of phyB appears to be under circadian control (Kozma-Bognar et al., 1999; Toth et al., 2001), and immunoblot analysis of total phyB protein concentrations have shown that it can change by 50% over the course of a day (Kozma-Bognar et al., 1999; Sharrock and Clack, 2002). This 50% variation in phyB protein indicates that although PPE_e provides an estimate of P_{fr} to P_{total}, the actual

concentration of P_{fr} could fluctuate by 50%. Some of the other phytochromes (e.g. phyA) have shown an even more dramatic fluctuation over the course of the day. Additionally, activated phyB interacts with the transcriptional factors phytochrome interacting factors (PIFs) resulting in their ubiquitination followed by proteasomal degradation (Ni et al., 2014). This means that the rate of degradation depends on the concentration of PIFs. Further, the concentration of phyB is not as light stable as is commonly thought (Klose et al., 2015). Overall, these findings indicate that the total pool of phytochrome at a given point in the day can vary based on the circadian rhythm, the expression of PIFs and the length of time in the dark or the light.

Recent complex modelling approaches in *Arabidopsis* (Klose et al., 2015; Sellaro et al., 2019) have estimated the pool of active phyB (P_{fr}-P_{fr} homodimer) in the nucleus by including not only photoconversions, but also thermal reversions (mentioned above) and synthesis/degradation rates. This model includes a specific degradation rates for each of the three potential states of the dimer. The rates of synthesis are assumed to be constant although this is likely not the case. Finally, there is no certainty as to how predictive this more complex model is for species other than *Arabidopsis*.

6. ***Chlorophyll*** in leaves attenuate the photon flux at different wavelengths. Therefore, P_{fr}/P_{total} (PPE_m or PPE_e) only represent the ratio at the top epidermal layer of leaves (Gardner and Graceffo, 1982; Morgan and Smith, 1978). However, even this may not be true, as back scattering and reflectance of photons may actually make the photon intensity in the initial layer of a leaf higher than that just above the leaf

(Mancinelli, 1988a; Seyfried and Fukshansky, 1983). Morgan and Smith (1978) demonstrated that the correlation between log-stem extension rate and PPE_e deviated from linearity when measured under a leaf with high chlorophyll content. Action spectra studies have shown that the peak wavelength of phytochrome responses in green tissue shift to shorter wavelengths than expected (Jose and Schafer, 1978; Kasperbauer et al., 1963), indicating that some photon attenuation is occurring.

These considerations bring the mechanistic relationship between P_{fr}/P_{total} and morphology into question. Early studies that compared PPE_m to growth responses used the technique described in Appendix E. This technique could only measure the P_{fr}/P_{total} ratio and does not indicate concentrations of either P_{total} or P_{fr} (but see Appendix E). Because measurements and estimations of P_{fr}/P_{total} have predicted morphological responses they were widely used as the primary metric, but due to the considerations discussed above, what do PPE_m and PPE_e actually indicate?

As mentioned previously, studies have used a constant background spectrum and only adjusted amounts of R and FR (Kalaitzoglou et al., 2019; Morgan and Smith, 1976, 1978, 1979; Park and Runkle, 2017, 2018), meaning that the responses are equally well predicted by environmental factors like the R:FR ratio.

3.8 R and FR Photons as Environmental Signals

These challenges of mechanistically modeling phytochrome protein dynamics and linking them with morphological responses across a wide range of species and environments

mean that simple environmental signals may be more broadly applicable. Small factors in complex biological models can have large impacts on outputs, especially when downstream processes remain unknown.

Environmental signals like temperature are easily measureable. Smith (1982) eloquently described the importance of environmental signals:

> "*For an environmental signal to be valuable to a perceiving organism it must be: (a) unambiguous, (b) reliable, (c) readily detectable, and (d) related to an ecologically important condition in some quantitatively predictive manner*."

Smith went on to state that the R:FR ratio perfectly fit these criteria as an environmental signal of vegetative shade, as other environmental photobiological signals of shade, like photon intensity, do not meet the same standard of reliability. Many authors investigating phytochrome action with mutant *Arabidopsis* avoid P_{fr}/P_{total} and simply use the R:FR ratio (de Wit et al., 2016; Trupkin et al., 2014; Wang et al., 2015).

3.9 Effect of Wavelength Range on the R:FR Ratio

Similar to the lack of standardization regarding weighting factors to calculate PPE_e, with some authors using data from Sager et al. (1988) and others using data from Kelly and Lagarias (1985), there is little standardization in the wavelength ranges for R and FR photons fluxes to calculate the R:FR ratio. This can result in different values of the R:FR ratio for a single light sources that has a constant SPD. One of the earliest and most commonly used ranges was the integration of the photon flux between 655 to 665 nm divided by the photon flux between 725 to 735 nm. This range was widely used by H. Smith and colleagues (Holmes and Smith, 1977a, 1977b; Smith and Holmes, 1977). Smith, in correspondence with

J. Monteith, settled on the Greek letter ζ (lower case zeta) to represent the ratio (Holmes and Smith, 1977a; Monteith, 1976). Smith reported that the R:FR ratio of sunlight following this method was 1.19 (Smith, 1982). He reported that there is surprisingly little variation in the R:FR ratio under a variety of environmental conditions (Smith, 1982), but that does not appear to be the case (Appendix F). A second method to calculate the R:FR ratio is to simply divide the photon flux at 660 nm by the flux at 730 nm (Deitzer et al., 1979; Pausch et al., 1991; Warrington et al., 1989). This single wavelength method for obtaining R and FR often uses alternative wavelengths like 645, 650, 725 and/or 735 nm (Casal et al., 1985; Kasperbauer, 1987; Kasperbauer and Karlen, 1994; Taylorson and Borthwick, 1969). M. Kasperbauer favored measuring R at 645 nm instead of 660 nm due to the apparent maximum sensitivity of floral inhibition by night break lighting at 645 nm (Kasperbauer et al., 1963) instead of the expected 660 nm (Butler et al., 1959). This shift in sensitivity when using green versus etiolated tissue was speculated to be due to chlorophyll absorption. Jose and Schafer (1978) found a similar shift in the action spectra for lengths of green hypocotyls. Finally, a third approach has been to calculate the R:FR ratio based on the flux between 600 to 700 nm divided by the flux between 700 to 800 nm (Li and Kubota, 2009; Mortensen and Stromme, 1987; Rajapakse et al., 1992; Rajapakse and Kelly, 1994; Runkle and Heins, 2001). Figure 3-2 shows a comparison of four wavelength ranges using the ASTM G173-03 reference of global tilt solar energy flux [American Society for Testing and Materials, 2012 (converted to a photon flux)] and a measurement made at Utah State University (Logan, UT) at noon on 10 June 2020 using a spectroradiometer (PS-300, Apogee Instruments, Logan UT). These three methods result in a 6% to 7% difference. These differences would be larger

under narrow bandwidth LEDs. While these are the most common methods used to calculate the R:FR ratio from spectral distribution measurements, there are numerous variations.

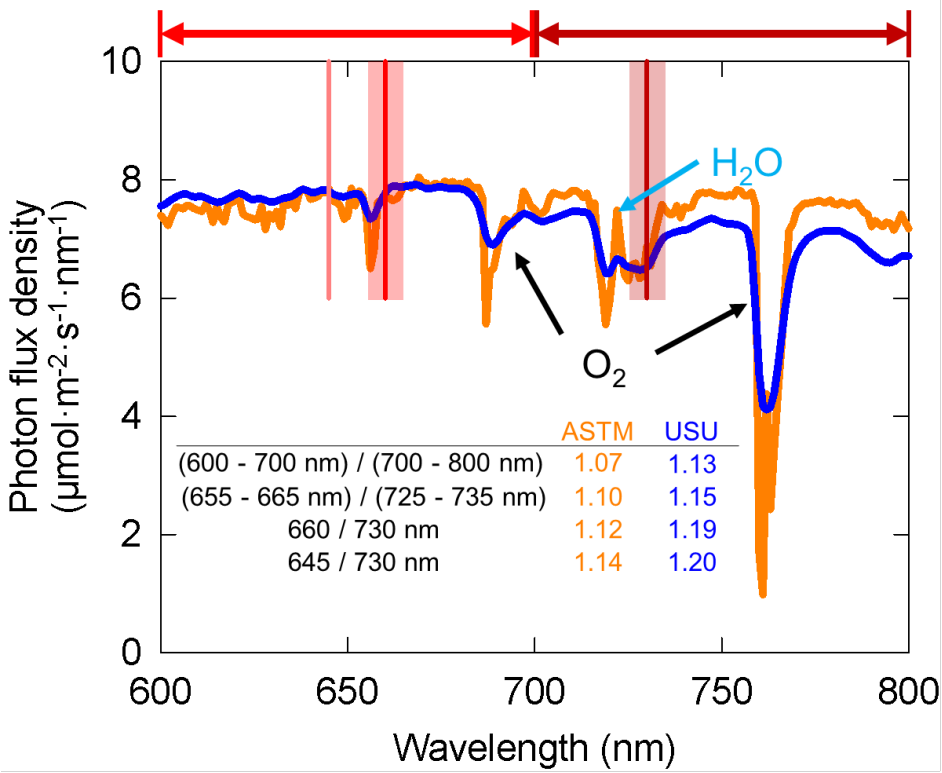

Fig. 3-2. Spectral photon distribution of the ASTM G173-03 reference of global tilt energy converted to photon flux [American Society for Testing and Materials, 2012 (orange line)] and a measurement made at Utah State University at noon on 10 June 2020 (blue line). Four ranges used for obtaining the red to far-red ratio (R:FR ratio) are shown as lines or bands in the figure: 1) 600 to 700 nm / 700 to 800 nm shown as arrows at the top of the figure, 2) 655 to 665 nm / 725 to 735 nm shown as shaded regions, 3) 660 / 730 nm shown as vertical lines and 4) 645 / 730 nm shown as a separate vertical line. The corresponding calculation of the R:FR ratio is shown in inset table. This figure also demonstrates potential variation due to environmental conditions. The light blue arrow shows a water vapor absorbance band and the black arrows show an oxygen absorbance band.

Sensors with dual detectors have been widely used to calculate an R:FR ratio. These sensors include photodiodes sensitive to photons in the R and FR regions. An early commercial model was the 660/730-nm sensor (SKR110, Skye Instruments, Llandrindod Wells, UK), which used to be sensitive to photons from 630 to 665 for the R region, but this

range was modified in 2010 to 645 to 675 nm. The FR range remained mostly unchanged from 715 to 740 nm, although it appears to have narrowed (Fig. 3-3). The Skye R:FR sensor was reported to provide a ratio of 1.1 in sunlight (Messier et al., 1989); we recently confirmed this measurement as 1.05. More recently, an R:FR sensor was developed with a wavelength range of 645 to 665 nm for R and 720 to 740 nm for FR (model S2, Apogee Instruments). R:FR sensors do not evenly weigh the photons between these wavelengths (Fig. 3-3), but are less expensive, more portable, have a faster response time, and are more durable than spectroradiometers. Inexpensive spectroradiometers are now widely available but these have lower spectral resolution (often greater than 24 nm bandwidth).

When calculating the R:FR ratio (and subsequent metrics described below), we recommend that the most appropriate range for FR is 730 ± 10 nm. This is a larger range than the commonly used recommendation from H. Smith, but the variation in reported maximum absorbance of P_{fr} in the FR region justifies this wider range (Kelly and Lagarias, 1985; Sager et al., 1988; Seyfried and Schafer, 1985). Broader ranges (e.g. 700 to 800 nm) could overestimate phytochrome responses from the Sun or from LEDs that have peaks beyond 750 nm. The R range is more difficult to determine due to chlorophyll screening and the apparent shift in maximum sensitivity from ≈660 nm to ≈630 or 645 nm (Jose and Schafer, 1978; Kasperbauer et al., 1963). Either choice of peak wavelength for R photons can be appropriate with justification. Similar to FR, a wider range (± 10 nm) seems appropriate. Commercially available R:FR sensor use these wider ranges and are a good choice for quickly and affordably assessing incoming R and FR photons. When reporting spectral data in wider contexts than phytochrome responses, broader ranges may still be appropriate.

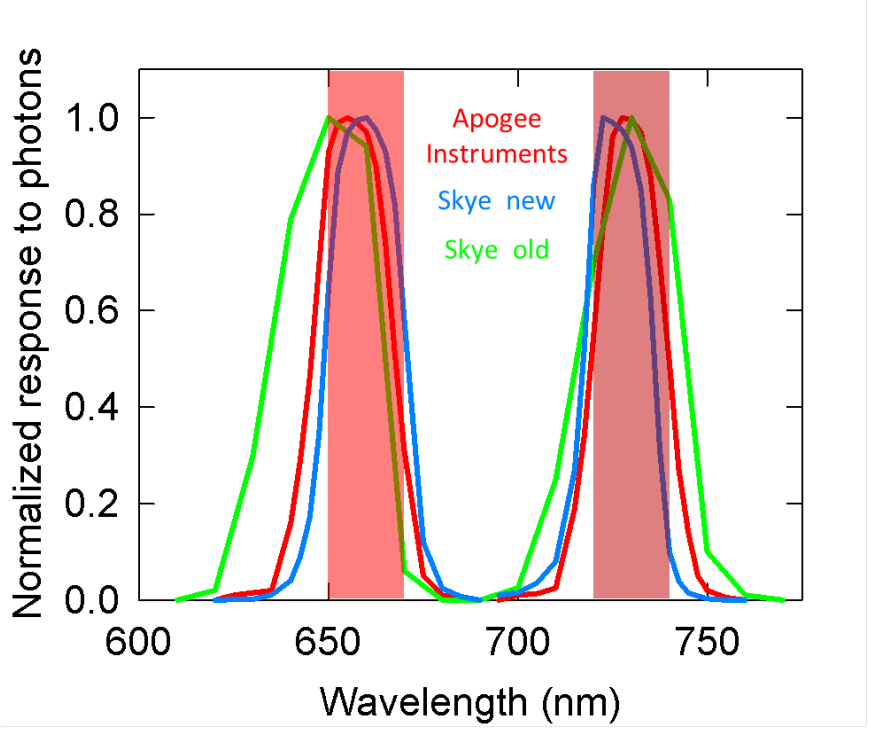

Fig. 3-3. Sensitivity of the red and far-red photodiodes in three red to far-red ratio sensors from Apogee instruments (Logan, UT) and Skye Instruments (Llandrindod Wells, UK). The shaded red regions represent our recommended ranges for calculating the R:FR ratio.

3.10 Units to Measure the R:FR Ratio: Energy Flux vs. Photon Flux

Although some studies have used energy units to measure R and FR fluxes (Salisbury, 1981; Taylorson and Borthwick, 1969), most studies have used photon fluxes because photons were known to be the driving factor for phytochrome responses as far back as 1964 (Butler et al., 1964; Siegelman and Hendricks, 1964). This is also described by the Stark-Einstein Law/photochemical equivalence law (Roth, 2001). Photons at 660 nm are more energetic than photons at 730 nm, so an R:FR ratio (660/730 nm) in sunlight based on energy units is 1.24, while the ratio based on photon flux is 1.12. These measurements can be interconverted using Planck's equation (*micromoles of photons = Joules of energy* × λ *(in nm)*×*0.008359*).

3.11 Effect of Environmental Conditions on R and FR Photon Flux

Atmospheric conditions also affect the R:FR ratio in natural environments. Kotilainen et al. (2020) demonstrated that atmospheric conditions, latitude, and time of day cause more variation in the R:FR ratio in the natural environment than previously thought. Photobiologists studying phytochrome responses in the natural environment need to be aware of this variation. We summarize these factors in Appendix F.

3.12 The Relationship between R:FR Ratio and PPE is Highly Nonlinear

The R:FR ratio has been an adequate metric for the natural environment because the highest value is ≈1.4 around midday (Kotilinen et al., 2020). Nonetheless, as measurements move from full sunlight to deep shade the relative amount of FR increases and the R:FR ratio decreases. This confines the R:FR ratio in the natural environment to values ranging from ≈0 to 1.

Smith and Holmes (1977) plotted the relationship between R:FR ratio and PPE_m under sunlight, vegetative shade and some electric lights. This analysis showed that PPE_m was highly sensitive to R:FR ratios found in shade. Smith (1982) recommends that this curve can be used to estimate P_{fr}/P_{total} from the R:FR ratio in natural environments, but he warns against using it in controlled environments, saying,

> "*the curve may be reliably used for all natural broadband sources except those, which contain a high portion of blue. Its use with artificial far-red sources is limited because of the difficulty of accurate read-out on the steepest part of the curve*."

Under electric lights the flux of FR can approach zero and the R:FR ratio approaches infinity. Although P_{fr}/P_{total}, may be unreliable, it does generally describe phytochrome status

and it is useful to understand the relationships with the R:FR ratio. Figure 3-4A shows the relationship between R:FR ratio measured with a Skye R:FR sensor and PPE_e calculated from spectral measurements and weighting factors published by Sager et al. (1988). The relationship is highly nonlinear. Under LEDs with minimal FR, the R:FR ratio nearly flat-lines above 3, and values continue to slightly increase up to 1800. Some publications have reported R:FR ratios above 100 (Hernandez and Kubota, 2016), while others have avoided the infinity problem by reporting the R:FR ratio as 1:0 (Park and Runkle, 2017, 2018). These issues mean that the R:FR ratio has little predictive value under electric lights.

3.13 R Fraction: An Intermediate Solution

A simple improvement is to use the red fraction (R fraction), first reported by Smith (1990), which is calculated as:

$$R\ fraction = \frac{R}{R+FR} = \frac{R{:}FR}{1 + R{:}FR}$$

Eq. [3.1]

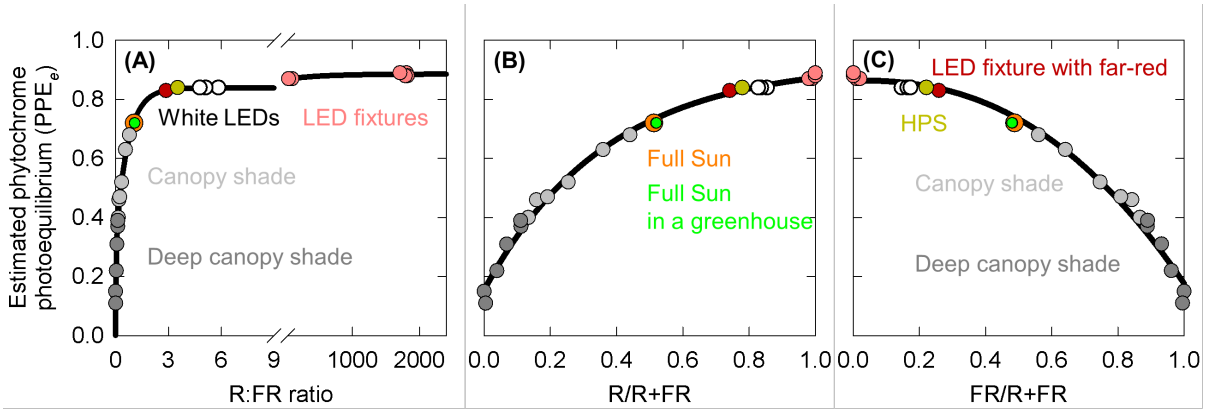

Fig. 3-4. Relationship between the R:FR ratio, R fraction, FR fraction and estimated phytochrome photoequilibrium. (A) Relationship between red to far-red ratio (R:FR ratio), measured with an R:FR sensor (SKR110, Skye Instruments, Llandrindod Wells, UK) and

estimated phytochrome photoequilibrium (PPE_e) using weighting factors from Sager et al. (1988). The R:FR ratio approaches infinity, but PPE_e reaches a maximum of 0.89. (B) Relationship between Red fraction [R/(R+FR)] and estimated PPE_e. The curve is more linear. (C) Relationship between FR fraction and PPE. This ratio is positively correlated with growth parameters like stem length and leaf area so this may be the preferred ratio. Both PPE and R fraction are negatively correlated with stem length and leaf area.

This confines the fraction (or ratio) to values between 0 and 1. We recommend the same ranges for R and FR as previously discussed for the R:FR ratio, but we note that confining the ratio from 0 to 1 can have a bigger impact than the wavelength range. We plot the same data as Fig. 3-4A using the new R fraction instead of the R:FR ratio in Fig. 3-4B.

Smith (1990) showed that the relationship between the R fraction and the change in stem extension rate in *Sinapis alba* was more linear than the relationship between PPE_m and the change in stem extension rate. But, the implications were not heavily discussed and the metric never became widely used.

P_{fr}/P_{total}, like the R fraction, is confined to values between 0 and 1. Although, based on the photochemical properties, P_{fr}/P_{total} is actually confined to values between 0 and 0.89 (Lagarias et al., 1987, Fig. 3-4). R activates P_r into P_{fr} and FR reconverts P_{fr} back into P_r, so it makes sense that the R fraction [R/(R+FR)] is well correlated with PPE [P_{fr} / (P_r + P_{fr})].

3.14 FR Fraction: An Improved Metric

The active form of phytochrome (P_{fr}) suppresses stem elongation by interacting with and degrading PIFs, which are involved in the expression of shade avoidance (cell wall and auxin related) genes (Casal, 2012; de Lucas and Prat, 2014). Therefore, P_{fr}/P_{total}, R fraction and the R:FR ratio have an inverse relationship with the parameters of interest in controlled

environments like stem length (Morgan and Smith, 1976, 1978, 1979; Park and Runkle, 2017, 2018). Perhaps many researchers have used the R:FR ratio because in the natural environment it is generally confined to values between ≈0 and 1. An FR:R ratio would not be confined in the same way. But positive correlations are more intuitive than negative correlations, and thus the FR fraction more intuitive than the R fraction. The FR fraction is the mirror image of the R fraction (Fig. 3-4C) and use the same wavelength ranges described previously. It is calculated as:

$$FR\ fraction\ = \frac{FR}{R+FR} = \frac{1}{1 + R{:}FR}$$

Eq. [3.2]

An FR:R ratio was used by M. Kasperbauer in several studies that investigated neighbor perception (Kasperbauer, 1971; Kasperbauer and Karlen, 1994) or reflectivity of colored mulches (Decoteau et al., 1990; Kasperbauer and Hunt, 1992). These studies do not provide an explanation for the use of the FR:R ratio, but the ratio is positively correlated with growth parameters.

3.15 Comparison of a Related Ratio that Evolved to Eventually Range from 0 to 1

The evolution to a simpler, more intuitive ratio has similarities with metrics used in remote sensing of vegetation. Jorden (1969) proposed the ratio vegetation index [RVI (reflectance at 900 nm divided by the reflectance at 680 nm)] to assess chlorophyll content and fraction of ground cover by leaves. But like the R:FR ratio, this original metric was non-linear and approached infinity in dense vegetation. To reduce these issues, Tucker (1978) introduced the difference vegetation index (the difference in intensity between 900 and 680 nm). But this difference increased with light intensity, so it was later normalized to the

intensity by dividing by the total photon flux. This resulted in a metric that ranges from 0 to 1 as the canopy density increases from bare soil to complete cover. This improved metric is now widely used and called the normalized difference vegetation index [NDVI (Gamon et al., 1995)].

Another metric that is still evolving is root mass fraction (root mass divided by total mass). Many researchers still publish root:shoot ratio (root mass divided by shoot mass), but this ratio starts at infinity in a germinating seed and decreases nonlinearly as the plant ages. By contrast, root mass fraction starts at 1 and slowly decreases over the life cycle. Metrics that use a total in the denominator are more intuitive.

3.16 A Comparison of Metrics

To demonstrate the value of this improved index we normalize (to the grand mean of both studies) and regraph geranium (*Pelargonium ×hortorum* 'Pinto Premium Orange Bicolor') stem length data from Park and Runkle (2017, 2018) using PPE_e, the R:FR ratio and the FR fraction as the independent variable (Fig. 3-5). It should be noted that the R:FR ratio and FR fraction are calculated with wider 100-nm bandwidths rather than the narrower 20-nm bandwidths we suggested earlier. This is because these authors reported R and FR in these 100-nm bands. Additionally, because these data come from a study that uses LEDs centered at ≈660 and 730 nm (with no white LEDs) the 100-nm range and the 20-nm range would produce very similar results. We exclude data from the most recent publication by these authors because it also altered the amount of blue, inducing morphological effects outside the R and FR ranges (Park and Runkle, 2019). This data contains three R:FR ratios

that do not have any FR, which the authors report as 1:0. Because division by zero is undefined we arbitrarily set FR equal to 0.01, 0.025 and 0.05 (relative to R = 1) in these cases (Fig. 3-5B and C). The alternative is to assign these FR values the same low value, but this would have caused clumping of data, which may not occur in LED fixtures (see the flat part of Fig. 3-4A). Additionally, the arbitrary values demonstrate the hyperbolic function often seen when graphing data with the R:FR ratio. Our arbitrary values can be obtained with a spectroradiometer, but the measurement depends on the dark calibration and signal-to-noise ratio.

Between 0 to 10, the R:FR ratio is still a good predictor of stem length (Fig. 3-5B, inset). But, large R and small FR values significantly alter the correlation between the R:FR ratio and stem length (Fig. 3-5B) and the curve is highly nonlinear. Especially in sole-source LED plant factories, which often lack FR, the R:FR ratio is clearly a poor metric to predict phytochrome controlled responses. Zhang et al. (2020) similarly concluded that the R:FR

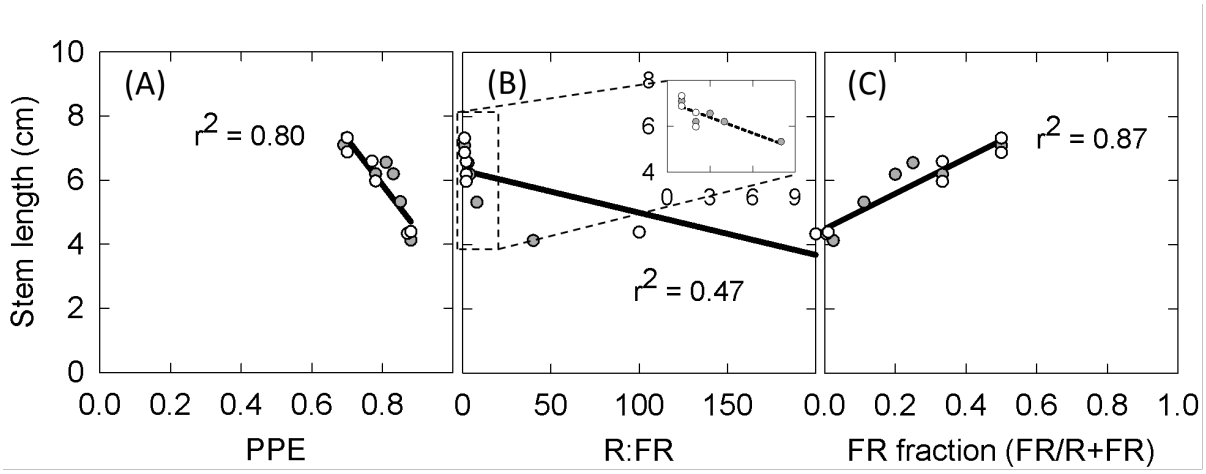

Fig. 3-5. Comparison of phytochrome photoequilibrium, the R:FR ratio and FR fraction on the prediction of stem length. Re-presented geranium ('Pinto Premium Orange Bicolor') stem length data estimated from two papers by Park and Runkle (2017, 2018). These data come from Fig. 2 in both papers. Grey circles are from the 2017 paper and were grown for 29 to 30 d. The open circles are from the 2018 paper and were grown for 36 to 39 d. Data is normalized to the grand mean of both studies. (A) The reported estimate of phytochrome

photoequilibrium (PPE_e) compared to stem length. (B) The red to far-red ratio (R:FR ratio) compared to stem length. Because Park and Runkle report R:FR ratios with no FR as 1:0, we arbitrarily chose 0.005, 0.025 and 0.01 (relative to R = 1). Notice the extremely large scale of the x-axis and how the data is sensitive to the small value of FR that might be provided by a spectroradiometer. These values are not unreasonable as they depend on the dark calibration and signal to noise ratio. (C) FR faction (FR/R+FR) compared to stem length. (C) uses the same data as (B) and are calculated using Eq. [3.2]. Notice that the FR fraction is not nearly as sensitive to small quantities of FR compared to the R:FR ratio.

ratio could change drastically while PPE_e remained relatively constant. They further found that the growth in *Antirrhinum majus*, *Petunia ×hybrida* and *Zinnia elegans* was better correlated with PPE_e than the R:FR ratio indicating that this was the superior metric. PPE_e presented here also appears to be a reasonably good metric. However, as we have discussed previously there are good reasons to be skeptical of this approach. As we learn more about phytochrome kinetics and downstream processes, this ratio may be incorporated into complex and mechanistic models that have better predictive ability, but for now perhaps environmental signals are better metrics.

The FR fraction (and the R fraction, not shown) is not sensitive to extremely high R or low FR (Fig. 3-5C). These examples demonstrates that the FR fraction is intuitively correlated with shade avoidance growth parameters and confined to values from 0 to 1. This metric is well suited to controlled environment plant production. Additionally, because experiments performed in controlled environments are used to predict responses in the natural environment this may indicate that it is also a better metric under natural conditions.

It is important to remember that the R:FR ratio, PPE_e, and the FR fraction can only predict morphological responses caused by phytochrome. The effects of blue light are not assessed with these metrics. Although PPE_e includes some sensitivity to violet and ultra-violet photons, these effects are minimal compared to blue light receptors like cryptochromes

(Park and Runkle, 2019; Runkle and Heins, 2001). Cryptochromes interact with many of the same transcription factors as phytochrome (de Wit et al., 2016). Blue and green photons have been proposed to act antagonistically in a similar manner to R and FR (Banerjee et al., 2007; Bouly et al., 2007), and thus models describing cryptochrome kinetics have been developed that resemble phytochrome kinetic models (Procopio et al., 2016). Future studies should investigate interactions of the R and blue photons antagonistically acting against FR and green photons.

3.17 Literature Cited

American Society for Testing and Materials. 2012. Committee G03 on Weathering and Durability. Standard tables for reference solar spectral irradiances: Direct normal and hemispherical on 37° tilted surface. ASTM International, West Conshohocken, PA.

Aukerman, M.J., M. Hirschfeld, L. Wester, M. Weaver, T. Clack, R.M. Amasino, and R.A. Sharrock. 1997. A deletion in the PHYD gene of the *Arabidopsis* Wassilewskija ecotype defines a role for phytochrome D in red/far-red light sensing. Plant Cell 9:1317-1326. doi: 10.1105/tpc.9.8.1317

Banerjee, R., E. Schleicher, S. Meier, R.M. Viana, R. Pokorny, M. Ahmad, R. Bittl, and A. Batschauer. 2007. The signaling state of *Arabidopsis* cryptochrome 2 contains flavin semiquinone. J. Biol. Chem. 282:14916-14922. doi: 10.1074/jbc.M700616200

Borthwick, H.A., S.B. Hendricks, M.W. Parker, E.H. Toole, and V.K. Toole. 1952. A reversible photoreaction controlling seed germination. Proc. Natl. Acad. Sci. USA 38:662-666. doi: 10.1073/pnas.38.8.662

Bouly, J.P., E. Schleicher, M. Dionisio-Sese, F. Vandenbussche, D. Van Der Straeten, N. Bakrim, S. Meier, A. Batschauer, P. Galland, R. Bittl, and M. Ahmad. 2007. Cryptochrome blue light photoreceptors are activated through interconversion of flavin redox states. J. Biol. Chem. 282:9383-9391. doi: 10.1074/jbc.M609842200

Butler, W.L., K.H. Norris, H.W. Siegelman, and S.B. Hendricks. 1959. Detection, assay, and preliminary purification of the pigment controlling photoresponsive development of plants. Proc. Natl. Acad. Sci. USA 45:1703-1708. doi: 10.1073/pnas.45.12.1703

Butler, W.L., H.C. Lane, and H.W. Siegelman. 1963. Nonphotochemical transformations of phytochrome in vivo. Plant Physiol. 38:514-519. doi: 10.1104/pp.38.5.514

Butler, W.L., S.B. Hendricks, and H.W. Siegelman. 1964. Action spectra of phytochrome *in vitro*. Photochem. Photobiol. 3:521-528. doi: 10.1111/j.1751-1097.1964.tb08171.x

Casal, J.J., V.A. Deregibus, and R.A. Sanchez. 1985. Variations in tiller dynamics and

morphology in *Lolium multiflorum* Lam. vegetative and reproductive plants as affected by differences in red/far-red irradiation. Ann. Bot. 56:553-559. doi: 10.1093/oxfordjournals.aob.a087040

Casal, J.J. 2012. Shade avoidance. Arabidopsis Book 10:e0157. doi: 10.1199/tab.0157

Chen, M., and J. Chory. 2011. Phytochrome signaling mechanisms and the control of plant development. Trends Cell Biol. 21:664-671. doi: 10.1016/j.tcb.2011.07.002

Cumming, B.G. 1963. The dependence of germination on photoperiod, light quality, and temperature in *Chenopodium* spp.. Can. J. Bot. 41:1211-1233. doi: 10.1139/b63-102

de Lucas, M., and S. Prat. 2014. PIF s get BR right: PHYTOCHROME INTERACTING FACTORs as integrators of light and hormonal signals. New Phytol. 202:1126-1141. doi: 10.1111/nph.12725

de Wit, M., D.H. Keuskamp, F.J. Bongers, P. Hornitschek, C.M. Gommers, E. Reinen, C. Martínez-Cerón, C. Fankhauser, and R. Pierik. 2016. Integration of phytochrome and cryptochrome signals determines plant growth during competition for light. Current Biol. 26:3320-3326. doi: 10.1016/j.cub.2016.10.031

Decoteau, D.R., M.J. Kasperbauer, and P.G. Hunt. 1990. Bell pepper plant development over mulches of diverse colors. HortScience 25:460-462. doi: 10.21273/HORTSCI.25.4.460

Deitzer, G.F., R. Hayes, and M. Jabben. 1979. Kinetics and time dependence of the effect of far red light on the photoperiodic induction of flowering in Wintex barley. Plant Physiol. 64:1015-1021. doi: 10.1104/pp.64.6.1015

Devlin, P.F., S.R. Patel, and G.C. Whitelam. 1998. Phytochrome E influences internode elongation and flowering time in *Arabidopsis*. Plant Cell 10:1479-1487. doi: 10.1105/tpc.10.9.1479

Devlin, P.F., P.R. Robson, S.R. Patel, L. Goosey, R.A. Sharrock, and G.C. Whitelam. 1999. Phytochrome D acts in the shade-avoidance syndrome in *Arabidopsis* by controlling elongation growth and flowering time. Plant Physiol. 119:909-916. doi: 10.1104/pp.119.3.909

Dooskin, R.H., and A.L. Mancinelli. 1968. Phytochrome decay and coleoptile elongation in *Avena* following various light treatments. Bul. Torrey Bot. Club 95:474-487. doi: 10.2307/2483479

Eichenberg, K., I. Bäurle, N. Paulo, R.A. Sharrock, W. Rüdiger, and E. Schäfer. 2000. *Arabidopsis* phytochromes C and E have different spectral characteristics from those of phytochromes A and B. FEBS Let. 470:107-112. doi: 10.1016/S0014-5793(00)01301-6

Franklin, K.A., S.J. Davis, W.M. Stoddart, R.D. Vierstra, and G.C. Whitelam. 2003. Mutant analyses define multiple roles for phytochrome C in *Arabidopsis* photomorphogenesis. Plant Cell 15:1981-1989. doi: 10.1105/tpc.015164

Franklin, K.A., and G.C. Whitelam. 2005. Phytochromes and shade-avoidance responses in plants. Ann. Bot. 96:169-175. doi: 10.1093/aob/mci165

Franklin, K.A., and P.H. Quail. 2010. Phytochrome functions in *Arabidopsis* development. J. Expt. Bot. 61:11-24. doi: 10.1093/jxb/erp304

Gamon, J.A., C.B. Field, M.L. Goulden, K.L. Griffin, A.E. Hartley, G. Joel, J. Peñuelas, and

R. Valentini. 1995. Relationships between NDVI, canopy structure, and photosynthesis in three Californian vegetation types. Ecol. Appl. 5:28-41. doi: 10.2307/1942049

Gardner, G., and M.A. Graceffo. 1982. The use of a computerized spectroradiometer to predict phytochrome photoequilibria under polychromatic irradiation. Photochem. Photobiol. 36:349-354. doi: 10.1111/j.1751-1097.1982.tb04385.x

Hartmann, K.M. 1966. A general hypothesis to interpret 'high energy phenomena' of photomorphogenesis on the basis of phytochrome. Photochem. Photobiol. 5:349-365. doi: 10.1111/j.1751-1097.1966.tb05937.x

Hendricks, S.B., and H.A. Borthwick. 1963. Control of plant growth by light, p. 233-262. In: L.T. Evans (ed.). Environmental control of plant growth. Academic Press, Cambridge, MA. doi: 10.1016/B978-0-12-244350-3.50018-5

Hernández, R., and C. Kubota. 2016. Physiological responses of cucumber seedlings under different blue and red photon flux ratios using LEDs. Environ. Expt. Bot. 12:66-74. doi: 10.1016/j.envexpbot.2015.04.001

Holmes, M.G., and H. Smith. 1975. The function of phytochrome in plants growing in the natural environment. Nature 254:512-514. doi: 10.1038/254512a0

Holmes, M.G., and H. Smith. 1977a. The function of phytochrome in the natural environment—I. Characterization of daylight for studies in photomorphogenesis and photoperiodism. Photochem. Photobiol. 25:533-538. doi: 10.1111/j.1751-1097.1977.tb09124.x

Holmes, M.G., and H. Smith. 1977b. The function of phytochrome in the natural environment—II. The influence of vegetation canopies on the spectral energy distribution of natural daylight. Photochem. Photobiol. 25:539-545. doi: 10.1111/j.1751-1097.1977.tb09125.x

Johnson, R.E., Y. Kong, and Y. Zheng. 2020. Elongation growth mediated by blue light varies with light intensities and plant species: A comparison with red light in arugula and mustard seedlings. Environ. Expt. Bot. 169:103898. doi: 10.1016/j.envexpbot.2019.103898

Jordan, C.F. 1969. Derivation of leaf-area index from quality of light on the forest floor. Ecology 50:663-666. doi: 10.2307/1936256

Jose, A.M., and E. Schäfer. 1978. Distorted phytochrome action spectra in green plants. Planta 138:25-28. doi: 10.1007/BF00392909

Jung, J.H., M. Domijan, C. Klose, S. Biswas, D. Ezer, M. Gao, A.K. Khattak, M.S. Box, V. Charoensawan, S. Cortijo, M. Kumar, A. Grant, J.C.W. Locke, E. Schäfer, K.E. Jaeger, and P.A. Wigge. 2016. Phytochromes function as thermosensors in *Arabidopsis*. Science 354:886-889. doi: 10.1126/science.aaf6005

Kalaitzoglou, P., W. van Ierpen, J. Harbinson, M. van der Meer, S. Martinakos, K. Weerheim, C.C.S. Nicole, and L.F.M. Marcelis. 2019. Effects of continuous or end-of-day far-red light on tomato plant growth, morphology, light absorption, and fruit production. Front. Plant Sci. 10:322. doi: 10.3389/fpls.2019.00322

Kasperbauer, M.J., H.A. Borthwick, and S.B. Hendricks. 1963. Inhibition of flowering of *Chenopodium rubrum* by prolonged far-red radiation. Bot. Gaz. 124:444-451. doi: 10.1086/336234

Kasperbauer, M.J. 1971. Spectral distribution of light in a tobacco canopy and effects of end-

of-day light quality on growth and development. Plant Physiol. 47:775-778. doi: 10.1104/pp.47.6.775

Kasperbauer, M.J. 1987. Far-red light reflection from green leaves and effects on phytochrome-mediated assimilate partitioning under field conditions. Plant Physiol. 85:350-354. doi: 10.1104/pp.85.2.350

Kasperbauer, M.J., and P.G. Hunt. 1992. Cotton seedling morphogenic responses to FR/R ratio reflected from different colored soils and soil covers. Photochem. Photobiol. 56:579-584. doi: 10.1111/j.1751-1097.1992.tb02205.x

Kasperbauer, M.J., and D.L. Karlen. 1994. Plant spacing and reflected far-red light effects on phytochrome-regulated photosynthate allocation in corn seedlings. Crop Sci. 34:1564-1569. doi: 10.2135/cropsci1994.0011183X003400060027x

Kelly, J.M., and J.C. Lagarias. 1985. Photochemistry of 124-kilodalton *Avena* phytochrome under constant illumination in vitro. Biochemistry 24:6003-6010. doi: 10.1021/bi00342a047

Kendrick, R.E., and B. Frankland. 1968. Kinetics of phytochrome decay in *Amaranthus* seedlings. Planta 82:317-320. doi: 10.1007/BF00386434

Kendrick, R.E., and C.J.P. Spruit. 1977. Phototransformations of phytochrome. Photochem. Photobiol. 26:201-214. doi: 10.1111/j.1751-1097.1977.tb07473.x

Kendrick, R.E., J. Kome, and P.A.P.M. Jaspers. 1985. Kinetics of Pfr appearance in *Amaranthus caudatus*. Photochem. Photobiol. 42:785-787. doi: 10.1111/j.1751-1097.1985.tb01648.x

Kilsby, C.A.H., and C.B. Johnson. 1982. The *in vivo* spectrophotometric assay of phytochrome in two mature dicotyledonous plants. Photochem. Photobiol. 35:255-260. doi: 10.1111/j.1751-1097.1982.tb03843.x

Kim, H.J., M.Y. Lin, and C.A. Mitchell. 2019. Light spectral and thermal properties govern biomass allocation in tomato through morphological and physiological changes. Environ. Expt. Bot. 157:228-240. doi: 10.1016/j.envexpbot.2018.10.019

Klein, W.H., J.L. Edwards, and W. Shropshire. 1967. Spectrophotometric measurements of phytochrome in vivo and their correlation with photomorphogenic responses of *Phaseolus*. Plant Physiol. 42:264-270. doi: 10.1104/pp.42.2.264

Klose, C., F. Venezia, A. Hussong, S. Kircher, E. Schäfer, and C. Fleck. 2015. Systematic analysis of how phytochrome B dimerization determines its specificity. Nature Plants 1:1-9. doi: 10.1038/nplants.2015.90

Klose, C. 2019. In vivo spectroscopy, p. 113-120. In: A. Hiltbrunner (ed.). Phytochromes. Humana Press, New York, NY. doi: 10.1007/978-1-4939-9612-4_8

Kotilainen, T., P.J. Aphalo, C.C. Brelsford, H. Böök, S. Devraj, A. Heikkilä, R. Hernández, A. Kylling, A.V. Lindfors, and T.M. Robson. 2020. Patterns in the spectral composition of sunlight and biologically meaningful spectral photon ratios as affected by atmospheric factors. Agr. For. Meteorol. 291:108041. doi: 10.1016/j.agrformet.2020.108041

Kozma-Bognár, L.K., A. Hall, É. Adám, S.C. Thain, F. Nagy, and A.J. Millar. 1999. The circadian clock controls the expression pattern of the circadian input photoreceptor, phytochrome B. Proc. Natl. Acad. Sci. USA 96:14652-14657. doi: 10.1073/pnas.96.25.14652

Kusuma, P., P. M. Pattison, and B. Bugbee. 2020. From physics to fixtures to food: current

and potential LED efficacy. Hort. Res. 7:1-9. https://doi.org/10.1038/s41438-020-0283-7

Lagarias, J.C., J.M. Kelly, K.L. Cyr, and W.O. Smith, Jr. 1987. Comparative photochemical analysis of highly purified 124 kilodalton oat and rye phytochromes *in vitro*. Photochem. Photobiol. 46:5-13. doi: 10.1111/j.1751-1097.1987.tb04729.x

Lamparter, T., J. Hughes, and E. Hartmann. 1994. A fully automated dual-wavelength photometer for phytochrome measurements and its application to phytochrome from chlorophyll containing extrace. Photochem. Photobiol. 60:179-183. doi: 10.1111/j.1751-1097.1994.tb05088.x

Legris, M., C. Klose, E.S. Burgie, C.C. Rojas, M. Neme, A. Hiltbrunner, P.A. Wigge, E. Schäfer, R.D. Vierstra, and J.J. Casal. 2016. Phytochrome B integrates light and temperature signals in *Arabidopsis*. Science 354:897-900. doi: 10.1126/science.aaf5656

Legris, M., Y.Ç. Ince, and C. Fankhauser. 2019. Molecular mechanisms underlying phytochrome-controlled morphogenesis in plants. Nature Commun. 10:1-15. doi: 10.1038/s41467-019-13045-0

Li, Q., and C. Kubota. 2009. Effects of supplemental light quality on growth and phytochemicals of baby leaf lettuce. Environ. Expt. Bot. 67:59-64. doi: 10.1016/j.envexpbot.2009.06.011

Mancinelli, A.L. 1986. Comparison of spectral properties of phytochromes from different preparations. Plant Physiol. 82:956-961. doi: 10.1104/pp.82.4.956

Mancinelli, A.L. 1988a. Some thoughts about the use of predicted values of the state of phytochrome in plant photomorphogenesis research. Plant Cell Environ. 11:429-439. doi: 10.1111/j.1365-3040.1988.tb01780.x

Mancinelli, A.L. 1988b. Phytochrome photoconversion *in vivo*: comparison between measured and predicted rates. Plant Physiol. 86:749-753. doi: 10.1104/pp.86.3.749

Mancinelli, A.L. 1994. The physiology of phytochrome action. In: R.E. Kendrick and G.H.M. Kronenberg (eds.). Photomorphogenesis in plants. Springer, Dordrecht, The Netherlands. doi: 10.1007/978-94-011-1884-2_10

Meng, Q., N. Kelly, and E.S. Runkle. 2019. Substituting green or far-red radiation for blue radiation induces shade avoidance and promotes growth in lettuce and kale. Environ. Expt. Bot. 162:383-391. doi: 10.1016/j.envexpbot.2019.03.016

Messier, C., T.W. Honer, and J.P. Kimmins. 1989. Photosynthetic photon flux density, red: far-red ratio, and minimum light requirement for survival of *Gaultheria shallon* in western red cedar–western hemlock stands in coastal British Columbia. Can. J. For. Res. 19:1470-1477. doi: 10.1139/x89-223

Monteith, J.L. 1976. Spectral distribution of light in leaves and foliage, p. 447-460. In: H. Smith (ed.). Light and plant development. Butterworth, London, UK. doi: 10.1016/B978-0-408-70719-0.50032-2

Morgan, D.C., and H. Smith. 1976. Linear relationship between phytochrome photoequilibrium and growth in plants under simulated natural radiation. Nature 262:210-212. doi: 10.1038/262210a0

Morgan, D.C., and H. Smith. 1978. The relationship between phytochrome-photoequilibrium and Development in light grown *Chenopodium album* L.. Planta 142:187-193. doi: 10.1007/BF00388211

Morgan, D.C., and H. Smith. 1979. A systematic relationship between phytochrome-controlled development and species habitat, for plants grown in simulated natural radiation. Planta 145:253-258. doi: 10.1007/BF00454449

Mortensen, L.M., and E. Strømme. 1987. Effects of light quality on some greenhouse crops. Scientia Hort. 33:27-36. doi: 10.1016/0304-4238(87)90029-X

Ni, W., S.L. Xu, J.M. Tepperman, D.J. Stanley, D.A. Maltby, J.D. Gross, A.L. Burlingame, Z.Y. Wang, and P.H. Quail. 2014. A mutually assured destruction mechanism attenuates light signaling in *Arabidopsis*. Science 344:1160-1164. doi: 10.1126/science.1250778

Park, Y., and E.S. Runkle. 2017. Far-red radiation promotes growth of seedlings by increasing leaf expansion and whole-plant net assimilation. Environ. Expt. Bot. 136:41-49. doi: 10.1016/j.envexpbot.2016.12.013

Park, Y., and E.S. Runkle. 2018. Far-red radiation and photosynthetic photon flux density independently regulate seedling growth but interactively regulate flowering. Environ. Expt. Bot. 155:206-216. doi: 10.1016/j.envexpbot.2018.06.033

Park, Y., and E.S. Runkle. 2019. Blue radiation attenuates the effects of the red to far-red ratio on extension growth but not on flowering. Environ. Expt. Bot. 168:103871. doi: 10.1016/j.envexpbot.2019.103871

Pausch, R.C., S.J. Britz, and C.L. Mulchi. 1991. Growth and photosynthesis of soybean (*Glycine max* L. Merr.) in simulated vegetation shade: influence of the ratio of red to far-red radiation. Plant Cell Environ. 14:647-656. doi: 10.1111/j.1365-3040.1991.tb01537.x

Patadia, F., R.C. Levy, and S. Mattoo. 2018. Correcting for trace gas absorption when retrieving aerosol optical depth from satellite observations of reflected shortwave radiation. Atmospheric Measurement Tech. 11:3205-3219. doi: 10.5194/amt-11-3205-2018

Poel, B.R., and E.S. Runkle. 2017. Spectral effects of supplemental greenhouse radiation on growth and flowering of annual bedding plants and vegetable transplants. HortScience 52:1221-1228. doi: 10.21273/HORTSCI12135-17

Pratt, L.H., and W.R. Briggs. 1966. Photochemical and nonphotochemical reactions of phytochrome in vivo. Plant Physiol. 41:467-474. doi: 10.1104/pp.41.3.467

Pratt, L.H. 1975. Photochemistry of high molecular weight phytochrome *in vitro*. Photochem. Photobiol. 22:33-36. doi: 10.1111/j.1751-1097.1975.tb06717.x

Procopio, M., J. Link, D. Engle, J. Witczak, T. Ritz, and M. Ahmad. 2016. Kinetic modeling of the Arabidopsis cryptochrome photocycle: FADHo accumulation correlates with biological activity. Front. Plant Sci. 7:888. doi: 10.3389/fpls.2016.00888

Rajapakse, N.C., R.K. Pollock, M.J. McMahon, J.W. Kelly, and R.E. Young. 1992. Interpretation of light quality measurements and plant response in spectral filter research. HortScience 27:1208-1211. doi: 10.21273/HORTSCI.27.11.1208

Rajapakse, N.C., and J.W. Kelly. 1994. Problems of reporting spectral quality and interpreting phytochrome-mediated responses. HortScience 29:1404-1407. doi: 10.21273/HORTSCI.29.12.1404

Rausenberger, J., A. Hussong, S. Kircher, D. Kirchenbauer, J. Timmer, F. Nagy, E. Schäfer,

and C. Fleck. 2010. An integrative model for phytochrome B mediated photomorphogenesis: from protein dynamics to physiology. PLoS One 5:e10721. doi: 10.1371/journal.pone.0010721

Roth, H.D. 2001. Twentieth century developments in photochemistry. Brief historical sketches. Pure Appl. Chem. 73:395-403.

Runkle, E.S., and R.D. Heins. 2001. Specific functions of red, far red, and blue light in flowering and stem extension of long-day plants. J. Amer. Soc. Hort. Sci. 126:275-282. doi: 10.21273/JASHS.126.3.275

Ruddat, A., P. Schmidt, C. Gatz, S.E. Braslavsky, W. Gärtner, and K. Schaffner. 1997. Recombinant type A and B phytochromes from potato. Transient absorption spectroscopy. Biochemistry 36:103-111. doi: 10.1021/bi962012w

Sager, J.C., W.O. Smith Jr., J.L. Edwards, and K.L. Cyr. 1988. Photosynthetic efficiency and phytochrome photoequilibria determination using spectral data. Trans. Am. Soc. Agric. Eng. 31:1882-1889. doi: 10.13031/2013.30952

Salisbury, F.B. 1981. Twilight effect: initiating dark measurement in photoperiodism of *Xanthium*. Plant Physiol. 67:1230-1238. doi: 10.1104/pp.67.6.1230

Schäfer, E. 1978. Variation in the rates of synthesis and degradation of phytochrome in cotyledons of *Cucurbita pepo* L. during seedling development. Photochem. Photobiol. 27:775-780. doi: 10.1111/j.1751-1097.1978.tb07676.x

Schmidt, R., and H. Mohr. 1982. Evidence that a mustard seedling responds to the amount of P_{fr} and not to the P_{fr}/P_{tot} ratio. Plant Cell Environ. 5:495-499. doi: 10.1111/1365-3040.ep11611856

Sellaro, R., R.W. Smith, M. Legris, C. Fleck, and J.J. Casal. 2019. Phytochrome B dynamics departs from photoequilibrium in the field. Plant Cell Environ. 42:606-617. doi: 10.1111/pce.13445

Seyfried, M., and L. Fukshansky. 1983. Light gradients in plant tissue. Appl. Optics 22:1402-1408. doi: 10.1364/AO.22.001402

Seyfried, M., and E. Schäfer. 1985. Action spectra of phytochrome *in vivo*. Photochem. Photobiol. 42:319-326. doi: 10.1111/j.1751-1097.1985.tb08947.x

Sharrock, R.A., and T. Clack. 2002. Patterns of expression and normalized levels of the five Arabidopsis phytochromes. Plant physiol. 130:442-456. doi: 10.1104/pp.005389

Siegelman, H.W., and S.B. Hendricks. 1964. Phytochrome and its control of plant growth and development. Adv. Enzymol. Relat. Areas Mol. Biol. 26:1-33. doi: 10.1002/9780470122716.ch1

Smith, H. 1973. Light quality and germination: Ecological implications, p. 219-231. In: W. Heydecker (ed.). Seed ecology. Pennsylvania State University Press, Pennsylvania, PA.

Smith, H., and M.G. Holmes. 1977. The function of phytochrome in the natural environment—III. Measurement and calculation of phytochrome photoequilibria. Photochem. Photobiol. 25:547-550. doi: 10.1111/j.1751-1097.1977.tb09126.x

Smith, H. 1981. Evidence that P_{fr} is not the active form of phytochrome in light-grown maize. Nature 293:163-165. doi: 10.1038/293163a0

Smith, H. 1982. Light quality, photoperception, and plant strategy. Ann. Rev. Plant Physiol. 33:481-518. doi: 10.1146/annurev.pp.33.060182.002405

Smith, H. 1983. Is P_{fr} the active form of phytochrome?. Philosophical Trans. Royal Soc. London 303:443-452. Doi: 10.1098/rstb.1983.0105

Smith, H. 1990. Phytochrome action at high photon fluence rates: rapid extension rate responses of light-grown mustard to variations in fluence rate and red:far-red ratio. Photochem. Photobiol. 52:131-142. doi: 10.1111/j.1751-1097.1990.tb01766.x

Smith, H., and D.C. Fork. 1992. Direct measurement of phytochrome photoconversion intermediates at high photon fluence rates. Photochem. Photobiol. 56:599-606. doi: 10.1111/j.1751-1097.1992.tb02208.x

Smith, H. 1994. Sensing the light environment: The functions of the phytochrome family, p. 377-416. In: R.E. Kendrick and G.H.M. Kronenberg (eds.). Photomorphogenesis in plants. Springer, Dordrecht, The Netherlands. doi: 10.1007/978-94-011-1884-2_15

Smith, H. 1995. Physiological and ecological function within the phytochrome family. Ann. Rev. Plant Biol. 46:289-315. doi: 10.1146/annurev.pp.46.060195.001445

Taylorson, R.B., and H.A. Borthwick. 1969. Light filtration by foliar canopies: significance for light-controlled weed seed germination. Weed Sci. 17:48-51. doi: 10.1017/S0043174500030873

Tóth, R., E. Kevei, A. Hall, A.J. Millar, F. Nagy, and L. Kozma-Bognár. 2001. Circadian clock-regulated expression of phytochrome and cryptochrome genes in *Arabidopsis*. Plant Physiol. 127:1607-1616. doi: 10.1104/pp.010467

Trupkin, S.A., M. Legris, A.S. Buchovsky, M.B.T. Rivero, and J.J. Casal. 2014. Phytochrome B nuclear bodies respond to the low red to far-red ratio and to the reduced irradiance of canopy shade in *Arabidopsis*. Plant Physiol. 165:1698-1708. Doi: 10.1104/pp.114.242438

Tucker, C.J. 1978. Red and photographic infrared linear combinations for monitoring vegetation. Remote Sens. Environ. 8:127-150. doi: 10.1016/0034-4257(79)90013-0

Vierstra, R.D., and P.H. Quail. 1983a. Photochemistry of 124 kilodalton *Avena* phytochrome *in vitro*. Plant Physiol. 72:264-267. doi: 10.1104/pp.72.1.264

Vierstra, R.D., and P.H. Quail. 1983b. Purification and initial characterization of 124 kdalton phytochrome from *Avena*. Biochemistry 22:2498-2505. doi: 10.1021/bi00279a029

Wang, Y., T. Zhang, and K.M. Folta. 2015. Green light augments far-red-light-induced shade response. Plant Growth Regulat. 77:147-155. doi: 10.1007/s10725-015-0046-x

Warrington, I.J., D.A. Rook, D.C. Morgan, and H.L. Turnbull. 1989. The influence of simulated shadelight and daylight on growth, development and photosynthesis of *Pinus radiata*, *Agathis australis* and *Dacrydium cupressinum*. Plant Cell Environ. 12:343-356. doi: 10.1111/j.1365-3040.1989.tb01951.x

Whitelam, G.C., E. Johnson, J. Peng, P. Carol, M.L. Anderson, J.S. Cowl, and N.P. Harberd. 1993. Phytochrome A null mutants of *Arabidopsis* display a wild-type phenotype in white light. Plant Cell 5:757-768. doi: 10.1105/tpc.5.7.757

Zhang, M., Y. Park, and E.S. Runkle. 2020. Regulation of extension growth and flowering of seedlings by blue radiation and the red to far-red ratio of sole-source lighting. Sci. Hort. 272:109478. doi: 10.1016/j.scienta.2020.109478

CHAPTER 4

IMPROVING THE PREDICTIVE VALUE OF PHYTOCHROME PHOTOEQUILIBRIUM: CONSIDERATION OF SPECTRAL DISTORTION WITHIN A LEAF[C]

4.1 Abstract

The ratio of active phytochrome (Pfr) to total phytochrome (Pr + Pfr), called phytochrome photoequilibrium (PPE; also called phytochrome photostationary state, PSS) has been used to explain shade avoidance responses in both natural and controlled environments. PPE is commonly estimated using measurements of the spectral photon distribution (SPD) above the canopy and photoconversion coefficients. This approach has effectively predicted morphological responses when only red and far-red (FR) photon fluxes have varied, but controlled environment research often utilizes unique ratios of wavelengths so a more rigorous evaluation of the predictive ability of PPE on morphology is warranted. Estimations of PPE have rarely incorporated the optical effects of spectral distortion within a leaf caused by pigment absorbance and photon scattering. We studied stem elongation rate in the model plant cucumber under diverse spectral backgrounds over a range of one to 45 percent FR (at total photon flux density, 400 to 750 nm, of 400 μmol m^{-2} s^{-1}) and found that PPE was not predictive when blue and green varied. Preferential absorption of red and blue photons by chlorophyll results in an SPD that is relatively enriched in green and FR at the phytochrome molecule within a cell (located both within the cytosol and the nucleus). This

[C] Kusuma, P., and B. Bugbee. Accepted in Frontiers in Plant Science.

can be described by spectral distortion functions for specific layers of a leaf. Multiplying the photoconversion coefficients by these distortion functions yields photoconversion weighting factors that predict phytochrome conversion at the site of photon perception within leaf tissue. Incorporating spectral distortion improved the predictive value of PPE when phytochrome was assumed to be homogeneously distributed within the whole leaf. In a supporting study, the herbicide norflurazon was used to remove chlorophyll in seedlings. Using distortion functions unique to either the green or the white cotyledons we came to the same conclusions as with whole plants in the longer-term study. Leaves of most species have similar spectral absorbance so this approach for predicting PPE should be broadly applicable. We provide a table of the photoconversion weighting factors. Our analysis indicates that the simple, intuitive ratio of FR (700 to 750 nm) to total photon flux (far-red fraction) is also a reliable predictor of morphological responses like stem length.

4.2 Introduction

LED technology provides a high degree of control over spectral output, which can be utilized to manipulate plant photoreceptors, but this manipulation requires an understanding of the photoreceptor activity. The action of phytochrome, the most well studied photoreceptor, has been extensively modeled (Sage, 1992), and our understanding continues to evolve (Sellaro et al., 2019; Smith and Fleck, 2019). In addition to predicting plant morphology in the field, phytochrome models must be able to predict morphology in controlled environments that can have unique background spectra.

Here we describe the historic and evolving modeling of phytochrome action that is largely based on stem/hypocotyl elongation. We discuss how these models have mostly ignored the issue spectral distortion by chlorophyll screening in green plants, and show that accounting for spectral distortion within leaves improves the predictive capability of classic phytochrome models.

4.2.1 A Historic Review of Phytochrome Modeling

Models of phytochrome action were developed in parallel with its discovery. The first models included the photon absorbing pigment phytochrome and reaction partners (Borthwick et al., 1952), where two forms of phytochrome were interconverted by red (R) and far-red (FR) photons. Later, Hartmann (1966) provided a hypothesis to explain how phytochrome controlled the high irradiance response. He simultaneously irradiated hypocotyls with photons at two wavelengths, and explained the results with an estimate of the ratio of Pfr to Ptotal [called phytochrome photoequilibrium (PPE) or the photostationary state (PSS)], where Ptotal is the sum of Pr plus Pfr.

Hartmann's work was praised by Smith (1975), who hypothesized that the PPE ratio explained phytochrome regulated responses in mature plants in the natural environment (Smith, 1973). Morgan and Smith (1976) provided evidence for this hypothesis by showing a direct linear relationship between PPE and the log of the stem extension rate. Morgan and Smith (1979) went on to show that this log linear relationship generally held for multiple species that evolved in a range of environments with the exception of understory plants that evolved in woodland areas, which had either a reduced or absent response. Child and Smith

(1987) further built upon this hypothesis, showing that the rapid percentage increase in stem extension rate after applying FR was linearly correlated with PPE.

Smith and collaborators either measured PPE directly in etiolated tissue (Morgan and Smith, 1976; Smith, 1990) or estimated it with the R:FR ratio (Morgan and Smith, 1978; Morgan and Smith, 1979). It is now common to predict PPE from the spectral photon distribution (SPD) above the canopy and photoconversion coefficients: σ_R for the conversion of Pr → Pfr, and σ_{FR} for the conversion of Pfr → Pr. These coefficients are essentially probability functions that predict the likelihood of photon absorbance at a given wavelength and subsequent conversion to the other form. The calculation to estimate PPE following this method is as follows:

$$\mathrm{PPE}\left(\frac{\mathrm{Pfr}}{\mathrm{Ptotal}}\right) = \frac{\sum_{\lambda=300\ \mathrm{nm}}^{\lambda=800\ \mathrm{nm}} I_\lambda\ \sigma_{R,\lambda}}{\sum_{\lambda=300\ \mathrm{nm}}^{\lambda=800\ \mathrm{nm}} I_\lambda\ \sigma_{R,\lambda}\ +\ \sum_{\lambda=300\ \mathrm{nm}}^{\lambda=800\ \mathrm{nm}} I_\lambda\ \sigma_{FR,\lambda}} \tag{4.1}$$

Where I_λ is the incident photon flux density at wavelength, λ. Photoconversion coefficients are calculated from *in vitro* measurements of the photochemical properties of phytochrome including: 1) absorbance spectra, 2) an estimation/calculation of PPE under actinic red photons, 3) the extinction coefficient of Pr at the peak in the red region (about 668 nm) and 4) quantum yields of Pr → Pfr and Pfr → Pr. Different photochemical properties are provided in at least ten publications (see Lagarias et al., 1987; Mancinelli, 1986, 1988, 1994). Thus it is possible to derive different photoconversion coefficients (Here, the term photoconversion coefficient refers to what has historically been called the photochemical/photoconversion cross-section, whereas the term photoconversion coefficient

historically refers to the photochemical cross-section divided by the natural log of 10. Because coefficient is a more friendly term, we use this term instead of cross-section).

These photoconversion coefficients, however, are primarily based on phytochrome-A (phyA) and not phyB. The phyB photoreceptor is the primary phytochrome photoreceptor responsible for sensing and responding to shade in the natural environment (Legris et al., 2019). Although phyA plays a larger role during de-etiolation (Mazzella and Casal, 2001), only monogenic mutants deficient in phyB (compared to monogenic mutants deficient in phyA, phyC, phyD or phyE) appear elongated when grown in white light indicating the dominant role of phyB past the stage of de-etiolation (Whitelam et al., 1993; Aukerman et al., 1997; Devlin et al., 1998, 1999; Franklin et al., 2003; Franklin and Quail, 2010). Some limited evidence suggests that the photochemical properties of phyA and phyB may be similar (Ruddat et al., 1997; Eichenberg et al., 2000). If so, the fact that the photoconversion coefficients are derivation from primarily phyA may not be a significant concern.

Estimates of PPE using photoconversion coefficients and the SPD above the leaf were used by Park and Runkle (2017, 2018, 2019) whose data shows a linear (as opposed to log linear) relationship between estimated PPE and stem length in several ornamental species. Overall, PPE estimates have resulted in a negative relationship with stem length. One limitation of most previous studies is that they typically performed under a single background of light and treatments often only change the amount of FR and occasionally the amount of R. Thus, the full extent of the reliability of estimated PPE to predict morphology has not been determined.

4.2.2 Recent PPE Modeling Efforts

The three-state model. The model described above (PPE = Pfr / Ptotal) is called *the two- state model*. A more complex model considers the dimerization of the phytochrome molecule in which the two arms of the dimer are activated independently. This is called *the three-state model*. It assumes only the Pfr-Pfr homodimer (called D_2) is the active form, while the Pr-Pr homodimer (D_0) and the Pr-Pfr heterodimer (D_1) are both inactive. Therefore *the three-state model* at photoequilibrium is equal to $D_2/(D_0+D_1+D_2)$, which can be calculated by squaring PPE calculated by *the two-state model* (PPE^2; Mancinelli, 1988, 1994). Although there is sufficient evidence to suggest that phytochrome exists as a dimer (Jones and Quail, 1986; Brockmann et al., 1987; Rockwell et al., 2006) the evidence that only D_2 is the active form is at present only based on mathematical analysis (Klose et al., 2015), and further investigation is required.

The cellular model. Thermal reversion, phytochrome destruction and nuclear body association/disassociation can either reduce or stabilize the pool of active phytochrome (Rausenberger et al., 2010; Klose et al., 2015). When these factors are considered the model is referred to as *the cellular model*. Sellaro et al. (2019) described that these other factors mainly play a role at low photon fluxes and/or high temperature, while only photoconversions apply at sufficiently high photon fluxes and low enough temperature. This model is thoroughly described in Smith and Fleck (2019). These complex models have yet to be used in applied research.

4.2.3 Spectral Distortions within Leaves

Leaves/cotyledons, and not stems/hypocotyls, were shown to be the primary site of red and far-red perception in *Cucumis sativa* (Black and Shuttleworth, 1974), *Sinapis alba* (Casal and Smith, 1988a), *Arabidopsis thaliana* (Tanaka et al., 2002; Endo et al., 2005) and *Brassica rapa* (Procko et al., 2016), while both organs were shown to be perceptive in a separate study in *Sinapis alba* (Casal and Smith, 1988b) and the epicotyl was shown to be the primary site of perception in *Vigna sinensis* (Garcia-Martinez et al., 1987). Upon far-red perception in leaves/cotyledons, signals (including auxin) are transported to the stem/hypocotyl to induce elongation (Tanaka et al., 2002; Procko et al., 2016). From these data, it seems likely that phytochrome in the leaves/cotyledons play a dominant role in controlling stem elongation, with stems/hypocotyls playing a secondary role.

A major issue with using photoconversion coefficients to estimate PPE is that they are applied to the SPD above the leaf, and not the SPD at the phytochrome molecule, which is distorted by chlorophyll and other pigments, as well as cell walls. Photons are scattered within leaves making the light diffuse within leaves (**Figure 4-1**). Due to this internal reflection, refraction and diffraction, leaves act as 'light traps' wherein the photon intensity in the epidermis can exceed the intensity above the leaf by several fold (Seyfried and Fukshansky, 1983; Vogelmann, 1994). Because the term attenuation specifically refers to a decrease in the photon intensity, we use the term distortion to describe spectral changes in leaves.

Both Morgan and Smith (1978) and Gardner and Graceffo (1982) discuss chlorophyll screening issues stating that estimates of PPE (above the leaf) are only accurate for the top epidermal layer of cells within a leaf. Gardner and Graceffo (1982) suggested that the

functional layer of phytochrome must be near the outer epidermal layer because of the linear relationship between PPE and the log stem extension rate seen in Morgan and Smith (1976). These assumptions are invalid because spectral distortions still occur in the epidermis, and additionally, several studies have shown that the peaks of phytochrome regulated action

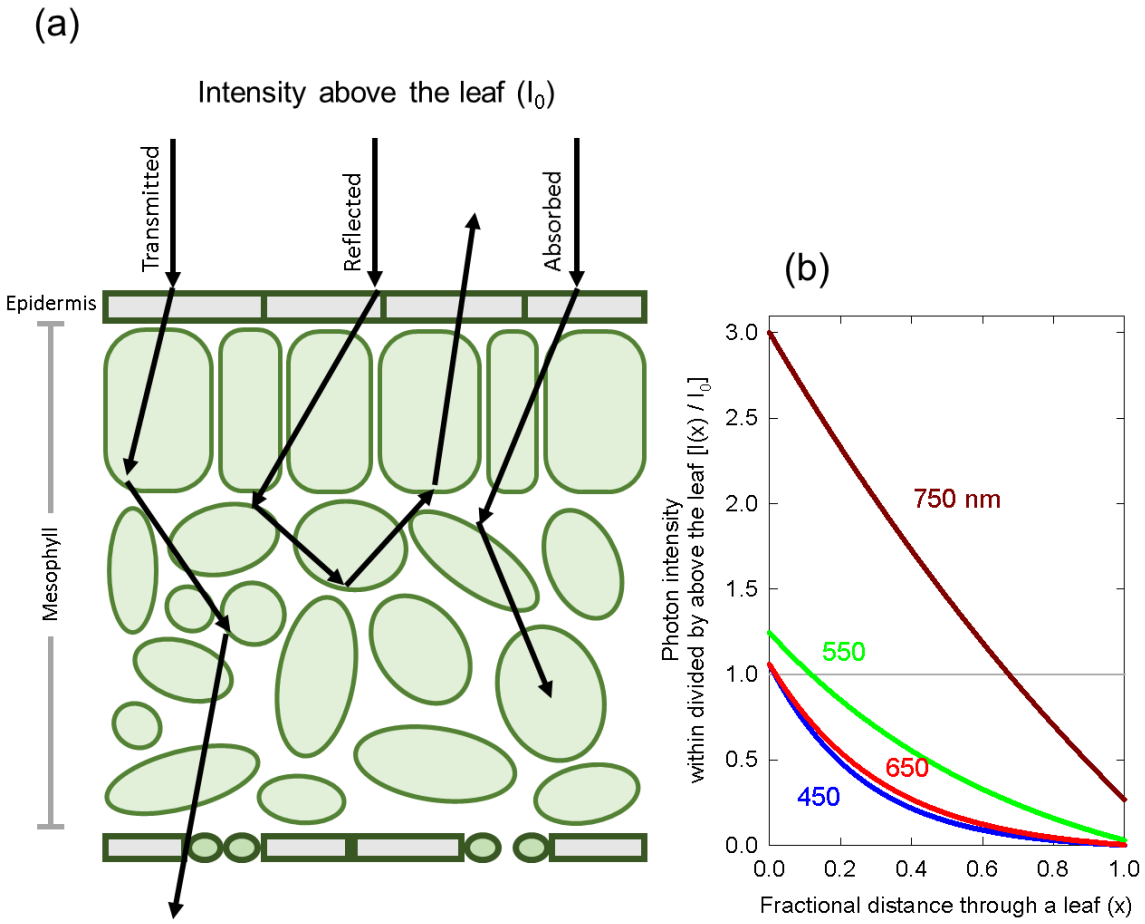

FIGURE 4-1: Basic principles of spectral distortion and photon scattering within a leaf. (a) A diagram of a cross section of a leaf showing the scattering of photons, which are eventually transmitted, reflected or absorbed. (b) A graphical representation of photon intensity at wavelengths 450, 550, 650 and 750 nm as a function of leaf depth. Because of reflections, diffraction and refraction, the photon intensity in the top layers of a leaf can exceed the intensity above the leaf. The Kubelka-Munk theory was used to calculate photon intensity with depth. The grey horizontal line represents the photon intensity just above the leaf.

spectra shift to lower wavelengths than the peak absorbance of extracted phytochrome, indicating that some degree of spectral distortion occurs within leaves. For example, Kasperbauer et al. (1963) observed that inhibition of flowering in *Chenopodium rubrum* was most affected by night break lighting at 645 nm, instead of the expected 660 (or 668) nm, an effect they attributed to spectral filtering by chlorophyll. Similarly, Jose and Schafer (1978) found that 630 nm photons induced the shortest hypocotyls and internodes in green tissue.

Several attempts have been made to account for spectral distortion within a leaf, especially via Kubelka-Munk theory. The Kubelka-Munk theory describes light propagation within a scattering medium like a leaf (Vogelmann, 1994). It simplifies to the Beer-Lambert law if extinction and scattering coefficients are assumed to be constant and not dependent on fractional distance through the leaf (Evans, 1995). Holmes and Fukshansky (1979) modeled PPE through a green leaf using the Kubelka-Munk theory and estimated that PPE decreased by about 40% as it moved through a leaf under full sunlight. Later, Kazarinova-Fukshansky et al. (1985) used the Kubelka-Munk theory to develop distortion functions that describe photon gradients within zucchini cotyledons. These distortion functions can be multiplied by the phytochrome photoconversion coefficients to develop weighting factors that can be used to predict the action spectra of phytochrome conversions within a certain layer of cotyledon tissue based on the incident photon flux above the leaf. Little has been done to test predictions of PPE with these weighting factors using experimental data. As such, despite the efforts of Kazarinova-Fukshansky et al. (1985), above-the-leaf estimates are still regularly employed.

Because the degree of spectral distortion depends on the specific layer of the leaf, it is important to ask whether all phytochrome is ‘functional’. The epidermis has been shown to

control the rate of elongation (Kutschera and Niklas, 2007; Savaldi-Goldstein et al., 2007), but whether the epidermis is where the light signals are perceived, especially in leaf/cotyledon tissue, remains undetermined. Phytochrome is expressed in all tissue (Somers and Quail, 1995), but Kim et al. (2016) concluded that only phytochrome in epidermal tissue (of the hypocotyl) controlled elongation under continuous R light and end-of-day FR. This conclusion was based on transgenic lines of *Arabidopsis thaliana* that controlled *PHYB* expression using hypocotyl-tissue-specific promoters, effectively limiting phyB to specific layers of hypocotyl tissue (i.e. epidermis, cortex, endodermis and vasculature). Endo et al. (2005) similarly expressed phytochrome in tissue specific organs and found that mesophyll-located phytochrome (in the cotyledons) controlled elongation.

Our objective was to use models of spectral distortion within a leaf (both for epidermal-located phytochrome and homogeneously distributed phytochrome) to improve the predictive relationship between PPE and morphological parameters.

4.3 Materials and Methods

Two studies were conducted:

1) Cucumber plants were grown for 10 to 15 days in growth chambers with unique spectral backgrounds and different doses of FR (long-term study)

2) Elongation of photobleached and green cucumber seedlings were compared after two days in the growth chambers with a gradient of FR (short-term photobleaching study)

In both studies, multiple models of spectral distortion were used to predict PPE in specific layers of tissue.

4.3.1 Plant Materials

4.3.1.1 Long-term Study

Tomato, lettuce, spinach, soybean and cucumber were screened for sensitivity to FR by applying either a low dose or no added FR. Cucumber was the most sensitive species to FR and was selected for further study (example data from one tomato study is shown in **Figure G-1**).

Seeds of cucumber (*Cucumis sativa* cv. Straight Eight) were planted into 1.7 L pots with a 1:1 mixture of peat/vermiculite by volume amended with 1.6 g per liter of dolomitic lime and 0.8 g per liter Gypsum ($CaSO_4$). Cotyledons emerged four days after planting and pots were moved from the greenhouse to the growth chambers (**Figure G-2**).

4.3.1.2 Short-term Photobleaching Study

Nine cucumber seeds were germinated on black felt saturated with nutrient solution (Utah hydroponic refill solution for dicots, USU Crop Physiology Laboratory, 2020) in each of 22 germination boxes (18×16.5 cm^2) at 21 ˚C. Black felt was used to minimize ground reflection so photons would primarily enter the cotyledons from above (**Figure G-3**). After three days the radicle had emerged, and nutrient solution was re-applied, with half of the germination boxes (11 boxes) receiving 50 μM norflurazon in the nutrient solution. Norflurazon is an herbicide that blocks the synthesis of carotenoids, leading to

photobleaching in high light, eventually killing the plant. Seeds were then moved into pretreatment conditions: two norflurazon treated and two non-treated boxes were moved into the dark and the remainder of the boxes were moved into a growth chamber with a continuous photosynthetic photon flux density (PPFD) of about 500 μmol m^{-2} s^{-1} (**Figure G-4**) and a temperature of 20 ˚C to finish emerging. 12% of the seeds either did not germinate or were not vigorous and all boxes had at least 6 seedlings. After three days in the pretreatment the norflurazon treated seedlings appeared white with an average hypocotyl length of 1.4 cm and the non-photobleached seedlings had an average hypocotyl length of 1.2 cm. Three days in continuous light reduces the concentration of highly light-labile phyA, which was shown to be reduced by 50- to 100-fold after 12 h under low red photon flux and were below detectable limits after 7 d in white light (Sharrock and Clack, 2002). This ensured that responses were primarily caused by phyB. The germination boxes were placed in seedling trays with one photobleached and one non-photobleached germination box in each tray. Trays were then placed in the growth chambers for 48 h. This was repeated four times.

4.3.2 Environmental Conditions

4.3.2.1 Long-term Study

Temperature was maintained at 27/22 ˚C day/night. Plants were watered as needed (typically every 2-3 days) with a complete nutrient solution at a concentration of 120 mg N per L (Peter's professional 20-10-20, 20N-4.4P-16.6K; Allentown PA). Potassium silicate (AgSil16H; Certis USA; Columbia MD) was added to the nutrient solution at 0.3 mM Si.

Chambers were enriched to 850 ppm CO_2. All studies contained six replicate plants per treatment. Plants were rotated every other day to minimize any position effects in the chamber. Individual plants were analyzed as replicates. Plant density was 20 plants per square meter.

4.3.2.2 Short-term Photobleaching Study

Temperature was maintained at a constant 20 ˚C. The norflurazon treated seedlings lost turgor at low humidity so water was added to the tray and the tray was covered to raise the humidity. Condensation formed on the lid of the seedling trays.

4.3.3 Spectral Treatment

Spectral measurements were made with a spectroradiometer (PS-300; Apogee instruments; Logan, UT). For both the long-term and the short-term studies, three growth chambers (1.25 × 0.9 × 1.2 m^3, L × W × H) provided separate background SPD from either cool white LED fixtures, 400-W high-pressure sodium (HPS) fixtures, or white+red LED fixtures. These background spectral distributions are common in controlled environment agriculture and are referred to here as high blue (cool white LED), high green (HPS) and high red (white+red LED). Spectral data for these background spectra are provided in **Table 4.1** and **Figure 4-2**.

TABLE 4.1: Ratios of colors for the three spectral backgrounds.

Treatment	%BLUE $\frac{\sum 400 - 499\ nm}{\sum 400 - 700\ nm}$	%GREEN $\frac{\sum 500 - 599\ nm}{\sum 400 - 700\ nm}$	%RED $\frac{\sum 600 - 699\ nm}{\sum 400 - 700\ nm}$	Total
HIGH BLUE	29	48	23	100
HIGH GREEN	6	52	42	100
HIGH RED	7	12	81	100

4.3.3.1 Long-term Photobleaching Study

Each chamber was separated in half with a white reflective board to provide a higher and lower level of FR from LEDs (peak of 730-735 nm). This allowed for two fractions of FR in each trial in time. Cucumber plants in the chambers at the end of one of these studies are shown in **Figure 4-3a**. The FR fraction was then varied among trials to achieve a collective range of 1 to 45% FR across seven replicate trials for a total of 14 doses of FR in each spectral background. Using regression analysis with plant rotation, this provided 84 replicates (six replicate plants × 14 doses of FR) for each spectral background.

Percent far-red (FR fraction) was calculated as:

$$\text{Percent far red} = \frac{\text{FR flux } (701 - 750\ \text{nm})}{\text{ePPFD } (400 - 750\ \text{nm})} \times 100 \tag{4.2}$$

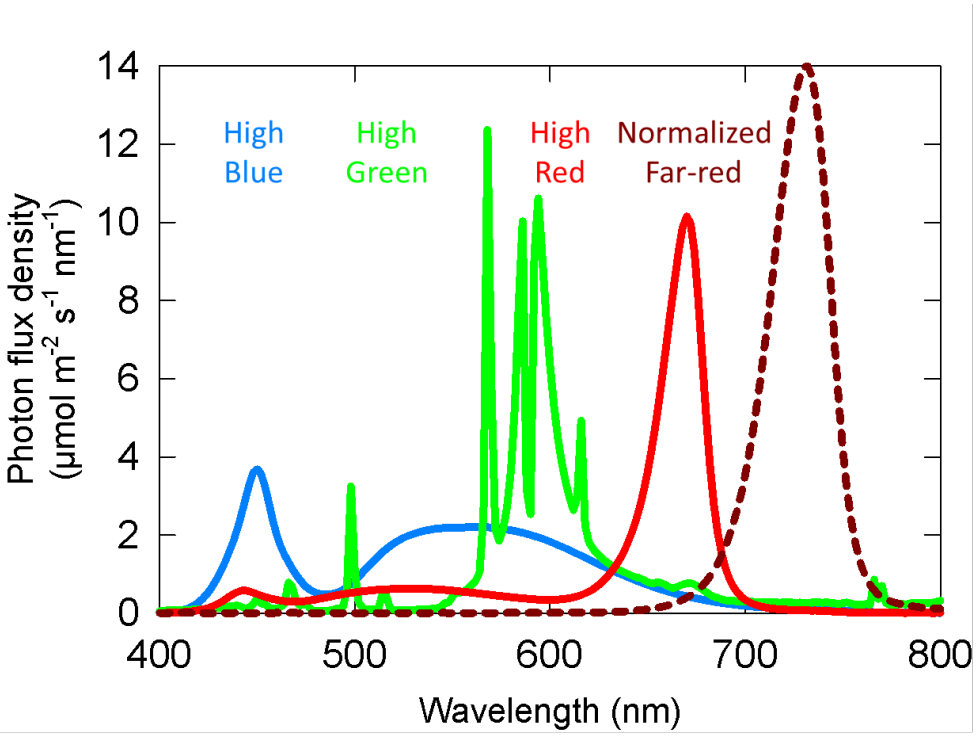

FIGURE 4-2: Representative spectral photon distributions (SPD) of the high blue, high green and high red spectra used in both the long-term and short-term studies. The dashed dark red line is the SPD of the far-red, which was variable among studies.

Because FR photons are photosynthetically active (Zhen and van Iersel, 2017; Zhen and Bugbee, 2020), the extended photosynthetic photon flux density (ePPFD: 400 – 750 nm) was kept constant among studies. This meant that as FR increased, the traditional PPFD (400 – 700 nm) decreased. For ePPFD, a cut-off wavelength of 750 nm may slightly overestimate photosynthetic photons (Zhen et al., 2018), but this definition is adequate for FR from LEDs. The average ePPFD was 400 and carefully adjusted so that it varied less than 10 µmol m^{-2} s^{-1} among the background spectra in each study. The photoperiod was 16 h. Detailed spectral information showing the one to 45% FR is provided in **Table G.1** and **Figure G-5**.

4.3.3.2 Short-term Photobleaching Study

The background light fixtures were placed at the top of one side of the chamber and FR LED bars were placed on the other side of the chamber to provide a gradient of FR that increased from right to left while PPFD increased from left to right. Seedling trays were placed on the left, middle and right sides of the chamber to obtain about 18, 31 and 50% FR for each background spectrum. A photo of the experimental set-up is provided in **Figure 4-3b**. The average ePPFD in these studies was 300 µmol m^{-2} s^{-1} and varied less than 15 µmol m^{-2} s^{-1} among the background spectra. The spectral photon distributions for these studies are shown in **Figure G-6**. Light was applied continuously for the whole 48 h treatment period.

4.3.4 Estimation of PPE

We calculated PPE (assuming *the two-state model*) following Eq (4.1). We used the photoconversion coefficients derived from the photochemical properties in Lagarias et al. (1987). These are different from other commonly used photoconversion coefficients (Kelly and Lagarias, 1985; Sager et al., 1988) on an absolute scale, but are similar when normalized to the Pr peak. The absolute magnitudes of the photoconversion coefficients are only important if other rates of phytochrome dynamics, like thermal reversions, are considered.

4.3.5 Estimation of the Three-state Model

We did not account for the additional factors in the cellular model proposed by Rausenberger et al. (2010) and modified by Klose et al. (2015). Sellaro et al. (2019) reported

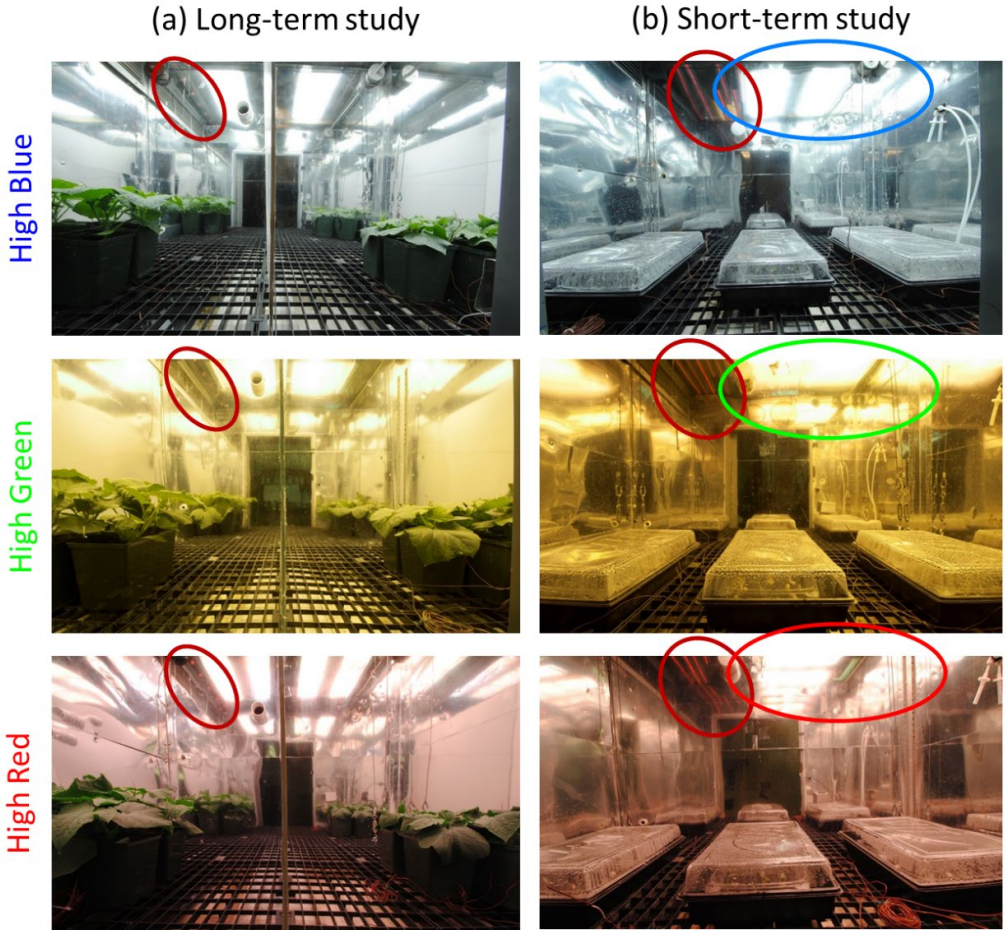

FIGURE 4-3: Experimental set-up of plants in the long-term and short-term studies. (a) Example photo of the plants in the high blue, green and red chambers from the long-term studies. In this example there was no added FR on the right side in each chamber. Treatments were randomized among studies. Each chamber was divided in half to supply two doses of FR. FR LEDs are circled in red. There is a second FR LED on the other side of the background LED (out of view, see **Figure G-2**) to improve the uniformity of FR. Additionally, in studies with higher fractions of FR, LEDs were placed across the top of the chamber. Uniformity within and between treatments was ensured by dimming lamps with either power supply capabilities or neutral density window screen. To achieve uniformity of spectral photon distribution (SPD) and extended photosynthetic photon flux density (ePPFD), the plants were grown on the sides of each half-chamber. (b) Photo of the experimental set-up for short-term photobleached seedling study. Each chamber was provided with a high dose of FR on one side of the chamber and the background light source on the other side of the chamber. This provided a gradient of percent far-red decreasing from left to right. FR LEDs are circled in red, and the background light source is circled in its respective color. Seedlings (in germination boxes) were kept in seedling trays that were brought to a high relative humidity by placing water in the bottom of the tray.

that when the temperature is 25 ˚C, the cellular model reaches 99% of the three-state model (assuming only photoconversions) at PPFD of about 450 μmol m^{-2} s^{-1}, and when the temperature is 20 ˚C, the cellular model reaches 99% of the three-state model at PPFD of about 350 μmol m^{-2} s^{-1}. These conditions are close to the environmental conditions used in these experiments. Therefore, we used the simplified three-state model assuming the temperature effects on phytochrome reversion were negligible. As mentioned previously, the three-state model is simply calculated by squaring PPE calculated by Eq (4.1) (Mancinelli, 1988).

4.3.6 Modeling Spectral Distortion within a Leaf

We use spectral distortion functions derived from Kazarinova-Fukshansky et al. (1985) to predict spectral distortion at the phytochrome molecule under the assumption that 'functional' phytochrome is either 1) only located in the epidermis (top 1% of the leaf), or 2) homogeneously distributed within all layers of the leaf. All curves from Kazarinova-Fukshansky et al. (1985) were obtained using GetData Graph Digitizer (http://getdata-graph-digitizer.com). Kazarinova-Fukshansky et al. (1985) modeled spectral distortion using the Kubelka-Munk theory within 7 d old *Cucurbita pepo* cv. "Senator" (zucchini), a species closely related to cucumber.

The Kubelka-Munk theory-based distortion functions use transmittance and reflectance measurements, so we include this data in **Figure 4-4a** for etiolated and green zucchini seedlings (Kazarinova-Fukshansky et al., 1985). **Figure 4-4b** shows the distortion functions for green plants assuming 'functional' phytochrome is 1) only in the epidermal

tissue (orange lines) or 2) homogenously distributed throughout the whole leaf (purple lines). **Figure 4-4c** shows the same distortion functions in etiolated tissue.

The photoconversion coefficients derived from Lagarias et al. (1987) were multiplied by the distortion functions to obtain modeled estimates of phytochrome conversion weighting factors (or action spectra) in specific layers of tissue (Eq 4.3).

$$\text{Photoconversion weighting factor for Pr}(\lambda) = \sigma_{\text{R}}(\lambda) \times \text{Distortion coefficient}(\lambda)$$
$$\text{Photoconversion weighting factor for Pfr}(\lambda) = \sigma_{\text{FR}}(\lambda) \times \text{Distortion coefficient}(\lambda) \quad (4.3)$$

4.3.7 Plant Measurements

4.3.7.1 Long-term Study

Plants were harvested when the stem length in the highest FR treatment was 25 to 30 cm long; this occurred 10 to 15 days after emergence. Stem length, petiole length and leaf area were recorded. Leaf area was measured with a leaf area meter (model Li-3000, LI-COR, Lincoln NE). Leaves, cotyledons and stems were separated and dried at 80 ˚C for 2 d, after which dry mass was measured and percent leaf and percent stem dry mass were calculated by dividing the respective dry mass by the total dry mass.

Stems typically elongate following a sigmoidal curve (Fisher et al., 1996; Bjorkman, 1999) with exponential elongation in young plants (Morgan and Smith, 1978), followed by linear elongation, and finally, exponential rise to a maximum. This means that elongation is best described as a natural logarithm function in the early stages of growth. For this reason

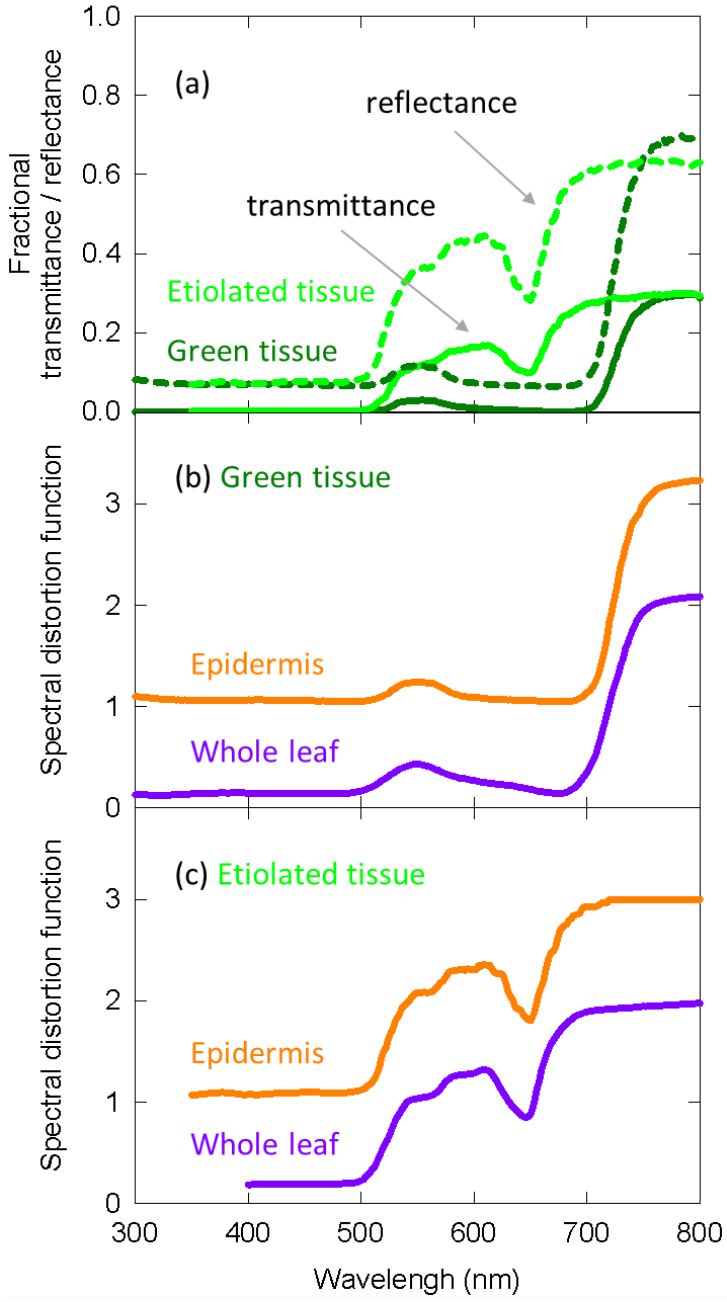

FIGURE 4-4: Spectral distortion functions developed from zucchini that were used in both the long-term and the short-term studies on elongation in cucumber. (a) Fractional transmittance (solid) and reflectance (dashed) spectra of green and etiolated zucchini cotyledons. Etiolated cotyledons represented norflurazon treated cotyledons. (b) Derived spectral distortion functions for green plants in epidermal tissue (orange) or the whole leaf (purple). (c) Derived spectral distortion functions in etiolated/white seedlings for epidermal tissue (orange) or the whole leaf (purple). All data are derived from Kazarinova-Fukshansky et al. (1985).

early studies regularly used log-linear stem elongation rates to predict elongation from phytochrome photoequilibrium (Morgan and Smith, 1976, 1978, 1979). , Thus in young plants, stem length at day (t) would be equal to:

$$\text{Stem length}(t) = \text{Stem length}(i)e^{\text{k}t} \tag{4.4}$$

Where Stem length(i) is the initial length. The assumptions to log-linear elongation is compared to linear elongation in **Figure G-7**. We can then calculate the exponential extension coefficient (the natural log of the stem extension rate; lnSER or k in Eq 4.4), assuming the initial stem length was equal to one, as follows:

$$\text{lnSER} = \frac{\ln(\text{Stem length at harvest})}{\text{days to harvest}} \tag{4.5}$$

The assumptions of Stem length(i) being equal to one is investigated in **Figure G-8**. This equation was also used to calculate the leaf expansion coefficient (natural log of the leaf expansion rate; lnLER) and the petiole extension coefficient (natural log of the petiole extension rate; lnPER). Chlorophyll concentration was measured with a chlorophyll meter (model MC-100, Apogee instruments, Logan UT).

4.3.7.2 Short-term Photobleaching Study

Cucumber hypocotyl lengths were measured with a ruler to the nearest 0.5 mm before and after they were moved into the treatments. The change in hypocotyl length over 48 h was normalized to the elongation of the respective dark control:

$$\text{Elongation relative to the control} = \frac{L_f - L_i}{L_{c,t2} - L_{c,t1}} \tag{4.6}$$

Where L_f is the final hypocotyl length, L_i is the initial hypocotyl length, and $L_{c,t1}$ and $L_{c,t2}$ are the average hypocotyl lengths of the dark controls before or after the cucumber seedlings were placed in the treatments. The change in hypocotyl length was normalized to its respective control (with or without applied norflurazon) due to the finding of Casal (1995) in which norflurazon treated seedlings grown in the dark were 15 to 20% shorter than untreated seedlings. For each replicate in time, the elongation relative to the control for all the seedlings in each treatment were averaged together.

4.3.8 Statistics

All data was analyzed using R statistical software (R Foundation for Statistical Computing; Vienna, Austria). Correlations were determined by calculating the r^2 value of a trend-line through the data. Trend-lines used either linear or exponential decay functions. Data was analyzed using a mixed effect linear model using *lmer* and *Anova* functions with the F statistic judged to be significant at $p < 0.05$. The background spectra (e.g. high blue) were treated as a categorical variable, while different methods for analyzing the effect of FR were treated as a continuous variable. Two examples of methods for analyzing the effects of far-red include percent FR and PPE modeled above the leaf. Chambers and replicates were treated as random factors.

4.4 Results

4.4.1 Long-term Photobleaching Study

The percent far-red ranged from less than 2% (which is only obtainable under LEDs) to 45% (typical of canopy shade). **Figure 4-5** shows the response of seven morphological parameters to increasing percent FR under three diverse spectral backgrounds. lnSER, lnLER, lnPER and percent stem mass all increase with increasing percent FR (**Figure 4-5a-c,g**). Chlorophyll concentration and percent leaf mass both decreased with increasing percent FR (**Figure 4-5d,f**). Specific leaf mass, which is calculated by dividing leaf mass by leaf area and is an indicator of leaf thickness, was unaffected by percent FR ($p = 0.19$, **Figure 4-5e**). Because lnSER had the highest correlation with percent FR it was used as the response variable for models of PPE within leaf tissue.

4.4.1.1 Accounting for Spectral Distortions in Predictions of PPE

Multiplying the spectral distortion functions (**Figure 4-4b**) by the photoconversion coefficients (Eq 4.3) provides weighting factors that predict local phytochrome conversions within a specific layer of tissue for a given SPD above the leaf (**Figure 4-6**). It is important to note that a) the photochemical properties of phytochrome, and thus the photoconversion coefficients, have not changed and that b) if no spectral distortion occurs within a leaf, then the photoconversion weighting factors are equal to the photoconversion coefficients.

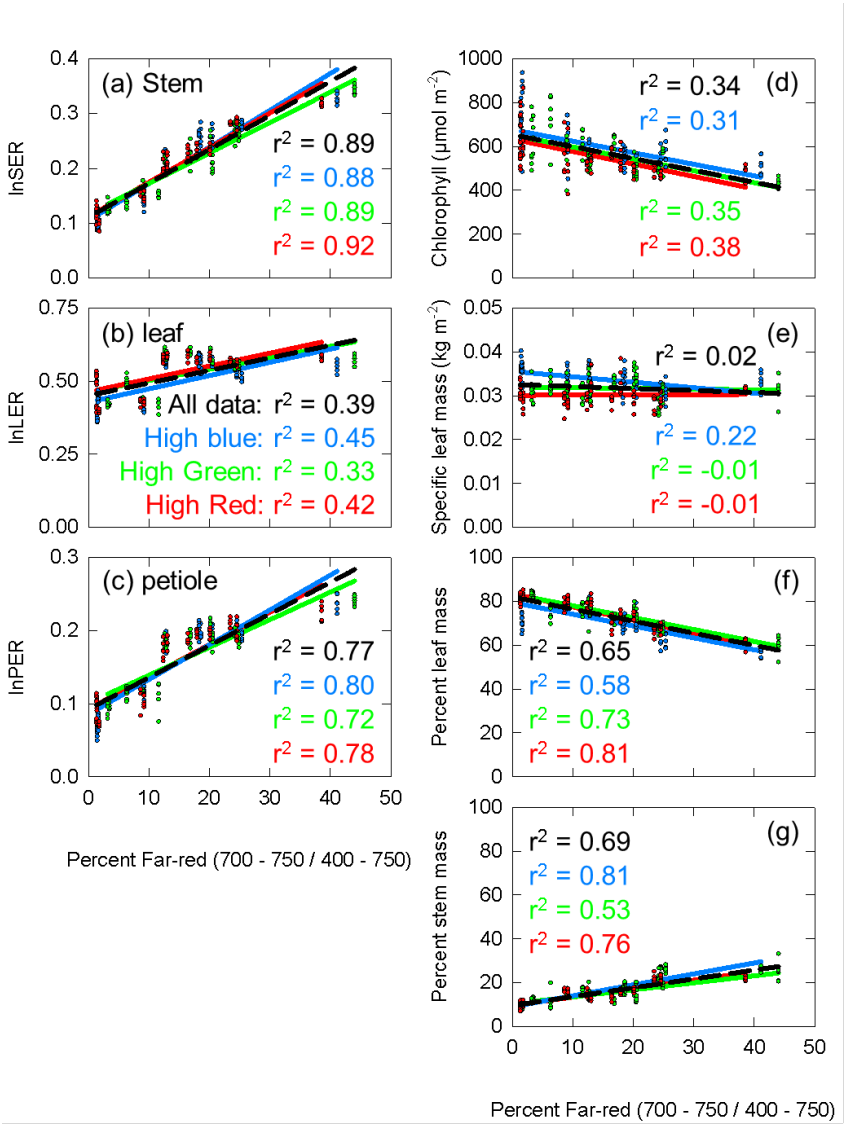

FIGURE 4-5: The response of seven physiological parameters to increasing percent far-red. The blue data and lines come from the chamber with spectral background containing a high portion of blue photons (high blue), the green data comes from the high green chamber, and the red data comes from the high red chamber. The r-squared value for each background is shown with the respective color. The black dashed line is a trend line running through all the data from all three background light sources, with the corresponding r-squared shown in black. (a) The stem extension rate constant (the natural log of the stem extension rate, lnSER; described in Eqs (4.3) and (4.4)). (b) The leaf expansion rate constant, calculated following the same method as lnSER, but using leaf area at harvest instead of stem length. (c) Petiole expansion rate constant, calculated following the same method as lnSER, but using petiole length at harvest instead of stem length. (d) Chlorophyll concentration at harvest (e) Specific leaf mass, leaf mass divided by leaf area. (f) Percent leaf mass, leaf mass divided by total shoot mass (g) percent stem mass, stem mass divided by total shoot mass.

Figure 4-6 shows that weighting factors for Pfr (Pfr → Pr) increase relative to Pr (Pr → Pfr) as the location of phytochrome moves from the epidermis to all leaf/cotyledon tissue. The weighting factors for Pr do not significantly shift the peak of action away from about 668 nm.

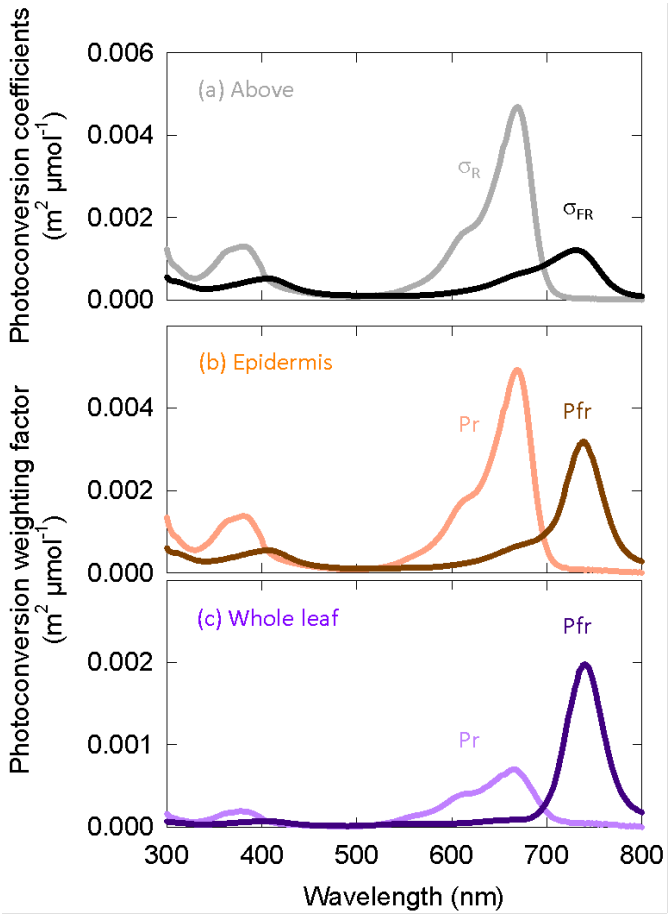

FIGURE 4-6: Photoconversion coefficients and photoconversion weighting factors for phytochrome conversion. (a) Photoconversion coefficients derived from Lagarias et al. (1987). These are used to estimate PPE above the canopy. The other two graphs are the photoconversion weighting factors for phytochrome that is (b) only in epidermal tissue or (c) homogeneously distributed through all leaf/cotyledon tissue.

Using σ_R and σ_{FR} (**Figure 4-6a**) in Eq (4.1) or substituting them with the Pr and Pfr weighing factors (**Figure 4-6b, c**) produces estimates PPE in three layers: PPE_{above},

$PPE_{epidermis}$ and $PPE_{whole\ leaf}$. We fit the lnSER data in **Figure 4-5a** to the estimates of PPE in these three layers assuming the commonly used *two-state model* (**Figure 4-7**). There was a high correlation between PPE estimated above the leaf (PPE_{above}) and lnSER for any single background SPD (**Figure 4-7a**; $r^2 = 0.91$, 0.89 and 0.85 for high blue, high green and high red, respectively). This relationship declines if PPE is compared to all the data (all three background spectra, dashed line, $r^2 = 0.47$). The correlation between PPE and lnSER for any single background spectrum remained relatively unchanged when PPE was estimated in the epidermal leaf tissue ($PPE_{epidermis}$) or the whole leaf ($PPE_{whole\ leaf}$), but the relationship with all the data was improved when predicted within the leaf (**Figure 4-7b, c**). $PPE_{whole\ leaf}$ produced the highest correlation between PPE and lnSER of all the data ($r^2 = 0.75$, **Figure 4-7c**).

4.4.1.2 Comparison between the *Two-state* and *Three-state models*

The two-state and *three-state models* of phytochrome were compared assuming the active phytochrome was a) in the epidermis and b) homogeneously distributed in all the leaf tissue (**Figure 4-8** compared to **Figure 4-7b, c**). Using regression analysis through all three spectral backgrounds, *the three-state model* did not improve the predictive power over the commonly used *two-state model* for any of the three assumed locations of phytochrome ($r^2 =$ 0.58 and 0.72 for $PPE_{epidermis}$ and $PPE_{whole\ leaf}$, respectively).

To further investigate differences between these four estimates of PPE (**Figure 4-7b, c** and **Figure 4-8**), the slopes and offsets for the three individual background spectra (blue, green and red lines) were compared using a linear mixed effects model, with the estimates of

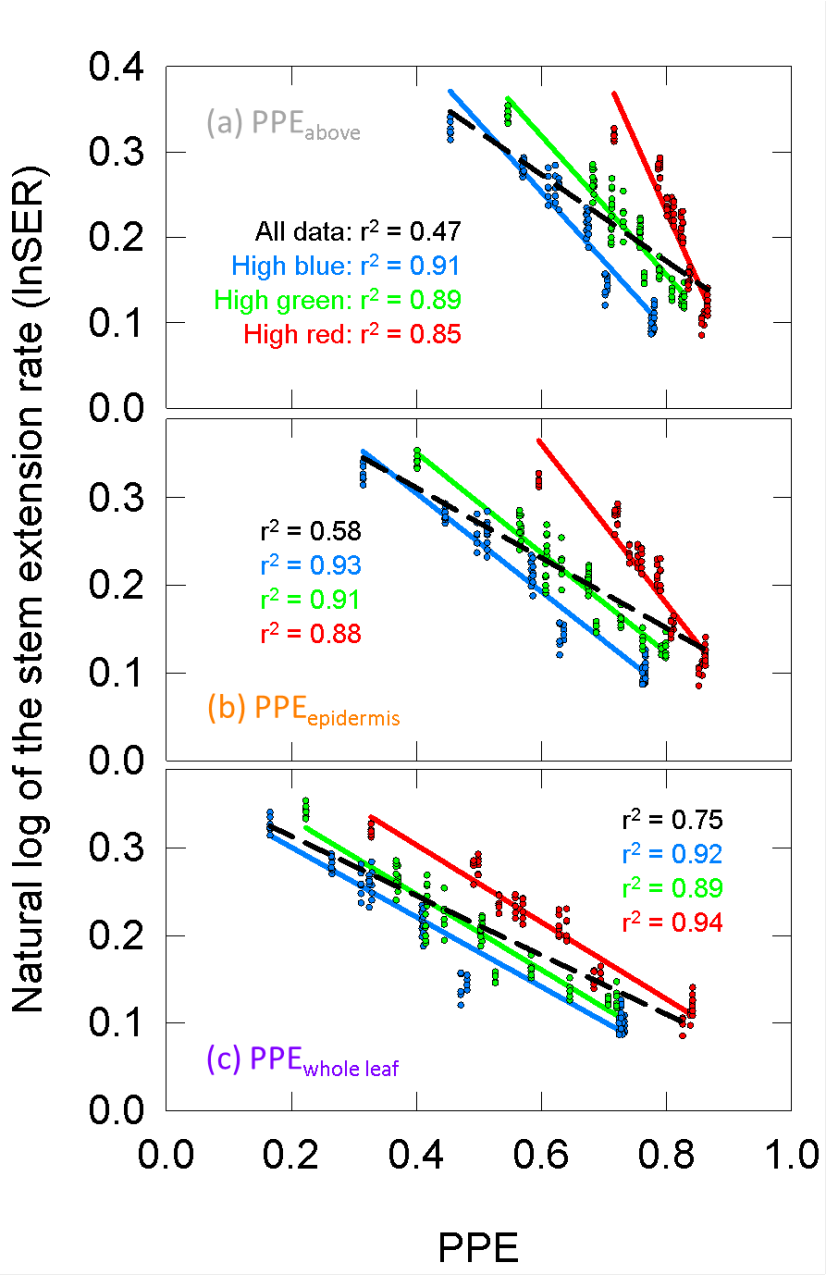

FIGURE 4-7: The response of the natural log of the stem extension rate (lnSER) to changes in the estimate of phytochrome photoequilibrium (PPE) in multiple layers of tissue. PPE is calculated with the two-state model. See **Figure 4-5** for an explanation of colors. (a) The relationship between PPE_{above} and lnSER. This is the most common method to model phytochrome activity using the spectral photon distribution above the leaf. Panels (b) and (c) use estimates of PPE for phytochrome that is (b) in epidermal tissue or (c) homogeneously distributed through the whole leaf.

PPE as a continuous variable and the background spectrum as a categorical variable. There was a significant effect of the background spectrum on the prediction of lnSER for all four estimates of PPE, indicating that the offsets for the linear models were significantly different ($p < 0.0001$ in all cases).

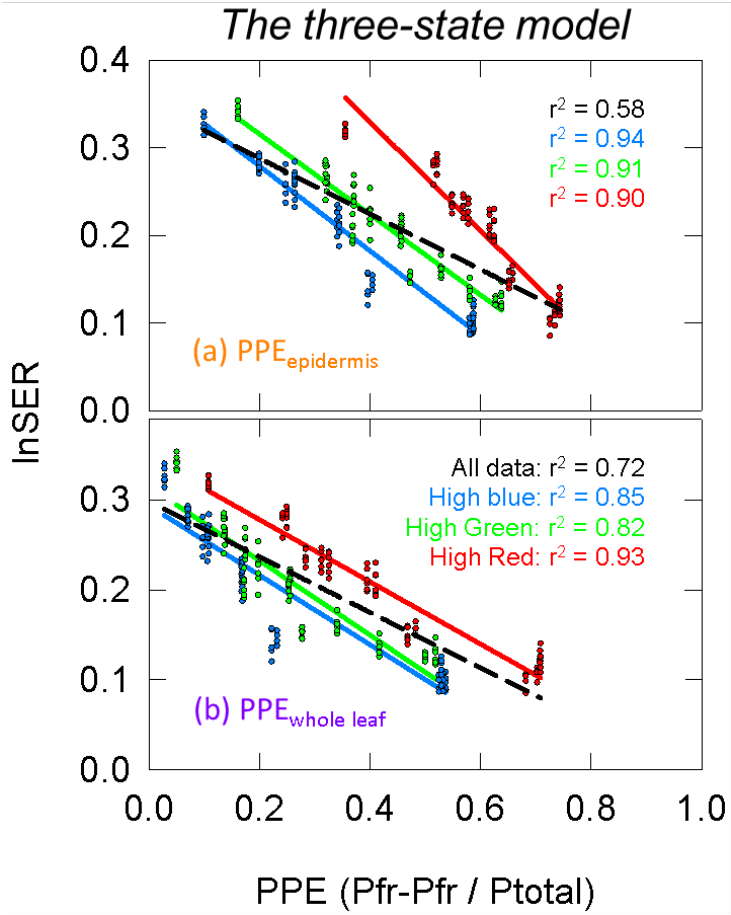

FIGURE 4-8: Modeling phytochrome activity with the three-state model. For this analysis, only phytochrome that is (a) in the epidermis or (b) homogeneously distributed within the whole leaf were considered. See **Figure 4-5** for an explanation of colors.

In the linear mixed effects model, an interaction effect between PPE and the background spectrum indicates that the slopes of the three lines are significantly different. This was the case for every model with the exception of only $PPE_{\text{whole leaf}}$ using *the three-*

state model ($p = 0.25$ compared to $p = 0.033$ for $PPE_{whole\ leaf}$ using the *two-state model*, and $p < 0.0001$ for $PPE_{epidermis}$ using both the *two-* and *three-state models*). This means that the three lines (blue, green and red) in this model ($PPE_{whole\ leaf}$ using the three-state model) of PPE are not significantly different (nearly parallel).

FIGURE 4-9: Representative plants at harvest from the short-term photobleaching study. Green seedlings are shown on the left and norflurazon-treated photobleached seedlings are shown on the right. There was some chlorophyll at the tips of some of the photobleached seedlings.

4.4.2 Short-term Photobleaching Study

To further investigate the role spectral distortion by chlorophyll on estimates of PPE and subsequent stem or hypocotyl elongation, seedlings were grown with or without chlorophyll using the herbicide norflurazon.

The photobleaching of the norflurazon treated seedlings was visually apparent, although some seedlings had chlorophyll at the tips of the cotyledons (**Figure 4-9**). Over the 48 h treatment period, the dark-grown norflurazon treated seedlings elongated an average of 8.5 cm, while the non-treated seedlings elongated an average of 9 cm. Elongation of seedlings in the light treatments relative to the dark controls are plotted as a function of

percent FR in **Figure 4-10**. The photobleached seedlings elongated significantly less than the green seedlings, but a higher fraction of FR induced more elongation in both green and photobleached seedlings.

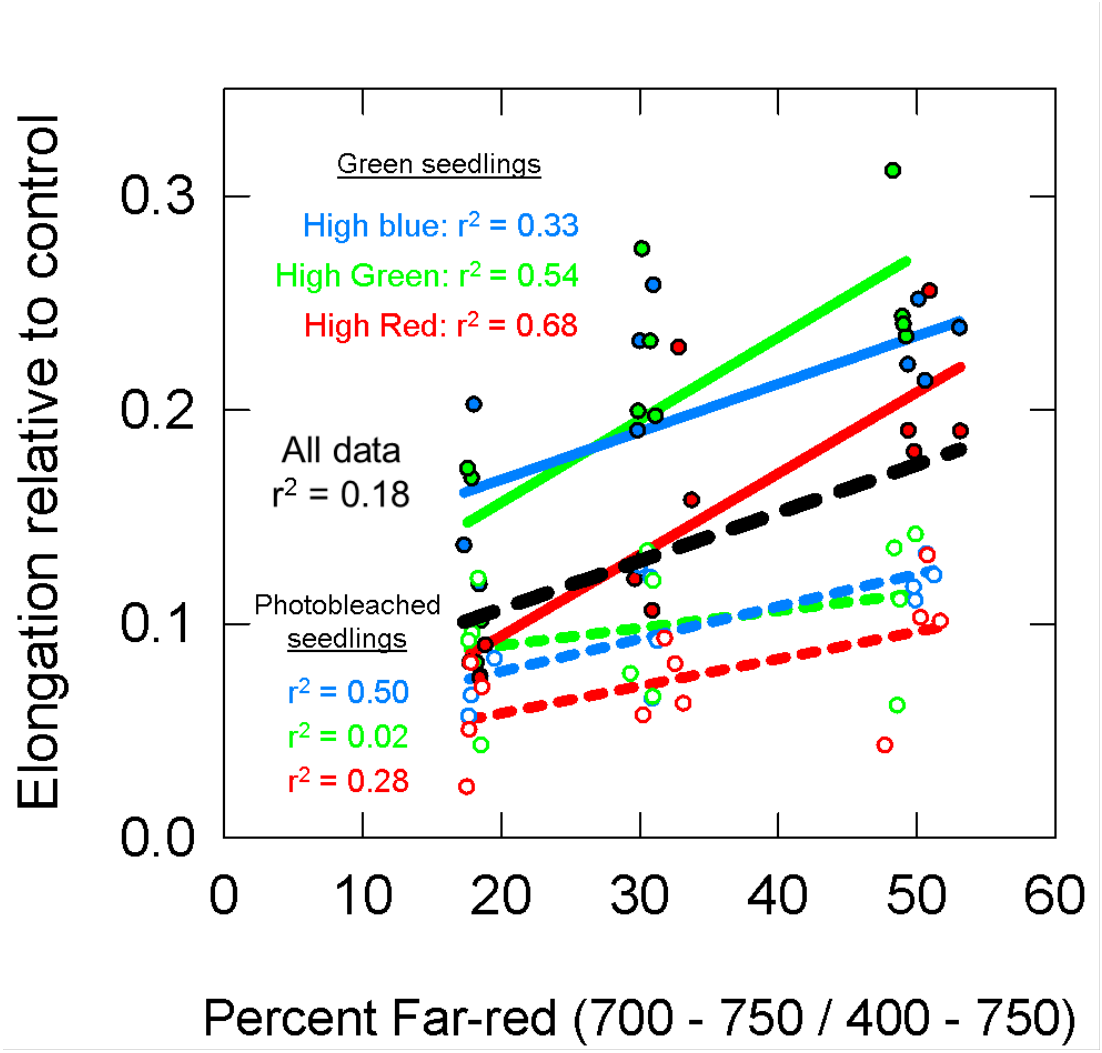

FIGURE 4-10: Elongation of green (closed circles, solid lines) and photobleached (open circles, dashed lines) seedlings over a 48 h period relative to dark controls. See **Figure 4-5** for an explanation of colors. Data show that photobleached seedlings elongated less then green seedlings.

Spectral distortion functions for etiolated seedlings (**Figure 4-4c**) were used to calculate weighting factors for phytochrome conversions in either the epidermis or the whole

leaf (**Figure G-9**). The photoconversion coefficients (**Figure 4-6a**) were substituted with the weighting factors for specific locations in green or etiolated cotyledons (**Figure 4-6b, c** and **Figure G-9**) in Eq (4.1) to estimate PPE in these treatments.

Figure 4-11 models the data in **Figure 4-10** with these estimates of PPE. For this analysis, both the green and photobleached seedlings grown under a single spectral background (e.g. high blue) were combined together for regression analysis. Similar to the long-term study, PPE estimated above the cotyledon produced a poor correlation when run through all the data from all three spectral backgrounds ($r^2 = 0.20$; **Figure 4-11a**), but unlike the long-term study, the regression through the data for a single spectral background also produced a poor correlation ($r^2 = 0.12$, 0.13 and 0.30 for high blue, high green and high red, respectively). Compared to PPE estimated above the cotyledon (PPE_{above}), the estimate of PPE within the epidermal tissue ($PPE_{epidermis}$) provided a slight improvement in predictive ability (**Figure 4-11b**). Corroborating the results of the long-term study, the assumptions that 'functional' phytochrome is homogeneously distributed within the whole leaf ($PPE_{whole\ leaf}$) provided the best correlations between PPE and elongation relative to the dark controls (**Figure 4-11c**). This was true for both correlations using all the data and correlations using each individual background spectrum.

Similar to the comparison between *the three-state* and *the two-state models* in the long-term study, there was little difference between the correlation between PPE and elongation relative to the control in a specific layer of tissue using either model. *The three- state model* for homogenously distributed 'functional' phytochrome required non-linear models to fit the data, and this resulted in a strong relationship (**Figure 4-11e**).

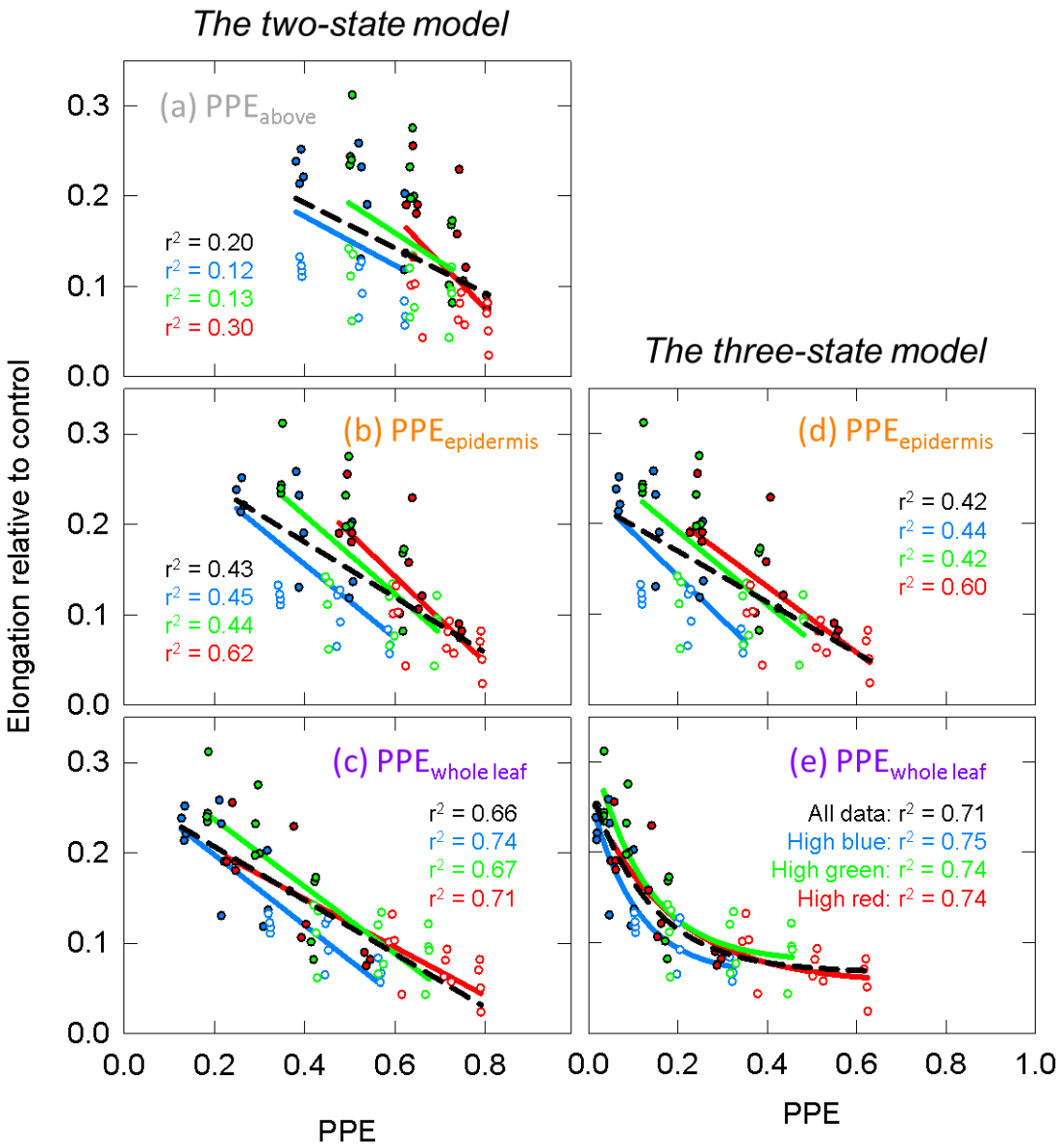

FIGURE 4-11: The response of green (closed circles) and photobleached (open circles) seedlings to models of PPE in specific leaf layers, using the same models as **Figure 4-7** and **Figure 4-8**. See **Figure 4-5** for an explanation of colors. Estimates of PPE are calculated using green or etiolated weighting factors. The green and photobleached seedlings from a single spectral treatment were combined for analysis. Panels (a) through (c) use estimates of PPE based on the two-state model for phytochrome that is (a) above the leaf, (b) in epidermal tissue or (c) homogeneously distributed in the whole cotyledon. Panels (d) and (e) use estimates of PPE based on the three-state model for phytochrome that is (d) in epidermal tissue or (e) homogeneously distributed in the whole cotyledons. All models use linear regression with the exception of (e), which fit the date with exponential decay functions. Each point represents an average of 6 to 9 seedlings. There were four replications in time.

4.5 Discussion

4.5.1 Effects of Spectral Distortion on the Action Spectrum of Phytochrome Conversion

Kazarinova-Fukshanky et al. (1985) previously estimated the weighting factors for *in vivo* (either green or etiolated tissue) phytochrome photoconversions based on *in vitro* determinations of the photoconversion coefficients and their spectral distortion functions. They used the original photoconversion coefficients from Butler et al. (1964), which are based on partially degraded 60 kDa phytochrome rather than *native* 124 kDa phytochrome (Mancinelli, 1986). Therefore, the weighting factors from Kazarinova-Fukshansky et al. (1985) required updating using the most accurate photoconversion coefficients. Here, photoconversion coefficients calculated from the photochemical properties in Lagarias et al. (1987) were used.

The application of photoconversion weighting factors did not significantly shift of the Pr peak away from 668 nm. Therefore, we could not explain why Kasperbauer et al. (1963) or Jose and Schafer (1978) observed shifts to 645 and 630 nm, respectively.

4.5.2 Analysis of Phytochrome Models

The high correlations between PPE_{above} and lnSER for each individual background in the long-term study is similar to previous reports that kept the background spectrum constant, and only adjusted levels of R or FR (Morgan and Smith, 1976, 1978, 1979; Park and Runkle, 2017, 2018), but there is a low correlation when using PPE_{above} to broadly estimate lnSER under any spectral background (**Figure 4-7a**). By comparison, the convergence of lnSER data in **Figure 4-7b, c** indicate that models that account for spectral distortion within a leaf

better predict phytochrome mediated plant responses under a broader range of spectral backgrounds.

Morgan and Smith (1978) found a linear relationship between PPE and lnSER when PPE was estimated under a leaf with a low chlorophyll concentration (380 μmol m^{-2}), but they reported a departure from linearity at a high chlorophyll concentration (660 μmol m^{-2}). Here, chlorophyll concentration in the leaves averaged 574 μmol m^{-2} across all treatments, although it ranged from 383 μmol m^{-2} to 937 μmol m^{-2} and decreased as percent FR increased (**Figure 4-5d**). Using only the transmitted spectrum, the relationship between PPE and lnSER was non-linear (**Figure G-10**). Phytochrome in the upper layers of a leaf would have a lower 'effective' chlorophyll concentration, and may be thought of as similar to the low chlorophyll leaf in Morgan and Smith (1978). Thus, the linear relationship between PPE and lnSER in the upper layers of leaf tissue ($PPE_{epidermis}$) is similar to previous findings (**Figure 4-7b**).

Results from our short-term photobleaching study were similar to Holmes and Wagner (1981), who measured the percent inhibition of elongation (relative to dark controls) of green and norflurazon-treated *Chenopodium rubrum* seedlings grown under a single spectral background with added R or FR. As PPE increased from 0.3 to 0.8 in their study, inhibition of hypocotyl elongation increased (i.e. shorter hypocotyls) for both the treated and untreated seedlings, although the effect appeared reduced in the green seedlings. Additionally, when white light was applied along with R and FR, the green seedlings were taller than the norflurazon treated seedlings. Broadly, their results are similar to ours (**Figure 4-10** and **Figure 4-11a**).

It is difficult to determine whether the relationship between PPE and lnSER should be linear (e.g. **Figure 4-7c**) or non-linear (e.g. **Figure 4-11e**). In the nucleus, activated phyB (Pfr or D_2) interacts with numerous transcription factors including PHYTOCHROME INTERACTING FACTORS (PIFs), often inactivating or phosphorylating them (Legris et al., 2019). PIFs transcriptionally promote the expression of genes related to auxins, gibberellins and cell walls, effectively leading to increased cell expansion (de Lucas and Prat, 2014). Thus, the down regulation of PIFs caused by higher relative concentrations of phyB-Pfr (high PPE) will cause a decrease in stem elongation, but with so many contributing factors, the exact relationship is difficult to determine. Additionally, post-transcriptional and translation regulation by phytochrome (Legris et al., 2019), the circadian control of phyB protein accumulation (Sharrock and Clack, 2002), and cytoplasmic roles of phytochrome (Hughes, 2013) all further complicate this relationship. We investigated the relationship between stem elongation and $PPE_{whole\ leaf}$ assuming the Michaelis-Menten kinetic equation (**Figure G-11**). The relationship between $PPE_{whole\ leaf}$ and stem elongation was not as strong as the simple linear models described previously.

The assumption that 'functional' phytochrome was homogeneously distributed throughout all leaf layers (whole leaf) provided better correlations with elongation than the assumption that 'functional' phytochrome was only in the epidermis (**Figure 4-7** and **Figure 4-11**). This corroborates the findings of Endo et al. (2005) who found that phyB expression in the mesophyll of the cotyledons restored the wild-type morphology in a *phyB* mutant. Kim et al. (2016) concluded that only phytochrome in the epidermis (of the hypocotyl) contributes to the control of hypocotyl elongation, but their results show a potential role for both epidermal and cortex located phytochrome in the control of hypocotyl elongation.

Cortex and mesophyll cells are both ‘ground’ tissue, comprising the majority of plant biomass. It seems likely that phytochrome in these cells (and the epidermis) modulate development in response to light signals, while phytochrome in vascular tissue does not (Endo et al., 2005; Kim et al., 2016).

The data presented here indicate that PPE estimated above a leaf is an inappropriate method for predicting phytochrome action. Under electric lights, above-the-leaf estimates of PPE are often above 0.8, which is higher than in sunlight. Some authors have concluded that the biological responses to treatments with PPE_{above} ranging from about 0.8 to 0.88 were likely not caused by phytochrome because it did not vary to a large degree (Barnes and Bugbee 1992; Dougher and Bugbee 2001a, b; Cope and Bugbee 2013). The proposed method of modifying the SPD that reaches phytochrome molecules demonstrates a high attenuation of R photons, resulting in lower rates of Pr to Pfr conversion than expected by above-the-leaf estimates. A re-evaluation of previous studies may be warranted.

4.5.3 Consideration of More Recent Models: Three-state and Cellular models

In the studies reported here, the intensity was kept close to the threshold intensities for a given temperature described by Sellaro et al. (2019) in order to minimize the contribution of thermal reversion on phytochrome dynamics. This simplified the estimates of PPE to only photoconversions, and therefore *the cellular model*, which accounts for other phytochrome dynamics, could be ignored.

The three-state model could still be investigated by simply squaring PPE calculated by *the two-state model* (Mancinelli, 1988). The correlations between PPE and elongation

were not greatly changed when using *the three-state* over the *two-state model* (**Figure 4-7b, c** compared to **Figure 4-8** and **Figure 4-11 b, c** compared to **Figure 4-11d, e**), but the linear models between PPE and lnSER for the estimate of phytochrome homogenously distributed in the whole leaf using *the three-state model* produced nearly parallel lines (more specifically, the slopes were not determined to be significantly different) for the three spectral backgrounds (**Figure 4-8b**). This means that a change in PPE is predicted to result in identical changes in elongation for the three spectral backgrounds. These results suggest that *the three-state model* for $PPE_{whole\ leaf}$ best predicts phytochrome action.

The three-state model assuming phytochrome is homogeneously distributed in all leaf tissue provided non-linear relationship between PPE and elongation in the short-term photobleaching study, and while linear responses may be more satisfying, it is possible that the response of stem extension to changes in PPE is non-linear (described above). Overall, it is difficult to conclude anything further regarding *the two-state* vs. th*e three-state models*.

Based on the principles of *the cellular model*, an interaction between intensity and percent far-red is expected (i.e. increasing percent far-red should have a more pronounced effect on stem elongation at lower intensities than higher intensities). Although specific effects of intensity have been well documented in the literature (Smith 1982), the interactions between intensity and percent far-red on the stem length or stem extension rate have been less well documented.

Hitz et al. (2019) applied three FR fractions (1, 7 and 20% FR) to a PPFD of 100 $\mu mol\ m^{-2}\ s^{-1}$ and a PPFD of 400 $\mu mol\ m^{-2}\ s^{-1}$, and saw an increase in stem length both when the percent FR was increased and when the PPFD was decreased, as *the cellular model* would generally predict. However, when the data from Hitz et al. (2019) is considered as a

percent increase from the treatments with no added FR, there appears to be no effect of intensity (**Figure G-12**). Child and Smith (1987) saw no difference in the relationship between PPE and the change in stem extension rate at intensities between 50 to 150 μmol m^{-2} s^{-1} of white light. Smith (1990) saw only transient changes in stem extension rate when rapidly increasing or decreasing the total intensity while keeping the R:FR ratio constant. Park and Runkle (2018) did not observe an interaction between PPE and intensity on stem length in petunia, geranium or coleus, but they did observe an independent effect of intensity on petunia stem length. These contradictions are difficult to explain because intensity in these studies, unlike our own, dropped below the thresholds described by Sellaro et al. (2019). Our study may not be representative of a traditional cucumber propagation environment because of the high intensity utilized to minimize this thermal reversion. Further studies at various intensities are required to test the robustness of *the cellular model*.

4.5.4 Blue and Green Responses

Although stem and hypocotyl elongating were primarily explained by changes in PPE, it cannot be rules out the background spectra would not have significantly different effects on elongation. The high green and high red treatments had roughly the same percentage of blue photons, which make them comparable to each other, but less comparable to the high blue treatment (Table 4.1), especially on a PPE basis. This is because the blue light receptors, cryptochromes, must be considered. Blue photons decrease stem elongation in cucumbers (Hernandez and Kubota, 2016; Snowden et al., 2016). When the data from both the long-term and short-term studies were plotted with PPE (*two-state* or *three-state*) as the

independent variable (**Figure 4-7**, **Figure 4-8**, **Figure 4-11**) the background spectral treatments generally increased in elongation in the order of high blue, high green then high red at the same value of PPE. This indicates a role of blue photons (through cryptochrome), and possibly green photons, in shifting the offset of the PPE model. These results are consistent with Park and Runkle (2019).

Research in the last 15 years has indicated that blue and green photons, sensed through the photoreceptor cryptochrome, act in a similarly antagonistic manner as R and FR. For example, green photons were found to reverse the blue induced decrease in hypocotyl elongation (Bouly et al., 2007). This has led to models of cryptochrome action similar to the phytochrome models described above (Procopio et al., 2016). It might be expected that green photons would increase stem elongation similar to FR, but neither Hernandez and Kubota (2016) nor Snowden et al. (2016) saw this response in cucumber. Additionally, although Sellaro et al. (2010) demonstrated that a blue/green ratio reliably predicted hypocotyl lengths, their data showed that increasing the flux of green photons, like blue photons, also decreased hypocotyl elongation, but to a lesser extent than the blue photons. It is difficult to determine what caused this green induced decrease in hypocotyl length, but this effect may explain the differences in offsets for the high blue and high green data compared to high red data (**Figure 4-7**, **Figure 4-8**, **Figure 4-11**).

4.5.5 Future Directions and Potential Improvements

Kusuma and Bugbee (2021) recently outlined six issues with using PPE as a model to predict morphological responses. These included 1) differences in photoconversion

coefficients from different studies, 2) multiple phytochromes, 3) thermal reversions, 4) phytochrome intermediates, 5) fluctuations in Ptotal, and 6) spectral distortion by chlorophyll. In this study, photoconversion coefficients derived from Lagarias et al. (1987) were used, which are derived from measurements of highly pure phytochrome *in vitro*. Our experiments were constructed to primarily obtain effects from phyB and minimize contributions of thermal reversion, but fluctuations in Ptotal and the formation of intermediates were not accounted for. Finally, the results presented here provide evidence that spectral distortion by chlorophyll must be considered in estimating PPE, but several further considerations could improve the robustness of PPE prediction of morphology based on spectral measurements.

As discussed previously, the leaves and cotyledons are likely the primary location of photon perception by phytochrome, but hypocotyls also contribute to photon perception. The planting density in the long-term study was 20 plants per m^2, which likely led to additional FR enrichment caused by reflection by neighboring plants. Because FR induced auxin signals can move within the plant (Roig-Villanova and Martinez-Garcia, 2016) it is important to determine how FR signals are integrated across different tissues across the plant.

The spectral distortion functions used in this study were derived from Kazarinova-Fukshansky et al. (1985). These distortion functions were calculated from transmission and reflectance measurements using the Kubelka-Munk theory from Kazarinova-Fukshansky et al. (1985), who made their measurements in 7 d old zucchini seedlings grown under 16000 lx of white light (it is difficult to determine what this is in PPFD, but we estimate that it is about 250 to 300 μmol m^{-2} s^{-1}). Because spectral reflectance and transmittance have roughly the same shape for all plants with chlorophyll, these distortion functions may have relatively

universal utility, but environmental conditions contribute to a few key changes in plant internal structure that could decrease the reliability of the presented distortion functions.

4.5.5.1 Potential shifts in spectral distortion functions

Increasing the FR fraction (decreasing PPE) decreased the leaf chlorophyll concentration (**Figure 4-5d**), and there was no effect of percent FR on specific leaf mass, with the exception of a small effect in the high blue treatment (**Figure 4-5e**). This means that this change in chlorophyll concentration (μmol per square meter of leaf) was unlikely caused by changes in leaf thickness, but rather was caused by differences in chlorophyll synthesis or retention. Decreasing the concentration of chlorophyll within the leaves is expected to increase the penetration of photons into deeper layers of tissue, increasing the average photon intensity within a leaf. This would result in spectral distortion functions (and thus photoconversion weighting factors) that are intermediate between the epidermis and whole leaf estimates (**Figure 4-4b**, **Figure 4-6b, c**).

The change in the spectral distortion function with changing chlorophyll concentrations will depend on the distribution of the chlorophyll within the leaves. Nishio et al. (1993) reported that carotenoid and chlorophyll concentrations peaked halfway through a spinach leaf if the plants were grown in sunlight, but peaked at a depth of about 30% through the leaf when grown in the shade. When chlorophyll/carotenoids are concentrated toward the adaxial side of the leaf, photons in the will be attenuated more rapidly, decreasing the average photon flux within the leaf. It seems unlikely that the shade (FR) induced changes in both chlorophyll concentration and chlorophyll distribution will perfectly offset each other,

but nonetheless the two effects would antagonistically alter the average SPD within the leaf. If chlorophyll distributions favor the adaxial side under higher FR, this may mean that the FR induced decrease in chlorophyll concentration will minimally affect the average spectral distortion within the leaf.

High photon intensity and blue photons can increase leaf thickness and reorient chloroplasts. Cui et al. (1991) suggested that increased leaf thickness via palisade elongation promoted photon penetration deeper into leaf tissue, although there was little difference in fractional leaf penetration between thick and thin leaves in their study. Chloroplast orientation along the sides of cell walls at high photon intensity induces a sieve effect allowing photon penetration deeper into leaf tissue (Davis et al., 2011; Parry et al. 2014). Again, this results in spectral distortion functions intermediate between the whole leaf and epidermis estimates (**Figure 4-4b**).

Developing leaves tend to have lower chlorophyll concentrations than mature leaves. As plants mature and chlorophyll concentrations increase, the average fluxes of blue and red photons within a leaf will decrease. This means that the phytochrome dynamics in older leaves would shift to lower average Pfr concentrations than younger leaves under identical SPD. Younger leaves were more receptive to far-red than older cotyledons in Casal and Smith (1988b). This response is the opposite of what would be expected assuming chlorophyll concentrations were higher in older cotyledon tissue compared to younger leaf tissue. Therefore, younger leaves may be more receptive to photon signals than older leaves. Nonetheless, as these younger leaves develop and chlorophyll concentrations increase, photon penetration into leaves will decrease, shifting the spectral distortion functions from similar to the epidermis estimate to lower than the whole leaf estimate (**Figure 4-4b**).

The combined effects of photon quality and quantity on leaf internal structure and chlorophyll concentration/distribution could result in changes in the internal SPD. Modifications to the spectral distortion functions to account for these changes could improve the model. Additional research is warranted.

4.5.6 A Simpler Intuitive Metric: The FR Fraction

Phytochrome and cryptochrome, when activated, interact with some of the same transcription factors (de Wit et al., 2016). The chromophore at the center of the photoreceptor cryptochrome is a flavin adenine dinucleotide (FAD) molecule, a coenzyme associated with numerous proteins. FAD absorbs photons in the UV-A and blue regions of the spectrum. FAD absorbance drops substantially around 500 nm (Banerjee et al., 2007; Procopio et al., 2016). The inactive form of phytochrome absorbs across the entire biologically active spectrum (300 to 800 nm), but is primarily activated by red photons. Chlorophyll-induced spectral distortions may mean that phytochrome is also significantly activated by (longer wavelength) green photons (**Figure 4-6c**). Therefore, blue, green and red photons may push back against FR photons to affect morphology. Percent far-red (FR fraction) was shown to be an excellent predictor of lnSER in the long-term study ($r^2 = 0.89$), although the expected blue (and possibly green) offsets are not present. Percent far-red did not appear to be a good predictor of morphology in seedlings (**Figure 4-10**).

Due to the issues with PPE outlines above, Kusuma and Bugbee (2021) suggested that environmental signals might be more reliable than photo-molecular models, like PPE. Environmental pressure drives evolution, and thus genetically regulated molecular machinery

could be expected to conform to the incoming signals (in so much as it provides a survival advantage). The R:FR ratio is often used as a metric to describe the degree of shade, but percent far-red may be a better ratio because it integrates the action of multiple photoreceptors that co-evolved to detect the extent of shade. Although our improvements to the PPE model indicate some important mechanistic aspects of photon perception within a leaf, the FR fraction is a simple intuitive metric that may be widely applicable across many conditions.

4.6 Summary

PPE is generally estimated from the spectral photon distribution above the leaf, which does not account for the spectral distortion caused by absorbance and scattering within a leaf, and is thus an inadequate metric for estimating phytochrome induced morphology. Estimates of PPE for phytochrome that is homogeneously distributed throughout the whole leaf accounted for spectral distortions and was a better predictor of morphological responses. The distortion functions used here were from a different species than the species investigated and yet improved predictions. We thus believe the distortion functions used here have universal utility.

Percent far-red is an intuitive environmental metric that accounts for photon effects from 400 to 750 nm on stem elongation rate, possibly because it accounts for cryptochrome and phytochrome action. This is an empirical metric but it appears to have excellent predictive power.

The use of LEDs in controlled environments allows an unprecedented opportunity to manipulate plant growth. FR LEDs have a high efficacy and may thus contribute to these manipulations, but the phytochrome mediated responses to FR must be better understood to utilize their potential.

4.7 Literature Cited

Aukerman, M. J., Hirschfeld, M., Wester, L., Weaver, M., Clack, T., Amasino, R. M., and Sharrock, R. A. (1997). A deletion in the PHYD gene of the *Arabidopsis* Wassilewskija ecotype defines a role for phytochrome D in red/far-red light sensing. *Plant Cell* 9, 1317–1326. doi: 10.1105/tpc.9.8.1317

Banerjee, R., Schleicher, E., Meier, S., Muñoz Viana, R., Pokorny, R., Ahmad, M., et al. (2007). The signaling state of Arabidopsis cryptochrome 2 contains flavin semiquinone. *J. Biol. Chem*. 282, 14916–14922. doi: 10.1074/jbc.M700616200

Barnes, C., and Bugbee, B. (1992). Morphological responses of wheat to blue light. *J. Plant Physiol.* 139, 339–342. doi: 10.1016/S0176-1617(11)80347-0

Björkman, T. (1999). Dose and timing of brushing to control excessive hypocotyl elongation in cucumber transplants. *HortTechnology* 9, 224–226. doi: 10.21273/HORTTECH.9.2.224

Black, M., and Shuttleworth, J. E. (1974). The role of the cotyledons in the photocontrol of hypocotyl extension in *Cucumis sativus* L. *Planta* 117, 57–66. doi: 10.1007/BF00388678

Borthwick, H. A., Hendricks, S. B., Parker, M. W., Toole, E. H., and Toole, V. K. (1952). A reversible photoreaction controlling seed germination. *Proc. Natl. Acad. Sci.* U.S.A. 38, 662–666. doi:10.1073/pnas.38.8.662

Bouly, J.P., Schleicher, E., Dionisio-Sese, M., Vandenbussche, F., Van Der Straeten, D., Bakrim, N., et al. (2007). Cryptochrome bluelight photoreceptors are activated through interconversion of flavinredox states. *J. Biol. Chem.* 282, 9383–9391. doi: 10.1074/jbc.M609842200

Brockmann, J., Rieble, S., Kazarinova-Fukshansky, N., Seyfried, M., and Schäfer, E. (1987). Phytochrome behaves as a dimer *in vivo*. *Plant Cell Environ*. 10, 105–111. doi: 10.1111/1365-3040.ep11602037

Butler, W. L., Hendricks, S. B., and Siegelman, H. W. (1964). Action spectra of phytochrome in vitro. *Photochem. Photobiol*. 3, 521–528. doi: 10.1111/j.1751-1097.1964.tb08171.x

Casal, J. J. (1995). Coupling of phytochrome B to the control of hypocotyl growth in Arabidopsis. *Planta* 196, 23–29. doi: 10.1007/BF00193213

Casal, J. J., and Smith, H. (1988a). Persistent effects of changes in phytochrome status on

internode growth in light-grown mustard: occurrence, kinetics and locus of perception. *Planta* 175, 214–220. doi: 10.1007/BF00392430

Casal, J. J., and Smith, H. (1988b). The loci of perception for phytochrome control of internode growth in light-grown mustard: promotion by low phytochrome photoequilibria in the internode is enhanced by blue light perceived by the leaves. *Planta* 176, 277–282. doi: 10.1007/BF00392456

Child, R., and Smith, H. (1987). Phytochrome action in light-grown mustard: kinetics, fluence-rate compensation and ecological significance. *Planta* 172, 219–229. doi: 10.1007/BF00394591

Cope, K. R., and Bugbee, B. (2013). Spectral effects of three types of white light-emitting diodes on plant growth and development: absolute versus relative amounts of blue light. *HortScience* 48, 504–509. doi: 10.21273/HORTSCI.48.4.504

Cui, M., Vogelmann, T. C., and Smith, W. K. (1991). Chlorophyll and light gradients in sun and shade leaves of *Spinacia oleracea*. *Plant Cell Environ*. 14, 493–500. doi: 10.1111/j.1365-3040.1991.tb01519.x

Davis, P. A., Caylor, S., Whippo, C. W., and Hangarter, R. P. (2011). Changes in leaf optical properties associated with light-dependent chloroplast movement. *Plant Cell Environ.* 34, 2047–2059. doi: 10.1111/j.1365-3040.2011.02402.x

de Lucas, M., and Prat, S. (2014). PIFs get BRright: PHYTOCHROME INTERACTING FACTORs as integrators of light and hormonal signals. *New Phytol.* 202, 1126–1141. doi: 10.1111/nph.12725

de Wit, M., Keuskamp, D. H., Bongers, F. J., Hornitschek, P., Gommers, C. M., Reinen, E., et al. (2016). Integration of phytochrome and cryptochrome signals determines plant growth during competition for light. *Curr. Biol.* 26, 3320–3326. doi: 10.1016/j.cub.2016.10.031

Devlin, P. F., Patel, S. R., and Whitelam, G. C. (1998). Phytochrome E influences internode elongation and flowering time in *Arabidopsis*. *Plant Cell* 10, 1479–1487. doi: 10.1105/tpc.10.9.1479

Devlin, P. F., Robson, P. R., Patel, S. R., Goosey, L., Sharrock, R. A., and Whitelam, G. C. (1999). Phytochrome D acts in the shade-avoidance syndrome in *Arabidopsis* by controlling elongation growth and flowering time. *Plant Physiol*. 119, 909–916. doi: 10.1104/pp.119.3.909

Dougher, T. A., and Bugbee, B. (2001a). Differences in the Response of Wheat, Soybean and Lettuce to Reduced Blue Radiation. *Photochem. Photobiol.* 73, 199-207. doi: 10.1562/0031-8655(2001)0730199DITROW2.0.CO2

Dougher, T. A., and Bugbee, B. (2001b). Evidence for Yellow Light Suppression of Lettuce Growth. *Photochem. Photobiol.* 73, 208-212. doi: 10.1562/0031-8655(2001)0730208EFYLSO2.0.CO2

Eichenberg, K., Bäurle, I., Paulo, N., Sharrock, R. A., Rüdiger, W., and Schäfer, E. (2000). Arabidopsis phytochromes C and E have different spectral characteristics from those of phytochromes A and B. *FEBS letters* 470, 107–112. doi: 10.1016/S0014-5793(00)01301-6

Endo, M., Nakamura, S., Araki, T., Mochizuki, N., and Nagatani, A. (2005).

Phytochrome B in the mesophyll delays flowering by suppressing FLOWERING LOCUS T expression in Arabidopsis vascular bundles. *Plant Cell* 17, 1941–1952. doi: 10.1105/tpc.105.032342

Evans, J. R. (1995). Carbon fixation profiles do reflect light absorption profiles in leaves. *Aust. J. Plant Physiol.* 22, 865–873. doi: 10.1071/PP9950865

Fisher, P. R., Heins, R. D., and Lieth, J. H. (1996). Quantifying the relationship between phases of stem elongation and flower initiation in poinsettia. *J. Am. Soc. Hort. Sci.* 121, 686–693. doi: 10.21273/JASHS.121.4.686

Franklin, K. A., Davis, S. J., Stoddart, M. W., Vierstra, R. D., and Whitelam, G. C. (2003). Mutant analyses define multiple roles for phytochrome C in *Arabidopsis* photomorphogenesis. *Plant Cell* 15, 1981–1989. doi: 10.1105/tpc.015164

Franklin, K. A., and Quail, P. H. (2010). Phytochrome functions in *Arabidopsis* development. *J. Expt. Bot.* 61, 11–24. doi: 10.1093/jxb/erp304

García-Martínez, J. L., Keith, B., Bonner, B. A., Stafford, A. E., and Rappaport, L. (1987). Phytochrome regulation of the response to exogenous gibberellins by epicotyls of *Vigna sinensis*. *Plant Physiol*. 85, 212–216. doi: 10.1104/pp.85.1.212

Gardner, G., and Graceffo, M. A. (1982). The use of a computerized spectroradiometer to predict phytochrome photoequilibria under polychromatic irradiation. *Photochem. Photobiol.* 36, 349–354. doi: 10.1111/j.1751-1097.1982.tb04385.x

Hartmann, K. M. (1966). A general hypothesis to interpret 'high energy phenomena' of photomorphogenesis on the basis of phytochrome. *Photochem. Photobiol.* 5, 349–365. doi: 10.1111/j.1751-1097.1966.tb05937.x

Hernández, R., and Kubota, C. (2016). Physiological responses of cucumber seedlings under different blue and red photon flux ratios using LEDs. *Environ. Exp. Bot.* 121, 66–74. doi: 10.1016/j.envexpbot.2015.04.001

Hitz, T., Hartung, J., Graeff-Hönninger, S., and Munz, S. (2019). Morphological response of soybean (*Glycine max* (L.) Merr.) cultivars to light intensity and red to far-red ratio. *Agronomy* 9, 428. doi: 10.3390/agronomy9080428

Holmes, M. G., and Fukshansky, L. (1979). Phytochrome photoequilibria in green leaves under polychromatic radiation: a theoretical approach. *Plant Cell Environ.* 2, 59–65. doi: 10.1111/j.1365-3040.1979.tb00774.x

Holmes, M. G., and Wagner, E. (1981). Phytochrome control of hypocotyl extension in light-grown Chenopodium rubrum. *Physiologia Plantarum* 53, 233–238. doi: 10.1111/j.1399-3054.1981.tb04492.x

Hughes, J. (2013). Phytochrome cytoplasmic signaling. *Annu. Rev. Plant Biol.* 64, 377–402. doi: 10.1146/annurev-arplant-050312-120045

Jones, A. M., and Quail, P. H. (1986). Quaternary structure of 124-kilodalton phytochrome from *Avena sativa* L. *Biochemistry* 25, 2987–2995. doi: 10.1021/bi00358a038

Jose, A. M., and Schäfer, E. (1978). Distorted phytochrome action spectra in green plants. *Planta* 138, 25–28. doi: 10.1007/BF00392909

Kasperbauer, M. J., Borthwick, H. A., and Hendricks, S. B. (1963). Inhibition of flowering of *Chenopodium rubrum* by prolonged far-red radiation. *Bot. Gaz.* 124, 444–451. doi: 10.1086/336234

Kazarinova-Fukshansky, N., Seyfried, M., and Schäfer, E. (1985). Distortion of action

spectra in photomorphogenesis by light gradients within the plant tissue. *Photochem. Photobiol.* 41, 689–702. doi: 10.1111/j.1751-1097.1985.tb03624.x

Kelly, J. M., and Lagarias, J. C. (1985). Photochemistry of 124-kilodalton *avena* phytochrome under constant illumination in vitro. *Biochemistry* 24, 6003–6010. doi: 10.1021/bi00342a047

Kim, J., Song, K., Park, E., Kim, K., Bae, G., and Choi, G. (2016). Epidermal phytochrome B inhibits hypocotyl negative gravitropism non-cell-autonomously. *Plant Cell* 28, 2770–2785. doi: 10.1105/tpc.16.00487

Klose, C., Venezia, F., Hussong, A., Kircher, S., Schäfer, E., and Fleck, C. (2015). Systematic analysis of how phytochrome B dimerization determines its specificity. *Nat. Plants* 1:15090. doi: 10.1038/nplants.2015.90

Kusuma, P., and Bugbee, B. (2021). Far-red Fraction: An Improved Metric for Characterizing Phytochrome Effects on Morphology. *J. Am. Soc. Hort. Sci.* 146, 3–13. doi: 10.21273/JASHS05002-20

Kutschera, U., and Niklas, K. J. (2007). The epidermal-growth-control theory of stem elongation: an old and a new perspective. *J. Plant Physiol.* 164, 1395–1409. doi: 10.1016/j.jplph.2007.08.002

Lagarias, J. C., Kelly, J. M., Cyr, K. L., and Smith Jr, W. O. (1987). Comparative photochemical analysis of highly purified 124 kilodalton oat and rye phytochromes *in vitro*. *Photochem. Photobiol.* 46, 5–13. doi: 10.1111/j.1751-1097.1987.tb04729.x

Legris, M., Ince, Y. Ç, and Fankhauser, C. (2019). Molecular mechanisms underlying phytochrome-controlled morphogenesis in plants. *Nat. Commun.* 10:5219. doi: 10.1038/s41467-019-13045-0

Mancinelli, A. L. (1986). Comparison of spectral properties of phytochromes from different preparations. *Plant physiol*. 82, 956–961. doi: 10.1104/pp.82.4.956

Mancinelli, A. L. (1988). Some thoughts about the use of predicted values of the state of phytochrome in plant photomorphogenesis research. *Plant Cell Environ.* 11, 429–439. doi: 10.1111/j.1365-3040.1988. tb01780.x

Mancinelli, A. L. "The physiology of phytochrome action". In: Kendrick RE and Kronenberg GHM, editors. *Photomorphogenesis in plants*. Springer, Dordrecht (1994). p. 211-269.

Mazzella, M. A., and Casal, J. J. (2001). Interactive signalling by phytochromes and cryptochromes generates de-etiolation homeostasis in Arabidopsis thaliana. *Plant Cell Environ.* 24, 155–161. doi: 10.1111/j.1365-3040.2001.00653.x

Morgan, D. C., and Smith, H. (1976). Linear relationship between phytochrome photo-equilibrium and growth in plants under simulated natural radiation. *Nature* 262, 210–212. doi: 10.1038/262210a0

Morgan, D., and Smith, H. (1978). The relationship between phytochrome-photoequilibrium and development in light grown *Chenopodium album* L. *Planta* 142, 187–193. doi: 10.1007/BF00388211

Morgan, D. C., and Smith, H. (1979). A systematic relationship between phytochrome controlled development and species habitat. *Planta* 145, 253–258. doi: 10.1007/BF00454449

Morgan, D. C., O'Brien, T., and Smith, H. (1980). Rapid photomodulation of stem

extension in light-grown *Sinapis alba* L. *Planta* 150, 95–101. doi: 10.1007/BF00582351

Nishio, J. N., Sun, J. D., and Vogelmann, T. C. (1993). Carbon fixation gradients across spinach leaves do not follow internal light gradients. *Plant Cell* 5, 953–961. doi: 10.1105/tpc.5.8.953

Park, Y., and Runkle, E. S. (2017). Far-red radiation promotes growth of seedling by increasing leaf expansion and whole-plant net assimilation. *Environ. Exp. Bot.* 136, 41–49. doi: 10.1016/j.envexpbot.2016.12.013

Park, Y., and Runkle, E. S. (2018). Far-red radiation and photosynthetic photon flux density independently regulate seedling growth but interactively regulate flowering. *Environ. Exp. Bot.* 155, 206–216. doi: 10.1016/j.envexpbot.2018.06.033

Park, Y., and Runkle, E. S. (2019). Blue radiation attenuates the effects of the red to far-red ratio on extension growth but not on flowering. *Environ. Exp. Bot.* 168, 103871. doi: 10.1016/j.envexpbot.2019.103871

Parry, C., Blonquist, J. M., and Bugbee, B. (2014). *In situ* measurement of leaf chlorophyll concentration: analysis of the optical/absolute relationship. *Plant Cell Environ.* 37, 2508–2520. doi: 10.1111/pce.12324

Procko, C., Crenshaw, C. M., Ljung, K., Noel, J. P., and Chory, J. (2014). Cotyledon-generated auxin is required for shade-induced hypocotyl growth in *Brassica rapa*. *Plant Physiol*. 165, 1285–1301. doi: 10.1104/pp.114.241844

Procopio, M., Link, J., Engle, D., Witczak, J., Ritz, T., and Ahmad, M. (2016). Kinetic modeling of the Arabidopsis cryptochrome photocycle: FADH accumulation correlates with biological activity. *Front. Plant Sci.* 7:888. doi: 10.3389/fpls.2016.00888

Rausenberger, J., Hussong, A., Kircher, S., Kirchenbauer, D., Timmer, J., Nagy, F., et al. (2010). An integrative model for phytochrome B mediated photomorphogenesis: from protein dynamics to physiology. *PLoS ONE* 5:e10721. doi: 10.1371/annotation/4563eaf4-e45b-4d9e-ab06-5f1794bf11e3

Rockwell, N. C., Su, Y., and Lagarias, J. C. (2006). Phytochrome structure and signaling mechnaisms. *Annu. Rev. Plant Biol.* 57, 837–858. doi: 10.1146/annurev.arplant.56.032604.144208

Roig-Villanova, I., and Martinez-Garcia, J. F. (2016). Plant responses to vegetation proximity: a whole life avoiding shade. *Front. Plant Sci.* 7:236. doi: 10.3389/fpls.2016.00236

Ruddat, A., Schmidt, P., Gatz, C., Braslavsky, S. E., Gärtner, W., and Schaffner, K. (1997). Recombinant type A and B phytochromes from potato. Transient absorption spectroscopy. *Biochemistry* 36, 103–111. doi: 10.1021/bi962012w

Sage, L.C. *Pigment of the Imagination*. Boston: Academic Press (1992). 562 p.

Sager, J. C., Smith, W. O., Edwards, J. L., and Cyr, K. L. (1988). Photosynthetic efficiency and phytochrome photoequilibria determination using spectral data. *Trans. Am. Soc. Agric. Biol. Eng.* 31, 1882–1889. doi: 10.13031/2013.30952

Savaldi-Goldstein, S., Peto, C., and Chory, J. (2007). The epidermis both drives and restricts plant shoot growth. *Nature* 446, 199–202. doi: 10.1038/nature05618

Sellaro, R., Crepy, M., Trupkin, S. A., Karayekov, E., Buchovsky, A. S., Rossi, C., et al.

(2010). Cryptochrome as a sensor of the blue/green ratio of natural radiation in Arabidopsis. *Plant Physiol.* 154, 401–409. doi: 10.1104/pp.110.160820

Sellaro, R., Smith, R. W., Legris, M., Fleck, C., and Casal, J. J. (2019). Phytochrome B dynamics departs from photoequilibrium in the field. *Plant Cell Environ.* 42, 606–617. doi: 10.1111/pce.13445

Seyfried, M., and Fukshansky, L. (1983). Light gradients in plant tissue. *Applied optics* 22, 1402–1408. doi: 10.1364/AO.22.001402

Sharrock, R. A., and Clack, T. (2002). Patterns of expression and normalized levels of the five Arabidopsis phytochromes. *Plant Physiol.* 130, 442–456. doi: 10.1104/pp.005389

Smith, H. "Light quality and germination: ecological implications". In: Heydecker W, editor. *Seed ecology*. Butterworths (1973). p. 219–231.

Smith, H. "The photomorphogenic response systems and their photoreceptors". In: Smith H, editor. *Phytochrome and Photomorphogenesis*. McGraw-Hill, London (1975). p. 22–53.

Smith, H. (1982). Light quality, photoperception, and plant strategy. *Annu. Rev. Plant Physiol.* 33, 481–518. doi: 10.1146/annurev.pp.33.060182.002405

Smith, H. (1990). Phytochrome action at high photon fluence rates: rapid extension rate responses of light-grown mustard to variations in fluence rate and red: far-red ratio. *Photochem. Photobiol*. 52, 131–142. doi: 10.1111/j.1751-1097.1990.tb01766.x

Smith, R. W., and Fleck, C. "Basic Phytochrome B Calculations". In: Hiltbrunner A, editor. *Phytochromes: Methods and Protocols*. Humana, New York (2019). p. 121–133.

Snowden, C. M., Cope, K. R., and Bugbee, B. (2016). Sensitivity of seven diverse species to blue and green light: integrations with photon flux. *PLoS ONE* 11:e0163121 doi: 10.1371/journal.pone.0163121

Somers, D. E., and Quail, P. H. (1995). Temporal and spatial expression patterns of PHYA and PHYB genes in Arabidopsis. *Plant J.* 7, 413–427. doi: 10.1046/j.1365-313X.1995.7030413.x

Tanaka, S. I., Nakamura, S., Mochizuki, N., and Nagatani, A. (2002). Phytochrome in cotyledons regulates the expression of genes in the hypocotyl through auxin-dependent and-independent pathways. *Plant Cell Physiol.* 43, 1171–1181. doi: 10.1093/pcp/pcf133

USU Crop Physiology Laboratory (2020). *"Utah Monocot/Dicot Solution" Nutrients. Paper 2.* Available at: https://digitalcommons.usu.edu/cgi/viewcontent.cgi?article=1001&context=cpl_nutrients.

Vogelmann, T. C. (1994). "Light within the plant". In: Kendrick RE and Kronenberg GHM, editors. *Photomorphogenesis in plants*. Springer, Dordrecht (1994). p. 491-535.

Whitelam, G. C., Johnson, E., Peng, J., Carol, P., Anderson, M. L., Cowl, J. S., and Harberd, N. P. (1993). Phytochrome A null mutants of *Arabidopsis* display a wild-type phenotype in white light. *Plant Cell* 5, 757–768. doi: 10.1105/tpc.5.7.757

Zhen, S., and van Iersel, M. W. (2017). Far-red light is needed for efficient

photochemistry and photosynthesis. *J. Plant Physiol.* 209, 115–122. doi: 10.1016/j.jplph.2016.12.004

Zhen, S. Y., Haidekker, M., and van Iersel, M. W. (2018). Far-red light enhances photochemical efficiency in a wavelength-dependent manner. *Physiol. Plant.* 167,21–33.doi:10.1111/ppl.12834

Zhen, S., and Bugbee, B. (2020a). Far-red photons have equivalent efficiency to traditional photosynthetic photons: Implications for redefining photosynthetically active radiation. *Plant Cell Environ.* 43, 1259–1272. doi: 10.1111/pce.13730

CHAPTER 5

FAR-RED INCREASES THE LEAF AREA OF LETTUCE AT HIGH PHOTON FLUXES, BUT DECREASES LEAF AREA AT LOW FLUXES

5.1 Summary

- The first signal of oncoming competition for sunlight from neighboring vegetation is an increase in the far-red photon flux (FR; 700 to 750 nm). Then as shade becomes more severe, the flux of photosynthetically active radiation (PAR; 400 to 700 nm) will decrease. Increased leaf expansion is a critical shade acclimation response, as reduced leaf area will limit photon capture and thus biomass accumulation. Previous reports have been inconsistent regarding the response of leaf area to FR showing increases, decreases and no response. Additionally, studies are often confounded by recent findings that FR is photosynthetic, possibly resulting in an increased leaf expansion through increased growth, rather than a morphological adjustment.
- Extended photosynthetic photon flux density (ePPFD; PAR+FR) was maintained at three levels, as the percentage of FR [100×FR/(PAR+FR)] was adjusted in the growth spectrum of lettuce and cucumber.
- In lettuce, FR increased leaf expansion at high ePPFD, but decreased it at low ePPFD. This interaction was attributed to FR effects on biomass partitioning between leaves and stems under these conditions, which favored stems at low ePPFD, but was unaffected at high ePPFD. In cucumber, FR increased leaf expansion under all ePPFD.

- Implications for horticulture are discussed.

5.2 Introduction

Limited resources limit plant growth (El-Sharkawy, 2011). As sessile organisms, plants must modulate their growth and development to efficiently compete for access to these resources. One of the primary resources that plants compete for is sunlight, which has led to the evolution for a high degree of plant plasticity in response to shaded environments.

Before plants are truly shaded, i.e. before they experience a decrease in photosynthetically active radiation (PAR; 400 to 700 nm), the flux of far-red (FR; 700 to 750 nm) will increase due to reflections from neighboring vegetation primarily in the horizontal direction. This increase in FR (decrease in the R:FR ratio), caused by preferential absorption of photons in the PAR region for photosynthesis and scattering of FR photons by leaf tissue, is perceived by the photoreceptor phytochrome (Ballare *et al*., 1987, 1991; Casal, 2012). As plants grow, they begin to overlap, decreasing the overall photon flux of PAR and FR, although the percentage of FR [100×FR / (PAR + FR)] will remain enriched compared to sunlight. Many plant species adjust their morphology in response to both FR and PAR to maximize survival in a process called shade avoidance (Ballare *et al*., 1991; Schmitt, 1997; Kurepin *et al*., 2009; Pierik & de Wit, 2014). Shade avoidance responses are often defined by increases in stem and petiole elongation, an increase in biomass allocation to stems, increased specific leaf area (SLA; leaf area divided by leaf mass), upward leaf movement (hyponasty), and increased apical dominance (Casal, 2012; Gommers *et al*., 2013; Pierik & de Wit, 2014).

Biomass accumulation is highly correlated with leaf area (Monteith, 1977; Gifford *et al*., 1984; Zhen & Bugbee, 2020a), as leaves are the photon-collecting organs with higher photosynthetic capacity than other organs (Xu *et al*., 1997). Thus, leaf area/expansion in response to shade is a vital parameter for the survival of a plant. SLA, which is often reported to increase in shade, only indicates a change in leaf area given a certain amount of biomass partitioning to the leaves, therefore total plant leaf area is also dependent on the biomass partitioning within plants, which tends to favor stems over leaves in shaded environments (Morgan & Smith, 1979; Ballare *et al*., 1987, 1991; Poorter *et al*., 2012).

The response of leaf area/expansion to an increased percentage of FR (decreased R:FR ratio) has been reported to vary significantly (Casal & Smith, 1989; Casal, 2012; Demotes-Mainard *et al*., 2016), with increases (Lopez-Juez *et al*., 1990; Kurepin *et al*., 2007; Lee *et al*., 2016; Park & Runkle, 2017, 2019; Kalaitzoglou *et al*., 2019; Zou *et al*., 2019; Zhen & Bugbee, 2020a; Legendre & van Iersel, 2021), decreases (Holmes & Smith, 1975; Robson *et al*., 1993; Devlin *et al*., 1999) or no effect (Miyashita *et al*., 1994; Kurepin *et al*., 2007; Lee *et al*., 2015; Park & Runkle, 2017, 2019; Zhang *et al*., 2020). These differences in response are likely species dependent, but they also depend on other environmental conditions. For example, Franklin *et al*. (2003) noted an apparent (unmeasured) increase in leaf area with increased FR, which was contradictory to previous findings and attributed to the lower temperature than the studies they compared to (e.g. Robson *et al*., 1993; Devlin *et al*., 1999). Other studies have noted different effects of FR on leaf area/expansion at different intensities of PAR (Kurepin *et al*., 2007), while others have noted no interaction (Park & Runkle, 2018).

One highly confounding factor with many of these studies is that FR photons are added to a constant flux of traditionally defined PAR. Recent evidence has demonstrated that FR photons are photosynthetic (Zhen & Bugbee, 2020a,b) through excitation of PSI (Zhen & van Iersel, 2017). Because many studies add FR to traditionally defined PAR, they increase the flux of total photosynthetic photons, potentially leading to increases in leaf area through increases in biomass accumulation. It is thus important to properly separate the two effects. Maintaining extended photosynthetic photon flux density (ePPFD = PAR+FR; 400 to 750 nm), while adjusting levels of FR, is one way to separate these two responses.

We sought to investigate the interactions of FR and ePPFD on plant morphology in two widely produced crops, lettuce and cucumber. While plant responses to FR are modulated only by phytochrome (Holmes & Smith, 1975; Franklin *et al*., 2003; Casal, 2012), responses to a decrease in ePPFD are modulated by phytochromes (Millenaar *et al*., 2009; Trupkin *et al*., 2014), cryptochromes (Keller *et al*., 2011; Pedmale *et al*., 2016), and possibly photosynthetic signals (Millenaar *et al*., 2009). Cryptochromes and phytochromes interact with many of the same transcription factors in order to modulate gene expression (de Wit *et al*., 2016), but cryptochrome interaction was shown to regulate genes related to cell wall elasticity while FR was associated with auxin genes (Pedmale *et al*., 2016). Phytochrome responses depend on the ePPFD because thermal reversion (Pfr back to Pr) significantly affects phytochrome dynamics at lower photon fluxes (Sellaro *et al*., 2019). Additionally, hormonal signals in response to FR have different patterns of expression at low and high ePPFD (Hersch *et al*., 2014).

Altogether, the signaling pathways in response to changes in photon quality and quantity are complex, as photoreceptor-controlled responses have appeared both

additive/independent (Neff & Chory, 1988; Keller *et al*., 2011; Pedmale *et al*., 2016) and synergistic (Casal & Mazzella, 1998; Sellaro *et al*., 2009; de Wit *et al*., 2016) in different studies. We hypothesize that increasing the percentage of FR will have a more significant effect on plant development at lower levels of ePPFD, and that FR and ePPFD will interact in the prediction of leaf area. We show that in lettuce increasing FR increases leaf area and dry mass accumulation at high intensities, but decreases leaf area and dry mass accumulation at lower intensities, while in cucumber leaf expansion increased with increasing far-red at all intensities.

5.3 Materials and Methods

5.3.1 Plant Material and Cultural Conditions

Green butterhead lettuce (*Lactuca sativa* 'Rex') and cucumber (*Cucumis sativa* 'Straight eight') seeds were direct seeded then thinned for uniformity after emergence leaving four plants per root module. Root modules measured 20 × 18 × 13 (4680 cm^3) and contained a 1:1 ratio of peat and vermiculite by volume with 0.75 g per L wetting agent (AquaGro G), 1 g per L hydrated lime, and 5 g per module of uniformly mixed slow-release fertilizer (Nutricote total; 18-6-8, N-P-K, type 70). Planted root modules were randomly placed into the 12 treatment chambers. Each chamber had dimensions of 20 × 23 × 30 (L × W × H, 13800 cm^3) with gloss white walls. Fans provided an air velocity of 0.5 m s^{-1} at the top of the canopy. Root modules were watered to 10% excess as needed with dilute fertilizer solution at a rate of 100 mg N per L (21-5-20; Peters Excel; EC = 1 dS m^{-1}), and allowed to passively drain. Type-E Thermocouples connected to a data logger (CR1000, Campbell

Scientific, Logan UT) continuously monitored ambient air temperature. Day/night temperature averaged 23.4±1.2/20.9±0.8 ˚C, with less than a 1˚C variation among chambers. CO_2 concentration was continuously monitored and was identical for all treatments and varied over time between 450 to 500 ppm.

Fig. 5-1 Experimental design of the study. Treatments included four percentages of far-red at three levels of extended photosynthetic photon flux density (ePPFD). The lowest ePPFD in the cucumber study was 50, not 100, µmol m^{-2} s^{-1}.

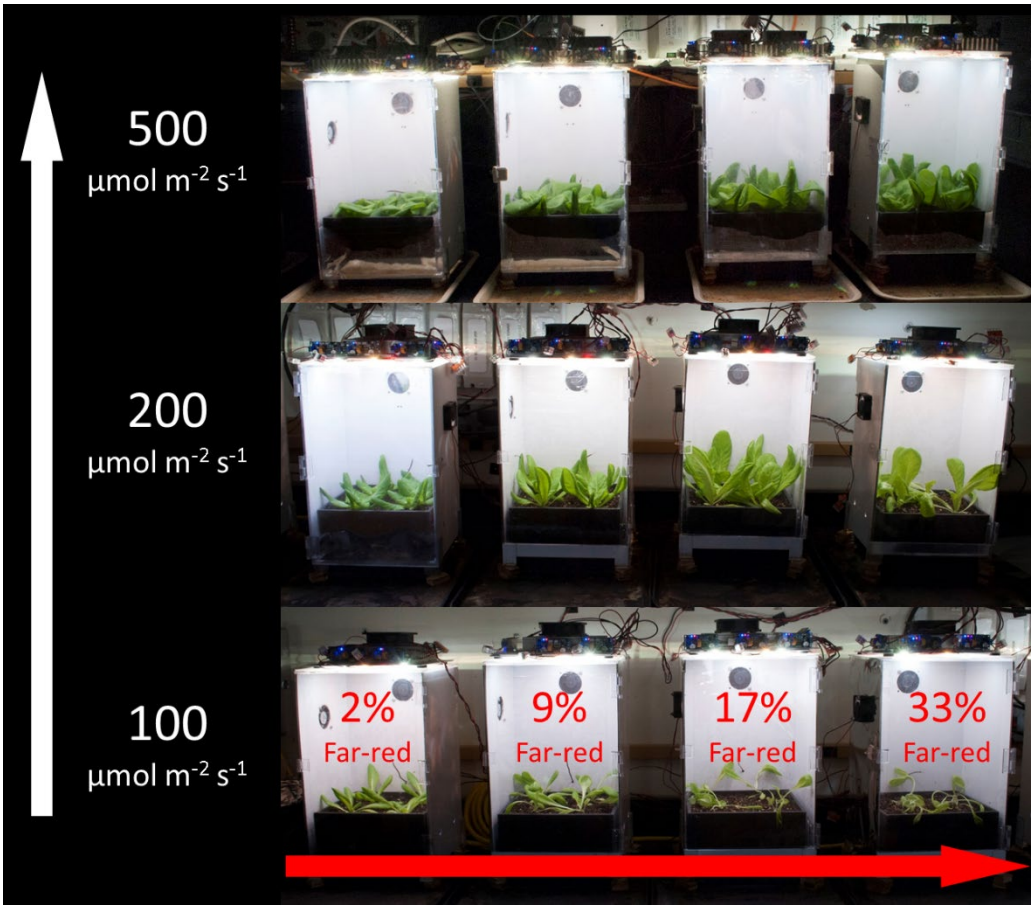

5.3.2 Treatments

The system included 12 chambers with four percentages of FR (Fig. 5-1 and Fig. 5-2) at three levels of ePPFD (4×3 = 12 treatments) for a 16 h photoperiod. In the cucumber study the three levels of ePPFD were 50, 200 and 500 µmol m^{-2} s^{-1} (DLI: 2.88, 11.52 and 28.8 mol m^{-2} d^{-1}). In the lettuce study, the lowest ePPFD treatment (ePPFD: 50 µmol m^{-2} s^{-1}) was increased to 100 µmol m^{-2} s^{-1} (DLI = 5.76 mol m^{-2} d^{-1}) because 50 µmol m^{-2} s^{-1} was below the light compensation point.

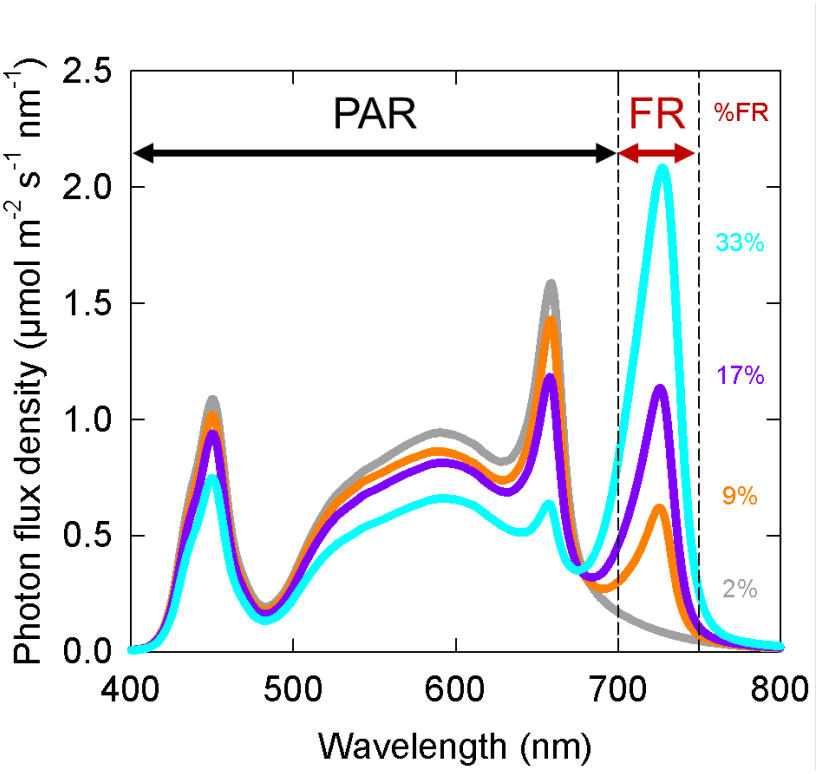

Fig. 5-2 Representative spectral photon distributions for the four fractions of far-red. Spectral photon distribution from the ePPFD: 200 µmol m^{-2} s^{-1} intensity. Spectral distributions from the other studies have the same shape with a different scale on the y-axis. Photon fluxes of blue, green and red were maintained at 20, 40 and 40%, respectively, as a percent of photosynthetically active radiation (PAR; 400 to 700 nm) for each treatment of far-red (FR). Percent far-red (%FR) treatments included 2% (grey), 9% (orange), 17% (purple), and 33% (cyan).

Treatments were developed using phosphor-converted white (2700 and 6500 K), red (peak about 658 nm) and far-red (peak 726 nm) LEDs (Lumileds LLC, San Jose, CA) to output 20, 40 and 40% blue, green and red photons, respectively, as a fraction of PAR. Treatments were then designed to reduce traditionally defined photosynthetic photon flux density (PPFD) while increasing FR photon flux density. Percent FR, as calculated by dividing the FR flux density by the ePPFD and multiplying by 100, was 2, 9, 17 and 33% (Fig. 5-1 and Fig. 5-2). Spectral photon distributions of the treatments were measured before each replicate study with a spectroradiometer (model PS-300; Apogee Instruments, Logan UT). ePPFD was measured with an ePPFD sensor (MQ-260, Apogee Instruments, Logan UT) at the top of the plant canopy throughout the study, and chambers were adjusted to maintain ePPFD at ± 5%. Root modules were rotated every three days to increase the uniformity of treatments within the chamber.

5.3.3 Plant Measurements

Plants were harvested at canopy closure. This occurred 17 or 18 days after emergence in lettuce and 9, 10, or 11 days after emergence in cucumber. At harvest, stem length, leaf area, chlorophyll concentrations and fresh mass were measured. Leaf area was measured using a leaf area meter (LI-3000; LI-COR, Lincoln NE). Petiole length was measured in the cucumber study and leaf length and leaf width were measured in the lettuce study. Leaves and stems (and cotyledons in cucumber) were separated, and dry mass of each organ (DM) was measured after the tissue was dried at 80 ˚C for 48 hours. Percent stem mass was calculated by dividing stem dry mass by total shoot dry mass, multiplied by 100; roots were

not included. Specific leaf area (SLA, m^2_{LA} kg DM_{leaf}^{-1}) was calculated by dividing the leaf area by the dry mass.

5.3.4 Statistical Analysis

The lettuce study was replicated three times and the cucumber study was replicated five times. Every replicate in time contained four plants in each treatment. All data was analyzed using R statistical software (R Foundation for Statistical Computing; Vienna, Austria). ePPFD was treated as a categorical variable with three levels for all analysis. Percent FR was treated as either a continuous variable or a categorical variable depending on the type of analysis. Responses that were linear with increasing percent FR were analyzed with linear mixed-effects regression analysis (percent FR treated as a continuous variable) and non-linear responses were analyzed with two-way ANOVA analysis (percent FR treated as a categorical variable). Replicates in time were treated as random factors in all statistical analyses. Significant effects were determined at the $p < 0.05$ level. Detailed statistical analysis for specific parameters are provided below.

5.4 Results

Fig. 5-3 shows the overhead view of all the plants from each treatment in one replicate study. Fig. 5-4 shows the side view of the plants from each treatment in one replicate study. These photos show approximate diameters and heights of the plants in different treatments.

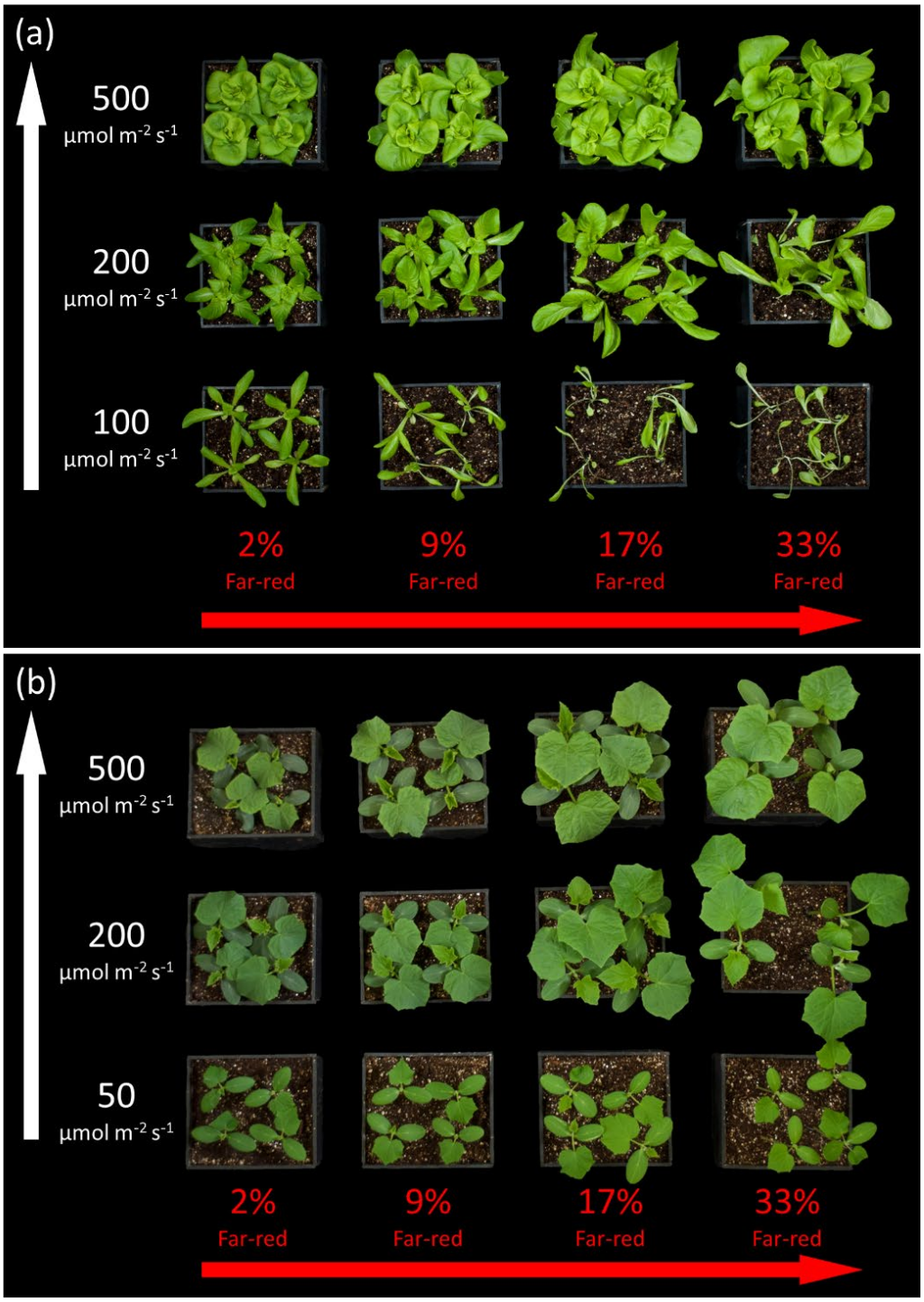

Fig. 5-3 Overhead view of all the treatments in one replicate for (a) lettuce and (b) cucumber. The white arrow on the left indicates increasing extended photosynthetic photon flux density (ePPFD) and the red arrow on the bottom indicates increasing percent far-red.

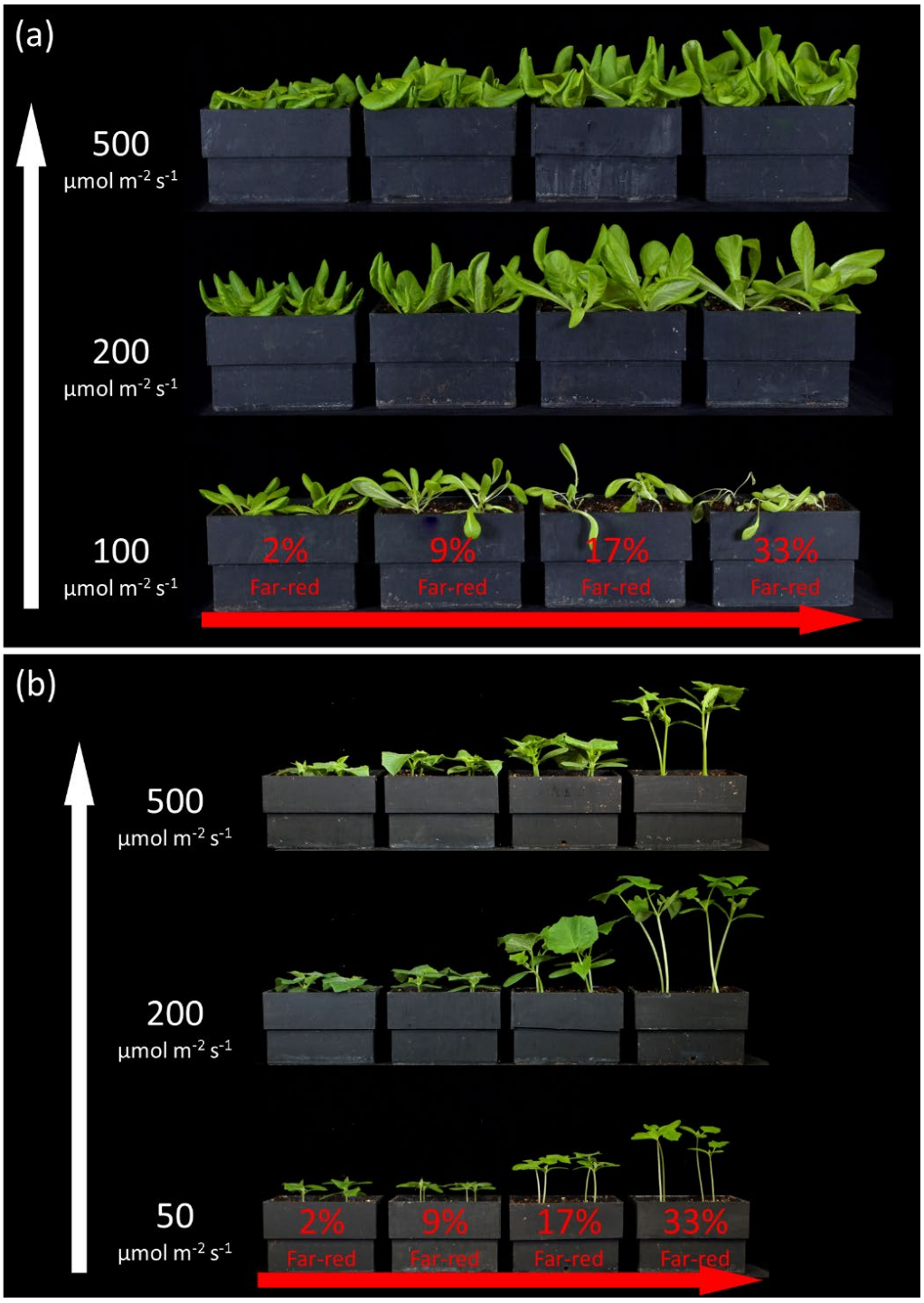

Fig. 5-4 Side view of all the treatments in one replicate for (a) lettuce and (b) cucumber. The white arrow on the left indicates increasing extended photosynthetic photon flux density (ePPFD) and the red arrow on the bottom indicates increasing percent far-red.

5.4.1 Dry Mass

Fig. 5-5a and 5-5b show the effect of ePPFD and percent FR on total shoot dry mass of lettuce and cucumber. The response was non-linear in both species, thus two-way ANOVA analysis and Tukey's post hoc test were used (with percent FR treated as a categorical variable) to separate the significant differences between treatments. The relatively smaller values and variance of total dry mass in the low ePPFD treated plants resulted in reduced statistical power to determine significant difference between percent FR treatments. Therefore, the data of each replicate in time was normalized to its respective 2% (no added FR) control, and this normalized response was analyzed with 1) two-way ANOVA analysis/Tukey's post hoc test to determine significant differences between treatments and 2) a student's t-test to determine if the normalized response was statistically different from one, which represented the response of no added FR. This normalized response is presented in Fig. 5-5c and 5-5d.

Unsurprisingly, higher levels of ePPFD produced more biomass than lower levels in both species. Percent FR and ePPFD interacted to predict biomass accumulation in lettuce, with an increase in dry mass with increasing percent FR at the high ePPFD, but a decrease in dry mass with increasing percent FR at the low ePPFD. This decrease occurred in both the 100 and 200 $\mu mol\ m^{-2}\ s^{-1}$ ePPFD treatments. There was also an interaction between percent FR and ePPFD in cucumber, where the highest percent FR at the lowest ePPFD had a no effect compared to higher ePPFD (Fig. 5-5d). In general, the response of shoot dry mass in cucumber showed no effect of increasing percent FR from 2 to 9%, a sharp increase between 9 and 17% FR, and little response between 17 and 33% FR. Additionally, the normalized dry

mass response in cucumber showed no significant difference from one at the lowest ePPFD and highest percent FR treatment (Fig. 5-5d).

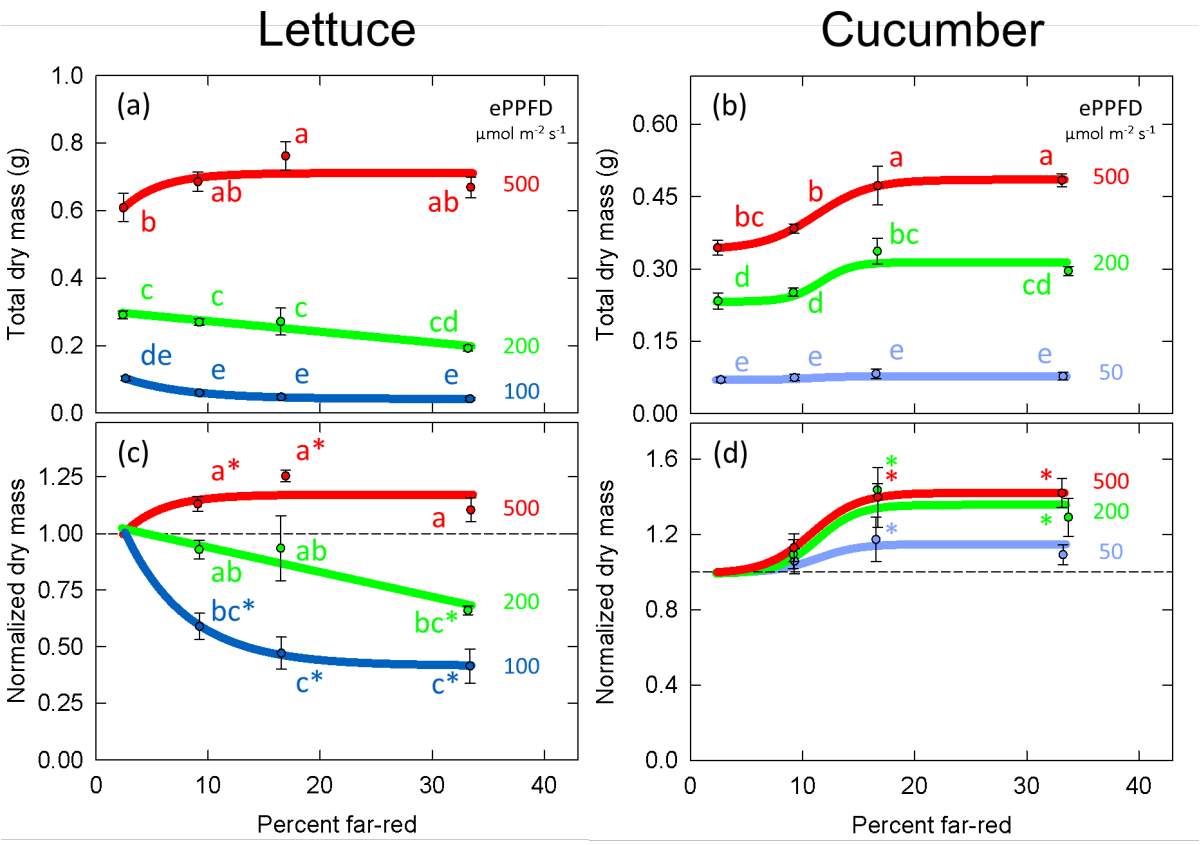

Fig. 5-5 Effects of percent far-red (FR) and extended photosynthetic photon flux density (ePPFD) on shoot dry mass in lettuce (a,c) and cucumber (b,d). (a) and (b) represent absolute values of dry mass and (c) and (d) are the normalized response, where data from each replicate in time was normalized to its respective 2% FR (no added FR) control treatment for each ePPFD. In (c) and (d), * indicates that the treatment is statistically different from 1 (using a student's t-test), which represents the response of the 2% FR control. Trend lines are included to guide the eye, and not meant to be used as a statistical representation. Error bars represent standard error for n = 3 replicates in lettuce and n = 5 replicates in cucumber. Letters are not included in (d) because the treatments were not determined to be statistically different from each other, although treatments were significantly different from the control.

5.4.2 Total Leaf Area

Average plant leaf area is presented in Fig. 5-6. This graph shows similar trends to shoot dry mass, indicating that leaf area significantly affected photon capture and biomass accumulation (leaf area is highly correlated with growth). Due to the similar non-linear response of leaf area to percent FR and ePPFD, this response was analyzed with the same methods as total dry mass.

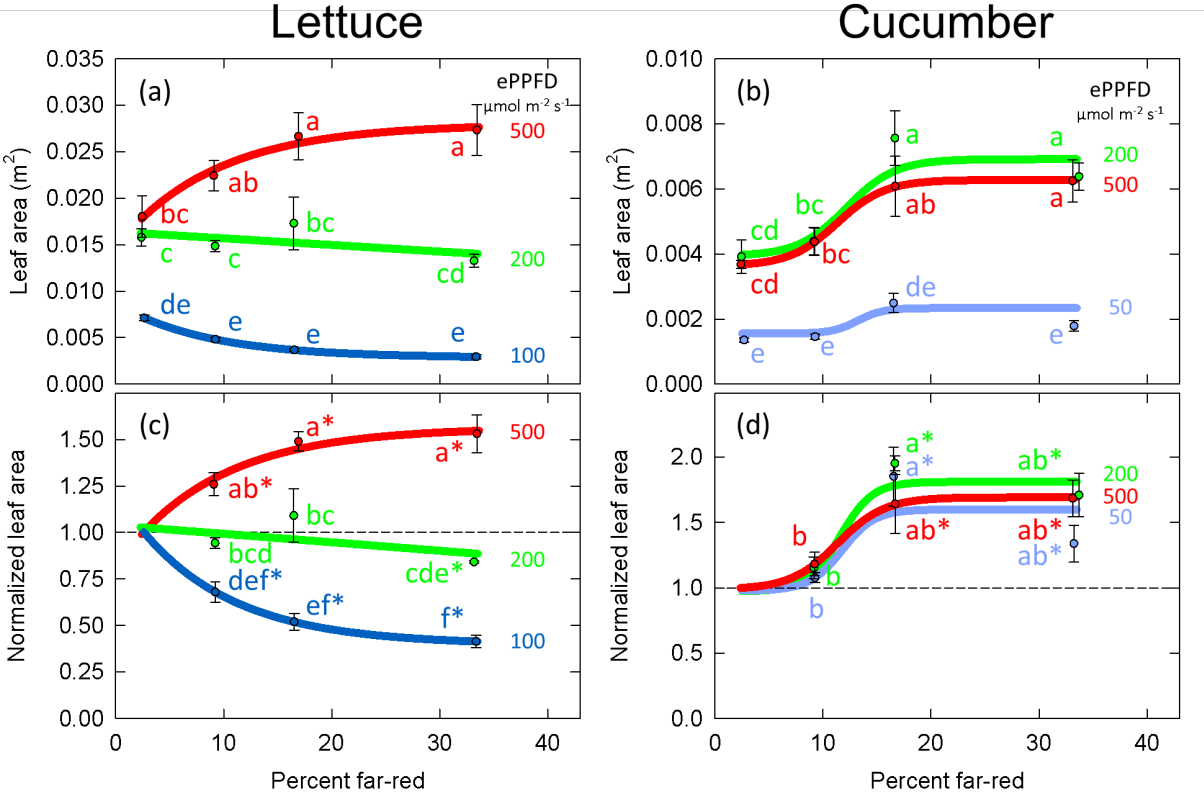

Fig. 5-6 Effect of percent far-red (FR) and extended photosynthetic photon flux density (ePPFD) on leaf area in lettuce (a,c) and cucumber (b,d). (a) and (b) represent absolute values of leaf area and (c) and (d) are the normalized response, where data from each replicate in time has been normalized to its respective 2% FR control treatment for each level of ePPFD. In (c) and (d), * indicates that the treatment is statistically different from 1 (using a student's t-test), which represents the effect of the 2% FR control. Trend lines are included to guide the eye, and not meant to be used as a statistical representation. Error bars represent standard error for n = 3 replicates in lettuce and n = 5 replicates in cucumber.

Because leaf area/expansion is a driver of biomass accumulation, it is valuable to better understand the interaction between the two treatments in controlling this response in lettuce – decreased leaf area with increasing percent FR at 100 and 200 μmol m^{-2} s^{-1}, but increased leaf area with increasing percent FR at 500 μmol m^{-2} s^{-1}. Leaf lengths increased with percent FR at all three levels of ePPFD, while the response of leaf width was similar to the response of leaf area (Fig. H-1a and H-1b). This resulted in cuneate rather than orbicular shaped leaves at higher percent FR (Fig. H-1c). Although an increase in leaf length may be expected under shaded conditions, the change in leaf shape does not explain the interaction between percent FR and ePPFD in predicting total leaf area in lettuce.

5.4.3 Specific Leaf Area

Changes in specific leaf area (SLA) indicate the change leaf area given the biomass partitioning to the leaves. It is widely reported to increase with shade. The response of SLA to percent FR at different levels of ePPFD appeared more linear than the response of dry mass or total leaf area, thus this parameter was analyzed with linear mixed-effects regression with percent FR as a continuous variable and ePPFD as a categorical variable. Increasing the percent FR and decreasing the ePPFD increased SLA in both species (Fig. 5-7a and 5-7b).

Because ePPFD had a large effect on SLA (the lowest ePPFD induced a 2.5 to 3 times higher SLA than the high ePPFD in both species), the best way to determine if there is an interaction between percent FR and ePPFD was to normalize the response. This is because the non-normalized response could indicate an interaction even if the effect of percent FR induced the same fractional change at all three levels of ePPFD. Fig. 5-7c and 5-7d normalize

the SLA response to the average 2% FR effect at each ePPFD. Linear mixed-effects regression analysis was then performed on this normalized data, which found no interaction between ePPFD and percent FR for either species, although the interaction approached significant in cucumber (Fig. 5-7d).

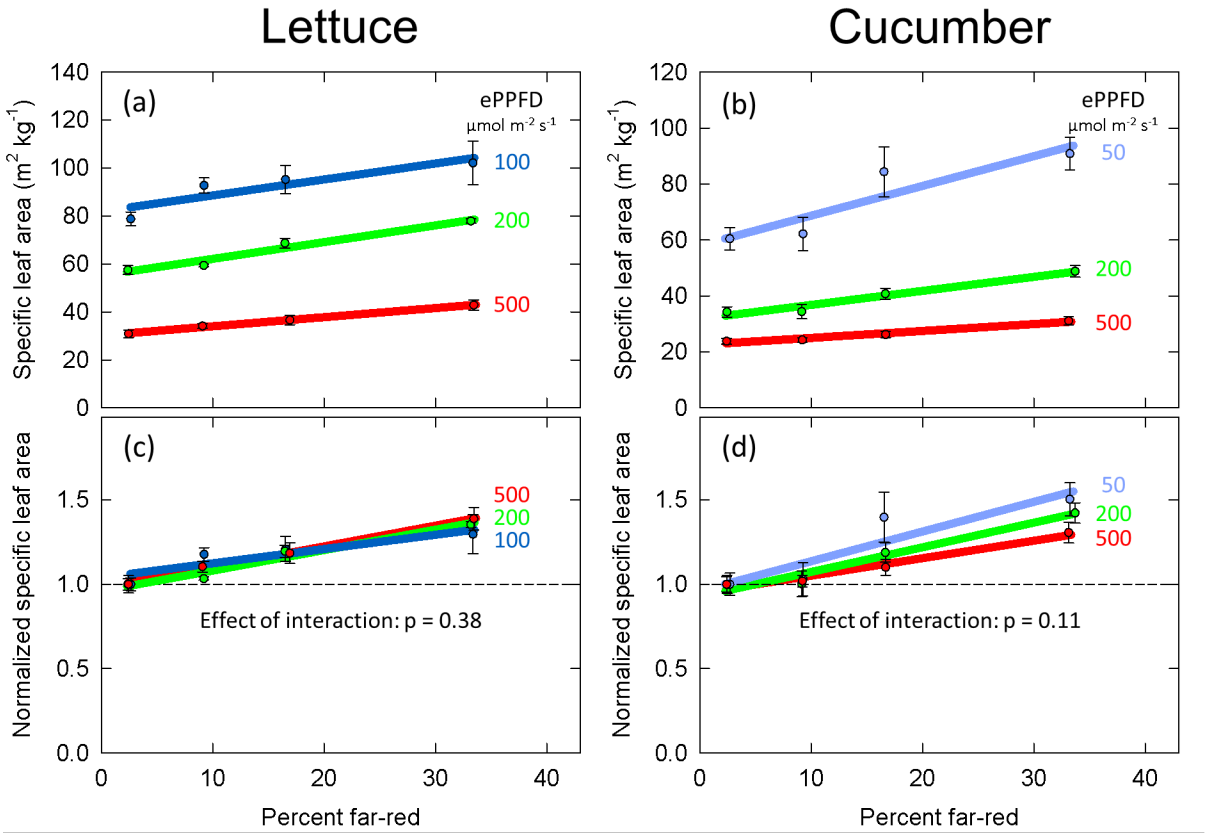

Fig. 5-7 Effect of percent far-red (FR) at different levels of extended photosynthetic photon flux density (ePPFD) on specific leaf area (SLA) in lettuce (a,c) and cucumber (b,d). (a) and (b) represent absolute values of SLA, while (c) and (d) are the normalized response, where data has been normalized to the average response in the 2% FR control treatment for each ePPFD. Increasing the percent FR and decreasing the ePPFD increased SLA in both species. Error bars represent standard error for n = 3 replicates in lettuce and n = 5 replicates in cucumber.

Overall, the increase in SLA in response to both increasing percent FR and decreasing ePPFD has been regularly observed in previous studies. However, because there was no interaction between the two treatments to predict SLA, this parameter (SLA) does not explain the interaction between to two treatments to predict total leaf area (Fig. 5-6a and 5-6c).

5.4.4 Biomass Partitioning

Increased shade is often reported to increase stem lengths, and this is often associated with an increase in biomass partitioning to stems. Percent stem mass, a metric that assesses partitioning to stems, is calculated by dividing stem dry mass by total shoot dry mass (and multiplying by 100). Subtracting percent stem mass from 100 is the shoot biomass allocation to leaves (and cotyledons for cucumber).

In lettuce, the effects of percent FR and ePPFD on percent stem mass were analyzed with linear mixed-effects regression following the same procedure as SLA (Fig.5-7a). In cucumber, the effect of percent FR on percent stem mass was non-linear, and was thus analyzed with two-way ANOVA analysis and Tukey's post hoc test.

In cucumber, there was no difference between percent stem mass at 2 and 9% FR for any of the three levels of ePPFD (Fig. 5-8b), then increasing percent FR from 9 to 33% increased biomass partitioning to stems at all three levels of ePPFD.

In lettuce, there was also an effect of percent FR, ePPFD and an interaction between the two treatments in the prediction of percent stem mass. The most striking impact of the interaction between percent FR and ePPFD in lettuce was that increasing percent FR from 2 to 33% increased percent stem mass by 2.5-fold at the lowest ePPFD, but had no effect at the

highest ePPFD (Fig. 5-8a). Similar to the effect of ePPFD at the lowest percent FR in cucumber (dotted lines in Fig. 5-8b), percent stem mass in lettuce tended to be higher at 100 µmol m^{-2} s^{-1} than the higher two levels of ePPFD at 2% FR. But, this was not statistically significant at the p = 0.05 level using Tukey's post hoc test from a two-way ANOVA (p = 0.09 and 0.06 for 100 compared to 200 and 100 compared to 500 µmol m^{-2} s^{-1}, respectively).

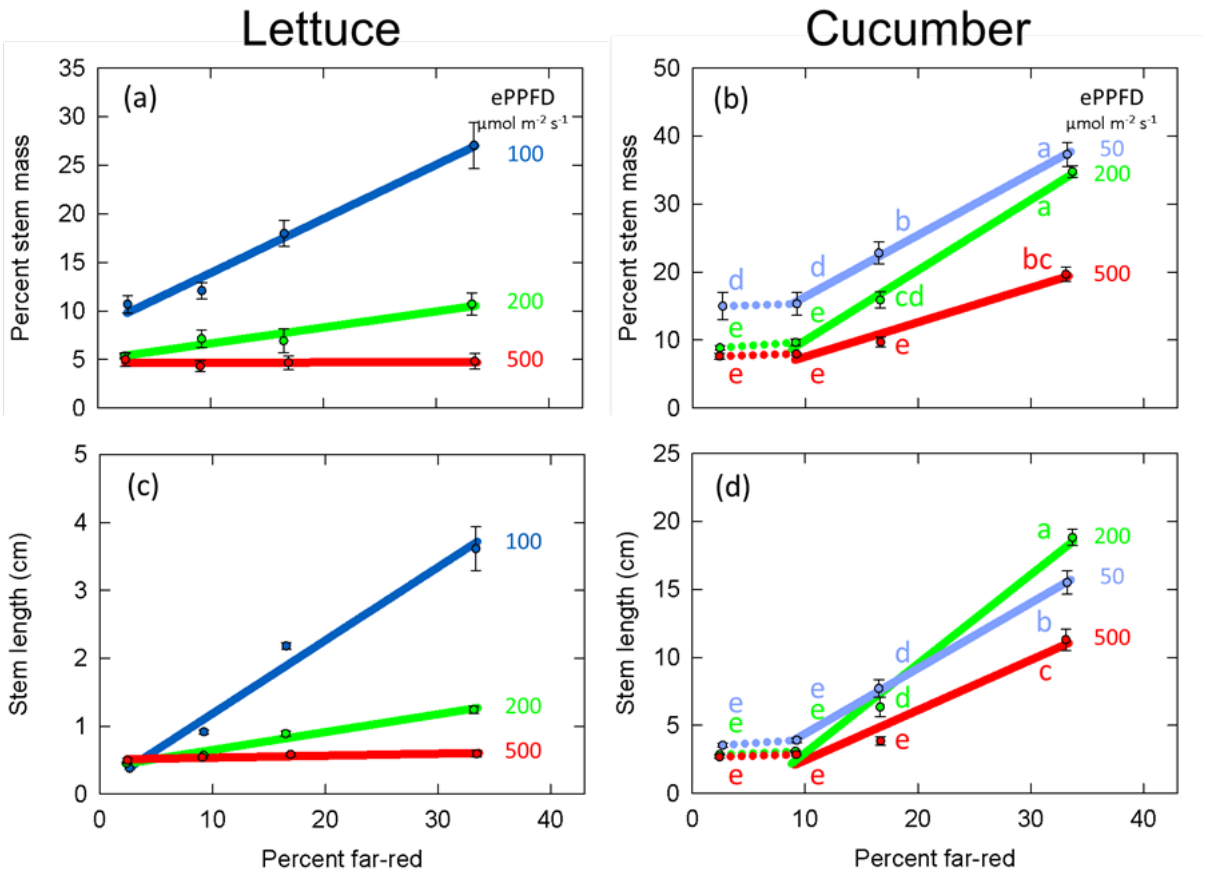

Fig. 5-8 Effects of percent far-red (FR) at different levels of extended photosynthetic photon flux density (ePPFD) on stems. (a) Percent stem mass in lettuce, representative of biomass partitioning to stems, (b) percent stem mass in cucumber, (c) stem length in lettuce, and (d) stem length in cucumber. The lettuce data was analyzed with linear mixed-effects regression analysis, and the cucumber data was analyzed with a two-way ANOVA analysis. Error bars represent standard error for n = 3 replicates in lettuce and n = 5 replicates in cucumber.

This striking interaction in lettuce between percent FR and ePPFD in the prediction of percent stem mass explain the interaction between the two treatments in the prediction of total plant leaf area. As percent stem mass (biomass allocation to stems) increases, percent leaf mass (biomass allocation to leaves) decreases. Because SLA increased with increasing percent FR at all levels of ePPFD (Fig. 5-7c), total leaf area increased under the highest ePPFD as biomass partitioning to leaves was unaffected. However, at the lowest ePPFD, even though the FR treatments increased SLA by about 30%, biomass was redirected away from the leaves to a significant enough degree to reduce leaf area.

Due to thermal reversion of phytochrome, ePPFD and FR have been combined into one unifying model called the cellular model, which accounts for both increased thermal reversion at higher temperatures and the larger contribution of thermal reversion on phytochrome dynamics at lower ePPFD. This model was unable to explain the response of percent stem mass in cucumber (Fig. H-2), indicating a contribution of other factors (e.g. cryptochrome and/or photosynthate signals).

5.4.5 Stem Length

The responses of lettuce and cucumber stem lengths were similar to the response of percent stem mass, and they data for each species was analyzed using the same methods as percent stem mass (Fig. 5-8). This indicates that the increase in biomass allocation to stems was to support their rapid elongation. There was an effect of percent FR, ePPFD and an interaction between the two in the prediction of stem length in both species. In cucumber, the tallest plants at the highest percent FR occurred at the middle ePPFD instead of the lowest

ePPFD. A similar response was observed in longest petiole length (Fig. H-3). This is likely a direct result of lower photosynthesis resulting in reduced growth.

5.5 Discussion

Leaves are primarily responsible for carbon gain with higher photosynthetic capacity than stems, petioles and fruits (Xu *et al*., 1997). Despite the importance of this organ, the response of total leaf area to shade signals (specifically an increase in FR) has been inconsistent (see introduction). Here, we show that the effect of percent FR on leaf expansion/leaf area can depend on the ePPFD (Fig. 5-6a, c). We conclude that this interaction is a byproduct of the differences in biomass allocation between stems and leaves under these conditions, and not a response of SLA which increased with FR under all levels of ePPFD. This interaction between ePPFD and percent FR is also dependent on species as it only occurred in lettuce.

In cucumber, increasing percent FR increased leaf area at all three levels of ePPFD despite a similar interaction between percent FR and ePPFD as lettuce in the prediction of biomass partitioning to stems. This contradiction may be explained by 1) the effect of increasing FR on percent stem mass was only reduced at the highest ePPFD in cucumber, whereas it was eliminated entirely in lettuce; and 2) there was an insignificant ($p = 0.11$, Fig. 5-7d) trend of a larger effect of increasing percent FR on SLA at lower levels of ePPFD in cucumber. Therefore, the morphological effects of SLA may have offset the effects of biomass partitioning in cucumber resulting in similar total leaf areas.

Increased percent stem mass was associated with increased stem length (Fig. 5-8). Biomass allocation between leaves and stems has been reported to be sensitive to both FR and ePPFD (Morgan & Smith, 1979, 1981; Ballare *et al*., 1987; Poorter *et al*., 2011; Yang *et al*., 2018). Faster rates of stem elongation may require an increase in sugars to support the upregulated metabolism. As such, increases in percent FR have been associated with 1) a decrease in expression of genes related to photosynthesis, the Calvin cycle, and sucrose/starch biosynthesis in *Arabidopsis* hypocotyls (but not cotyledons) suggesting a decrease in local sugar production in the hypocotyl and thus an increase in stem sink strength; and 2) an increase in the transport of radiolabeled carbon from cotyledons to hypocotyls (de Wit *et al*., 2016). This transported carbon was allocated to multiple pools of carbon within the hypocotyl including amino acids, lipids, neutral sugars, proteins and cell walls. Of these, the insoluble portion (cell walls and proteins) and the ethanol soluble portion (lipids/cell membranes) both increased over 3-fold from the high R:FR treated to the low R:FR treated seedlings. The increases in these two pools indicate an increase to structural components, meaning an increase in biomass accumulation. In addition to this change in carbon transport, auxin (which is upregulated in the shade, see below), inhibits cytokinin expression in leaf primordia (Carabelli *et al*., 2007), which leads to an inhibition of cell proliferation in leaves and reduced leaf area (Rielfer *et al*., 2006; Wu *et al*., 2017). This provides a second mechanism by which biomass allocation to stems increases in the shade. Low ePPFD has been reported to decrease the root mass fraction while increasing the stem and leaf mass fractions, while the R:FR ratio has been shown to have little effect on root mass fraction (Poorter *et al*., 2011), but we did not measure root mass fraction.

Shade symptoms are often reported to increase in response to both and decreases in photon intensity and increases in FR. The response to photon intensity are often associated with a decrease in blue photons specifically (de Wit *et al*., 2016; Pedmale *et al*., 2016), although this is not always the case (Millenaar *et al*., 2009). Previous studies have shown similar interactions between low blue (low photon intensity) and increased FR, with synergistic shade responses under both conditions compared to one shade condition alone (de Wit *et al*., 2016). This is similar to the results obtained in this study, especially for stem elongation (Fig. 5-8). This interaction is hypothesized to be related to both the PHYTOCHROME INTERACTING FACTOR (PIF) family of transcription factors and the E3 ubiquitin ligase formed by CONSTITUTIVELY PHOTOMORPHOGEIC 1 (COP1) and SUPRESSOR OF PHYA-105(SPA) proteins (Su *et al*., 2017), both of which are regulated by the phytochrome and cryptochrome photoreceptors (Legris *et al*., 2019).

5.5.1 Photosynthetic Considerations

Often, studies investigating plant responses to FR will typically supplement with FR, rather than substitute traditionally defined PAR with FR. Increasing percent FR while maintaining ePPFD (decreasing traditionally defined PAR) removes the potential impact of photosynthesis on leaf expansion through increased growth rates. Assuming PAR and FR photons both drive photosynthesis with equal efficiencies, then the studies performed here (substituting PAR with FR) would at most result in equal photosynthesis. However, this 1:1 assumption is likely not the case. Zhen & Bugbee (2020b) noted that the photosynthetic relationship of 400 to 700 nm photons and 701 to 750 nm photons began to deviate from a

1:1 equivalency when FR was added in excess of 40% of PAR (29% FR based on the definition used here). Furthermore, Zhen *et al*. (2018) showed that photons at 752 nm did not increase the quantum yield of PSII (the fraction of absorbed photons used for photochemistry), indicating that photons at 752 nm did not contribute to photosynthesis (the next lowest wavelength measured was 731 nm). These considerations indicate that 1) extending the definition of photosynthetic photons out to 750 nm may overestimate the photosynthetic response, and b) 33% FR used in this study would have deviated from a 1:1 photosynthetic relationship FR and PAR.

Despite this limitation of our experimental design, the decreased contribution of FR to photosynthesis further highlight the effect of increasing FR on leaf expansion in cucumber and lettuce (at high photon fluxes in the latter).

5.5.2 Implications for Horticulture

The results presented here have substantial implications for the horticultural industry – especially in sole-source lighting environments, where electric lighting from LEDs has been rapidly increasing. Providing photons for crop production is expensive, especially when considering the electrical power required to operate the LEDs. FR LEDs are among the highest efficacy LEDs (µmol of photons per joule input electrical energy), primarily because of the lower energy of the photons (Kusuma *et al*., 2020). Interest in FR for horticultural environments has increased in the past five years where studies have often found that adding FR increases leaf area or plant diameter in lettuce, resulting in an increase in fresh and dry mass (Lee *et al*., 2016; Meng & Runkle, 2019; Zou *et al*., 2019; Zhen & Bugbee, 2020a;

Legendre & van Iersel, 2021). But, these studies often supplemented with FR rather than substituting PAR photons for FR photons. The addition of FR LEDs in fixtures increases the price for two reasons: 1) FR LEDs are lower demand, meaning they are more expansive, and 2) operating these additional LEDs increases the power requirements. Thus, substitution of PAR with FR is much more reasonable for practical applications. Zhen & Bugbee (2020a) found that substituting 14% of PAR with FR at an ePPFD of 350 μmol m^{-2} s^{-1} resulted in similar quantum yields for CO_2 fixation in 'Waldmann's Dark Green' lettuce, but increased biomass accumulation by 29 to 31% via an increase in photon capture (leaf expansion). Similarly, Legendre & van Iersel (2021) concluded that FR photons were between 57 to 183% more effective at increasing photon capture than PAR photons in 'Green Salad Bowl' lettuce, and were thus 93 to 162% more effective at increasing biomass accumulation. Interestingly, they observed no interaction between PPFD and FR, when PPFD varied between 111 and 245 μmol m^{-2} s^{-1}. Here, we show a clear interaction between both of these parameters in 'Rex' lettuce, with no benefit of substituting PAR with FR when the total ePPFD was 100 and 200 μmol m^{-2} s^{-1}. Additionally, substituting 33% of the PAR for FR photons resulted in decreases in leaf expansion and dry mass accumulation at these two photon intensities (Fig. 5-5 and Fig. 5-6). Thus, the addition of FR appeared to only be beneficial at high ePPFD in this study, possibly indicating that FR will not be beneficial in some cultivars if the ePPFD is too low, and it may actually be detrimental. Further research is required to determine how common this response is across cultivars of lettuce and other leafy greens.

Producers can increase yields by including FR LEDs in lighting fixtures because FR photons will increase leaf expansion and photon capture, while decreasing electrical input

(depending on operating conditions and other LEDs in the fixture). Based on current definitions, FR photons are not considered in the calculation of photosynthetic photon efficacy (PPE), which is the flux of photosynthetic photons (μmol s^{-1}) divided by the input power (W), resulting in μmol per J. Currently, photosynthetic photons are considered to only be those with wavelengths between 400 to 700 nm based on studies by McCree (1971, 1972). Because this definition excludes photons between 700 to 750 nm, the benefits of photons from FR LEDs, both on leaf expansion and photosynthesis are excluded. These definitions ought to be reconsidered, but at the same time, FR must be used with caution, as we have shown it can be detrimental in some conditions.

5.6 Literature Cited

Ballaré CL, Sánchez RA, Scopel AL, Casal JJ, Ghersa CM. 1987. Early detection of neighbour plants by phytochrome perception of spectral changes in reflected sunlight. *Plant, Cell & Environment* **10**: 551–557.

Ballaré CL, Scopel AL, Sánchez RA. 1991. Photocontrol of stem elongation in plant neighbourhoods: effects of photon fluence rate under natural conditions of radiation. *Plant, Cell & Environment* **14**: 57–65.

Ballaré CL, Pierik R. 2017. The shade-avoidance syndrome: Multiple signals and ecological consequences. *Plant, Cell & Environment* **40**: 2530–2543.

Carabelli M, Possenti M, Sessa G, Ciolfi A, Sassi M, Morelli G, Ruberti I. 2007. Canopy shade causes a rapid and transient arrest in leaf development through auxin-induced cytokinin oxidase activity. *Genes & Development* **21**: 1863–1868.

Casal JJ. 2012. Shade avoidance. *The Arabidopsis Book/American Society of Plant Biologists* **10**: e0157.

Casal JJ, Mazzella MA. 1998. Conditional synergism between cryptochrome 1 and phytochrome B is shown by the analysis of phyA, phyB, andhy4 simple, double, and triple mutants in Arabidopsis. *Plant Physiology* **118**: 19–25.

Casal, JJ, Smith H. 1989. The function, action and adaptive significance of phytochrome in light-grown plants. *Plant, Cell & Environment* **12**: 855–862.

Demotes-Mainard S, Péron T, Corot A, Bertheloot J, Le Gourrierec J, Pelleschi-Travier S, Crespel L, Morel P, Huché-Thélier L, Boumaza R et al. 2016. Plant responses to red and far-red lights, applications in horticulture. *Environmental and Experimental Botany* **121**: 4–21.

Devlin PF, Robson PR, Patel SR, Goosey L, Sharrock RA, Whitelam GC. 1999. Phytochrome D acts in the shade-avoidance syndrome in Arabidopsis by controlling elongation growth and flowering time. *Plant Physiology* **119**: 909–916.

de Wit M, George GM, Ince YÇ, Dankwa-Egli B, Hersch M, Zeeman SC, Fankhauser C. 2018. Changes in resource partitioning between and within organs support growth adjustment to neighbor proximity in *Brassicaceae* seedlings. *Proceedings of the National Academy of Sciences* **115**: E9953–E9961.

de Wit M, Keuskamp DH, Bongers FJ, Hornitschek P, Gommers CM, Reinen E, Martínez-Cerón C, Fankhauser C, Pierik R. 2016. Integration of phytochrome and cryptochrome signals determines plant growth during competition for light. *Current Biology* **26**: 3320–3326.

El-Sharkawy MA. 2011. Overview: Early history of crop growth and photosynthesis modeling. *BioSystems* **103**: 205–211.

Franklin KA, Praekelt U, Stoddart WM, Billingham OE, Halliday KJ, Whitelam GC. 2003. Phytochromes B, D, and E act redundantly to control multiple physiological responses in Arabidopsis. *Plant Physiology* **131**: 1340–1346.

Fraser DP, Hayes S, Franklin KA. 2016. Photoreceptor crosstalk in shade avoidance. *Current Opinion in Plant Biology* **33**: 1–7.

Gifford RM, Thorne JH, Hitz WD, Giaquinta RT. 1984. Crop productivity and photoassimilate partitioning. *Science* **225**: 801–808.

Gommers CM, Visser EJ, St Onge KR, Voesenek LA, Pierik R. 2013. Shade tolerance: when growing tall is not an option. *Trends in Plant Science* **18**: 65–71.

Hersch M, Lorrain S, de Wit M, Trevisan M, Ljung K, Bergmann S, Fankhauser C. 2014. Light intensity modulates the regulatory network of the shade avoidance response in Arabidopsis. *Proceedings of the National Academy of Sciences* **111**: 6515–6520.

Holmes MG, Smith H. 1975. The function of phytochrome in plants growing in the natural environment. *Nature* **254**: 512–514.

Kalaitzoglou P, Van Ieperen W, Harbinson J, van der Meer M, Martinakos S, Weerheim K, Nicole CCS, Marcelis LF. 2019. Effects of continuous or end-of-day far-red light on tomato plant growth, morphology, light absorption, and fruit production. *Frontiers in Plant Science* **10**: 322.

Keller MM, Jaillais Y, Pedmale UV, Moreno JE, Chory J, Ballaré CL. 2011. Cryptochrome 1 and phytochrome B control shade-avoidance responses in Arabidopsis via partially independent hormonal cascades. *The Plant Journal* **67**: 195–207.

Kurepin LV, Emery RN, Pharis RP, Reid DM. 2007. Uncoupling light quality from light irradiance effects in *Helianthus annuus* shoots: putative roles for plant hormones in leaf and internode growth. *Journal of Experimental Botany* **58**: 2145–2157.

Kusuma P, Pattison PM, Bugbee B. 2020. From physics to fixtures to food: current and potential LED efficacy. *Horticulture Research* **7**: 1–9.

Lee MJ, Park SY, Oh MM. 2015. Growth and cell division of lettuce plants under various ratios of red to far-red light-emitting diodes. *Horticulture, Environment, and Biotechnology* **56**: 186–194.

Lee MJ, Son KH, Oh MM. 2016. Increase in biomass and bioactive compounds in

lettuce under various ratios of red to far-red LED light supplemented with blue LED light. *Horticulture, Environment, and Biotechnology* **57**: 139–147.

Legendre R, van Iersel MW. 2021. Supplemental Far-Red Light Stimulates Lettuce Growth: Disentangling Morphological and Physiological Effects. *Plants* **10**: 166.

Legris M, Ince YÇ, Fankhauser C. 2019. Molecular mechanisms underlying phytochrome-controlled morphogenesis in plants. *Nature Communications* **10**: 1–15.

López-Juez E, Buurmeijer WF, Heeringa GH, Kendrick RE, Wesselius JC. 1990. Response of light-grown wild-type and long hypocotyl mutant cucumber plants to end-of-day far-red light. *Photochemistry and Photobiology* **52**: 143–149.

McCree, KJ. 1971. The action spectrum, absorptance and quantum yield of photosynthesis in crop plants. *Agricultural Meteorology* **9**: 191–216.

McCree, KJ. 1972. Test of current definitions of photosynthetically active radiation against leaf photosynthesis data. *Agricultural Meteorology* **10**: 443–453.

Meng Q, Runkle ES. 2019. Far-red radiation interacts with relative and absolute blue and red photon flux densities to regulate growth, morphology, and pigmentation of lettuce and basil seedlings. *Scientia Horticulturae* **255**: 269–280.

Millenaar FF, Van Zanten M, Cox MC, Pierik R, Voesenek LA, Peeters AJ. 2009. Differential petiole growth in Arabidopsis thaliana: photocontrol and hormonal regulation. *New Phytologist* **184**: 141–152.

Miyashita Y, Kitaya Y, Kozai T, Kimura T. 1994. Effects of red and far-red light on the growth and morphology of potato plantlets in vitro: using light emitting diode as a light source for micropropagation. *Environmental Effects and their Control in Plant Tissue Culture* **393**: 189–194.

Monteith JL. 1977. Climate and the efficiency of crop production in Britain. *Philosophical Transactions of the Royal Society of London. B, Biological Sciences* **281**: 277–294.

Morgan DC, Smith H. 1979. A systematic relationship between phytochrome-controlled development and species habitat, for plants grown in simulated natural radiation. *Planta* **145**: 253–258.

Morgan DC, Smith H. 1981. Control of development in Chenopodium album L. By shadelight:the effect of light quantity (total fluence rate) and light quality (red. Far-red ratio). *New Phytologist* **88**: 239–248.

Neff MM, Chory J. 1998. Genetic interactions between phytochrome A, phytochrome B, and cryptochrome 1 during Arabidopsis development. *Plant Physiology* **118**: 27–35.

Park Y, Runkle ES. 2017. Far-red radiation promotes growth of seedlings by increasing leaf expansion and whole-plant net assimilation. *Environmental and Experimental Botany* **136**: 41–49.

Park Y, Runkle ES. 2018. Far-red radiation and photosynthetic photon flux density independently regulate seedling growth but interactively regulate flowering. *Environmental and Experimental Botany* **155**: 206–216.

Park Y, Runkle ES. 2019. Blue radiation attenuates the effects of the red to far-red ratio on extension growth but not on flowering. *Environmental and Experimental Botany* **168**: 103871.

Pedmale UV, Huang SSC, Zander M, Cole BJ, Hetzel J, Ljung K, Reis PAB, Sridevi

P, Nito K, Nery JR et al. 2016. Cryptochromes interact directly with PIFs to control plant growth in limiting blue light. *Cell* **164**: 233–245.

Pierik R, de Wit M. 2014. Shade avoidance: phytochrome signalling and other aboveground neighbour detection cues. *Journal of Experimental Botany* **65**: 2815–2824.

Poorter H, Niklas KJ, Reich PB, Oleksyn J, Poot P, Mommer L. 2012. Biomass allocation to leaves, stems and roots: meta-analyses of interspecific variation and environmental control. *New Phytologist* **193**: 30–50.

Riefler M, Novak O, Strnad M, Schmülling T. 2006. Arabidopsis cytokinin receptor mutants reveal functions in shoot growth, leaf senescence, seed size, germination, root development, and cytokinin metabolism. *The Plant Cell* **18**: 40–54.

Robson PR, Whitelam GC, Smith H. 1993. Selected components of the shade-avoidance syndrome are displayed in a normal manner in mutants of *Arabidopsis thaliana* and *Brassica rapa* deficient in phytochrome B. *Plant Physiology* **102**: 1179–1184.

Schmitt J. 1997. Is photomorphogenic shade avoidance adaptive? Perspectives from population biology. *Plant, Cell & Environment* **20**: 826–830.

Sellaro R, Hoecker U, Yanovsky M, Chory J, Casal JJ. 2009. Synergism of red and blue light in the control of Arabidopsis gene expression and development. *Current Biology* **19**: 1216–1220.

Sellaro R, Smith RW, Legris M, Fleck C, Casal JJ. 2019. Phytochrome B dynamics departs from photoequilibrium in the field. *Plant, Cell & Environment **42**:* 606–617.

Su J, Liu B, Liao J, Yang Z, Lin C, Oka Y. 2017. Coordination of cryptochrome and phytochrome signals in the regulation of plant light responses. *Agronomy* **7**: 25.

Trupkin SA, Legris M, Buchovsky AS, Rivero MBT, Casal JJ. 2014. Phytochrome B nuclear bodies respond to the low red to far-red ratio and to the reduced irradiance of canopy shade in Arabidopsis. *Plant Physiology* **165**: 1698–1708.

Wu Y, Gong W, Yang W. 2017. Shade inhibits leaf size by controlling cell proliferation and enlargement in soybean. *Scientific Reports* **7**: 1–10.

Xu HL, Gauthier L, Desjardins Y, Gosselin A. 1997. Photosynthesis in leaves, fruits, stem and petioles of greenhouse-grown tomato plants. *Photosynthetica* **33**: 113–123.

Yang F, Fan Y, Wu X, Cheng Y, Liu Q, Feng L, Chen J, Wang Z, Wang X, Yong T, Liu W. 2018. Auxin-to-gibberellin ratio as a signal for light intensity and quality in regulating soybean growth and matter partitioning. *Frontiers in Plant Science* **9**: 56.

Zou J, Zhang Y, Zhang Y, Bian Z, Fanourakis D, Yang Q, Li T. 2019. Morphological and physiological properties of indoor cultivated lettuce in response to additional far-red light. *Scientia Horticulturae* **257**: 108725.

Zhang M, Park Y, Runkle ES. 2020. Regulation of extension growth and flowering of seedlings by blue radiation and the red to far-red ratio of sole-source lighting. *Scientia Horticulturae* **272**: 109478.

Zhen S, Bugbee B. 2020a. Substituting far-red for traditionally defined photosynthetic photons results in equal canopy quantum yield for CO_2 fixation and increased photon capture during long-term studies: Implications for re-defining PAR. *Frontiers in Plant Science* **11**: 1433.

Zhen S, Bugbee B. 2020b. Far-red photons have equivalent efficiency to traditional

photosynthetic photons: Implications for redefining photosynthetically active radiation. *Plant, Cell & Environment* **43**: 1259–1272.

Zhen S, Haidekker M, van Iersel MW. 2019. Far-red light enhances photochemical efficiency in a wavelength-dependent manner. *Physiologia Plantarum* **167**: 21–33.

Zhen S, van Iersel MW. 2017. Far-red light is needed for efficient photochemistry and photosynthesis. *Journal of Plant Physiology* **209**: 115–122.

CHAPTER 6

PHOTONS FROM NIR LEDS CAN DELAY FLOWERING IN SHORT-DAY SOYBEAN AND *CANNABIS*: IMPLICATIONS FOR PHYTOCHROME ACTIVITY

6.1 Abstract

Photons during the dark period delay flowering in short-day plants (SDP). Red photons applied at night convert phytochromes to the active far-red absorbing form (P_{fr}), leading to inhibition of flowering. Far-red photons (greater than 700 nm) re-induce flowering when applied after a pulse of red photons during the dark period. However, far-red photons at sufficiently high intensity and duration delay flowering in sensitive species. Mechanistically, this response occurs because phytochrome-red (P_r) absorbance is not zero beyond 700 nm. We applied nighttime photons from near infrared (NIR) LEDs over a 12 h dark period. Compared to control plants without nighttime photons, photons from NIR LEDs delayed flowering in two sensitive species: 3 days in *Glycine max* (at an intensity of 3.8 μmol m^{-2} s^{-1}) and 12 days in *Cannabis sativa* (5.2 μmol m^{-2} s^{-1}). This suggests that photons from NIR LEDs can activate phytochromes (convert P_r to P_{fr}) and thus alter plant development.

6.2 Introduction

Phytochromes are a class of plant photoreceptors that modulate development throughout the life cycle of a plant. They interconvert between two major forms upon photon absorption: the inactive form (P_r), which is most sensitive to red photons, and the active form (P_{fr}), which is most sensitive to far-red photons [1]. Although P_r and P_{fr} are named for the

region that they are most sensitive to, both forms absorb across the entire biologically active range of radiation (300 to 800 nm). Historically, a metric called phytochrome photoequilibrium (PPE) has been used to predict phytochrome-mediated plant developmental responses. PPE is an estimate of the fraction of active P_{fr} to the total phytochrome pool, and it is calculated from the spectral photon distribution (SPD) of the incident light and photoconversion cross-sections for P_r and P_{fr} at each wavelength. Photoconversion cross-sections are closely related to absorption spectra and, when multiplied by the photon intensity at specific wavelengths, they provide an estimate of the rates of conversion between the two forms of phytochrome. Several studies have separately derived the photochemical parameters necessary to calculate these photoconversion cross-sections. Fig 6-1a shows four P_r cross-section values that are derived from 1) Seyfried and Schafer [2], 2) Kelly and Lagarias [3], 3) Lagarias et al. [4] and 4) Sager et al. [5] for 650 to 800 nm. Shinomura et al. [6] used a spectrograph (a device that uses prisms to provide narrow bandwidths of radiation) to determine an action spectrum of seed germination and found that it closely matched the absorbance spectra of P_r (Fig 6-1a). Phytochrome absorbance spectra above 800 nm have not been rigorously determined, but Schafer et al. [7] predicted the photoconversion cross-sections out to 1100 nm with the action spectra of both inhibition and promotion, respectively, of mesocotyl and coleoptile elongation. These data show a log-linear decrease in the relative photoconversion cross-section between about 700 to 800 nm, above which it the relationship deviates from log-linearity, e.g. Gaussian to Lorenzian; but there are no apparent peaks in sensitivity between 800 and 1100 nm. Therefore, although the ability of

photons to activate P_r into P_{fr} decreases rapidly above 700 nm (and even 800 nm), responses can still occur in these regions with high enough photon intensities.

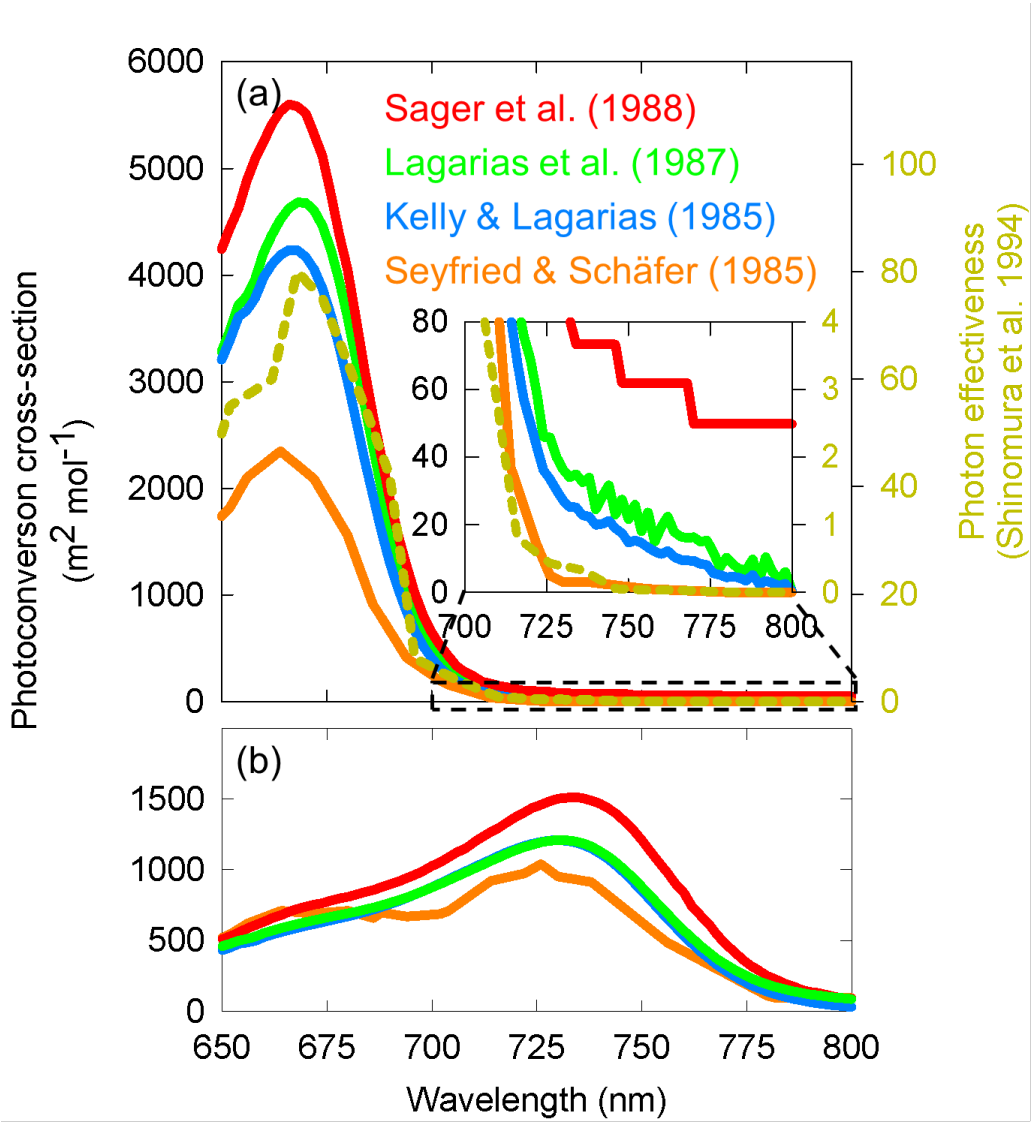

Fig 6-1. Photoconversion cross-sections of P_r and P_{fr} from four studies. (a) Left axis, Photoconversion cross-sections of P_r determined by Seyfried and Schafer [2], Kelly and Lagarias [3], Lagarias et al. [4] and Sager et al. [5]. Photoconversion cross-sections are related to absorbance spectra. Right axis, action spectrum of seed germination [6]. Inset: P_r photoconversion cross-section at 700 to 800 nm. Note the inconsistency of P_r action above 750 nm determined by different research groups. (b) Photoconversion cross-sections of P_{fr}.

Photoconversions for the conversion of P_{fr} back to P_r are also available for many of these studies [2-5] (Fig 6-1b). These show a higher sensitivity than P_r cross-sections between 700 to 800 nm, but similar to P_r, P_{fr} photoconversion cross-sections are not available for wavelengths above 800 nm.

A common NIR LED for night vision has a peak at about 850 nm with a full width at half maximum (FWHM) of 25 to 40 nm and outputs photons down to at least 750 nm. This LED is used in security cameras for night vision in greenhouses and controlled environment agriculture. Because of their regular use in controlled plant growth environments, especially during the dark periods, it is valuable to investigate the potential role they may play in altering plant growth and development. The photons from this LED may affect plant growth and development either by 1) the activation of P_r to P_{fr} (Fig 6-1a), or 2) the inactivation of phytochrome from P_{fr} to P_r. The activation of phytochromes (i.e. convert P_r to P_{fr}) can be assessed by floral initiation in short-day plants (SDP), while the inactivation of phytochrome (i.e. convert P_{fr} to P_r) can be assessed with stem elongation.

SDP undergo floral initiation when the period of un-interrupted darkness is longer than a critical length [8]. The application of photons for 4 hours or less during the dark period, called a night-break or night-interruption, is a common practice to delay or inhibit flowering in SDP in ornamental crop production. Similarly, low levels of constant light throughout the dark period, here called nighttime photons, can also disrupt flowering in SDP. P_{fr} plays a vital role in this process [9]; however, the mechanisms governing the response are only partially understood. It involves complex interactions between phytochromes (phyA, phyB and phyC in the SDP rice [10]) and 1) the circadian rhythm [11], 2) transcriptional regulation [12], and 3) possibly post-transcription stabilization [13].

Early studies that contributed to the discovery of phytochrome investigated the action spectrum of floral inhibition by night-break lighting in SDP. Using a spectrograph, these studies found strong inhibitory responses to red photons (600 to 700 nm), and minimal responses to the yet unnamed far-red photons, especially beyond 720 nm, although they still observed some inhibition at 770 nm – no response was observed out to 840 nm [14]. Following the landmark flip-flop seed germination study with red and far-red photons [15], studies found that far-red could reverse red night-break inhibition of flowering in SDP [16,17]. Although flowering was able to be re-induced by a far-red pulse after a red pulse, it differed from the germination response in that each additional 'flip-flop' had a reduced response. After four cycles of flip-flopping, flowering was almost entirely inhibited [17]. Follow-up studies determined that high doses (dependent on intensity and duration) of far-red (with or without prior night-break with red) inhibited flowering of SDPs compared to a control without night-break lighting [17-20].

Table 6.1 summarizes the effect of far-red night-breaks lighting compared to controls without night breaks reported in studies spanning 63 years. The older studies report stage of floral development as an index, and the newer studies typically report time to flowering. Additionally, the older studies typically used a spectrograph with filters while the newer studies apply far-red photons with LEDs that have a peak at about 730 nm. Some studies show a delay in flowering (see [21]), indicating that the applied photons (700 and 750 nm) are able to activate phytochrome into P_{fr} and inhibit flowering. By contrast, some studies under similar conditions show no significant response (see [22]). These contradictions may be due to differences in the duration of the dark period, intensity of the far-red, duration of the night-break and sensitivity of the species. Floral initiation is a complex molecular

process, and different species/cultivars will have different thresholds for a photo-molecular process to occur. Therefore, it is important to choose species known to be sensitive to night-break/nighttime photons when investigating the ability of photons from NIR LEDs to activate phytochromes and inhibit flowering. Soybean (*Glycine max*) and *Cannabis sativa* are highly sensitive to nighttime photons [8].

Photons from NIR LEDs could also potentially affect plant growth and development by inactivating P_{fr} back into P_r. Far-red photons are often reported to increase stem elongation [28], a process that is modulated through the inactivation of phytochrome [29].

We investigate the ability of photons from NIR LEDs applied over a 24 h photoperiod to 1) delay flowering in two sensitive short-day species, and 2) elongate stems. We found that at high enough doses, photons from NIR LEDs can affect both of these plant responses.

Table 6.1. Summary of the effect of far-red night-break lighting on flowering development or time to flowering. Results differed between studies, possibly due to the difference in treatments (also described). Stage of flowering refers to a flowering development index, different publications use different scales. R: red; FR: far-red; NB: night break; SD: short-day

Species	Reported FR intensity	FR source	Night break length	Photoperiod conditions (day/night)	Effect on flowering development	Citation	Comment
Xanthium pensylvanicum Wallr.	unclear	filtered sunlight with output near 735 nm	12 min	12h/12h	Reduced stage of flowering from 6 to 4 (scale from 0 to 7) - 33% reduction	Downs [17]	Provided after R (about 50 µmol m^{-2} s^{-1})
Chrysanthemum morifolium cv. Indianapolis Yellow	unclear	Filtered incandescent	81 min	9h/15h	Reduced stage of flowering from 4.1 to 0.4 (scale from 0 to 10) - 90% reduction	Cathey and Borthwick [18]	
Chrysanthemum morifolium cv. Shasta					Reduced stage of flowering from 3.7 to 0 (scale from 0 to 10) - inhibited		
Chrysanthemum morifolium cv. Honey Sweet					Reduced stage of flowering from 3.7 to 0 (scale from 0 to 10) - inhibited		

Chenopodium rubrum	14 µmol m^{-2} s^{-1}	Spectrograph centered at 730 nm (about 720 to 740 nm)	16 min	8h/16h	Reduced stage of flowering from 9 to 6.7 (scale from 0 to 9) - 26% reduction	Kasperbauer et al. [19]	
Xanthium pensylvanicum Wallr.	about 50 µmol m^{-2} s^{-1}	Filtered incandescent quantified from 710 to 800 nm	1 h	12h/12h	Reduced stage of flowering from 6.7 to 4.9 (scale from 0 to 7) - 27% reduction	Mancinelli and Downs [20]	
				8h/16h	Reduced stage of flowering from 6.8 to 3.1 (scale from 0 to7) - 55% reduction		
				4h/20h	Reduced stage of flowering from 6.7 to 0.9 (scale from 0 to 7) - 87% reduction		
Oryza sativa (rice)	18000 µmol m^{-2}	Acrylic filtered fluorescent. Shortest wavelength ≈ 710 nm, peak ≈ 765 nm	"flash"	10h/14h	no effect	Ishikawa et al. [23]	
Tagetes erecta (African Marigold) cv. America Antigua Yellow	1.3 - 1.6 µmol m^{-2} s^{-1}	LED peak at about 730 nm, quantified from 700 to 800 nm	4 h	9h/15h	9 day delay	Craig and Runkle [21]	only significant in one of two replicate studies
Chrysanthemum morifolium Ramat. cv. Reagan	62.5 µmol m^{-2} s^{-1}	LED peak at about 740 nm, quantified from 300 to 900 nm	4 h	12h/12h	1.7 day delay	Higuchi et al. [24]	
Chrysanthemum ×morifolium cv. Adiva Purple	1.3 - 1.6 µmol m^{-2} s^{-1}	LED peak at about 735 nm, quantified from 700 to 800 nm	4 h	9h/15h	no effect	Craig and Runkle [25]	Data for Dahlia should be interpreted with caution because there was incomplete flowering in SD and FR NB treatments
Dahlia hortensis cv. Carolina Burgundy					11 day delay		
Dahlia hortensis cv. Figaro Mix					8 day delay		
Tagetes erecta (African Marigold) cv. America Antigua Yellow					10 day delay		
Chrysanthemum seticuspe	20 µmol m^{-2} s^{-1}	LED peak at about 740 nm	10 min	8h/16h	no effect	Higuchi et al. [26]	Supplementary data
Chrysanthemum morifolium Ramat. cv. Iwa no hakusen	6.6 µmol m^{-2} s^{-1}	LED peak at 728 nm, quantified from 400 to 800 nm	6 h	12h/12h	Reduced stage of flowering from 0.86 to 0.27 (scale from 0 to 1) - 96% reduction	Liao et al. [27]	R NB similar to SD
Chrysanthemum morifolium Ramat. cv. Jimba					no effect		

Dendranthema grandiforum cv. Gaya Yellow	10 µmol m^{-2} s^{-1}	LED peak at 730 nm	4 h	10h/14h	no effect	Park and Jeong [22]

6.3 Material and Methods

6.3.1 Plant Materials

Soybean (*Glycine max* cv. Hoyt) were seeded into 1.7 L pots inside a greenhouse. Rooted cuttings of medicinal hemp (*Cannabis sativa* L. cv. T1 "Trump") were transplanted into 6.5 L pots filled with a 3:1 mixture of peat/vermiculite. The media was amended with 1.6 g per L of dolomitic lime to bring the pH to 5.8 and 0.8 g per L Gypsum ($CaSO_4$) to provide additional sulfur. Soybeans emerged four days after planting and were moved from the greenhouse into the growth chamber (CMP 3023, Conviron, Winnipeg, Canada). After transplanting, the *Cannabis* was grown in the greenhouse for one week (28/25 ˚C day/night; 18/6 h day/night) before moving into the growth chamber.

6.3.2 Spectral Treatments

A growth chamber (0.77 ×1.8 m) was split in half with white reflective cardboard to minimize light contamination between sections. The background spectrum for both sides was provided by white + red LEDs (Icarus Vi, BIOS, Melbourne FL), which had 10% blue (400 to 500 nm), 22% green (500 to 600 nm), and 68% red (600 to 700 nm). Two NIR LED fixtures (Ray 22 custom spectra; Fluence Bioengineering, Austin, TX) with a peak at about 850 nm were added to one side of the chamber. The other side received no NIR photons.

For soybean, two studies were conducted in time, one with a control and a low NIR treatment [nighttime NIR photon flux density (700 to 900 nm) = 44 μmol m^{-2} s^{-1}], and a second study with a control and a high NIR treatment (nighttime NIR photon flux density = 87 μmol m^{-2} s^{-1}). Each study contained 12 plants per treatment. The *Cannabis* study was conducted across three studies in time. In addition to the controls, the first study contained a high night far-red flux density (nighttime NIR photon flux density = 62 μmol m^{-2} s^{-1}) with four replicate plants and the second and third studies contained a low night far-red flux density (nighttime NIR photon flux density = 121 μmol m^{-2} s^{-1}) with three replicate plants.

The white + red background light was applied for a 12 h photoperiod and the NIR was applied for the full 24 h. Measurements were made with a spectroradiometer (PS-300; Apogee instruments; Logan, UT) with 13 measurements made for each treatment. Spectral traces from the *Cannabis* study are shown in Fig 6-2. The spectral data is summarized in Table 6.2. To increase the accuracy of far-red measurements (700 to 800 nm) a high integration time was used to improve the signal to noise ratio. Table 6.2 splits the flux f photons from NIR LEDs into three regions: FR-A (700 to 749 nm), FR-B (750 to 799 nm) and FR-C (800 to 900 nm). Nighttime PPE was calculated assuming only photoconversions (no thermal reversion; see more details in Discussion) using data from Kelly and Lagarias [3], Lagarias et al. [4] and Sager et al. [5].

Table 6.2. Spectral analysis of near infrared (NIR) treatments. Values in this table represent averages from 13 measurements in each chamber. Additionally, treatments with the same level of NIR are averaged together.

	Soybean					
	Day			Night		
	control	low NIR	high NIR	control	low NIR	high NIR
PPFD (400 - 700 nm)	646	638	651	-	-	-
FR photon flux density						
FR-A (700 - 749 nm)	10	10	10	0.0	0.1	0.2
FR-B (750 - 799 nm)	3.2	4.8	7	0.1	1.7	3.8
FR-C (800 - 900 nm)	4.7	41	83	2.0	42	83
PPE						
Kelly and Lagarias (1985)	0.87	0.87	0.87	-	0.11	0.12
Lagarias et al. (1987)	0.86	0.86	0.86	-	0.11	0.11
Sager et al. (1988)	0.88	0.88	0.87	-	0.21	0.20

	Cannabis					
	Day			Night		
	control	low NIR	high NIR	control	low NIR	high NIR
PPFD (400 - 700 nm)	832	840	837	-	-	-
FR photon flux density						
FR-A (700 - 749 nm)	13	13.6	14	0.0	0.1	0.3
FR-B (750 - 799 nm)	4.3	6.4	8.9	0.1	2.6	5.2
FR-C (800 - 900 nm)	5.8	55	114	2.0	59	116
PPE						
Kelly and Lagarias (1985)	0.87	0.86	0.87	-	0.08	0.12
Lagarias et al. (1987)	0.86	0.86	0.86	-	0.09	0.12
Sager et al. (1988)	0.88	0.87	0.87	-	0.19	0.21

6.3.3 Environmental Conditions

Temperature was a constant 26 °C day/night in the growth chambers (Fig 6-3). CO_2 was maintained at 400 ppm. Inductive photoperiods (12/12 h day/night) began when plants were moved into the growth chambers. Plants were irrigated daily to a 10% excess with a complete liquid fertilizer [Peter's Peat-lite professional 20-10-20 (20N-4.4P-16.6K), Everris NA, Inc., Dublin, OH] at a rate of 120 mg N per L. Greencare micronutrients (Greencare

Fertilizers, Inc., Kankakee, IL) were added at a rate of 7 mg per L. AgSil 16H (PQ Corporation, Malvern, PA) was added using a second proportioner for the liquid fertilizer at a rate of 8.4 mg Si (0.3 mmol Si) per L. Electrical conductivity (EC) of the nutrient solution was 1.2 mS cm^{-1} and pH was 6.8.

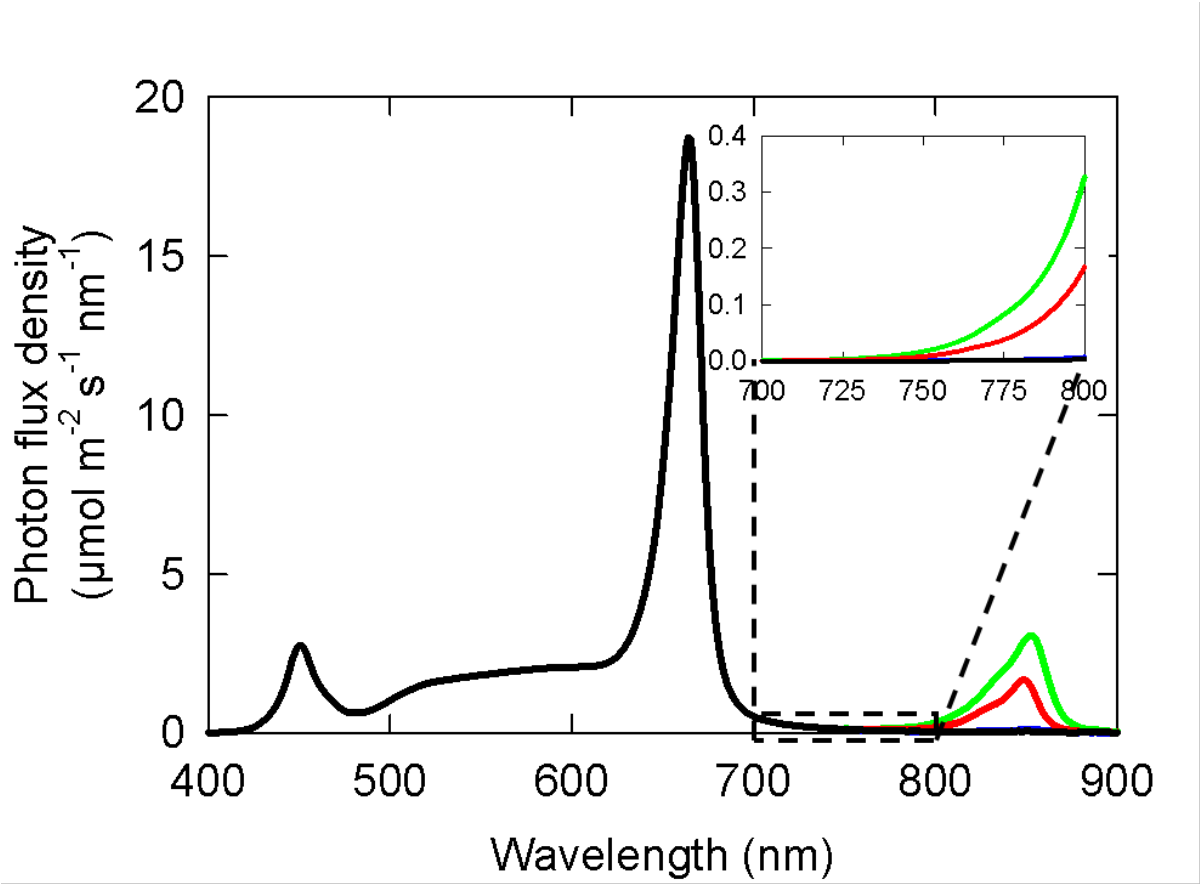

Fig 6-2. Spectral distribution from the *Cannabis* studies. The black line is the background spectral distribution used in all treatments including the control. The red and green lines show the two intensities of added photons from a near-infrared (NIR) LED (low NIR and high NIR in Table 2). Inset: spectral distribution between 700 and 800 nm of nighttime light pollution from NIR LEDs. Spectral distributions in the soybean study had the same shapes but with lower overall intensities.

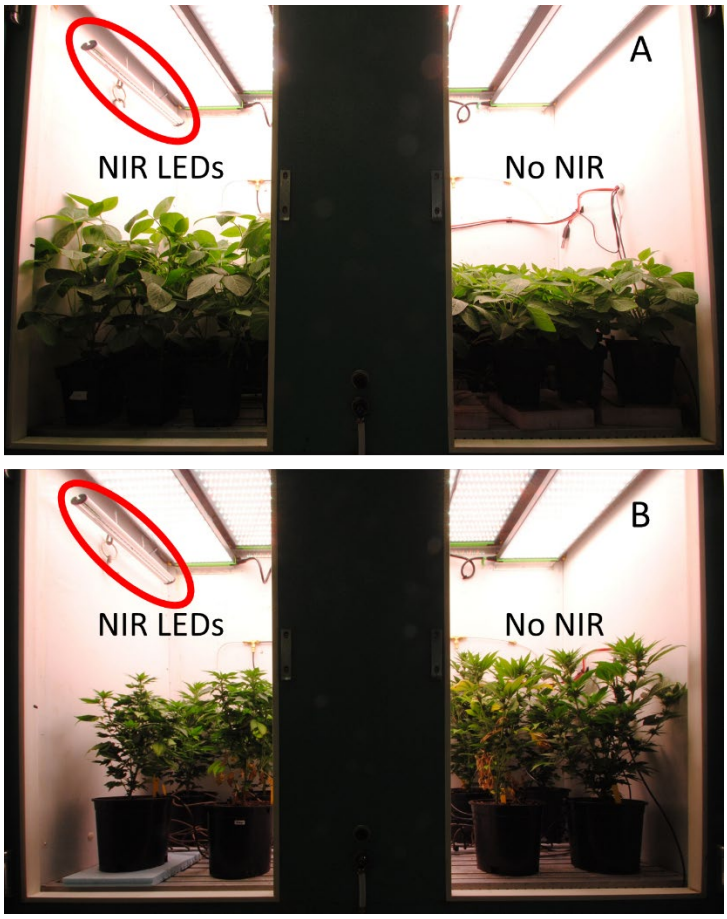

Fig 6-3. Photo at the end of the soybean (A) and *Cannabis* (B) study. The near infra-red (NIR) LEDs, circled in red, were provided for the full 24 h, while the background light was provided for a 12 h photoperiod. The no NIR treatment was a control with a long (12 h uninterrupted) night.

6.3.4 Plant Measurements

Plants were monitored daily to determine time to flowering. In soybean, time to flowering was determined by emergence of the first colored flower. In *Cannabis*, time to flowering was determined as when the apical inflorescence reached 2 mm. Stem length of soybean was measured from the base of the stem to the apical meristem when flowering first occurred.

6.3.5 Statistics

All data were analyzed using SigmaPlot graphical/statistical software (Systat Software, Inc., San Jose CA). All plants within each treatment were averaged together and analyzed using linear regression.

6.4 Results & Discussion

6.4.1 Flowering

Increasing the photon flux density from NIR LEDs delayed flowering (increased time to flowering) in both soybean ($p = 0.056$) and *Cannabis* (Fig 6-4, $p = 0.014$). On average, the high NIR treatment flowered 3 and 12 d later than the dark SD control in soybean and *Cannabis*, respectively. All soybean plants flowered within three days of each other and all *Cannabis* plants flowered within four days of each other. Plants were not rotated in the chambers, and thus only the average response within the chamber was used for statistical analysis.

Previous studies have provided conflicting evidence regarding the effects of night-break photons beyond 700 nm on time to flower (Table 6.1). Flowering is a complex process, and the molecular/genetic mechanisms regulating photoperiodic flowering continue to be investigated. Many details of this process, as well as the universality of metabolic pathways remain uncertain [12]. Nevertheless, it is well established that phytochromes play an essential role in flowering [9], but these photoreceptor proteins act on at least three separate metabolic pathways: the circadian oscillator [11,30], transcriptional regulation [12] and post-transcriptional stabilization [13]. Circadian control and transcription both require the nuclear

localization of phytochrome. Only the P_{fr} form of phytochrome can enter the nucleus to disrupt flowering in night-break or nighttime photon conditions. The necessary thresholds of P_{fr} to affect these responses are not known and likely differ among species [31]. Kasperbauer et al. [19] speculated from their data that just 1 to 2% of phytochrome in the active form for varied significantly for the night period (Table 6.2). Nonetheless, they estimated that between 10 to 20% of the total pool of phytochrome was in the P_{fr} form during the night in this study

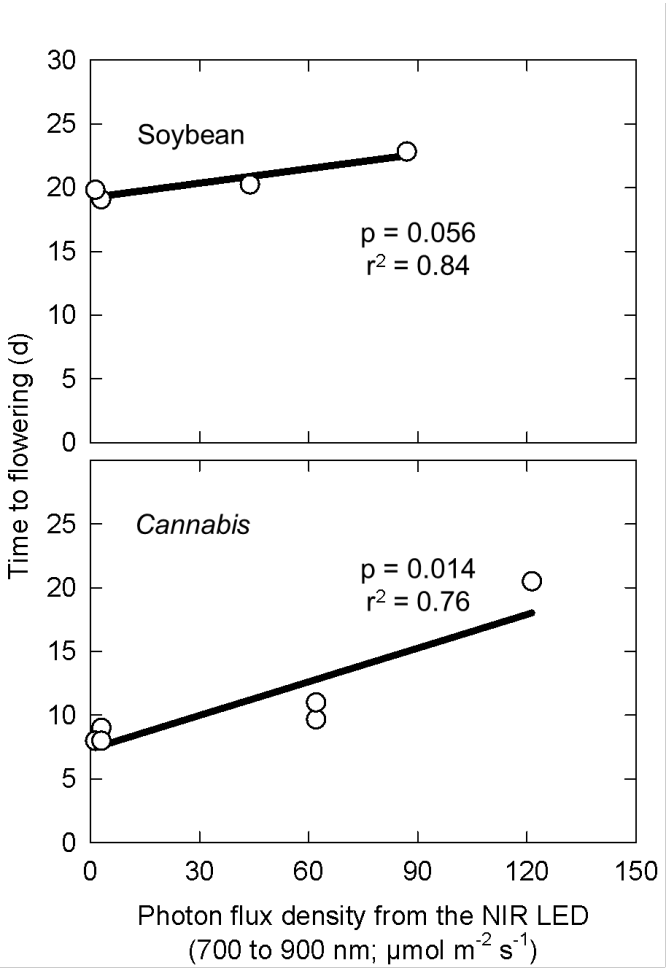

Fig 6-4. Effect of photons (700 and 900 nm) on time to flowering in soybean and *Cannabis*. Data points are the average effect within each treatment.

(Table 6.2). These estimations of P_{fr} as a fraction of P_{total} are likely too high because they do not include thermal reversion of P_{fr} back to P_r. Schafer et al. [7] estimated the lowest

theoretical PPE under monochromatic longer-wavelength (greater than 780 nm) photons is about 0.0001 or 0.01% P_{fr}.

Reversion/relaxation of P_{fr} back into P_r occurs in a non-photochemical process that is temperature dependent. This process was historically called dark reversion, but is now called thermal reversion. Thermal reversion has been well studied [32], but it has only recently been incorporated into estimates of P_{fr} to P_{total}, especially in low light [33-35].

Jung et al. [36] determined that *Arabidopsis thaliana* phyB-P_{fr} had a half-life of about 52 minutes at 27 ˚C, the approximate temperature of this study. This half-life likely only applies to phyB at 27 ˚C. Warmer temperatures result in shorter half-lives compared to cooler temperatures. Additionally, different types of phytochromes have different stabilities. For example, phyA demonstrates thermal reversion in multiple species [32], phyD is thermally unstable, and phyE is highly thermostable [37]. Osugi et al. [10] determined that all phytochromes in rice (phyA, phyB and phyC) play a role in flowering, making it difficult to estimate the thermal reversion of the phytochromes in the species used in this study. Altogether, it was difficult to predict the nighttime PPE due to variation (and possible inaccuracy) in the photoconversion cross-sections, spectral distortions within leaves [2,19] and unknown thermal reversion rates.

Nonetheless, the photoconversion cross-sections determined *in vitro* are not zero beyond 750 nm (Fig 6-1), which overlaps with the spectral output from the NIR LED, indicating that some amount of P_r will be converted into P_{fr} during the night period with NIR photons.

There are concerns in the *Cannabis* industry that photons from NIR LEDs cause monecious flowering. *Cannabis* is naturally dioecious; only female plants are desired for medical *Cannabis* cultivation. Monoecious flowering is often confused with hermaphroditism. Botanically, these terms are distinct: monoecious refers to the presence of separate male and female flowers on the same plant, while hermaphrodite refers to the presence of both male and female reproductive organs within an individual flower [38]. In practice, the distinction is not important because monoecious and hermaphroditic *Cannabis* produce pollen and potentially reduce product quality and value [39]. The tendency of

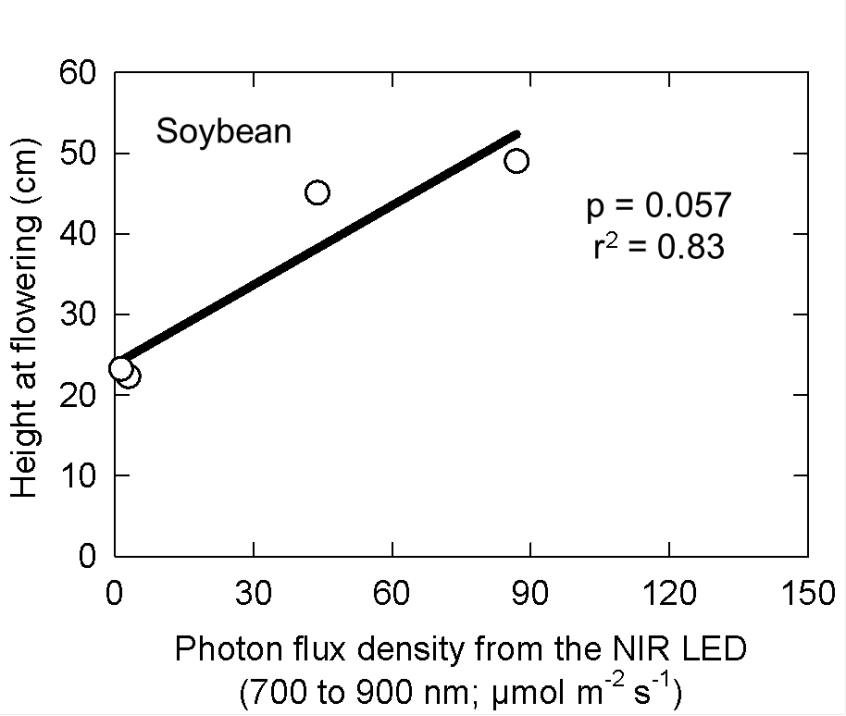

Fig 6-5. Effect of photons (between 700 and 900 nm) on soybean height at flowering. Data points are the average effect within each treatment.

Cannabis to form monoecious or hermaphroditic plants is under genetic and environmental influence [40,41]. No monoecious or hermaphrodite plants were observed in this study, but we did not grow the plants to maturity.

6.4.2 Stem Length

Soybean plant height at flowering was increased by photons from the NIR LEDs (Fig 6-5). The coefficient of variation (standard deviation divided by the mean) of plant height at flowering in each treatment was at most 0.15.

Far-red photons have a powerful effect on stem elongation in soybeans [28], so the effect of photons from NIR LEDs on soybean plant height ($p = 0.057$) was not entirely surprising (Figs 6-3 and Fig 6-5). P_{fr} inhibits the activity of transcription factors that promote stem elongation meaning that this elongation response is caused by the inactivation of phytochrome, P_{fr} to P_r [29].

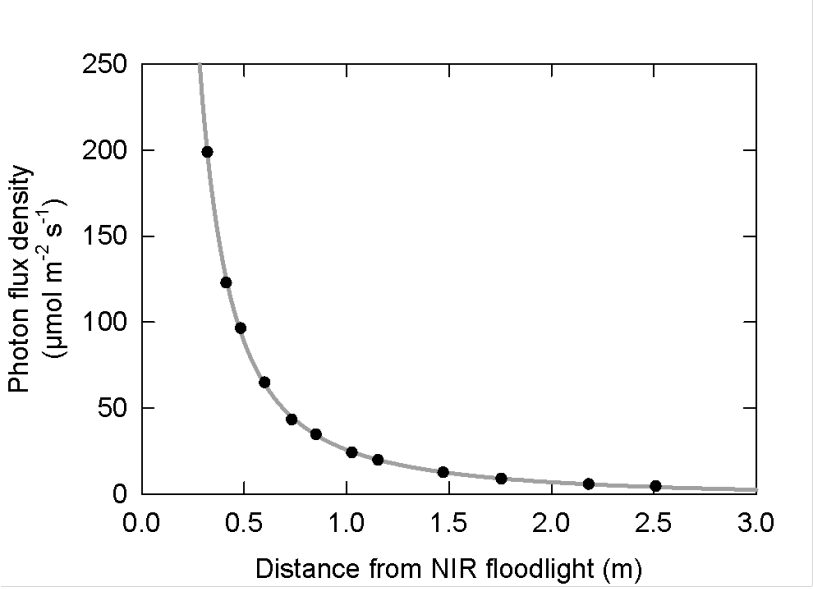

Fig 6-6. Total photon flux density from a near infrared (NIR) LED floodlight as a function of distance. These measurements were made directly below the floodlight at increasing distances, and they follow the inverse square law.

We conclude that photons from NIR LEDs applied for 24 h per day can both inactivate P_{fr} to P_r inducing stem elongation and activate P_r to P_{fr} delaying flowering in sensitive SDP. For practical applications, this means that the NIR LEDs in security cameras for night-vision in controlled environment plant growth have the potential to alter plant

development. We measured the photon flux from an NIR floodlight, which is used to increase the range of night-vision for a security camera, to determine the intensities that plants might be exposed to in commercial setting (Fig 6-6). The photon flux density at one meter of the floodlight was about 25 μmol m^{-2} s^{-1}. Our data indicate that this intensity may be enough to delay flowering by one day in soybean and two days in *Cannabis*. Additionally, this intensity from the NIR LEDs is enough to increase stem elongation by 33% in soybean. It should be noted that these measurements were made with a floodlight, which represents a much higher flux of NIR photons compared to the flux of just a security camera – although, floodlights can be used in controlled environment settings. Additionally, most plants would not be within one meter of the NIR LEDs. By a distance of about 3 m, the photon flux from these LEDs drops to about one μmol m^{-2} s^{-1}, which is likely too low to have any noticeable effects. Therefore, although NIR photons from security cameras can have affect plant growth and development, intensities are likely too low to be effective.

6.5 Literature Cited

1. Smith H. Phytochromes and light signal perception by plants—an emerging synthesis. Nature. 2000; 407: 585-591. doi: 10.1038/35036500
2. Seyfried M, Schäfer E. Action spectra of phytochrome in vivo. Photochem Photobiol. 1985; 42: 319-326. doi: 10.1111/j.1751-1097.1985.tb08947.x
3. Kelly JM, Lagarias JC. Photochemistry of 124-kilodalton Avena phytochrome under constant illumination in vitro. Biochemistry. 1985; 24: 6003-6010. doi: 10.1021/bi00342a047
4. Lagarias JC, Kelly JM, Cyr KL, Smith Jr WO. Comparative photochemical analysis of highly purified 124 kilodalton oat and rye phytochromes in vitro. Photochem Photobiol. 1987; 46:5-13. doi: 10.1111/j.1751-1097.1987.tb04729.x
5. Sager JC, Smith WO, Edwards JL, Cyr KL. Photosynthetic efficiency and phytochrome photoequilibria determination using spectral data. Trans Am Soc Agri. Eng. 1988; 31: 1882-1889. doi: 10.13031/2013.30952

6. Shinomura T, Nagatani A, Hanzawa H, Kubota M, Watanabe M, Furuya M. Action spectra for phytochrome A-and B-specific photoinduction of seed germination in Arabidopsis thaliana. Proc Natl Acad Sci USA. 1996; 93: 8129-8133. doi: 10.1073/pnas.93.15.8129
7. Schäfer E, Lassig TU, Schopfer P. Phytochrome-controlled extension growth of *Avena sativa* L. seedlings. Planta 1982; 154: 231-240.
8. Vince-Prue D. The role of the dark period and its interaction with light. In: Vince-Prue D, editor. Photoperiodism in plants. London: McGraw-Hill; 1975. pp. 70-97.
9. Vince-Prue D. The duration of light and photoperiodic responses. In: Kendrick RE, Kronenberg GHM, editors. Photomorphogenesis in plants. Dordrecht: Springer; 1994. pp. 447-490. doi: 10.1007/978-94-011-1884-2_17
10. Osugi A, Itoh H, Ikeda-Kawakatsu K, Takano M, Izawa T. Molecular dissection of the roles of phytochrome in photoperiodic flowering in rice. Plant Physiol. 2011; 157: 1128-1137. doi: 10.1104/pp.111.181792
11. Wang H, Wang H. Phytochrome signaling: time to tighten up the loose ends. Mol Plant. 2015; 8: 540-551. doi: 10.1016/j.molp.2014.11.021
12. Song YH, Shim JS, Kinmonth-Schultz HA, Imaizumi T. Photoperiodic flowering: time measurement mechanisms in leaves. Annu Rev Plant Biol. 2015; 66: 441-464. doi: 10.1146/annurev-arplant-043014-115555
13. Zheng T, Sun J, Zhou S, Chen S, Lu J, Cui S, Tian Y, Zhang H, Cai M, Zhu S, Wu M. Post-transcriptional regulation of Ghd7 protein stability by phytochrome and OsGI in photoperiodic control of flowering in rice. New Phytologist. 2019; 224: 306-320. doi: 10.1111/nph.16010
14. Parker MW, Hendricks SB, Borthwick HA, Scully N. Action spectrum for the photoperiodic control of floral initiation of short-day plants. Bot Gaz. 1946; 108: 1-26. doi: 10.1086/335392
15. Borthwick HA, Hendricks SB, Parker MW, Toole EH, Toole VK. A reversible photoreaction controlling seed germination. Proc Natl Acad Sci USA. 1952; 38: 662-666. doi: 10.1073/pnas.38.8.662
16. Borthwick HA, Hendricks SB, Parker MW. The reaction controlling floral initiation. Proc Natl Acad Sci USA. 1952; 38: 929-934. doi: 10.1073/pnas.38.11.929
17. Downs RJ. Photoreversibility of Flower Initiation. Plant Physiol. 1956; 31: 279-284. doi: 10.1104/pp.31.4.279
18. Cathey HM, Borthwick HA. Photoreversibility of floral initiation in chrysanthemum. Bot Gaz. 1957; 119: 71-76. doi: 10.1086/335964
19. Kasperbauer MJ, Borthwick HA, Hendricks SB. Inhibition of flowering of Chenopodium rubrum by prolonged far-red radiation. Bot Gaz. 1963; 124: 444-451. doi: 10.1086/336234
20. Mancinelli AL, Downs RJ. Inhibition of flowering of Xanthium pensylvanicum Wallr. By prolonged irradiation with far red. Plant Physiol. 1967; 42: 95-98. doi: 10.1104/pp.42.1.95
21. Craig DS, Runkle ES. Using LEDs to quantify the effect of the red to far-red ratio of night-interruption lighting on flowering of photoperiodic crops. Acta Hort. 2012; 956: 179-185. doi: 10.17660/ActaHortic.2012.956.18

22. Park YG, Jeong BR. Night interruption light quality changes morphogenesis, flowering, and gene expression in Dendranthema grandiflorum. Hort. Environ. Biotechnol. 2019; 60: 167-173. doi: 10.1007/s13580-018-0114-z
23. Ishikawa R, Shinomura T, Takano M, Shimamoto K. Phytochrome dependent quantitative control of Hd3a transcription is the basis of the night break effect in rice flowering. Genes Genet Sys. 2009; 84: 179-184. doi: 10.1266/ggs.84.179
24. Higuchi Y, Sumitomo K, Oda A, Shimizu H, Hisamatsu T. Day light quality affects the night-break response in the short-day plant chrysanthemum, suggesting differential phytochrome-mediated regulation of flowering. J Plant Physiol. 2012; 169: 1789-1796. doi: 10.1016/j.jplph.2012.07.003
25. Craig DS, Runkle ES. A moderate to high red to far-red light ratio from light-emitting diodes controls flowering of short-day plants. J Am Soc Hort Sci. 2013; 138: 167-172. doi: 10.21273/JASHS.138.3.167
26. Higuchi Y, Narumi T, Oda A, Nakano Y, Sumitomo K, Fukai S, Hisamatsu T. The gated induction system of a systemic floral inhibitor, antiflorigen, determines obligate short-day flowering in chrysanthemums. Proc Natl Acad Sci USA. 2013; 110: 17137-17142. doi: 10.1073/pnas.1307617110
27. Liao Y, Suzuki K, Yu W, Zhuang D, Takai Y, Ogasawara R, Shimazu T, Fukui H. Night Break Effect of LED Light with Different Wavelengths on Floral Bud Differentiation of Chrysanthemum morifolium Ramat 'Jimba'and Iwa no hakusen. Environ. Control Biol. 2014; 52: 45-50. doi: 10.2525/ecb.52.45
28. Hitz T, Hartung J, Graeff-Hönninger S, Munz S. Morphological response of soybean (Glycine max (L.) Merr.) cultivars to light intensity and red to far-red ratio. Agronomy. 2019; 9: 428. doi: 10.3390/agronomy9080428
29. Legris M, Ince YÇ, Fankhauser C. Molecular mechanisms underlying phytochrome-controlled morphogenesis in plants. Nat. Commun. 2019; 10: 1-5. doi: 10.1038/s41467-019-13045-0
30. Oakenfull RJ, Davis SJ. Shining a light on the Arabidopsis circadian clock. Plant Cell Environ. 2017; 40: 2571-2585. doi: 10.1111/pce.13033
31. Chen M, Chory J. Phytochrome signaling mechanisms and the control of plant development. Trends Cell Biol. 2011; 21: 664-671. doi: 10.1016/j.tcb.2011.07.002
32. Klose C, Nagy F, Schäfer E. Thermal reversion of plant phytochromes. Mol Plant. 2020; 13: 386-397. doi: 10.1016/j.molp.2019.12.004
33. Rausenberger J, Hussong A, Kircher S, Kirchenbauer D, Timmer J, Nagy F, Schäfer E, Fleck C. An integrative model for phytochrome B mediated photomorphogenesis: from protein dynamics to physiology. PLoS One. 2010; 5: e10721. doi: 10.1371/journal.pone.0010721
34. Klose C, Venezia F, Hussong A, Kircher S, Schäfer E, Fleck C. Systematic analysis of how phytochrome B dimerization determines its specificity. Nat Plants. 2015; 1: 1-9. doi: 10.1038/nplants.2015.90
35. Sellaro R, Smith RW, Legris M, Fleck C, Casal JJ. Phytochrome B dynamics departs from photoequilibrium in the field. Plant Cell Environ. 2019; 42: 606-617. doi: 10.1111/pce.13445

36. Jung JH, Domijan M, Klose C, Biswas S, Ezer D, Gao M, Khattak AK, Box MS, Charoensawan V, Cortijo S, Kumar M. Phytochromes function as thermosensors in Arabidopsis. Science. 2016; 354: 886-889. doi: 10.1126/science.aaf6005
37. Viczián A, Ádám É, Staudt AM, Lambert D, Klement E, Romero Montepaone S, Hiltbrunner A, Casal J, Schäfer E, Nagy F, Klose C. Differential phosphorylation of the N-terminal extension regulates phytochrome B signaling. New Phytologist. 2020; 225: 1635-1650. doi: 10.1111/nph.16243
38. Lebel-Hardenack S, Grant SR. Genetics of sex determination in flowering plants. Trends Plant Sci. 1997; 2: 130-136. doi: 10.1016/S1360-1385(97)01012-1
39. Punja ZK, Holmes JE. Hermaphroditism in Marijuana (Cannabis sativa L.) Inflorescences–Impact on Floral Morphology, Seed Formation, Progeny Sex Ratios, and Genetic Variation. Front Plant Sci. 2020; 11 :718. doi: 10.3389/fpls.2020.00718
40. Moliterni VC, Cattivelli L, Ranalli P, Mandolino G. The sexual differentiation of Cannabis sativa L.: a morphological and molecular study. Euphytica. 2004; 140: 95-106. doi: 10.1007/s10681-004-4758-7
41. Faux AM, Berhin A, Dauguet N, Bertin P. Sex chromosomes and quantitative sex expression in monoecious hemp (Cannabis sativa L.). Euphytica. 2014; 196: 183-197. doi: 10.1007/s10681-013-1023-y

CHAPTER 7

SUMMARY AND CONCLUSIONS

7.1 Specific Objectives and Hypotheses

1) In addressing the first objective, to determine the effect and interactions of blue and green photons fluxes on plant morphology, we concluded that:
    a. Increasing the fraction of blue photons reduced leaf area and dry mass in lettuce, cucumber and tomato, while increasing the fraction of green photons only increased leaf area and dry mass in tomato. Stem length was reduced by an increasing fraction of blue photons, and increased by an increasing fraction of green photons in both cucumber and tomato.
    b. Blue photon fraction interacted with intensity in predicting dry mass in cucumber, leaf area in cucumber, specific leaf mass in tomato, and plant height in tomato, but of these interactions, only plant height in tomato showed a larger response at low photon intensity.
    c. Blue photon fraction interacted with green photon fraction in predicting dry mass in lettuce, leaf area in lettuce and cucumber, plant height in tomato, and petiole length in cucumber. For all of these parameters, with the exception of plant height in tomato, this interaction showed that green photons had bigger effects when the fraction of blue photons was lower.
2) In addressing the second objective, to investigate metrics that are commonly used to predict morphological responses to far-red, we concluded that:

   a. We conclude that simple environmental metrics, like the FR fraction/percent far-red were as predictive as PPE.
   b. The R:FR ratio, a metric that is commonly used in photobiology, can theoretically approach infinity, and is therefore was not predictive.

3) In addressing the third objective, to improve the phytochrome photoequilibrium (PPE) model by accounting for spectral distortions within leaves, we conclude that:
   a. Accounting for spectral distortion within leaves resulted in predictions of PPE that better predicted stem elongation in cucumber.
   b. Assuming phytochrome was homogeneously distributed within all leaf tissue resulted in a better relationship between PPE and stem elongation than assuming phytochrome was only located in epidermal tissue.
4) In addressing the forth objective, to investigate how plant responses to far-red interacted with intensity, we conclude that:
   a. Photon flux density interacted with percent far-red to predict stem elongation biomass partitioning (between leaves and stems) in lettuce. Interactions were also present in cucumber, but less pronounced.
   b. The interactions between percent far-red and photon intensity on biomass partitioning resulted in far-red induced increases in leaf expansion at high photon fluxes, but decreases at low photon fluxes in lettuce.
6) In addressing the fifth objective, to determine if photons from NIR LEDs can affect plant growth and development, we conclude that:
   a. Photons from NIR LEDs can delay flowering of SDP when applied during the dark period.

b. Photons from NIR LEDs can increase stem elongation.
c. The intensities in practical applications are likely too low to induce these responses.

7.2 Broad Scientific Conclusions

Plants are highly responsive to changes in the photon environment, a phenomenon that has been extensively modeled. Photobiological models can be highly complex (Smith and Fleck, 2019), and still fail to predict responses (Fig. H-3). This failure is primarily due to the difficulty in incorporating all of the complex interactions between downstream factors within a plant.

Phytochrome photoequilibrium is one such model that has existed for over half a century (Hartmann, 1966). Its predictive capability was improved by accounting for spectral distortions within leaf tissue, solving only one of several problems with this model (Kusuma and Bugbee, 2021). Many molecular pathways have evolved to respond to environmental signals, thus, environmental signals, and not molecular models, may be better predictors of plant responses. One such metric is the far-red fraction. This was first proposed to be an improvement to the R:FR ratio, when equal to the flux of far-red (FR) divided by the flux of red (R) plus FR. However, this only predicts responses under phytochrome control, and other photoreceptors contribute to the final shape of a plant. Therefore, extending the FR fraction to include all wavelengths from 400 to 750 nm provides a simple method to integrate responses induced by multiple photoreceptors.

Photobiology studies have suggested that green photons act antagonistically to blue photons through the cryptochrome photoreceptor. Some shade avoidance responses were observed in response to green photons in cucumber and tomato, suggesting that the FR fraction could be improved if it incorporated both green and far-red in the numerator. However, another study showed that this was not necessary (Fig. 4-5a). It would be useful to understanding this discrepancy, and interactions that arise with variations in the extended photosynthetic photon flux density (ePPFD).

Although the FR fraction was shown to be a useful intuitive metric in many of the studies presented here, there were notable interactions with ePPFD. The interactions tended to be unsurprising in both molecular and ecological contexts, with more pronounced shade avoidance responses as ePPFD decreased. Even comparing two horticulturally relevant intensities (ePPFD: 200 and 500 μmol m^{-2} s^{-1}): at the lower intensity, increasing percent far-red increased shoot biomass partitioning to the stems (decreasing the biomass partitioning to the leaves), resulting in an overall decreased in total leaf area (despite an increased in SLA); while at the higher intensity, increasing percent far-red had no effect on shoot biomass partitioning resulting in an increase in total leaf area (with an increase in SLA). Nonetheless, it is difficult to incorporate this interaction into a comprehensive model, especially in the pursuit of simplicity.

Even if environmental signals may be better predictors of plant morphology than molecular models, it is still useful to understand the components of the complex cellular signaling because it may help identify specific modes of action or genes that can be manipulated to improve crop yields. In addition to improvements, negative consequences of certain photon environments may become more predictable. For example, the delay in

flowering observed when photons from an NIR LED were applied during the dark period of *Cannabis* and soybean.

7.3 Broad Applied Conclusions

From an applied perspective, the primary goal of photobiology in horticulture (and most applied fields for that matter) is to maximize outputs while minimizing inputs. Increasing leaf area increases photons capture, which increases yield. Therefore, in general, the optimum spectrum is one that induces faster leaf expansion. Unfortunately, responses are species specific, and therefore optimal spectra will be species specific.

The studies presented here show that substituting traditionally defined photosynthetically active radiation (PAR) with FR can result in increases in leaf area and dry mass, but responses tended to be more beneficial at higher levels of ePPFD (500 compared to both 100 and 200 μmol m^{-2} s^{-1}). Additionally, while there are clear benefits of adding about 20% FR from LEDs, effects beyond this remain undetermined. More studies are required to fine-tune the optimum fraction of FR.

Green photons increased biomass accumulation in tomato in a short-term study, but further investigation is required to test long-term plant yields. Ji et al. (2020) showed that FR, which is known to increase biomass partitioning to stems, increased tomato fruit sink strength – leading to increased yields. Perhaps green photons induce a similar response. Finally, lettuce and cucumber, two species that were statistically unresponsive to green photons, showed an interaction between blue and green photons in the prediction of leaf area, indicating that perhaps green is beneficial when the flux of blue photons is low.

Many studies indicate that blue photons ought to be minimized in a growth spectrum in order to maximize biomass accumulation (although higher fractions of blue can increase the concentrations of beneficial secondary metabolites). Some studies have shown that eliminating blue photons entirely can increase yields (Meng et al., 2020; Son and Oh, 2013; Wang et al., 2016) while other studies show decreased yields (Hernández and Kubota, 2016; Snowden et al., 2016; Yorio et al., 2001). Like many photobiological responses, effects are species specific.

7.4 Literature Cited

Hartmann, K.M. 1966. A general hypothesis to interpret 'high energy phenomena' of photomorphogenesis on the basis of phytochrome. Photochem. Photobiol. 5:349-365.

Hernández, R. and C. Kubota. 2016. Physiological responses of cucumber seedlings under different blue and red photon flux ratios using LEDs. Environ. Exp. Bot. 121:66-74.

Ji, Y., D. Nuñez Ocaña, D. Choe, D.H. Larsen, L.F. Marcelis, E. Heuvelink. 2020. Far-red radiation stimulates dry mass partitioning to fruits by increasing fruit sink strength in tomato. New Phytol. 228:1914-1925.

Meng, Q., J. Boldt, and E.S. Runkle. 2020. Blue radiation interacts with green radiation to influence growth and predominantly controls quality attributes of lettuce. J. Am. Soc. Hort. Sci. 145:75-87.

Son, K.H., and M.M. Oh. 2013. Leaf shape, growth, and antioxidant phenolic compounds of two lettuce cultivars grown under various combinations of blue and red light-emitting diodes. HortScience 48:988-995.

Smith, R.W., and C. Fleck. 2019. Basic Phytochrome B Calculations, p. 121-133. In: H. Hiltbrunner (ed). Phytochromes (pp. 121-133). Humana, New York.

Snowden, M.C., K.R. Cope, and B. Bugbee. 2016. Sensitivity of seven diverse species to blue and green light: interactions with photon flux. PLoS One 11:e0163121.

Wang, J., W. Lu, Y. Tong, and Q. Yang. 2016. Leaf morphology, photosynthetic performance, chlorophyll fluorescence, stomatal development of lettuce (Lactuca sativa L.) exposed to different ratios of red light to blue light. Front. Plant Sci. 7:250.

Yorio, N.C., G.D. Goins, H.R. Kagie, R.M. Wheeler, and J.C. Sager. 2001. Improving spinach, radish, and lettuce growth under red light-emitting diodes (LEDs) with blue light supplementation. HortScience 36:380-383.

APPENDICES

APPENDIX A

HISTORY AND PHYSICS OF LIGHTING TECHNOLOGIES

A.1 History of Lighting Technologies

For most of human history fires, candles and oil lamps provided light for human vision in the dark. Then, over 200 years ago, advances in electric technology began to revolutionize lighting. The first practical electric light was the carbon arc lamp, which was commercialized decades before the well-known incandescent light bulb[D]. Arc lamps conduct electricity through the air, ionizing the gaseous particles in the process. These ionized atoms can transfer electrons as they collide. When an ionized gaseous atom accepts an electron, the electron "relaxes" to a lower energy level, releasing a photon in the process. Carbon arc lamps were phased out in favor of Thomas Edison's safer and more reliable incandescent light bulb. Incandescent bulbs use electricity to heat a filament until it glows (following the Stefan-Boltzmann law), providing light in a similar manner to the Sun. The incandescent bulb dominated for much of the 20th century but towards the mid to end of the century fluorescent lamps, a type of gaseous discharge lamp, began to dominate due to their higher efficiency. Gaseous discharge lamps operate in the same manner as carbon arc lamps, but ionize a specific, contained gas rather than simply ionizing air. Fluorescent lamps, which ionize mercury gas, are so named because they use a material called a phosphor to absorbs ultra-violet (UV) photons and re-emit them in the visible region - a process called fluorescence. Fluorescent lamps have low internal gas pressures, but by increasing the pressures, high intensity discharge (HID) lamps such as high-pressure sodium and metal halide lamps became popular in the latter half of the 20th century and are still widely used

[D] The invention of incandescent light bulb predated carbon arc lamps by four years, but these early incandescent bulbs were too short-lived to have practical application.

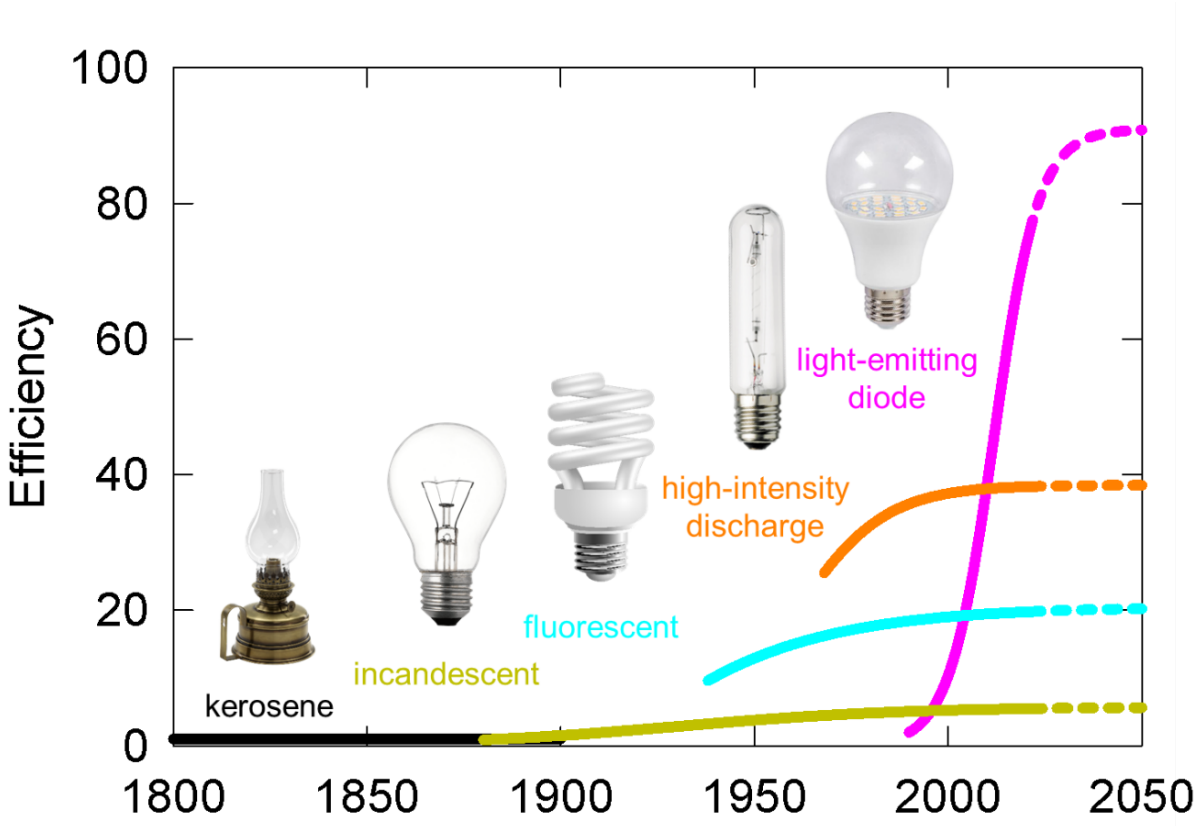

Figure A-1: Historical increase in efficiency of lighting technologies. Efficiency here describes the photon energy output (400 to 700 nm) divided by the electrical energy input. Dashed lines indicate the projected increase in technologies for the next 30 years. LED efficiency in this graph represents efficiency of a combination of red and blue LEDs at about 350 mA per mm^{-2}. Under lower drive currents, the efficiency of these LEDs can approach 90%.

(e.g., for streetlights). These HID lamps are even more efficient than fluorescent lamps and typically have high power ratings (e.g., 400, 600, and 1000 W). Within the last two decades, fluorescent lamps and even some HID lamps have been phased out in favor of much higher efficiency light-emitting diodes (LEDs), a solid-state-lighting-technology. Like gaseous discharge lamps, LEDs also emit photons through the relaxation of excited electrons, but LEDs conduct charge through a solid material rather than a gas and operate at low voltage

instead of high voltage. Each technology replaced its predecessor due to improvements in their efficiencies (Figure A-1; Nakamura et al., 2010).

A.2 Lighting Technologies for Plant Growth

Electric lighting for use in plant growth environments closely followed developments in human lighting (Wheeler et al., 2008). Early plant photobiology research utilized both carbon arc and incandescent lamps to provide sole-source lighting in indoor environments (Sage, 1992), but carbon arcs were generally not favored due to their high maintenance requirement and hazardous operation. In these early days of plant photobiology, studies investigated the effects of different colors on crop growth by using colored filters and prisms (Sage, 1992). With the development of fluorescent lamps, many growth chambers in the latter half of the 20th century were fitted with fluorescent and incandescent lamps (Downs, 1977). Fluorescent lamps could be designed with specific phosphors that re-emitted the absorbed photons at specific wavelengths, thus fluorescent lamps could output (for example) a green or red dominant spectrum. This further allowed the investigation of the effect of specific wavelength photons on plant growth. But, as with human lighting, these technologies are being phased out for LEDs. Broad spectrum white LEDs contain a phosphor, like fluorescent lamps, that absorb blue photons and re-emit longer wavelength photons, but LEDs can also be designed to output narrow spectrum photons across the visible spectrum.

A.3 Physics of Spectral Output

Regarding the investigation of spectral effects on plant growth, it is interesting to consider the physics related to unique spectral output from specific types of lamps. In gaseous discharge lamps and LEDs, as electrons "relax" the wavelength of the emitted photon depends on the energy difference between the excited and relaxed states. Therefore, the spectral photon distribution from gaseous discharge lamps depends on the emission spectrum of the specific gas, which is determined by the potentially energy states of the excited electron. Under low pressure, the atoms are dispersed and in a relatively uniform energy state, limiting the emission spectrum to fewer and fewer wavelengths, but at higher pressures, the atoms are packed in higher density, decreasing the uniformity of energy states, and therefore the energy difference between the exited and relaxed states becomes increasingly broad, as does the spectral photon distribution. LEDs can de designed to carefully control the energy bandgap between the excited and relaxed states of the electrons, limiting the photons to narrow bandwidths (in a relatively Gaussian distribution). The spectral photon distribution of incandescent lamps, on the other hand, is determined by their temperature, as well as both the Stefan-Boltzmann and Wien's laws. In terms of converting power to electromagnetic radiation, incandescent lamps are very efficient, but most of the radiation is in the infrared. Halogen lamps are a type of incandescent lamp that can reach higher temperatures than traditional incandescent lamps, shifting the spectrum to shorter (blue) wavelengths. The high temperature required to produce this higher flux of shorter wavelength (higher energy) blue photons in a halogen bulb evaporates the tungsten in the filament. This would shorted the life of a normal incandescent lamp, but the halogen bulb contains an inert noble gas mixed with a small portion of a halogen (iodine or bromine),

which sets up a reversible reaction cycle wherein the evaporated tungsten is deposited back onto the filament.

Although the history and physics of these older lighting technologies are interesting, LEDs are far superior – both because of their narrow spectrum and because of their much higher efficiency. These two considerations (efficiency and spectrum) make indoor farming possible.

A.4 Literature Cited

Downs, R.J. 1977. Incandescent lamp maintenance in plant growth chambers. HortScience 12: 330–332.

Narukawa, Y., Ichikawa, M., Sanga, D., Sano, M., & Mukai, T. (2010). White light emitting diodes with super-high luminous efficacy. Journal of physics D: Applied physics, 43(35), 354002.

Sage, L. C. (1992). Pigment of the imagination: a history of phytochrome research. Elsevier.

Wheeler, R. M. (2008). A historical background of plant lighting: an introduction to the workshop. HortScience, 43(7), 1942-1943.

APPENDIX B

FROM PHYISCS TO FIXTURES TO FOOD:

CURRENT AND POTENTIAL

LED EFFICACY[E]

[E] Kusuma, P., P.M. Pattison, and B. Bugbee. Published in Horticulture Research.

B. 1 Overview

Light emitting diodes (LEDs) have enabled a historic increase in the conversion of electric energy to photons, but this is approaching a physical limit. The theoretical maximum efficiency occurs when all input energy is converted to energy in photosynthetic photons. Blue LEDs can be 93% efficient, phosphor-converted "whites" 76% efficient, and red LEDs 81% efficient. These improvements open new opportunities for horticultural lighting. Here we review 1) fundamental physics and efficiency of LEDs, 2) the current efficacy of LEDs 3) the effect of spectral quality on crop yield and 4) the potential efficacy of horticultural fixtures. Advances in the conversion of photons to yield can be achieved by optimization of spectral effects on plant morphology, which vary among species. Conversely, spectral effects on photosynthesis are remarkably similar across species, but the conventional definition of photosynthetic photons (400–700 nm) may need to be modified. The upper limit of LED fixture efficacy is determined by the LED package efficacy multiplied by four factors inherent to all fixtures: current droop, thermal droop, driver (power supply) inefficiencies, and optical losses. With current LED technology, the calculations indicate efficacy limits of 3.4 μmol J^{-1} for white+red fixtures and 4.1 μmol J^{-1} for blue+red fixtures. Adding optical protection from water and high humidity reduces these values by about 10%. We describe tradeoffs between peak efficacy and cost.

B.2 Physics

The term *efficiency* applies to ratios with the same units in the numerator and denominator, which can be expressed as a percentage. LED efficiency describes the optical

power output divided by the electrical power input (watt/watt or %). The term *efficacy* applies to ratios with different units. In horticultural lighting, efficacy refers to micromoles of photon output per second, per watt of input power. Since a watt is a joule per second, this simplifies to μmol per joule. The relationship between photon energy and wavelength is expressed in the Planck-Einstein relation, often just called Planck's equation. This equation states that energy is inversely proportional to wavelength ($E=hc/\lambda$). This equation is used to convert between efficiency and efficacy, and it is used to calculate the maximum possible photosynthetic photon efficacy for a given spectrum.

By converting LED efficiency into efficacy we get the appropriate units for determining the impact of photons on plants per input electrical power. This follows another physical law called the Stark-Einstein Law, which states that for every photon absorbed, only one molecule can react. This Law can be restated to say that one photon excites one electron. In this paper, photon efficacy is limited to photons between 400 and 700 nm, except in the case of far-red LEDs, where photons from up to 800 nm are included. LED package manufacturers often report efficacy in lumens per watt, because this is a meaningful metric for human lighting, but it is not applicable for horticultural lighting because it is a measure of photons weighted for human vision based on the human eye response to different colors.

> [*In this paper, LED refers to an LED package, which is the LED chip inside a housing. The housing/packaging enables mechanical and electrical connections to the fixture, provides a thermal path, affects photon distribution, and includes the phosphor layer for white LEDs (see below). LED performance specifications are for LED packages. An LED fixture refers to LED packages integrated into a fixture.*]

B.2.1 Fundamental Efficiency of LEDs

The fundamental efficiency of LEDs (LED packages) is the product of the following three sub-efficiencies:

1. Electrical efficiency: the ratio of the emitted photon energy expressed in electron volts to the applied voltage (V_{photon}/V_f), affected by internal electrical resistance of the LED.
2. The internal quantum efficiency (photon per electron): the conversion of electrons to photons, affected by non-radiative recombination pathways including impurities and microphysical defects.
3. Photon extraction efficiency: the ratio of photons that exit the LED semiconductor material to total generated photons, affected by internal reflection and reabsorption. Losses in extracting photons out of an LED package are termed 'package losses' within the LED industry. These can vary greatly among LED package types.

Table B.1: Efficiency and efficacy of some common LEDs at 100 mA per mm^2 (near-optimal efficacy) and a 25 ˚C junction temperature. Data derived from company websites (see below). The conversion of efficiency to photon efficacy depends on spectral distribution.

LED	Peak wavelength or correlated color temperature	Efficiency (W W^{-1})	Photon efficacy (µmol J^{-1})
Blue	450 nm	0.93	3.5
Green	530 nm	0.42	1.9
Red	660 nm	0.81	4.5
Far-red	730 nm	0.77	4.7
Cool White	6500 K	0.76	2.9
Warm White	2700 K	0.69	2.6

For a more comprehensive description of LED efficiency, see ref. [1]. Incremental improvements have been made to each of the three factors above resulting in a substantial improvement of LED packages over the past 10 years. Now, far-red, red, white and blue LEDs, respectively, can be 77, 81, 76 and 93% efficient (Table B.1).

B.2.2 White LEDs

White LEDs consist of blue LEDs with a luminescent material coating (e.g. a phosphor material, typically $Y_3Al_5O_{12}$:Ce) that absorbs blue photons and luminesces at longer wavelengths. Phosphor-converted white LEDs are designed to transmit some blue photons, with the remainder converted to longer wavelengths. Types and amounts of phosphor are varied to create multiple hues and color qualities. Figure B-1 shows a general relationship between correlated color temperature (CCT) and percentage of blue photons (400–500 nm). This relationship generally follows Wien's Displacement Law, which indicates that as the CCT increases the peak wavelength decreases. Therefore, white LEDs with a high CCT have a higher percentage of blue photons. In addition to CCT, electric lights are qualified/quantified by other metrics including CRI and TM-30 (ref. [2]). Both CRI and the TM-30 metric of R_f use a scale of 0–100 to describe color fidelity. A high color fidelity facilitates observing subtle color differences. This is important to human observers for visual identification of tiny insects, nutritional disorders, and diseases. Suitable color fidelity is also necessary for machine vision.

Commonly used terms to associate names with color temperatures are warm white (2500–3500 K), neutral white (3500–4500 K), cool white (4500–5500 K) and daylight

(5500–7500 K). A lower CCT (2700–4000 K) and higher CRI (greater than 80) are often preferred for indoor lighting to provide incandescent-like light qualities for humans[3].

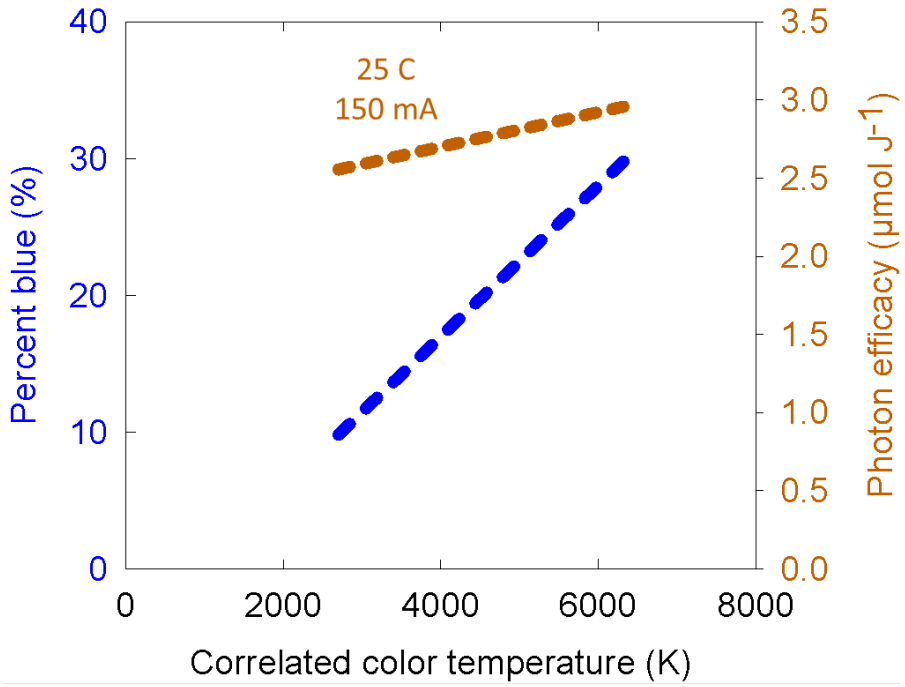

Fig. B-1 The general relationship between color temperature on percent blue photons (left axis), and the effect of color temperature on photon efficacy (right axis). Exact values vary among manufacturers. Photon efficacy in this graph is presented at a junction temperature of 25 ˚C and 150 mA. The efficacy values will shift if these inputs are changed, see below.

Increased density of phosphor coatings and increased use of red phosphor materials decreases efficiency. A 6500 K LED (daylight) with about 30% blue photons can have 95% of the photon output of its non-phosphor-converted blue LED counterpart, but this value decreases to 80–85% for a warm white LED with 10% blue photons. Additionally, as the optical output of white LEDs increases, the phosphor efficiency will decrease. This is due to conversion, energy, and optical losses within the phosphor conversion process.

B.2.3 Current Droop

LEDs are designed for performance at specific current ranges. Moderate LED drive current density enables higher efficiency, but at very low drive currents, efficiency decreases. LED loss mechanisms are typically a function of current density. So at a given current, increasing the size on an LED chip can increase the efficacy of an LED by reducing the current density. Unfortunately, chip area is often confidential and LED manufacturers only report LED specs at the total LED drive current, not drive current density.

Figures B-2 and B-3 are calculated using data from Lumileds (Amsterdam, Netherlands) (Wouter Soer, personal communication)[4], Osram (Munich, Germany) [5-7] and Samsung (Seoul, South Korea)[8]. These companies provide LED efficacy data in μmol J^{-1}. Additional LED manufacturers include Nichia (Anan, Japan)[9], Cree (Durham, North Carolina, USA)[10], Epistar (Hsinchu, Taiwan)[11], and many others. As technology improves, see the companies' websites to find the latest LED package efficacy information, and apply the principles described below to determine potential fixture efficacy. Figure 2 shows the decrease in efficacy as a function of drive current density for typical LEDs. This effect is referred to as current 'droop'. Current droop is the decrease in radiative efficiency of the LED as current is increased. For a blue LED current droop is caused by Auger recombination[12,13]. For a white LED, which has a blue LED and a phosphor conversion layer, the droop is caused by Auger in the blue LED and reduction in phosphor conversion efficiency at higher optical flux concentrations[14]. For red and far-red LEDs, the current droop is caused by carrier leakage due to poor confinement of electrons in the active regions[15]. In general, decreasing the drive current increases the efficacy, but eventually Shockley-Read-Hall defect losses will dominate at very low drive current[16]. LED

manufacturers continue to both increase LED peak efficiency and reduce current droop. The theoretical maximum lines for red (centered at 660 nm) and blue (centered at 450 nm) LEDs are based on the assumption of 100% power efficiency of the LED or hypothetical photon generating device (1 W electricity input = 1 W photon output) followed by a conversion to number of photons using Planck's equation. White LEDs would be as efficient as blue LEDs if phosphor conversion was 100% efficient. However, phosphor conversion efficiencies range from 80 to 95% depending on amount of phosphor, phosphor material, temperature,

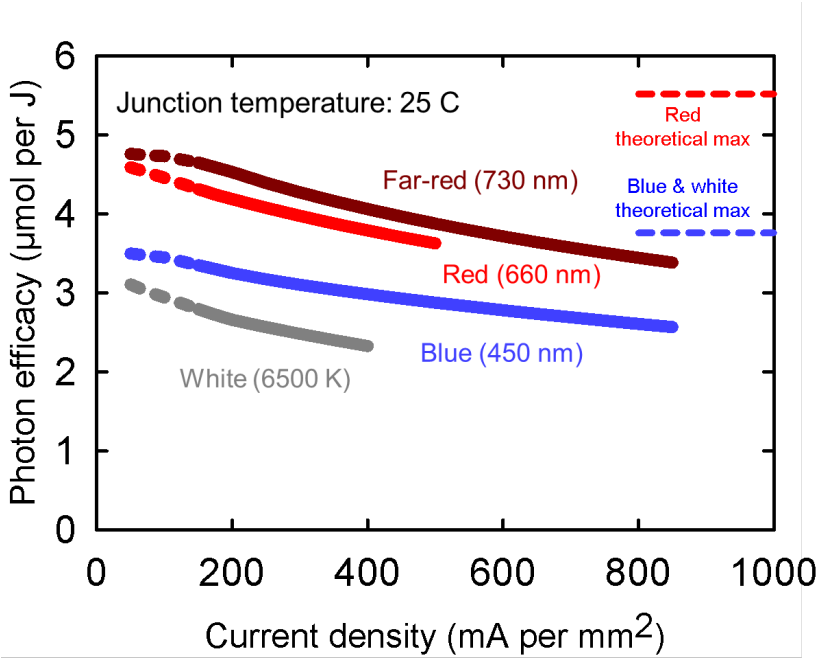

Fig. B-2 Effect of drive current on photon efficacy at a junction temperature of 25 ˚C. The dashed lines in this graph represent inadequate test data at low drive currents. However, low drive current (e.g. 65 mA) is used in LED fixtures. Blue photons have a lower theoretical maximum efficacy than red photons, based on Planck's equation, which states that energy is inversely proportional to wavelength (E = hc/wavelength). Blue photons centered at 450 nm can provide 3.76 µmol J^{-1} and red photons centered at 660 nm can provide 5.52 µmol J^{-1}. This is really less of a characteristic of the photons than of the LEDs that make them.

and photon flux density. A color-mixed "white" fixture using direct emitting (not phosphor converted) green LEDs (550 nm) as well as red and blue LEDs would have a theoretical

maximum of about 4.6 µmol J^{-1}, but direct-emitting green LEDs currently have low efficiency (referred to as the green gap[17]) resulting in low efficacy (about 1.9 µmol per J)[18].

B.2.4 Thermal Droop

Junction temperature refers to the operating temperature at the actual diode. There are two temperature standards for reporting the efficacy of LEDs: 25 and 85 ˚C. Efficacy decreases about 10% as the temperature increases from 25 to 85 ˚C (thermal droop). Thermal droop is typically worse in red compared to blue LEDs.

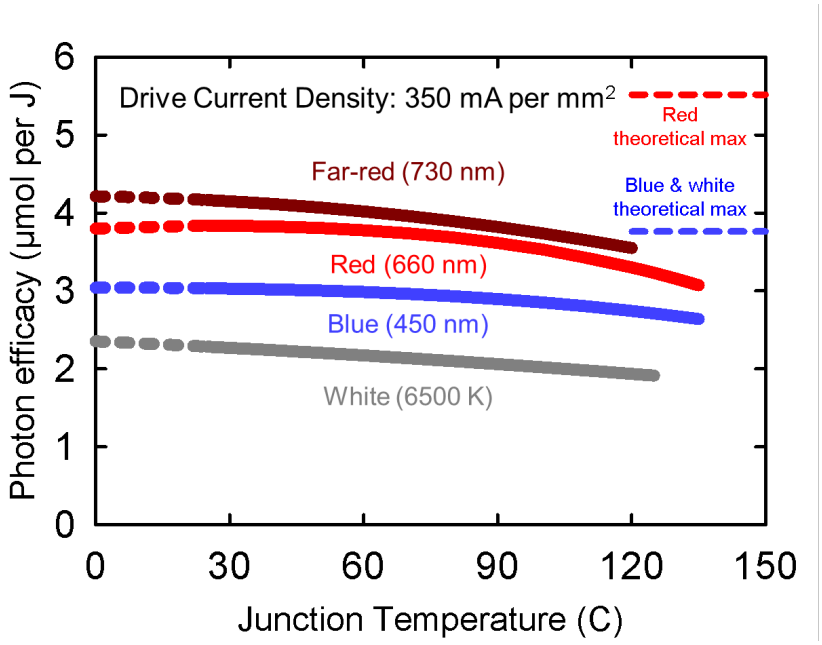

Fig. B-3 Effect of junction temperature on photon efficacy. Note that higher drive currents increase the junction temperature. The dashed lines in this graph represent temperatures below 25 ˚C, and therefore temperatures below ambient conditions. Reducing the temperature below ambient would be an energy requiring process.

B.2.5 Projected Efficacy

A timeline of the historic and projected increases in LED efficacy is presented in Figure B-4 (ref. [19]).

Figure B-4 has been updated to include an estimation of the efficacy of current LED technology. This estimation indicates LED efficacy is approaching a practical maximum. The theoretical maximum assumes 100 percent efficiency, but is difficult to attain. Therefore efficacy is expected to level off at a practical maximum that is 90% of the theoretical maximum.

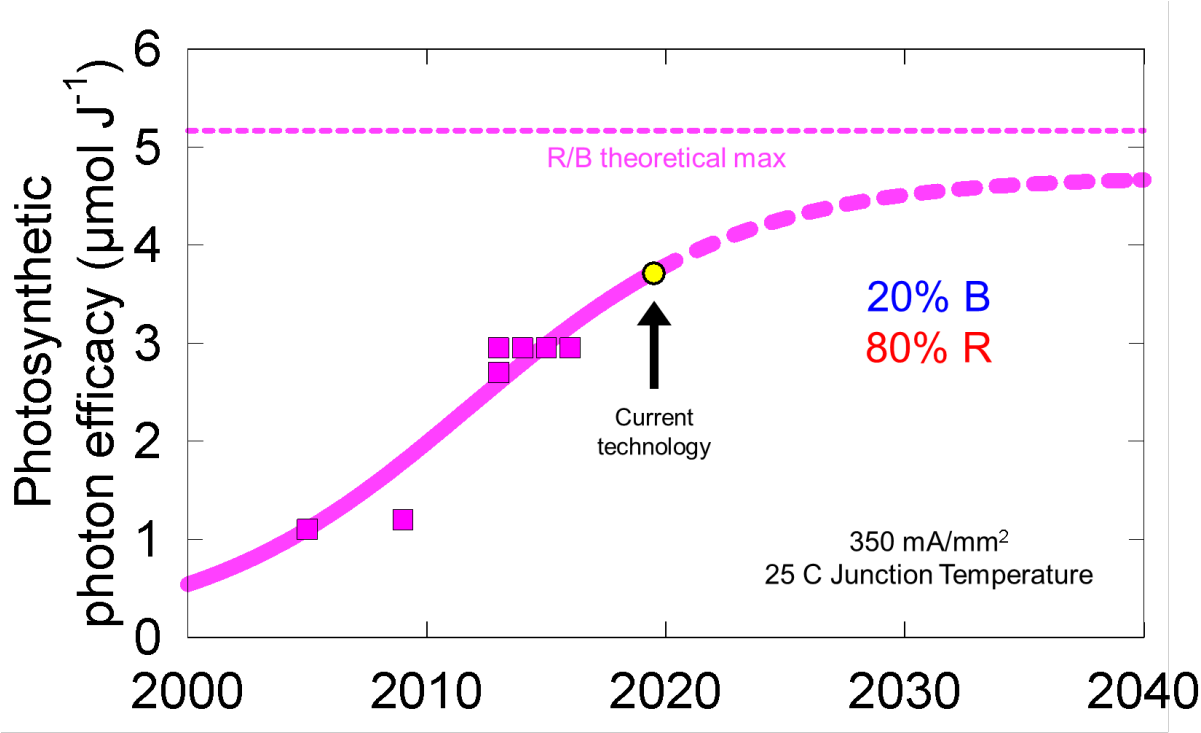

Fig. B-4 Historical, current and projected LED package combination efficacy of a 20/80% ratio of blue and red LEDs. This is an average of the two LEDs. The figure constrains LED performance to specific current and temperature operating conditions as discussed below. The current technology point is not constrained to these conditions so will be higher compared to the figure data.

B. 3 LEDs for Horticultural Applications

Horticultural LED fixtures typically contain combinations of red (peak ≈ 660 nm), blue (peak ≈ 450 nm), white, and/or far-red (peak ≈ 730 nm) emitting LEDs. Other peak wavelengths are available, but they have lower efficiencies and efficacies and are less common. Fixture manufacturers choose the ratios of these LEDs for specific applications and based on their perception of best practices and market demands.

B.3.1 History of Horticultural LED Fixtures

Morrow discussed the significance of LEDs for horticultural lighting and reviewed the early adoption of the technology[20]. The first LED-produced photons used to grow plants were red[21], which was shortly followed by the development of high output blue LEDs[22]. For a review of the historical significance of this Nobel prize-winning discovery, see ref. [23]. Before widespread adoption of blue LEDs, early studies demonstrated the value of blue photons for plant growth using blue fluorescent fixtures to supplement red photons from LEDs[24,25].

The first commercial horticultural LED fixtures were blue+red combinations. These fixtures, which produced a spectrum that appeared magenta, had a higher efficacy than white or white+red fixtures. Many people thought that these blue+red fixtures would enhance photosynthesis compared to full spectrum fixtures due to their close match to the chlorophyll absorption spectrum, which shows peak absorption in the blue and red regions of the photosynthetically active radiation (PAR, 400–700 nm) spectrum. This thinking was advanced by early LED manufacturers, even though green photons have long been known to

be effective for photosynthesis[26,27]. Due to widespread use in lighting applications for human vision, white LED packages are now ≈20% of the cost of red LEDs. This has contributed to the increase in the fraction of white LEDs to more than 60%, in some horticultural fixtures.

B.3.2 Spectral Effects on Plant Shape and Photosynthesis

Photons excite electrons and photobiology is thus driven by the number of photons, not energy or lumens. Biologically active photons must have sufficiently high energy to excite pigment photoreceptors, and there are multiple photoreceptors with weighting functions for wavelengths, which are biophysically or empirically derived. Lumens are an example of a weighting function applied to a photon flux and spectral distribution for human visual function.

The effect of spectral quality on plant shape is synergistic among wavelengths, interacts with intensity, varies among species[28] and may vary over the plant life cycle. Some principles, however, apply across all species. The impacts of spectrum on plant growth and development are much greater in sole-source lighting than in greenhouse supplemental lighting where electric lighting makes up only a small portion of the plant lighting diet.

In plant biology spectra are traditionally separated into the following coarse categories.

Ultra-violet photons are further separated into three broad categories: UV-C (100–280 nm), UV-B (280–315/320 nm) and UV-A (315/320–400 nm). The wavelength at which UV-C and UV-B are separated (280 nm) is determined by the shortest wavelength of solar radiation that reaches the surface of Earth. The wavelength at which UV-B and UV-A are

separated (315 or 320 nm) is generally determined by the effect of sun on human skin sunburn (315 nm) or skin cancer (320 nm). There is no universal agreement on the wavelength transition between UV-B and UV-A, both are equally used. Fortunately, UV-C photons are completely blocked by our atmosphere because they are highly damaging to biological organisms. UV-B photons are also damaging, but can have beneficial effects including increased production of secondary metabolites[29]. UV-A photons are less damaging than UV-B, and can have either stimulatory or inhibitory effects on plant growth depending on species and interacting environmental factors[30].

At 25 ˚C and 350 mA, UV-B and UV-C LEDs are only ≈3% efficient[31], but these photons can have large biological effects in small quantities. At 25 C and 700 mA, the efficiency of UV-A LEDs increases from 50 to 60% as the wavelength increases from 370 to 395 nm[32]. A violet LED with a peak between 402 to 408 nm is ≈65% efficient, and has 15–30% of its photons below 400 nm. Efficiency will increase as current density decreases.

Based on studies by McCree[26, 27], PAR only includes photons with wavelengths between 400 to 700 nm. However, McCree's studies show significant differences in the photosynthetic efficiency of species at wavelengths below ≈425 nm. Some species, like radish, have equal photosynthesis between 375 and 500 nm. Photons above 350 nm can be photosynthetic, but a high-fraction are typically absorbed by non-photosynthetic pigments.

Blue photons (400–500 nm) reduce plant height and leaf expansion in nearly all species[28,33-35]. Because of absorption by inactive pigments (e.g. anthocyanin), blue photons are ≈20% less photosynthetically efficient than photons from the most common red LED (660 nm)[26,27]. However, the blue-induced decreases in leaf area (reducing photon capture) may have a larger effect on overall plant growth than the blue-induced reduction in

photosynthetic rate[28]. A range of 5–30% blue is typically used in horticultural LED fixtures to inhibit excessive stem extension and reduce plant height, which is typically beneficial for controlled environment growth.

Green photons (500–600 nm) improve human perception of color. Unfortunately, monochromatic direct emitting (non-phosphor converted) green LEDs have low efficacy. White (phosphor-converted blue) LEDs are thus used to provide the green photons that are important to human vision; and they have the added benefit of providing blue and red photons. Green photons are up to 10% less photosynthetically efficient than photons from the most common red LED (660 nm)[26,27], but they penetrate deeper into plant canopies than blue or red photons[36].

The effect of green photons on plant shape is generally much less than the effects of blue or far-red photons. Studies in *Arabidopsis* suggest that green photons can reverse blue photon effects (e.g. inhibition of hypocotyl elongation)[37,38] or induce shade avoidance (e.g. increased stem elongation, reduced branching)[39,40]. Some studies suggest that green-induced shade avoidance also occurs in food crops and other economically valuable plants[28,35,41], but several other studies have shown minimal effects[28,33,41-45].

Red photons (600–700 nm) are well absorbed by leaves, are photosynthetically efficient, and are efficiently generated by LEDs so they are widely used in horticultural fixtures. The classical paradigm has been that red and far-red act antagonistically to inhibit or induce shade avoidance symptoms like stem elongation, hyponastic leaf orientation and/or reduced branching[46,47]. However, the high absorbance of red photons by chlorophyll means that the impact of red on shade responses may be overestimated[48]. Replacing green photons

with red photons has minimal effects on plant shape[43,45], but plants grown in the complete absence of red and green photons (sole-source blue LEDs) can rapidly elongate[28,33,49].

Far-red photons (700–800 nm) can have powerful effects on plant shape and are efficiently generated by LEDs so they are a promising addition to horticultural lighting. Along with several other laboratories, we are working to quantify the effects of far-red photons on plant morphology. In some species (especially lettuce), far-red photons beneficially increase leaf expansion, but they also significantly increase stem elongation in many other species[35,50], which may not be beneficial.

Despite the classic definition of PAR, recent studies indicate that far-red photons (700–750 nm) are photosynthetically synergistic with shorter wavelength photons[51,52]. These photons are thus being reconsidered for their role in photosynthesis. Far-red photons must be used with caution, particularly in sole-source environments, because they can induce stem elongation associated with shade avoidance.

B.4 Technology of LED Fixtures

B.4.1 Four Factors that Determine Fixture Efficacy

The upper limit of fixture efficacy is determined by the choice of LEDs and operating conditions. Different colors of LEDs have different efficacies, but the quality of LEDs within and among manufacturers also varies. In addition to the efficacy of the selected LEDs, fixture efficacy is determined by four additional factors[53]:

1. LED drive current
2. LED junction temperature

3. Driver efficiency
4. Optical losses in the fixture

1. ***Drive current***

   The effect of drive current on LED efficacy has been discussed above. Due to different types of efficiency reductions at high and low drive currents, efficiency can be maximized at some relatively low drive current (less than 100 mA). Fixture manufacturers seek to co-optimize fixture size, cost, output and efficacy for specific applications. While low drive currents will increase the efficacy of the fixture, the output of each LED would be relatively low. This increases the cost and complexity of the fixture.

2. ***LED junction temperature***

   The junction temperature of LEDs in fixtures depends on the drive current, ambient temperature and the heat dissipation (thermal management) of the fixture, but is typically around 85 ˚C[53]. Better thermal management may increase fixture cost, but it also increases efficacy and longevity of the LEDs (Fig. B-5).

   [*LEDs degrade with time as a function of temperature and current density. L70 is a metric that indicates the time at which a fixture output is 70% of the original output (sometimes referred as Q70 for horticultural products). A typical L70 for LED fixtures is 50,000 h. As the LEDs and fixture age, the efficacy will decline; a problem that is exacerbated by high junction temperatures. Rates of fixture aging can vary greatly among manufacturers. Most manufacturers characterize their fixture lifetime (L70, L90, Q70 or Q90) in terms of LED output depreciation based on a standard*

LED package test–IES LM-80, which can be interpolated into luminaire lumen maintenance. Projections of luminaire lumen maintenance based on LED depreciation cannot exceed six times of the duration that the LEDs were tested, so for a depreciation lifetime claim of 60,000 h the LEDs must have been tested for 10,000 h. Many fixtures that claim extended lifetimes are exceeding the allowable six times interpolation based on LED testing. Fixture lifetimes based on LED depreciation also do not include optical loss mechanisms in the fixture and accelerated aging of the LEDs due to higher temperatures. Also, typical lifetime claims do not consider catastrophic failure of the LED driver, which often fails before the LEDs have reached the L70.]

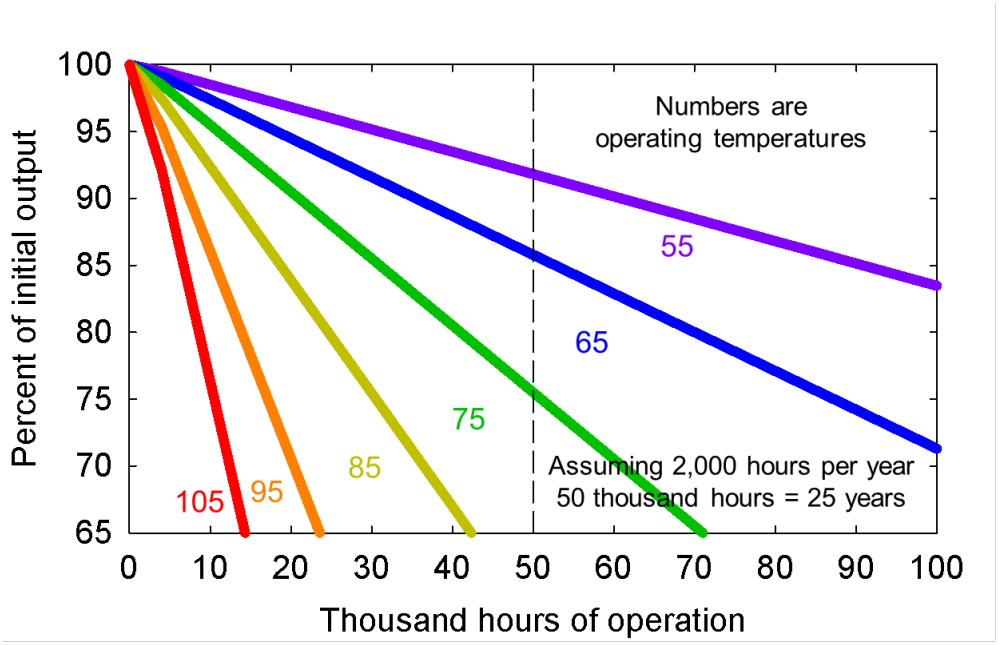

Fig. B-5 Long-term depreciation of LEDs based on temperature. LEDs will depreciate slower when operated at lower temperatures.

3. ***LED Drivers*** (also called power supplies) are necessary to convert AC to DC power and provide regulated voltage and current. The efficiency of LED drivers ranges

from 85 to 95%. LED drivers can be less efficient when they provide dimming, color control and/or communication functionality.

4. ***Optical losses*** occur when LEDs are mounted in fixtures. The sides of the fixture can obstruct low-angle photons. Protective transparent covers (e.g. glass) transmit up to 92% of the photons and thus reduce the output by 8%, but this protection can significantly improve the lifetime of a fixture. Fixtures with unprotected LEDs can have 99% optical efficiency, but may have shorter lifetimes in harsh growing environments (e.g., high humidity).

Optical covers can also diffuse the photons, which reduces efficiency, but can result in more uniform mixing of colors and improved photon penetration into plant canopies[54-56].

Photons must impact leaves to be absorbed, and this is an important consideration in fixture design. Early LED fixtures had focused photon output over a small area. This facilitated precise photon placement, but caused non-uniform distribution. LED package and fixture design has transitioned to a less-focused photon distribution but as long as the photons exit the fixture this does not affect our analysis of optical efficacy[57].

B.4.2 Potential Fixture Efficacy

Using the following near-maximum parameters, we now calculate an achievable fixture efficacy using presently-available technology:

1. Drive current minimized to achieve 104% of the reported LED efficacy (100 mA mm^{-2} to 50 mA mm^{-2})
2. Temperature rise minimized by sufficient heat dissipation (e.g. water cooling) to achieve 95% of the reported LED efficacy (at 25 ˚C)
3. The LED driver is 95% efficient
4. Unprotected LEDs in the fixture to achieve 99% optical efficiency

The resulting fixture efficacy would be 1.04 × 0.95 × 0.95 × 0.99 = 93% of the reported efficacy of the LED. The first two factors can be above 100% if the LEDs are operated at lower drive current and lower temperature than the reported specification (100 mA mm^{-2} and 25 ˚C here). Reducing drive current is much easier than reducing temperature.

Accordingly, a horticultural fixture with 90% red and 10% blue photons (i.e. a photon flux distribution of B10:R90, typical of magenta-colored fixtures) could potentially achieve an efficacy of 4.1 µmol J^{-1} if it used red and blue LEDs with efficacies of 4.5 and 3.5 µmol J^{-1}, respectively (Table B.1).

A fixture built using all white LEDs with an efficacy of 2.9 µmol J^{-1} (Table B.1) would result in a fixture efficacy of 2.7 µmol J^{-1}.

A broad spectrum fixture, with approximately equal portions of red and white LEDs could achieve an efficacy of 3.4 under optimal conditions if the best LEDs are used (Fig. B-6). The increased leaf expansion caused by far-red photons means that the addition of up to 30% far-red LEDs might be cost effective for lettuce and other leafy greens[35].

Table B.2: Examples of the highest efficacy values from independently-tested LED fixtures and an HPS fixture. TÜV SÜD America is an accredited testing laboratory.

Color	Efficacy (μmol J^{-1})	Reference
blue/red	2.55	Johnson et al. (2017)[53]
blue/red	2.64	Radetsky (2018)[54]
white/red	2.59	Radetsky (2018)[54]
blue/red	3	DLC(2019)[10]
white/red	2.78	DLC(2019)[10]
white/red	2.61	DLC(2019)[10]
3000 K	2.13	TÜV SÜD America (2019)
5000 K	2.43	TÜV SÜD America (2019)
1000 W double-ended HPS	1.72	Radetsky (2018)[54]

B.4.3 Typical Fixture Efficacy

Using more typical parameters:

1. Drive current achieves 90% of the reported LED efficacy
2. Temperature management achieves 90% of the reported LED efficacy (at 25 ˚C)
3. The LED driver is 90% efficient
4. Protected LEDs in the fixture achieve 92% optical efficiency

The resulting fixture efficacy would be 0.90 × 0.90 × 0.90 × 0.90 = 67% of the reported efficacy of the LEDs.

In 2014, the best LED fixtures had an efficacy of 1.7 μmol J^{-1} (ref. [57]). Now, fixture efficacies of 2.5 to 2.8 μmol J^{-1} for white+red fixtures and 3 μmol J^{-1} for blue+red fixtures have been achieved (Table B.2).

Certified test laboratories conduct comprehensive tests on fixtures to characterize their performance. This is the integrated measure of all the above factors. Fixture manufacturers should always be able to provide test results for their fixtures from certified third-party test laboratories.

The Design Lighting Consortium (DLC) maintains a list of horticultural lighting products that meet their listing requirements[58]. The DLC requires that products have a minimum efficacy of 1.9 µmol J^{-1} and meet photon flux maintenance, driver lifetime, warranty, and safety requirements.

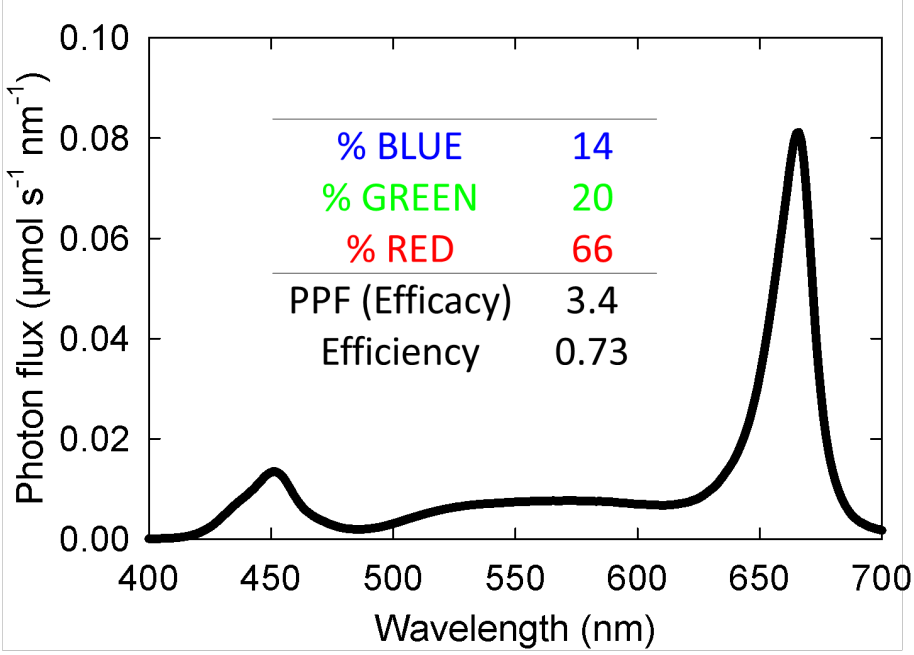

Fig. B-6 A suggested fixture for high efficacy. The y-axis assumes one watt of input power.

B.5 Additional Considerations

In addition to efficacy, several other factors affect fixture choice, including:

1. Initial fixture cost per photon s^{-1} of output capacity. HPS fixtures (1 kW) range from \$200 to \$350 USD per kW (5–9 μmol s^{-1} per \$). LED fixtures range from \$1000 to \$3000 USD per kW (0.5–1.5 μmol s^{-1} per \$). On a photon flux basis, the initial cost is therefore, 3–18 times higher for LED vs. HPS fixtures. The cost of both technologies has decreased but the cost of LED fixtures are expected to decrease faster than HPS fixtures. While initial cost is higher, LED fixtures reduce energy cost compared to HPS. Depending on usage periods and price of energy, the electric savings can equal the difference in initial cost after of 3–5 years for sole source applications and 5–8 years for supplemental applications[57].
2. Spectral quality for plant morphology and photon capture[35,59].
3. Adequate green photons to create "white" light to facilitate human comfort and visual identification of insects, diseases, and nutritional disorders[60].
4. Fixture reliability, including environmental protection of the LEDs.
5. Fixture operating temperatures, which affect LED and system longevity.
6. Uniformity and distribution of photon output. Many early LED fixtures had narrow beam angles, but more recent fixtures have a broader distribution of photons. High wattage HPS fixtures need to be mounted higher above the canopy than LED fixtures to achieve uniform distribution of photons.
7. Fixture size for shading in a greenhouse application.

Because LEDs can be cycled on and off over short intervals, there has been interest in rapid cycling of LED fixtures to improve plant growth. Unfortunately, high frequency flickering (10–10000 Hz) has been well studied and there is neither empirical nor theoretical evidence that this can be used to increase the quantum yield of photosynthesis. Plants appear

to integrate light intensity for photosynthesis[61,62]. However, some recent evidence indicates that longer term cycling of LEDs (minute to hours) can alter plant shape (hypocotyl length) and color (anthocyanin synthesis)[63].

B.6 Summary

- Blue LEDs are now 93% efficient, phosphor-converted "whites" are 76% efficient, and reds are 81% efficient when run at the near optimal conditions of 100 mA mm^{-2} and a junction temperature of 25 ˚C.
- Both junction temperature and drive current density will affect the photon efficacy of LEDs, and in general, the most efficient LED fixture will run their LEDs at low drive currents. However, a lower drive current results in a lower photon output per LED, and the resulting fixture will require many LEDs to achieve a high photon output and thus will be more expensive.
- Broad spectrum distribution of photons is important useful for uniform spectral reflectance and diagnosis of plant disorders. Broad spectrum lighting is not necessarily beneficial for with photosynthesis or plant growth. Unique spectra, selectively applied during specific stages of the life cycle, can however, have a beneficial effect on plant shape and development.
- The calculations in this paper show current possible performance levels of LED fixtures of 3.4 µmol J^{-1} for white+red fixtures and 4.1 µmol J^{-1} for blue+red fixtures. These values are significantly higher than current typical values of 2–3 µmol J^{-1}.

Although fixture efficacy is paramount, timing and angular delivery of photons to photosynthetic tissues, spectrum and intensity also determine the effectiveness of the photon delivery system. Efficient lighting is then coupled with optimal temperature, humidity, nutrition, plant water potential, atmospheric carbon dioxide concentration, delivery of oxygen to root surfaces and genetics. Both NASA and the USDA are funding research at universities to optimize these factors and improve the economic potential of electric lighting in in controlled environments: https://cubes.space/ ; https://www.hortlamp.org/index.html.

B.7 Literature Cited

1. Tsao, J. Y., Coltrin, M. E., Crawford, M. H. & Simmons, J. A. Solid-state lighting: an integrated human factors, technology and economic perspective. *Proc. IEEE* **98**, 1162-1179 (2010).
2. Illuminating Engineering Society of North America. IES TM-30-15. *IES method for evaluating light source color rendition*. (2015).
3. Pust, P., Schmidt, P. J. & Schnick, W. A revolution in lighting. *Nat. Mater.* **14**, 454-458 (2015).
4. *LUXEON 2835 line product datasheet DS216.* https://www.lumileds.com/uploads/603/DS216-luxeon-2835-line-datasheet-pdf (Lumileds Holding B.V., 2019).
5. *OSLON Square GH CSSRM3.24 product datasheet*. https://dammedia.osram.info/media/resource/hires/osram-dam-7718278/GH CSSRM3.24_EN.pdf (Osram Opto Semiconductors GmbH, 2019).
6. *OSLON SSL 150 GF CSHPM2.24 product datasheet*. https://dammedia.osram.info/media/resource/hires/osram-dam-9119319/GF CSHPM2.24_EN.pdf (Osram Opto Semiconductors GmbH, 2019).
7. *OSLON Square GD CSSRM2.14 product datasheet*. https://dammedia.osram.info/media/resource/hires/osram-dam-5658482/GD CSSRM2.14_EN.pdf (Osram Opto Semiconductors GmbH, 2019).
8. *Middle power LED series 3030 LM301H CRI80 product datasheet*. https://cdn.samsung.com/led/file/resource/2018/11/Data_Sheet_LM301H_CRI80_Rev.1.2.pdf (Samsung, 2019)
9. Nichia website. http://www.nichia.co.jp/en/product/led.html (Nichia Corporation, 2019).
10. Cree website. https://www.cree.com/led-components/products (Cree, Inc. 2019).

11. Epistar website. https://www.epistar.com/EpistarEn/ProdInfoApp?id=10 (Epistar Corporation, 2019).
12. Iveland, J., Martinelli, L., Peretti, J., Speck, J. S. & Weisbuch, C. Direct measurement of Auger electrons emitted from a semiconductor light-emitting diode under electrical injection: identification of the dominant mechanism for efficiency droop. *Phys. Rev. Lett.* **110**, 177406 (2013).
13. Shen, Y. C. *et al.* Auger recombination in InGaN measured by photoluminescence. *Appl. Phys. Lett.* **91**, 141101 (2007).
14. Shchekin, O. LED technology considerations for high luminance sources. DOE SSL R&D Workshop. https://www.energy.gov/sites/prod/files/2017/02/f34/shchekin_considerations_longbeach2017.pdf (2017).
15. Krames, M. R. *et al.* Status and future of high-power light-emitting diodes for solid-state lighting. *J. Disp. Technol.* **3**, 160-175 (2007).
16. Kuritzky, L. H., Weisbuch, C. & Speck, J. S. Prospects for 100% wall-plug efficient III-nitride LEDs. *Opt. Express* **26**, 16600-16608 (2018).
17. Pattison, P. M., Tsao, J. Y. & Krames, M. R. Light-emitting diode technology status and directions: opportunities for horticultural lighting. *Acta Hortic*. **1134**, 413-426 (2016).
18. *OSLON Square GT QSSPA1.13 product datasheet*. https://dammedia.osram.info/media/resource/hires/osram-dam-9945204/GT QSSPA1.13_EN.pdf (Osram Opto Semiconductors GmbH, 2019).
19. US DOE SSL Program. *Solid-State Lighting 2017 Suggested Research Topics Supplement: Technology and Market Context*. https://energy.gov/sites/prod/files/2017/09/f37/ssl_supplement_suggested-topics_sep2017_0.pdf (2017).
20. Morrow, R. C. LED lighting in horticulture. *HortSci.* **43**, 1947-1950 (2008).
21. Bula, R. J. *et al.* Light-emitting diodes as a radiation source for plants. *HortSci.* **26**, 203-205 (1991).
22. Nakamura, S., Mukai, T. & Senoh, M. Candela-class high-brightness InGaN/AIGaN double-heterostructure blue-light-emitting diodes. *Appl. Phys. Lett.* **64**, 1687-1689 (1994).
23. Tsao, J. Y., Han, J., Haitz, R. H. & Pattison, P. M. The blue LED Nobel prize: historical context, current scientific understanding, human benefit. *Ann. Phys.* **527**, A53-A61 (2015).
24. Goins, G. D., Yorio, N. C., Sanwo, M. M. & Brown, C. S. Photomorphogenesis, photosynthesis, and seed yield of wheat plants grown under red light-emitting diodes (LEDs) with and without supplemental blue lighting. *J. Exp. Bot.* **48**, 1407-1413 (1997).
25. Yorio, N. C., Goins, G. D., Kagie, H. R., Wheeler, R. M. & Sager, J. C. Improving spinach, radish, and lettuce growth under red light-emitting diodes (LEDs) with blue light supplementation. *HortSci*. **36**, 380-383 (2001).
26. McCree, K. J. The action spectrum, absorptance and quantum yield of photosynthesis in crop plants. *Agric. Meteorol.* **9**, 191-216 (1971).

27. McCree, K. J. Test of current definitions of photosynthetically active radiation against leaf photosynthesis data. *Agric. Meteorol.* **10**, 443-453 (1972).
28. Snowden, M. C., Cope, K. R. & Bugbee, B. Sensitivity of seven diverse species to blue and green light: interactions with photon flux. *PLoS ONE* **11**, e0163121 (2016).
29. Dou, H., Niu, G. & Gu, M. Pre-Harvest UV-B Radiation and Photosynthetic Photon Flux Density Interactively Affect Plant Photosynthesis, Growth, and Secondary Metabolites Accumulation in Basil (*Ocimum basilicum*) Plants. *Agronomy* **9**, 434 (2019).
30. Verdaguer, D., Jansen, M. A., Llorens, L., Morales, L. O. & Neugart, S. UV-A radiation effects on higher plants: Exploring the known unknown. *Plant Sci.* **255**, 72-81 (2017).
31. *NICHIA NCSU334A(T) product datasheet.* https://www.nichia.co.jp/specification/products/led/NCSU334A-E.pdf (Nichia Corporation, 2019).
32. *NICHIA NVSU119CT product datasheet.* https://www.nichia.co.jp/specification/products/led/NVSU119C-E.pdf (Nichia Corporation, 2019).
33. Hernández, R., & Kubota, C. Physiological responses of cucumber seedlings under different blue and red photon flux ratios using LEDs. *Environ. Exp. Bot.* **121**, 66-74 (2016).
34. Wang, J., Lu, W., Tong, Y. & Yang, Q. Leaf morphology, photosynthetic performance, chlorophyll fluorescence, stomatal development of lettuce (*Lactuca sativa* L.) exposed to different ratios of red light to blue light. *Front. Plant. Sci.* **7**, 1-10 (2016).
35. Meng, Q., Kelly, N. & Runkle, E. S. Substituting green or far-red radiation for blue radiation induces shade avoidance and promotes growth in lettuce and kale. *Environ. Exp. Bot.* **162**, 383-391 (2019).
36. Brodersen, C. R. & Vogelmann, T. C. Do changes in light direction affect absorption profiles in leaves?. *Funct. Plant Biol.* **37**, 403-412 (2010).
37. Bouly, J. P. *et al.* Cryptochrome blue light photoreceptors are activated through interconversion of flavin redox states. *J. Biol. Chem.* **282**, 9383-9391 (2007).
38. Sellaro, R. *et al.* Cryptochrome as a sensor of the blue/green ratio of natural radiation in Arabidopsis. *Plant Physiol.* **154**, 401-409 (2010).
39. Zhang, T., Maruhnich, S. A. & Folta, K. M. Green light induces shade avoidance symptoms. *Plant Physiol.* **157**, 1528-1536 (2011).
40. Wang, Y., Zhang, T. & Folta, K. M. Green light augments far-red-light-induced shade response. *Plant Growth Regul.* **77**, 147-155 (2015).
41. Park, Y. & Runkle, E. S. Spectral effects of light-emitting diodes on plant growth, visual color quality, and photosynthetic photon efficacy: White versus blue plus red radiation. *PloS ONE* **13**, e0202386 (2018).
42. Li, Q. & Kubota, C. Effects of supplemental light quality on growth and phytochemicals of baby leaf lettuce. *Environ. Exp. Bot.* **67**, 59-64 (2009).
43. Son, K. & Oh, M. Growth, photosynthetic and antioxidant parameters of two lettuce cultivars as affected by red, green, and blue light-emitting diodes. *Hortic. Environ. Biotechnol.* **56**, 639-653 (2015).

44. Chen, X., Xue, X., Guo, W., Wang, L. & Qiao, X. Growth and nutritional properties of lettuce affected by mixed irradiation of white and supplemental light provided by light-emitting diode. *Sci. Hortic.* **200**, 111-118 (2016).
45. Kang, W. H., Park, J. S., Park, K. S. & Son, E. S. Leaf photosynthetic rate, growth, and morphology of lettuce under different fractions of red, blue, and green light from light-emitting diodes (LEDs). *Hortic. Environ. Biotechnol.* **57**, 573-579 (2016).
46. Smith, H. Phytochromes and light signal perception by plants—an emerging synthesis. *Nature* **407**, 585-591 (2000).
47. Casal, J. J. Shade avoidance. *Arabidopsis Book* **10**, e0157 (2012).
48. Morgan, D. C. & Smith, H. The relationship between phytochrome-photoequilibrium and development in light grown *Chenopodium album* L.. *Planta* **142**, 187-193 (1978).
49. Kong, Y., Stasiak, M., Dixon, M. A. & Zheng, Y. Blue light associated with low phytochrome activity can promote elongation growth as shade-avoidance response: A comparison with red light in four bedding plant species. *Environ. Exp. Bot.* **155**, 345-359 (2018).
50. Park, Y. & Runkle, E. S. Far-red radiation promotes growth of seedlings by increasing leaf expansion and whole-plant net assimilation. *Environ. Exp. Bot.* **136**, 41-49 (2017).
51. Zhen, S. & van Iersel, M. W. Far-red light is needed for efficient photochemistry and photosynthesis. *J. Plant Physiol.* **209**, 115-122 (2017).
52. Zhen, S. & Bugbee, B. Far-red photons have equivalent efficiency to traditional photosynthetic photons: implications for re-defining photosynthetically active radiation. *Plant Cell Environ*. 1-14 (2020).
53. US DOE SSL Program. *Solid-State Lighting R&D Plan*. https://www.energy.gov/sites/prod/files/2015/06/f22/ssl_rd-plan_may2015_0.pdf (2015).
54. Sinclair, T. R., Shiraiwa, T. & Hammer, G. L. Variation in crop radiation-use efficiency with increased diffuse radiation. *Crop Sci.* **32**, 1281-1284 (1992).
55. Tubiello, F., Volk, T. & Bugbee, B. Diffuse Light and Wheat Radiation-Use Efficiency in a Controlled Environment. *Life Support Biosphere Sci*. **4**, 77-85 (1997).
56. Zhen, S. & Bugbee, B. Diffuse light and canopy photosynthesis. *Controlled Environments*. Paper 12. (2019) Digital commons.
57. Nelson, J. & Bugbee, B. Economic analysis of greenhouse lighting: light emitting diodes vs. high intensity discharge fixtures. *PLoS ONE*, **9**, e99010 (2014).
58. Design Lighting Consortium. *Horticultural lighting product search*. https://www.designlights.org/horticultural-lighting/search/ (2019).
59. Bugbee, B. Toward an optimal spectral quality for plant growth and development: the importance of radiation capture. *Acta Hortic.* **1134**, 1-12 (2016).
60. Pattison, M., Tsao J., Brainard, G. & Bugbee, B. LEDs for photons physiology and food. *Nature* **563**, 493-500 (2018).
61. Sager, J. C. & Giger Jr, W. Re-evaluation of published data on the relative photosynthetic efficiency of intermittent and continuous light. *Agric. Meteorol.* **22**, 289-302 (1980).

62. Tennessen, D. J., Bula, R. J. & Sharkey, T. D. Efficiency of photosynthesis in continuous and pulsed light emitting diode irradiation. *Photosynth. Res.* **44**, 261-269 (1995).
63. Song, S., Kusuma, P., Carvalho, S. D., Li, Y. & Folta, K. M. Manipulation of Seedling Traits with Pulsed Light in Closed Controlled Environments. *Environ. Exp. Bot.* **166**, 103803 (2019).
64. Johnson, J., Kusuma, P. & Bugbee, B. Efficacy of two HORTILED fixtures. *Controlled Environments*. Paper 11. https://digitalcommons.usu.edu/cpl_env/11 (2017).
65. Radetsky, L.C. LED and HID Horticultural Luminaire Testing Report. http://www.lrc.rpi.edu/programs/energy/pdf/HorticulturalLightingReport-Final.pdf (2018).

APPENDIX C

PHOTON EFFICACY IN HORTICULTURE: TURNING LED PACKAGES INTO LED LUMINAIRES[F]

[F] Kusuma, P., P.M. Pattison, and B. Bugbee. Published In: *Plant factory: basics, applications and advanced research*, Eds. T. Kozai, G. Niu & J. Masabni. Elsevier

C.1 Abstract

The final photon efficacy of an LED luminaire is determined by the inherent efficiency and photon wavelength of the LED package(s), multiplied by four losses associated with the design of the LED luminaire. Depending on the design of the LED luminaire and choice of operating conditions there can be additional LED package related losses of current droop and thermal droop; and there will be non-LED package losses related to power supply efficiency and optical efficiency. Here we describe the typical performance of a range of high-end LED packages with peak wavelengths across the photo-biologically active range of radiation (280 to 800 nm). We describe how current and thermal droops affect the efficiency of the LED luminaire. Finally, the performances of some state-of-the-art LED luminaires are described.

C.2 Introduction

The final photon efficacy[G] of an LED luminaire[H] is determined by the inherent efficiency and photon wavelength of the LED package(s)[I], multiplied by four losses associated with the design of the LED luminaire. Depending on the design of the LED luminaire and choice of operating conditions there can be additional LED package related losses of current droop and thermal droop; and there will be non-LED package losses related to power supply efficiency and optical efficiency. Here we describe the typical performance

[G] In this chapter, photon efficacy refers to µmol of *all* photons divided by joules of input energy (µmol J^{-1}). The term *photosynthetic* photon efficacy includes only photons with wavelengths between 400 to 700 nm.
[H] Here, the term LED luminaire refers to a "complete lighting unit" including LED packages mounted on a circuit board, power supplies, reflective surfaces, protective housing, electrical connections, and circuitry.
[I] An LED package refers to an LED chip/die within a housing, which provides a thermal path, enables electrical connections, and affects the angles of photon output. For white LED packages it also includes the phosphor.

of a range of high-end LED packages with peak wavelengths across the photo-biologically active range of radiation (280 to 800 nm). We describe how current and thermal droops affect the efficiency of the LED luminaire. Finally, the performances of some state-of-the-art LED luminaires are described.

Light-emitting diode (LED) technology is the most efficient lighting technology, with some LED luminaires now providing double the photon efficacy of the highest performing alternative technology, double-ended high-pressure sodium (DE-HPS) luminaires. LED luminaires can achieve a photosynthetic photon efficacy of over 3.4 compared to 1.7 µmol of photons per joule of input energy (µmol J^{-1})[J] for DE-HPS (DesignLights Consortium, 2021). But, these high photon efficacies are only possible under certain operating conditions and spectral combinations. Here we discuss the changes in efficiency/photon efficacy as LED packages are incorporated into LED luminaires. These include: 1) current droop, 2) thermal droop, 3) power supply efficiency, and 4) optical efficiency (Kusuma et al., 2020).

LED technology is rapidly evolving, with advancements driven by emerging applications for specific types of LEDs. LEDs can be categorized into three groups based on the typical/primary elemental composition of semiconductor materials: 1) GaN/AlGaN for LEDs with a peak wavelength between 220 and 360 nm, 2) InGaN for LEDs with a peak wavelength between 360 to 550 nm, and 3) AlInGaP for LEDs with a peak wavelength between 550 to 1000 nm. Improvements to InGaN LEDs have been enabled by

[J] The units for photon efficacy are µmol of photons per second divided by watts of input power. Because a watt is a joule per second, the seconds cancel in the numerator and the denominator resulting in µmol J^{-1}.

C.1 Typical LED Package Performance

Table C.1: Typical performance of select LED packages. Narrow bandwidth LED packages are described by their approximate peak wavelength and phosphor-converted (PC) white LED packages (bottom) are described by their correlated color temperature (CCT). Percent of theoretical maximum describes the efficiency of the LED packages. For the narrow bandwidth LED packages efficiency is the power output divided by the power input, while efficiency of the PC white LED packages is the product of the efficiency of the underlying 450 nm blue LED multiplied by the phosphor conversion efficiency. Both of these parameters must be 100% efficient for a PC white LED package to reach its theoretical maximum performance. The operating conditions to obtain the efficiencies (percent of theoretical maximum) and photon efficacies described here are a 25 ˚C junction temperature and a nominal drive current specified in the table. Choosing LED packages from the highest performance bin can increase the efficiency and photon efficacy values by 5 to 10%. Dividing the photon efficacy by the percent of theoretical maximum (as a fraction) provides the theoretical maximum efficacy for that LED package.

Wavelength (nm) or CCT (K)	nominal drive current (mA)	Photon efficacy (µmol J^{-1})	Percent of theoretical maximum
280	**100**	**0.08**	**3**
310	**20**	**0.03**	**1**
385	**500**	**0.9**	**28**
405	**500**	**1.6**	**48**
450	**350**	**2.8**	**74**
470	**350**	**2.4**	**62**
500	**350**	**2**	**50**
530	**350**	**1.3**	**30**
590	**350**	**1.1**	**21**
620	**350**	**3.4**	**64**
635	**350**	**2.5**	**47**
660	**700**	**4.1**	**74**
730	**350**	**3.6**	**59**
850	**1000**	**3**	**42**
3000	**65**	**2.8**	**74**
6500	**65**	**2.9**	**77**

advancements in material quality and device structures that have been driven by their large scale use in general illumination (Feezell and Nakamura, 2018; Tsao et al., 2015). Improvements in AlInGaP LEDs have historically been driven by signage, indicator, and automotive applications but are now being driven primarily by horticultural applications. Development of AlGanN based ultra-violet (UV) emitting LEDs has been driven by applications in sterilization and curing.

Table C.1 and Figure C-1 describe the efficiency and photon efficacy of commercially available LED packages with peaks from 280 to 850 nm (the data in Fig. 1 is normalized to one watt of electrical input). The data presented here and in subsequent figures were developed from data from the following companies: Nichia Corp. for the 280 nm LED package (Nichia, 2020); SeoulViosys Co. for the 310 nm LED package (SeoulViosys, 2020); Lumileds holding BV for the 385 and 405 nm LED packages (Lumileds, 2018), the 850 nm LED package (Lumileds, 2020), and the 3000 K and 6500 K LED packages (Lumileds, 2021); and OSRAM Opto Semiconductors GmbH for the 450 nm LED package (Osram, 2020c), 470 nm LED package (Osram, 2020b), 500 nm LEDpackage (Osram, 2020h), 530 nm LED package (Osram, 2020g), 590 nm LED package (Osram, 2020i), 620 nm LED package (Osram, 2020a), 635 nm LED package (Osram, 2020f), 660 nm LED package (Osram, 2020e), and 730 nm LED package (Osram, 2020d). The photon efficacy of all of these LED packages is reported at a junction temperature of 25 ˚C, and a nominal drive current specified in Table C.1. Values here differ from Kusuma et al. (2020) for three reasons: 1) these are reported at the nominal current densities for each type of LED package as opposed to 100 mA mm^{-2}, 2) these values represent typical performance rather than top bin performance, and 3) LEDs have continued to improve (this is most true of the 660 nm red

LED package). It is important to recognize that this is an evolving industry and improvements in efficiency will continue.

The LED package performances described here reflect both the fundamental LED material properties as well as commercial development focused on certain wavelengths. For example, green LEDs (with peak wavelengths between 500 to 600 nm) would be commercially viable, but LED material challenges in both the InGaN and AlInGaP LED materials systems limit the performance of green LEDs. Among LED scientists, this is referred to as the "green gap". An example of commercial impact is that, based on material properties, an LED at 635 nm should be more efficient than an LED at 620 nm (Table C.1), but the 620 nm LEDs are more important for general illumination, and thus developmental focus in 620 nm LEDs have led them to surpass 635 nm LEDs.

Figure C-1a shows the variation in the power flux (at 1 W electrical input) for direct emitting LED packages with different emission wavelengths and associated spectral bandwidths. Bandwidths are generally defined by the spectral width in nm at half of the maximum output, called the full width at half maximum (FWHM). Figure C-1 highlights the difference in efficiency for different wavelength LED packages, especially the green gap in LED performance. There are research examples that show it is possible for InGaN LEDs to provide emission across the visible spectrum, but for now, AlInGaP LEDs have a much better performance at emission wavelengths around the red portion of the spectrum (DOE BTO Lighting R&D Program, 2019).

Figure C-1b converts the power output in Figure C-1a into a photon output using Planck's equation, demonstrating the fact that LEDs with longer peak wavelengths have an advantage in that their photons have less energy. For example, although 450 nm blue and 660 nm red LED packages have similar efficiencies, the photon efficacy of 660 nm red is almost 50% higher than the 450 nm blue.

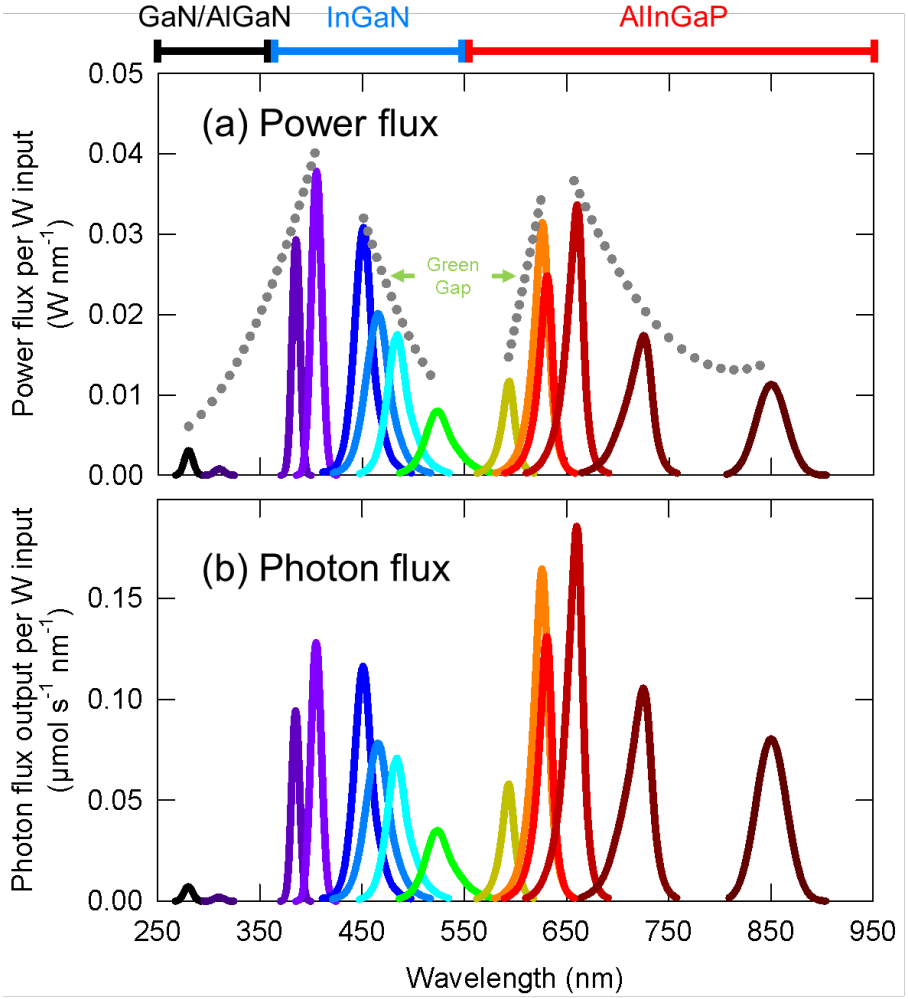

Figure C-1: Power flux and photon flux of 14 LED packages. (a) Power flux of 14 LED packages across the photo-biologically active region of radiation. These fluxes assume one watt of electrical input. (b) Data in (a) converted to a photon flux using Planck's equation.

C.4 Binning

Although the LED packages presented in Table C.1 and Figure C-1 are some of the highest performing products currently on the market, these values represent typical, and not maximum, performance of these products. LED package products are generally separated into bins based on the specific performance of that product. The performance characteristics that LED packages are binned by include photon output, forward voltage, and wavelength. The performance differences among individual LED packages are the result of the LED semiconductor crystal growth processes, which require very precise (high) temperature, pressure, and gas flow control in very clean chambers. Even with the best control there are variations in the semiconductor crystal properties that result in performance variations. The impact of binning is that LED packages from the same manufacturer can have a range of performance levels, so it is necessary for LED luminaire manufacturers to specify not just the color and the package type of the desired LED but also the specific performance bin. By choosing LED packages from a higher performance bin, the efficiencies and photon efficacies in Table C.1 may vary by 10% depending on the type of LED.

C.5 White LED Packages

There are two ways to generate white light with LEDs: phosphor-conversion (PC) and color-mixed (CM). PC white LEDs incorporate an optical down-conversion material (typically a phosphor) into an LED package with a blue (450 nm) LED. This material absorbs a portion of the blue photons and then re-emits them at longer wavelengths. The relative composition of blue light and the phosphor converted light can be engineered to achieve

different hues of white light. CM white LEDs are made up of a combination of the narrow-bandwidth LEDs described in Fig. C-1 and Table C.1. For example, combining 450, 530 and 620 nm LEDs would provide white light. The process of down-converting photons in a PC white LED introduces conversion efficiency losses. There are two typical phosphors used in generating white light from a blue LED, one with a broad emission that peaks at about 550 nm (green) and another with a peak emission at about 600 nm (red). The green phosphor is more efficient than the red phosphor, 88% compared to 81% photon efficiency at 150 ˚C and 1 W input (DOE BTO Lighting R&D Program, 2019). The photon efficiency of the phosphor material depends on the temperature and the photon intensity. The green and red phosphors have similar efficiencies at low drive currents.

The theoretical maximum photon efficacy of a PC white LED package is limited by its foundational 450 nm LED. Using Planck's equation, this theoretical maximum is equal to 3.76 μmol J^{-1}. This would require both the LED itself and the phosphor conversion (photons emitted / photons produced) to both be 100% efficient (the efficiency [percent of theoretical maximum] of the white LED packages in Table C.1 assume the product of these two efficiencies, rather than W_{out} / W_{in}). Because of this limitation, CM white LEDs have a higher potential photon efficacy than PC white LEDs, but for making white light the current green gap in the technology significantly limits CM white LEDs. Therefore, PC white LEDs dominate the market to provide broad spectrum white light. Additionally, the very high demand for PC white LEDs in human lighting has enabled price reductions and performance improvements that enable their effective use for horticulture.

C.6 LEDs for Horticulture

The lower photon efficacy of narrow bandwidth LED packages within the green gap, especially in comparison to PC white LED packages, limit their application in horticulture. But, green LED packages with peaks between 500 to 600 nm are a useful tool for research purposes. UV-A, UV-B and UV-C[K] LED packages may find a use in horticulture, as these wavelengths may have beneficial effects on crop quality, and can readily be incorporated into LED luminaires. However, UV LED packages with a peak below about 380 nm suffer from low efficiency, which can limit their practical effectiveness. Far-red LED packages (730 nm) have the potential to be a valuable addition to LED luminaires for their role in increasing leaf expansion, although caution should be taken as many species increase their stem length under far-red photons. Infrared LED packages (850 nm) are used in security cameras, which may be installed in plant factories with artificial lighting (PFALs). Photons at these long wavelengths have the potential to affect plant development, although effects are expected to be minimal.

The most commonly used LED packages in horticulture include PC white, 660 nm red, and 450 nm blue LED packages. Other LED packages including 730, 405, 385, 280, and 310 nm LED packages are being considered for incorporation into LED luminaires, but caution should be taken with their inclusion as many responses are intensity and species dependent.

[K] UV-C is most likely be used for germicidal or sterilization purposes.

C.7 Current Droop

The incorporation of LED packages into LED luminaires requires a number of operating and design considerations. Driving LED packages lower than the nominal drive current will increase the photon efficacy, while driving them higher than the nominal drive current will decrease it. This is known as current droop. This effect is a direct function of the current density (the current divided by the LED chip area), but the chip area is often not reported by LED package manufacturers. Figure C-2 normalizes the typical current droop as the fractional change in the drive current, with 1 being equal to the nominal drive current (note the differences in the nominal drive current between LED packages in Table C.1). Current droop is a result of a decrease in photon output per ampere input. At higher currents, LED packages also experience an increase in the forward voltage (related to electrical resistance within the LED device and package). This means there is both a relative decrease in the output and an increase in the input occur at higher current operation (electrical power, $W = V_f \cdot A$).

LED luminaire manufacturers often operate the LED packages at a low drive current in order to maximize photon efficacy with additional benefits of 1) reducing thermal management requirements and 2) extending the LED lifetime. The operating drive current for PC white LED packages in LED luminaires is often below 100 mA. However, increasing the drive current increases the output of the LED package. Therefore, a tradeoff exists between photon efficacy (along with thermal management and lifetime) and photon output. An LED luminaire with both high photon efficacy and high photon output requires the incorporation of many LED packages. Some luminaires contain more than 5,000 LED packages. This

means that although the photon output and the photon efficacy of the LED luminaire will both be high, the price of the LED luminaire will also be high. Because very low drive currents can cause excessively low photon outputs per LED package, the economics of the optimal drive current must be considered.

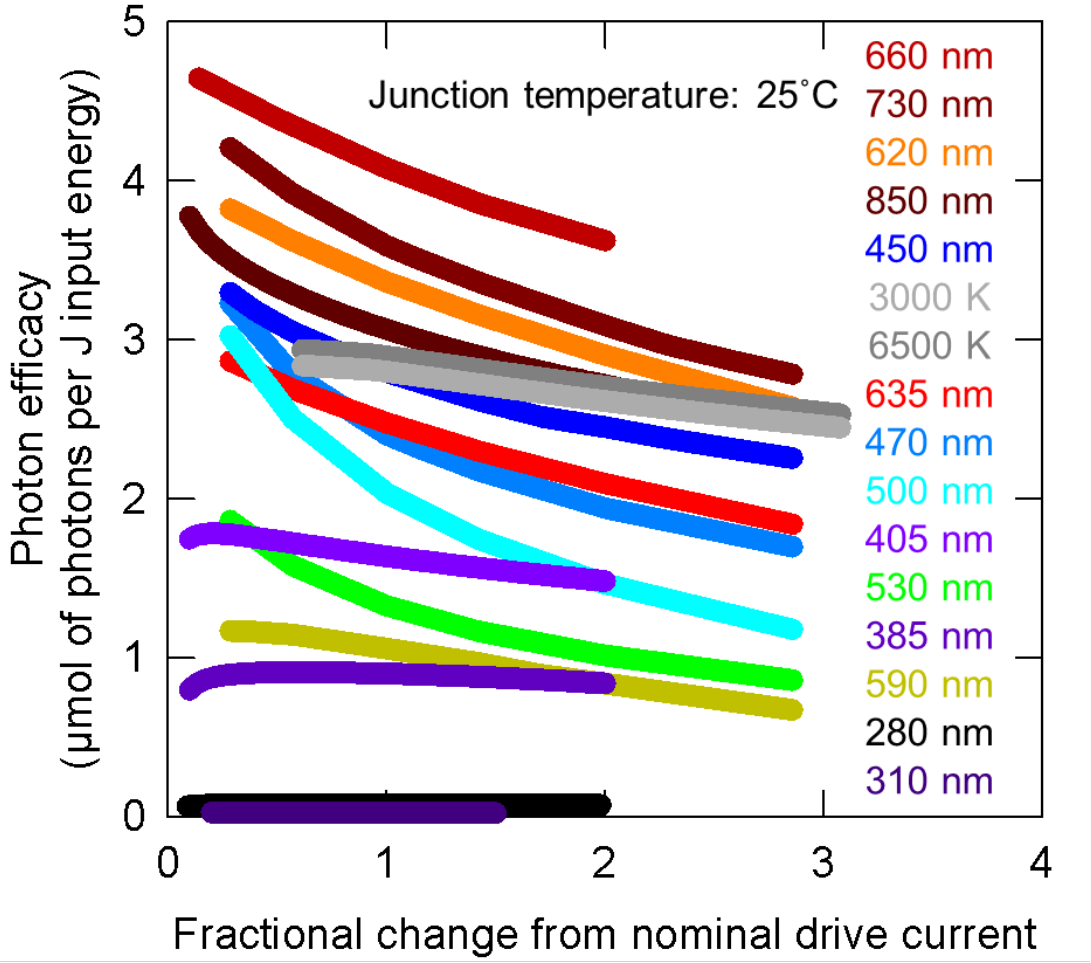

Figure C-2: Current droop of the 16 LED packages described in Table C.1. Current droop is plotted as a function of fractional change from the nominal drive current. This is because current droop is actually a function of current density and the die size of an LED package is often not reported. The junction temperature is specified at 25 ˚C and the type of each LED package is listed (roughly in order) on the right hand side of the figure.

Although a decrease in the drive current generally increases the photon efficacy, extremely low drive currents also cause a decrease in photon efficacy. At very low current, crystal defect and/or impurity related non-radiative recombination dominates, while at high drive currents, current droop dominates. With InGaN LEDs, Auger recombination causes droop. This can be thought of as the interaction of two excited charge carriers, which leads to an increase in the energy of one of the charge carriers, rather than the desired relaxation of the charge carrier. Relaxation of charge carriers is what causes the emission of a photon. For AlInGaP LEDs, droop is a result of charge carriers escaping from the LED active region and non-radiatively recombining elsewhere in the LED device structure. There is a range of drive currents between these two extremes (defects/impurity losses and droop losses) where luminaire manufacturers can operate the LED packages with optimal photon efficacy (and economics).

C.8 Thermal Droop

Efficiency losses in an LED package produce heat (100% efficiency minus LED package efficiency = unwanted heat). This leads to self-heating of the LED package and LED luminaire. LED packages decrease in photon efficacy when operated at high junction temperature, either due to self-heating or ambient conditions.

Junction temperature is the temperature at the LED *p-n* junction (also known as the active region). The LED junction temperature is measured at a defined temperature probe point with a known thermal resistance between that point and the junction, such that the junction temperature can be determined.

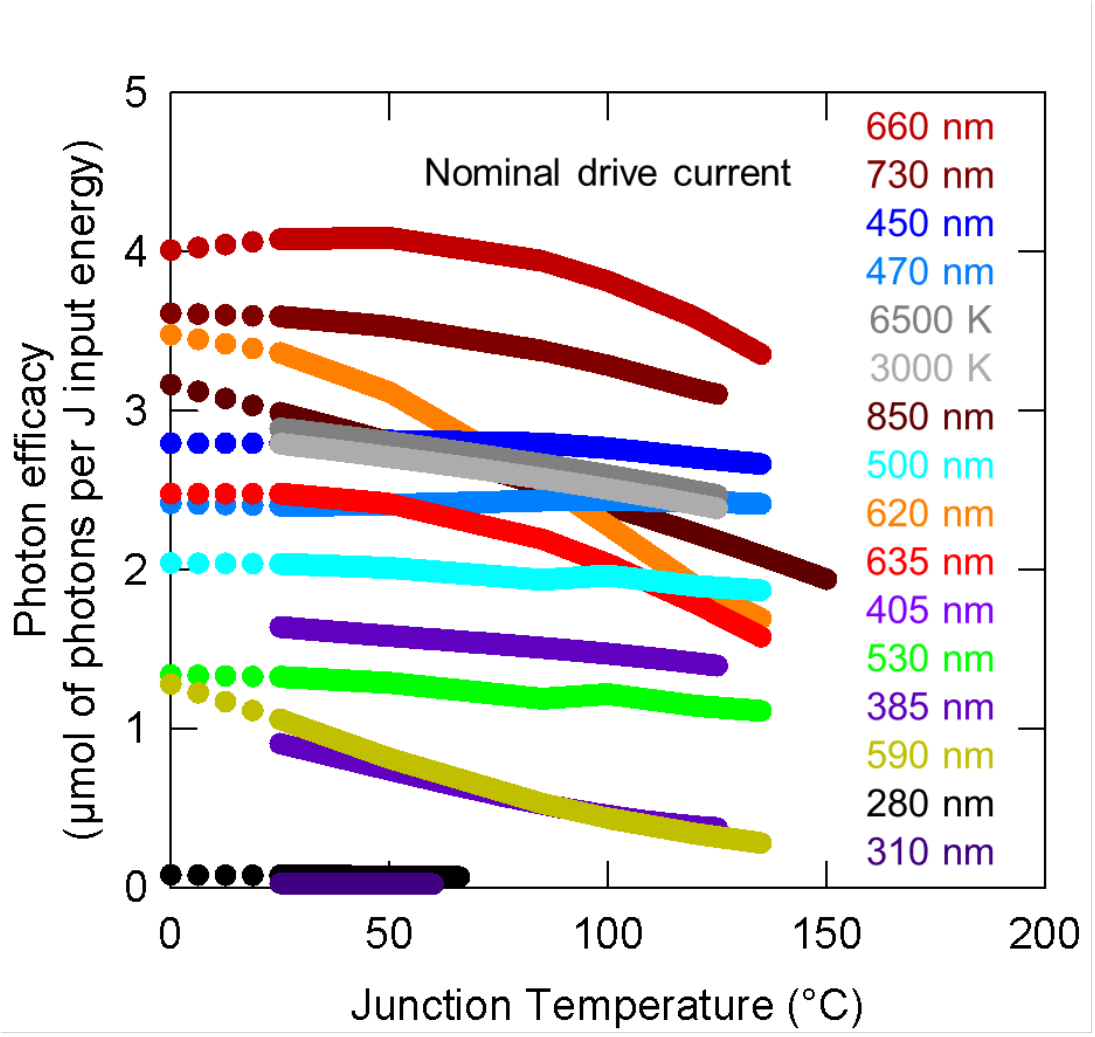

Figure C-3: Thermal droop of the 16 LED packages described in Table C.1. This data is specified at the nominal drive current described in Table C.1. Photon efficacy will continue to change as temperature decreases below 25 ˚C and data from LED package manufacturers has been specified down to -40 ˚C, but the junction temperature rarely drops to ambient temperature. A junction temperatures of -40 ˚C would require a high amount of energy input for cooling. Therefore, only a dotted line is shown for junction temperatures below 25 ˚C as these values are practically unrealistic.

The efficiencies and photon efficacies in Table C.1, Figure C-1, and Figure C.2 are specified for a junction temperature of 25 ˚C (with the exception of the 280 nm LED package, which is specified at an ambient temperature, the 310 nm LED package is specified at a solder joint temperature, and the 850 nm LED package is specified at a case

temperature). Typical LED packages, under typical operating conditions, will have junction temperatures between 55 and 100 ˚C. This is despite the fact that typical performance is often defined at 25 ˚C. As with current droop, this decrease in efficiency (and resulting photon efficacy) is caused by a decrease in photon output. Unlike increasing the current, increasing the temperature actually decreases the forward voltage - meaning a reduced input power, but the net effect is still that LED packages have reduced efficiency at higher temperatures.

Figure C-3 shows typical thermal droops from increasing junction temperature. It is apparent from this figure that AlInGaP based LEDs experience a greater degree of thermal droop compared to lnGaN and AlGaN based LEDs.

C.9 Power Supply Efficiency

LED luminaires require power supplies to convert AC to DC power. Most power supplies can achieve this power conversion with 80 to 95% efficiency. As with LED packages, higher performance power supplies are more expensive.

Power supplies can also provide dimming capabilities, either through current modulation or pulse width modulation, which is dimming achieved through pulsing the electrical power through the LED packages at a high frequency.

C.10 LED Luminaire Optical Efficiency

This efficiency describes the number of photons that are emitted from the LED luminaire divided by the number of photons produced by the LED packages. This efficiency can approach 100%. However, if a glass or plastic lens is used to engineer the optical

distribution (including making the light diffuse) or protect the LED packages then there can be optical losses due to reflection and absorption. The LED luminaire optical efficiency does not describe the percentage of emitted photons that reach and are absorbed by the plants. In some cases it may make sense to use lenses to more optimally distribute the light across the plant and improve yield, but this comes at the cost of optical losses that reduce the efficiency of the LED luminaire. This is another trade-off that horticultural lighting manufacturers and growers must consider. Optical performance and losses can occur through both refractive and reflective optical elements and these elements may degrade over time, especially in the greenhouse environment, which contributes to the depreciation of photon output.

C.11 LED Luminaire Photon Efficacy

Multiplying the LED package performance (photon efficacy) by the four efficiencies described above provides a final estimate of the LED luminaire photon efficacy.

$$\begin{matrix}\text{LED luminaire}\\ \text{photon efficacy}\end{matrix} = \begin{matrix}\text{LED package}\\ \text{photon efficacy}\end{matrix} \times \begin{matrix}\text{current}\\ \text{droop}\end{matrix} \times \begin{matrix}\text{thermal}\\ \text{droop}\end{matrix} \times \begin{matrix}\text{power supply}\\ \text{efficiency}\end{matrix} \times \begin{matrix}\text{optical}\\ \text{efficiency}\end{matrix}$$

Two example cases can be considered:

Case 1

An LED luminaire contains 90% 6500 K PC white LED packages and 10% 660 nm red LED packages (Table 7.1). The white LED packages are operated at the nominal drive current and the 660 nm LED packages are operated at about half of the nominal drive current (250 mA). It is assumed that under these conditions, both types of LED package will operate at a junction temperature of about 85 ˚C. The power supply for the while LED packages is

90% efficient and the power supply for the 660 nm red LED packages is 85% efficient. The LED packages are unprotected, achieving a high optical efficiency.

$$\text{White LEDs: } 2.9\frac{\mu\text{mol}}{\text{J}} \times 1.0 \times 0.92 \times 0.90 \times 0.99 = 2.4\frac{\mu\text{mol}}{\text{J}}$$

$$\text{Red LEDs: } 4.1\frac{\mu\text{mol}}{\text{J}} \times 1.07 \times 0.96 \times 0.85 \times 0.99 = 3.5\frac{\mu\text{mol}}{\text{J}}$$

One thing that is immediately obvious from this calculation is the fact that decreasing the drive current below the nominal provides an increase in photon efficacy rather than a decrease. The weighted average of the overall LED luminaire would be

$$\text{LED luminaire photon efficacy} = \left(0.9 \times 2.4\frac{\mu\text{mol}}{\text{J}}\right) + \left(0.1 \times 3.5\frac{\mu\text{mol}}{\text{J}}\right) = 2.5\frac{\mu\text{mol}}{\text{J}}$$

Case 2

An LED luminaire contains 90% 660 nm red LED packages and 10% 450 nm blue LED packages. Additionally, by choosing LED packages from a higher performance bin the performance can be assumed to be 5% better than indicated in Table 7.1. Both types of LED package are operated at about 100 mA. At this low drive current heating would be minimal and the junction temperature of the LED packages might be about 50 ˚C. The power supplies for both types of LED packages are 90% efficient and the LED packages are unprotected.

$$\text{Red LEDs: } 4.3\frac{\mu\text{mol}}{\text{J}} \times 1.14 \times 0.99 \times 0.90 \times 0.99 = 4.3\frac{\mu\text{mol}}{\text{J}}$$

$$\text{Blue LEDs: } 2.9\frac{\mu\text{mol}}{\text{J}} \times 1.15 \times 0.99 \times 0.90 \times 0.99 = 2.9\frac{\mu\text{mol}}{\text{J}}$$

The overall photon efficacy of the LED luminaire would be

$$\text{LED luminaire photon efficacy} = \left(0.9 \times 4.3\frac{\mu\text{mol}}{\text{J}}\right) + \left(0.1 \times 2.9\frac{\mu\text{mol}}{\text{J}}\right) = 4.2\ \frac{\mu\text{mol}}{\text{J}}$$

The first case represents typical operating conditions for an LED luminaire, while the second case represents a state-of-the-art LED luminaire – although even this theoretical LED luminaire could be further optimized. Table C.2 provides the measured photosynthetic photon efficacies of a variety of LED luminaires taken from the DesignLights Consortium (DLC) website (DesignLights Consortium, 2021; https://www.designlights.org/horticultural-lighting/search/). The DLC is a third-party testing organization that provides a list of products that qualify for rebates. One of the required qualifications is a photosynthetic photon efficacy of at least 1.9 μmol J^{-1}. Following the website link above, LED luminaires can be sorted by photosynthetic photon efficacy in ascending or descending order. The LED luminaires presented in Table C.2 may represent slightly higher photosynthetic photon efficacies than the average of that product, due to binning and self-selection. Additionally, the current average LED luminaire photosynthetic photon efficacy on the DLC website is about 2.5 μmol J^{-1}. It is apparent that the highest photosynthetic photon efficacy LED luminaires contain a high fraction of red photons, and that photon output (PPFD) does not appear to be correlated with photosynthetic photon efficacy.

Table C.2: Photosynthetic photon efficacies of a range of LED luminaires reported by the DesignLights Consortium. The types of LED packages used in the LED luminaire are described in the first column, although some of the LED luminaires with PC-W LED packages may also contain 450 nm blue LED packages. Ratios of blue (%B), green (%G), red (%R) and far-red (%FR) are all described as a percent of the PPFD and not total photon flux density. PC-W: Phosphor-converted white.

LED packages	PPFD	%B	%G	%R	%FR	Photosynthetic photon efficacy (μmol J^{-1})
PC-W	839	10	38	52	8	1.81
PC-W+660 nm	755	18	41	41	2	2.04
450 nm+660 nm+730 nm	700	26	0	74	9	2.06
PC-W+530 nm+660 nm+730 nm	1443	12	23	65	13	2.09
PC-W+660 nm	138	17	28	55	1	2.10
450 nm+660 nm+730 nm	1235	26	0	74	9	2.26
PC-W+660 nm	1969	18	45	37	2	2.30
PC-W+660 nm	766	17	30	53	1	2.35
PC-W	64	23	46	31	3	2.40
PC-W+660 nm	491	24	45	31	2	2.44
PC-W+660 nm	1593	19	41	40	2	2.49
450 nm+660 nm	498	17	0	83	0	2.55
PC-W+660 nm	1639	19	41	40	2	2.56
PC-W+660 nm+730 nm	1672	19	38	43	10	2.56
PC-W+660 nm	781	9	17	74	1	2.57
PC-W+660 nm	1727	22	41	37	2	2.67
PC-W+660 nm	277	27	70	73	0	2.72
450 nm+660 nm	1721	48	0	52	0	2.73
PC-W+660 nm	1681	8	9	83	1	2.77
PC-W+660 nm	1796	17	41	42	3	2.77
PC-W+660 nm	1805	12	23	65	1	2.88
PC-W+660 nm	506	11	5	84	1	2.90
450 nm+660 nm	1724	8	0	92	0	2.90
450 nm+660 nm	93	34	0	66	0	2.94
450 nm+660 nm	292	5	0	95	0	3.00
PC-W+660 nm	4971	16	26	58	1	3.18
PC-W+660 nm	1700	11	5	84	1	3.30
450 nm+660 nm	2196	5	0	95	0	3.40
450 nm+660 nm	2195	4	0	96	0	3.51
450 nm+660 nm	2311	4	0	96	0	3.69

One drawback of Table C.2 is that LED luminaires are classified by the photosynthetic photon efficacy (400 to 700 nm) rather than the total photon efficacy. This means that LED

luminaires that contain 730 nm far-red LED packages pay a penalty even though these photons are expected to have beneficial effects on the growth and development of many species (Zhen and Bugbee, 2020a, 2020b).

C.12 LED Luminaire Longevity

LED luminaires can operate well beyond 50,000 hours, which is longer than most other lighting technologies. LED packages rarely completely fail. They are highly reliable with a predictable degradation over time if the operating conditions (junction temperature and drive current) are known. When LED luminaires do fail, it is typically due to a failure in the power supply, electrical connections, or manufacturing defect (DOE BTO Lighting R&D Program, 2019).

Depreciation of LED packages within an LED luminaire is predicted from the depreciation of the LED packages over time under fixed conditions (junction temperature and drive current). The method of testing LED packages, called LM-80, is approved by the Illuminating Engineering Society (IES) (IESNA Testing Procedures Committee, 2008). LED package manufacturers perform these tests on their products and share the results with their customers (LED luminaire manufacturers). When the LED packages are engineered into an LED luminaire, the drive current is known, and the junction temperature can be measured. The depreciation of the LED packages within the LED luminaire can then be projected according to IES technical memo 21 (TM-21) (IESNA Testing Procedures Committee, 2011). This enables a consistent projection of photon maintenance among different LED luminaire manufacturers. However, TM-21 only allows for projection of up to six times the

LED package measurement duration under LM-80. For example, if an LED luminaire manufacturer claims a depreciation level for 60,000 hours then the LED packages must have been LM-80 tested for 10,000 hours.

LM-80 and TM-21 measure and project the depreciation of the LED packages. Other factors can increase the rate of depreciation of the LED luminaire. These factors include temperature extremes, humidity, chemical incursion (like sulfur which is a common fungicide), electrical surges (voltage and current), and depreciation of lenses or reflectors in the LED luminaire. For growers, photon output depreciation directly results in reduced plant growth, so it is important to predict depreciation and plan for lighting updates even if LED luminaires are still operational. Output depreciation is not unique to LED lighting technology, as all lighting technologies depreciate, but unlike LED luminaires the lamps typically fail before the depreciation is a major issue.

While LED packages generally degrade over time, LED luminaires can also catastrophically fail, meaning they stop emitting photons partially or entirely. This is generally due to failures in electrical connections or the power supply. A partial failure could occur when one circuit of LED packages loses its electrical connection, while the remaining circuits are still operational. Power supplies are also sensitive to environmental conditions such as temperature, humidity, chemical incursion, and electrical surges. The wide range of circuit types, operating conditions, and power quality (minimal surges) make the lifetime of a power supply less predictable than the LED packages. Quality of manufacturing and component selection plays a large role in power supply reliability. LED luminaire manufacturers can select power supplies that have been tested under wet and hot operating

conditions, under thermal cycling to check robustness of solder joints, and/or under vibration tests to check component integrity.

Ultimately, a conservative and practical estimate of the lifetime of a LED luminaire is the duration of the manufacturer warranty. Growers ought to inquire after the LM-80 data and TM-21 analysis for the LED luminaires. They should ask for failure rates and reliability testing, as well as documentation regarding the power supplies that are used. Lighting is a critical component for indoor plant growth and LED luminaire failures can have significant impacts on production. As such, LED luminaire purchasing decisions, including reliability, are paramount.

C.13 Continued Improvement

LED technology has rapidly advanced in the past decade, and the most common LED packages for horticulture use (PC white, 450 nm blue, 660 nm red, and 730 nm far-red). These LED packages are approaching their theoretical maximum performance. Advancements will continue, but will slow for these most advanced LED packages.

Closing the green gap would increase photon efficacy, especially for human lighting. The theoretical maximum photon efficacy of PC white LED packages is dependent on the higher energy 450 nm blue LEDs. Although green photons are photosynthetic (McCree, 1971), they are not required for plant growth. These LED packages are included in LED luminaires because 1) PC white LED packages are inexpensive and 2) green photons aid in human perception of plant color. As 530 nm green and 590 nm yellow LED packages improve these can replace PC white LED packages to achieve this human-centric goal.

The theoretical maximum photosynthetic photon efficacy is 5.85 μmol J^{-1} for photons concentrated at 700 nm, but this is not a practical maximum. A plant grown under only 700 nm photons would likely be subject to developmental problems. Several studies have shown that some plants require at least some blue photons for *normal* plant growth (Yorio et al., 2001; Hernandez and Kubota, 2016), although other studies have shown some plants can be grown under pure red (Son and Oh, 2013; Meng et al., 2020). Determining which species can grow normally under pure red may help maximize the theoretical potential in horticulture. Finally, recent studies have provided compelling evidence that the spectral range for photosynthesis should be extended to 750 nm (Zhen and Bugbee, 2020a, 2020b). This would allow the use of highly efficient far-red LED packages in selected horticulture applications.

C.14 Literature Cited

DesignLights Consortium, 2021. Horticultural Lighting. <https://www.designlights.org/horticultural-lighting/search/> (accessed 9 February 2021).

DOE BTO Lighting R&D Program, 2019. 2019 Lighting R&D Opportunities. <https://www.energy.gov/sites/prod/files/2020/01/f70/ssl-rd-opportunities2-jan2020.pdf> (accessed 9 February 2021).

Feezell, D., Nakamura, S., 2018. Invention, development, and status of the blue light-emitting diode, the enabler of solid-state lighting. Comptes Rendus Physique 19(3), 113–133.

Hernández, R., Kubota, C., 2016. Physiological responses of cucumber seedlings under different blue and red photon flux ratios using LEDs. Environmental and Experimental Botany 121, 66–74.

IESNA Testing Procedures Committee, 2008. LM-80-08: Measuring Lumen Maintenance of LED Light Sources. Illuminating Engineering Society.

IESNA Testing Procedures Committee, 2011. TM-21-11: Projecting Long Term Maintenance of LED LightSources. Illuminating Engineering Society.

Kusuma, P., Pattison, P.M., Bugbee, B., 2020. From physics to fixtures to food: current and potential LED efficacy. Horticulture research 7(1), 1–9.

Lumileds, 2018. DS185 LUXEON UV FC Line Product Datasheet.

<https://www.lumileds.com/wp-content/uploads/files/DS185.pdf> (accessed 9 February 2021).
Lumileds, 2020. DS191 LUXEON IR Domed Line Product Datasheet. <https://www.lumileds.com/wp-content/uploads/files/DS191-luxeon-ir-domed-line-datasheet-1.pdf> (accessed 9 February 2021).
Lumileds, 2021. DS267 LUXEON 3030 HE Product Datasheet. <https://www.lumileds.com/wp-content/uploads/DS267-LUXEON-3030-HE-datasheet.pdf> (accessed 9 February 2021).
McCree, K.J., 1971. The action spectrum, absorptance and quantum yield of photosynthesis in crop plants. Agricultural Meteorology 9, 191–216.
Meng, Q., Boldt, J., Runkle, E.S., 2020. Blue radiation interacts with green radiation to influence growth and predominantly controls quality attributes of lettuce. Journal of the American Society for Horticultural Science 145(2), 75–87.
Nichia, 2020. PART NO. NCSU434A(T) Datasheet. <https://www.nichia.co.jp/specification/products/led/NCSU434A-E.pdf> (accessed 9 February 2021).
Osram, 2020a. GA CSSPM1.23 Datasheet. <https://www.osram.com/ecat/OSLON%C2%AE%20SSL%20120%20GA%20CSSPM1.23/com/en/class_pim_web_catalog_103489/prd_pim_device_2402546/> (accessed 9 February 2021).
Osram, 2020b. GB CSHPM1.13 Datasheet. <https://www.osram.com/ecat/OSLON%C2%AE%20SSL%20150%20GB%20CSHPM1.13/com/en/class_pim_web_catalog_103489/prd_pim_device_2402541/> (accessed 9 February 2021).
Osram, 2020c. GD CSSPM1.14 Datasheet. <https://www.osram.com/ecat/OSLON%C2%AE%20SSL%20120%20GD%20CSSPM1.14/com/en/class_pim_web_catalog_103489/prd_pim_device_2402548/> (accessed 9 February 2021).
Osram, 2020d. GF CSSPM1.24 Datasheet. <https://www.osram.com/ecat/OSLON%C2%AE%20SSL%20120%20GF%20CSSPM1.24/com/en/class_pim_web_catalog_103489/prd_pim_device_2402545/> (accessed 9 February 2021).
Osram, 2020e. GH CSSRM4.24 Datasheet. <https://www.osram.com/ecat/OSLON%C2%AE%20Square%20GH%20CSSRM4.24/com/en/class_pim_web_catalog_103489/prd_pim_device_10285510/> (accessed 9 February 2021).
Osram, 2020f. GR QSSPA1.23 Datasheet. <https://www.osram.com/ecat/OSCONIQ%C2%AE%20P%203030%20GR%20QSSPA1.23/com/en/class_pim_web_catalog_103489/prd_pim_device_8882698/> (accessed 9 February 2021).
Osram, 2020g. GT CSSPM1.13 Datasheet. <https://www.osram.com/ecat/OSLON%C2%AE%20SSL%20120%20GT%20CSSPM1.13/com/en/class_pim_web_catalog_103489/prd_pim_device_2402547/> (accessed 9 February 2021).
Osram, 2020h. GV QSSPA1.13 Datasheet.

<https://www.osram.com/ecat/OSCONIQ%C2%AE%20P%203030%20GV%20QSSPA1.13/com/en/class_ppi_web_catalog_103489/prd_pim_device_8931522/> (accessed 9 February 2021).

Osram, 2020i. GY CSHPM1.23 Datasheet. <https://www.osram.com/ecat/OSLON%C2%AE%20SSL%20150%20GY%20CSHPM1.23/com/en/class_pim_web_catalog_103489/prd_pim_device_2402540/> (accessed 9 February 2021).

SeoulVioSys, 2020. UV CA3535 series Datasheet. <http://www.seoulviosys.com/en/product/PKG/?sub=13&seq=1> (accessed 9 February 2021).

Son, K.H., Oh, M.M., 2013. Leaf shape, growth, and antioxidant phenolic compounds of two lettuce cultivars grown under various combinations of blue and red light-emitting diodes. HortScience, 48(8) 988–995.

Tsao, J.Y., Han, J., Haitz, R.H., Pattison, P.M., 2015. The Blue LED Nobel Prize: Historical context, current scientific understanding, human benefit. Annalen der Physik (Leipzig), 527(SAND-2015-4440J).

Yorio, N.C., Goins, G.D., Kagie, H.R., Wheeler, R.M., Sager, J.C., 2001. Improving spinach, radish, and lettuce growth under red light-emitting diodes (LEDs) with blue light supplementation. HortScience 36(2), 380–383.

Zhen, S., Bugbee, B., 2020a. Substituting far-red for traditionally defined photosynthetic photons results in equal canopy quantum yield for CO2 fixation and increased photon capture during long-term studies: Implications for re-defining PAR. Frontiers in Plant Science 11, 1433.

Zhen, S., Bugbee, B., 2020b. Far-red photons have equivalent efficiency to traditional photosynthetic photons: Implications for redefining photosynthetically active radiation. Plant, cell & environment 43(5), 1259–1272.

APPENDIX D

SUMMARY OF BLUE AND GREEN EFFECTS ON LETTUCE, CUCUMBER AND TOMATO

Table D.1: Response of lettuce, cucumber and tomato growth (dry mass) and development (leaf area, stem length and petiole length) to blue photons (B). This analysis only includes the effects of increasing the fraction of blue between 5 and 75% blue, meaning that all treatments contain some red (600 to 699 nm) and blue photons. The complete absence of either red or blue photons often induces abnormal growth and development (Hernandez and Kubota, 2016; Snowden et al., 2016), likely caused by under-activation of the photoreceptors cryptochromes and phytochromes (Kong et al., 2019). In the Days column the number in bold is the number of days in the treatment, and the other number is the number of days between emergence/planting and moving the plants into the treatments.

Blue Effects											
Species	Cultivar	Range of treatments	PPFD (μmol m^{-2} s^{-1})	Photo-period (h)	Parameter	Effect	Citation	Comment	CO_2 (ppm)	Temp	Days
Lettuce	Waldmann's Green	8 and 16%	300	18	Dry Mass	NS	Yorio et al. 2001		1200	23	**21**
	Grand Rapids	6 to 26%	200 & 500	16	Leaf Area Dry Mass	NS ↑	Dougher & Bugbee 2001		1000	26/22	4+**18**
	Red Fire	10 and 26%	300	12	Leaf Area Dry Mass	↓ ↓	Ohashi-Kaneko et al. 2007		400	20/18	**37**
	Red Cross	16, 23 and 55%	300	16	Dry Mass	NS	Li & Kubota 2009		-	25/20	10+**12**
	Sunmang Grand Rapid TBR	13 to 59%	171	12	Leaf Area Dry Mass Leaf Area Dry Mass	↓ ↓ ↓ ↓	Son & Oh 2013	Grand Rapids lettuce at 47% blue did not fit the trend	400	20	18+**28**
	Waldmann's Green	11 to 28%	200 500	16	Leaf Area Dry Mass Leaf Area Dry Mass	- NS ↓ NS	Cope et al. 2014	Results for leaf area at 200 μmol m^{-2} s^{-1} are difficult to interpret	430	24.5	**21**
	Red Fire	15, 19 and 25%	100 200 300	16	Leaf Area Dry Mass Leaf Area Dry Mass Leaf Area Dry Mass	↓ NS NS - ↑ ↑	Furuyama et al. 2013	At 200 μmol m^{-2} s^{-1} the highest dry mass occurred in the middle treatment (19% B)	1000	23/20	4+11+**14**
	Jeokchima	10, 20 and 30%	230	16	Leaf Area Dry Mass	↓ NS	Lee et al. 2014	Decrease in leaf area only occurs between 20 and 30% B	800	22/18	**28**
	Ostinata	12 to 36%	150	16	Dry Mass	-	Kong et al. 2015	Results are difficult to interpret. No apparent trend	1200	25/18	**39**
	Sunmang Grand Rapid TBR	13 to 34%	173	12	Leaf Area Dry Mass Leaf Area Dry Mass	↓ ↓ ↓ ↓	Son & Oh 2015		400	20	18+**28**
	Green Oak Leaf	23, 30 and 45%	135	16	Dry Mass	-	Chen et al. 2016	Results are difficult to interpret. No apparent trend	350	22/18	**35**
	unspecified	8 to 50%	200	16	Leaf Area Dry Mass	↓ ↓	Wang et al. 2016		400	24/20	**30**
	Sunmang	8 to 31%	173	12	Leaf Area Dry Mass	↓ ↓	Son et al. 2016	Results are difficult to interpret. Appears to trend downward	400	20	18+**28**

Table D.1: continued

Species	Cultivar	Range of treatments	PPFD (µmol m^{-2} s^{-1})	Photo-period (h)	Parameter	Effect	Citation	Comment	CO_2 (ppm)	Temp	Days
Lettuce	Waldmann's Green	11 to 28%	200	16	Leaf Area	NS	Snowden et al. 2016		430	-	**21**
					Dry Mass	NS					
			500		Leaf Area	NS					
					Dry Mass	NS					
	Green Skirt	10 to 30%	150	16	Plant diameter	↓	Kang et al. 2016		1000	22/17	14+**28**
	Frill ice	20.7, 21.4 and 26.2%	200	14	Dry Mass	-	Yan et al. 2019b	At 200 µmol m^{-2} s^{-1} in 14 h, the highest dry mass occurred in the middle treatment (21.4% B)	800	22/18	20+ **20**
				16		NS					
			250	14		NS					
				16		NS					
	Rouxai	7 to 33%	180	20	Plant diameter	↓	Meng et al. 2019		379 to 402	20	**30**
					Fresh/Dry Mass	↓					
	Rex				Plant diameter	↓					
					Fresh/Dry Mass	↓					
	Rex	17 and 50%	180	24	Dry Mass	↓	Meng & Runkle 2019	Not including FR treatments	-	23	3 + **12**
	Cherokee				Dry Mass	↓					
	Ziwei	14 to 27%	100	14	Dry Mass	NS	Yan et al. 2019a	At 150, 200 and 250 µmol m^{-2} s^{-1}, treatments had significant differences, but the pattern is not always consistent.	800	22	20+ **20**
			150			-					
			200			-					
			250			-					
			300			↓					
	Rouxai	7 to 55%	180	20	Plant diameter	↓	Meng et al. 2020		410	22	**30/33**
					Dry Mass	↓					
	Green Oak Leaf	20 and 50%	200	18	Dry Mass	NS	Spalholz et al. 2020	A higher 80% B showed significant differences in Red Oak Leaf	704	20	**42**
	Red Oak Leaf				Dry Mass	NS					
	Tiberius	10, 25 and 28% B	210	16	Leaf Area	NS	Zou et al. 2020	The highest dry mass and leaf area occurred in the middle treatment	-(400)	23/21	**15**
					Dry Mass	NS					
Cucumber	Cumlaude	10 to 75%	100	18	Leaf Area	↓	Hernandez & Kubota 2016		512	24.5	**17**
					Dry Mass	↓					
					Stem Length	↓					
	Sweet Slice	11 to 28%	200	16	Leaf Area	NS	Snowden et al. 2016		430	-	**21**
					Dry Mass	NS					
					Stem Length	NS					
					Petiole Length	↓					
			500		Leaf Area	↓					
					Dry Mass	↓					
					Stem Length	↓					
					Petiole Length	↓					
	Zhongnong 26	14 to 27% B	200	12	Leaf Area	↓	Song et al. 2017	Results are difficult to interpret. Lowest dry mass and height were in intermediate treatments. Tallest plants occurred at the highest percent blue	500	25	**15**
					Dry Mass	-					
					Stem Length	- (↑)					
	Zhongnong 16	10, 25 and 28% B	230	16	Leaf Area	↓	Zou et al. 2020		-(400)	23/21	**15**
					Dry Mass	↓					
					Stem Length	↓					

Table D.1: continued

Species	Cultivar	Range of treatments	PPFD ($\mu mol\ m^{-2}\ s^{-1}$)	Photo-period (h)	Parameter	Effect	Citation	Comment	CO_2 (ppm)	Temp	Days
Tomato	Komeett	0, 4 and 16% B (supple-mental)	56 + GH	18	Leaf Area Dry Mass Stem Length	NS NS NS	Hernandez & Kubota 2012	Supplemental in GH	512	24.5	7+**11**
	Early Girl	25 and 50%	160	18	Leaf Area Dry Mass Stem Length	↓ NS NS	Wollaeger & Runkle 2014		-	20	**31/32**
	Early Girl	6 to 50%	160	18	Leaf Area Dry Mass Stem Length	NS NS ↓	Wollaeger & Runkle 2015		-	20	**31 to 33**
	Early girl	11 to 28%	200	16	Leaf Area Dry Mass Stem Length Petiole Length	↓ ↓ ↓ NS	Snowden et al. 2016		430	-	**21**
			500		Leaf Area Dry Mass Stem Length Petiole Length	↓ ↓ ↓ ↓					
	Komeett	10 to 75%	100	18	Leaf Area Dry Mass Stem Length	NS NS ↓	Hernandez et al. 2016		509	25	**21**
	Qianxi	25 to 75%	300	12	Leaf Area Dry Mass	- -	Liu et al. 2018	Significant differences, but no apparent trends	- (400)	28/18	**30**

Table D.2: Effect of green photons (G) on growth and development of lettuce, cucumber and tomato. The studies included in this summary generally maintained a constant fraction of blue photons (B), while increasing the fraction of green photons (by simultaneously decreasing the fraction of red photons). In the Days column the number in bold is the number of days in the treatment, and the other number is the number of days between emergence/planting and moving the plants into the treatments.

Green Effects											
Species	Cultivar	Range of treatments	PPFD ($\mu mol\ m^{-2}\ s^{-1}$)	Photo-period (h)	Parameter	Effect	Citation	Comment	CO_2 (ppm)	Temp	Days
Lettuce	Waldmann's Green	16% B with or without 24% G	150	18	Leaf Area Dry Mass	↑ ↑	Kim et al. 2004		1200	21	**28**
	Red Cross	31, 52 and 70% G	300	16	Dry Mass	NS	Li & Kubota 2009		-	25/20	10+**12**
	Ostinata	27% B with 23, 40 or 51% G	150	16	Dry Mass	↑	Kong et al. 2015		1200	25/18	**39**

Table D.2: continued

Species	Cultivar	Range of treatments	PPFD (μmol m^{-2} s^{-1})	Photo-period (h)	Parameter	Effect	Citation	Comment	CO_2 (ppm)	Temp	Days
Lettuce	Sunmang	14% B with or without 8% G	173	12	Leaf Area	NS	Son & Oh 2015		400	20	18+**28**
					Dry Mass	NS					
		24% B with or without 8% G			Leaf Area	NS					
					Dry Mass	↑					
	Grand Rapid TBR	14% B with or without 8% G			Leaf Area	NS					
					Dry Mass	NS					
		24% B with or without 8% G			Leaf Area	NS					
					Dry Mass	NS					
	Green Oak Leaf	23% B with 30 or 53% G	135	16	Dry Mass	NS/↓	Chen et al. 2016	NS compared to high yellow, ↓compared to high red	350	22/18	**35**
	Sunmang	About 20% B with 7 or 13% G	173	12	Leaf Area	↑	Son et al. 2016	Two 7% G treatments. NS compared to one, ↑ compared to other	400	20	18+**28**
					Dry Mass	NS/↑					
	Waldmann's Green	1.7 to 41% G in a background of 11 to 14% B	200	16	Leaf Area	↓	Snowden et al. 2016		430		**21**
					Dry Mass	NS					
			500		Leaf Area	NS					
					Dry Mass	NS					
	Green Skirt	10% G in a 10, 20 or 30% B background	150	16	Plant diameter	NS	Kang et al. 2016		1000	22/17	14+**28**
	Frill ice	21% B with 34 or 41% G	200	14	Dry Mass	↑	Yan et al. 2019b		800	22/18	20+**20**
				16		NS					
			250	14		NS					
				16		NS					
	Ziwei	18.5% B with 32 or 45% G	100	14	Dry Mass	NS	Yan et al. 2019a		800	22	20+**20**
			150			NS					
			200			↓					
			250			↓					
			300			↓					
	Rouxai	12% B with or without 32% G	180	20	Plant diameter	NS	Meng et al. 2020		410	22	**30/33**
					Dry Mass	NS					
		34% B with or without 33% G			Plant diameter	↓					
					Dry Mass	↓					
		55% B with or without 32% G			Plant diameter	NS					
					Dry Mass	↓					
	Tiberius	15% B with 0 or 25% G	150	16	Leaf Area	↑	Li et al. 2020		1000	24/20	**21**
					Dry Mass	NS					
	Tiberius	27% B with 35 or 45% G	210	16	Leaf Area	↓	Zou et al. 2020		-(400)	23/21	**15**
					Dry Mass	↓					

Table D.2: continued

Species	Cultivar	Range of treatments	PPFD (µmol m^{-2} s^{-1})	Photo-period (h)	Parameter	Effect	Citation	Comment	CO_2 (ppm)	Temp	Days
Cucumber	Cumlaude	28% G at 20%B	100	18	Leaf Area	NS	Hernandez & Kubota 2016	No departure from the trend set by B effects	512	24.5	**17**
					Dry Mass	NS					
					Stem Length	NS					
	Sweet Slice	13% B with 2 to 41% G	200	16	Leaf Area	NS	Snowden et al. 2016		430	-	**21**
					Dry Mass	NS					
					Stem Length	NS					
					Petiole Length	NS					
			500		Leaf Area	↑					
					Dry Mass	NS					
					Stem Length	NS					
					Petiole Length	NS					
	Zhongnong 26	20% B with 1 to 44% G	200	12	Leaf Area	NS	Song et al. 2017		500	25	**15**
					Dry Mass	↓					
					Stem Length	NS					
	Zhongnong 16	27% B with 35 or 45% G	230	16	Leaf Area	↓	Zou et al. 2020		-(400)	23/21	**15**
					Dry Mass	↓					
					Stem Length	↓					
Tomato	Early Girl	0 and 25% G as B decreases from 50 to	160	18	Leaf Area	NS	Wollaeger & Runkle 2014		-	20	**31/32**
					Dry Mass	NS					
					Stem Length	NS					
	Early girl	1.7 to 41% G in a background of 11 to 14% B	200	16	Leaf Area	NS	Snowden et al. 2016		430	-	**21**
					Dry Mass	NS					
					Stem Length	NS					
					Petiole Length	NS					
			500		Leaf Area	NS					
					Dry Mass	NS					
					Stem Length	↑					
					Petiole Length	NS					
	Komeett	28% G at 20% B	100	18	Leaf Area	NS	Hernandez et al. 2016	No departure from the trend set by B	509	25	**21**
					Dry Mass	NS					
					Stem Length	NS					

D.1 Literature Cited

Chen, X.L.; Xue, X.Z.; Guo, W.Z.; Wang, L.C.; Qiao, X.J. Growth and nutritional properties of lettuce affected by mixed irradiation of white and supplemental light provided by light-emitting diode. Sci. Hortic. 2016, 200, 111–118, doi:10.1016/j.scienta.2016.01.007.

Cope, K.R.; Snowden, M.C.; Bugbee, B. Photobiological interactions of blue light and photosynthetic photon flux: Effects of monochromatic and broad-spectrum light sources. Photochem. Photobiol. 2014, 90, 574–584, doi:10.1111/php.12233.

Dougher, T.A.; Bugbee, B. Differences in the response of wheat, soybean and lettuce to

reduced blue radiation. Photochem. Photobiol. 2001, 73, 199–207, doi:10.1562/0031-8655(2001)0730199DITROW2.0.CO2.

Furuyama, S.; Ishigami, Y.; Hikosaka, S.; Goto, E. Effects of blue/red ratio and light intensity on photomorphogenesis and photosynthesis of red leaf lettuce. Acta Hortic. 2013, 1037, 317–322, doi:10.17660/ActaHortic.2014.1037.38.

Hernández, R.; Kubota, C. Tomato seedling growth and morphological responses to supplemental LED lighting red: Blue ratios under varied daily solar light integrals. Acta Hortic. 2012, 956, 187–194, doi: 10.17660/ActaHortic.2012.956.19.

Hernández, R.; Eguchi, T.; Deveci, M.; Kubota, C. Tomato seedling physiological responses under different percentages of blue and red photon flux ratios using LEDs and cool white fluorescent lamps. Sci. Hortic. 2016, 213, 270–280, doi:10.1016/j.scienta.2016.11.005.

Hernández, R.; Kubota, C. Physiological responses of cucumber seedlings under different blue and red photon flux ratios using LEDs. Environ. Exp. Bot. 2016, 121, 66–74, doi:10.1016/j.envexpbot.2015.04.001.

Kang, W.H.; Park, J.S.; Park, K.S.; Son, J.E. Leaf photosynthetic rate, growth, and morphology of lettuce under different fractions of red, blue, and green light from light-emitting diodes (LEDs). Hortic. Environ. Biotechnol. 2016, 57, 573–579, doi:10.1007/s13580-016-0093-x.

Kim, H.H.; Goins, G.D.; Wheeler, R.M.; Sager, J.C. Green-light supplementation for enhanced lettuce growth under red-and blue-light-emitting diodes. HortScience 2004, 39, 1617–1622, doi:10.21273/HORTSCI.39.7.1617.

Kong, S.W.; Chung, H.Y.; Chang, M.Y.; Fang, W. The contribution of different spectral sections to increase fresh weight of boston lettuce. HortScience 2015, 50, 1006–1010, doi:10.21273/HORTSCI.50.7.1006.

Kong, Y.; Schiestel, K.; Zheng, Y. Maximum elongation growth promoted as a shade-avoidance response by blue light is related to deactivated phytochrome: A comparison with red light in four microgreen species. Canad. J. Plant Sci. 2019, 100, 314–326, doi:10.1139/cjps-2019-0082.

Lee, J.S.; Lim, T.G.; Yong, H.K. Growth and phytochemicals in lettuce as affected by different ratios of blue to red LED radiation. Acta Hortic. 2014, 1037, 843–848, doi:10.17660/ActaHortic.2014.1037.112.

Li, Q.; Kubota, C. Effects of supplemental light quality on growth and phytochemicals of baby leaf lettuce. Environ. Exp. Bot. 2009, 67, 59–64, doi:10.1016/j.envexpbot.2009.06.011.

Li, L.; Tong, Y.X.; Lu, J.L.; Li, Y.M.; Yang, Q.C. Lettuce Growth, Nutritional Quality, and Energy Use Efficiency as Affected by Red–Blue Light Combined with Different Monochromatic Wavelengths. HortScience, 55, 613–620. doi: 10.21273/HORTSCI14671-19

Liu, X.Y.; Jiao, X.L.; Chang, T.T.; Guo, S.R.; Xu, Z.G. Photosynthesis and leaf development of cherry tomato seedlings under different LED-based blue and red photon flux ratios. Photosynthetica 2018, 56, 1212–1217, doi:10.1007/s11099-018-0814-8.

Meng, Q.; Kelly, N.; Runkle, E.S. Substituting green or far-red radiation for blue

radiation induces shade avoidance and promotes growth in lettuce and kale. Environ. Exp. Bot. 2019, 162, 383–391, doi:10.1016/j.envexpbot.2019.03.016.
Meng, Q.; Runkle, E.S. Far-red radiation interacts with relative and absolute blue and red photon flux densities to regulate growth, morphology, and pigmentation of lettuce and basil seedlings. Sci. Hortic. 2019, 255, 269–280, doi:10.1016/j.scienta.2019.05.030.
Meng, Q.; Boldt, J.; Runkle, E.S. Blue radiation interacts with green radiation to influence growth and predominantly controls quality attributes of lettuce. J. Am. Soc. Hortic. Sci. 2020, 145, 75–87, doi:10.21273/JASHS04759-19.
Ohashi-Kaneko, K.; Takase, M.; Kon, N.; Fujiwara, K.; Kurata, K. Effect of light quality on growth and vegetable quality in leaf lettuce, spinach and komatsuna. Environ. Control Biol. 2007, 45, 189–198, doi:10.2525/ecb.45.189.
Snowden, M.C.; Cope, K.R.; Bugbee, B. Sensitivity of seven diverse species to blue and green light: Interactions with photon flux. PLoS ONE 2016, 11, e0163121, doi:10.1371/journal.pone.0163121.
Son, K.H.; Oh, M.M. Leaf shape, growth, and antioxidant phenolic compounds of two lettuce cultivars grown under various combinations of blue and red light-emitting diodes. HortScience 2013, 48, 988–995, doi:10.21273/HORTSCI.48.8.988.
Son, K.H.; Oh, M.M. Growth, photosynthetic and antioxidant parameters of two lettuce cultivars as affected by red, green, and blue light-emitting diodes. Hortic. Environ. Biotechnol. 2015, 56, 639–653, doi:10.1007/s13580-015-1064-3.
Son, K.H.; Jeon, Y.M.; Oh, M.M. Application of supplementary white and pulsed light-emitting diodes to lettuce grown in a plant factory with artificial lighting. Hortic. Environ. Biotechnol. 2016, 57, 560–572, doi:10.1007/s13580-016-0068-y.
Song, J.; Meng, Q.; Du, W.; He, D. Effects of light quality on growth and development of cucumber seedlings in controlled environment. Int. J. Agric. Biol. Eng. 2017, 10, 312–318, doi:10.3965/j.ijabe.20171003.2299.
Spalholz, H.; Perkins-Veazie, P.; Hernández, R. Impact of sun-simulated white light and varied blue: Red spectrums on the growth, morphology, development, and phytochemical content of green-and red-leaf lettuce at different growth stages. Sci. Hortic. 2020, 264, 109195, doi:10.1016/j.scienta.2020.109195.
Wang, J.; Lu, W.; Tong, Y.; Yang, Q. Leaf morphology, photosynthetic performance, chlorophyll fluorescence, stomatal development of lettuce (Lactuca sativa L.) exposed to different ratios of red light to blue light. Front. Plant Sci. 2016, 7, 250, doi:10.3389/fpls.2016.00250.
Wollaeger, H.M.; Runkle, E.S. Growth of impatiens, petunia, salvia, and tomato seedlings under blue, green, and red light-emitting diodes. HortScience 2014, 49, 734–740, doi:10.21273/HORTSCI.49.6.734.
Wollaeger, H.M.; Runkle, E.S. Growth and acclimation of impatiens, salvia, petunia, and tomato seedlings to blue and red light. HortScience 2015, 50, 522–529, doi:10.21273/HORTSCI.50.4.522.
Integr. Agric. 2020, 19, 2027–2034, doi:10.1016/S2095-3119(20)63209-9.
Yan, Z.; He, D.; Niu, G.; Zhai, H. Evaluation of growth and quality of hydroponic lettuce at harvest as affected by the light intensity, photoperiod and light quality at seedling stage. Sci. Hortic. 2019a, 248, 138–144, doi:10.1016/j.scienta.2019.01.002.

Yan, Z.; He, D.; Niu, G.; Zhou, Q.; Qu, Y. Growth, nutritional quality, and energy use efficiency of hydroponic lettuce as influenced by daily light integrals exposed to white versus white plus red light-emitting diodes. HortScience 2019b, 54, 1737–1744, doi:10.21273/HORTSCI14236-19.

Yorio, N.C.; Goins, G.D.; Kagie, H.R.; Wheeler, R.M.; Sager, J.C. Improving spinach, radish, and lettuce growth under red light-emitting diodes (LEDs) with blue light supplementation. HortScience 2001, 36, 380–383, doi:10.21273/HORTSCI.36.2.380.

Zou, J.; Zhou, C.B.; Xu, H.; Cheng, R.F.; Yang, Q.C.; Li, T. The effect of artificial solar spectrum on growth of cucumber and lettuce under controlled environment. J.

APPENDIX E

METHOD AND THEORY OF DIRECTLY MEASURING PPE (P_{FR}/P_{TOTAL}) IN ETIOLATED TISSUE

E.1 Method

This method is primarily explained by Klein et al. (1967), Kendrick and Frankland (1968) and Klose (2019). The technique was modified from Butler et al. (1963).

These measurements must be made with chlorophyll deficient tissue because chlorophyll affects the measurements, even at small concentrations. This means that either dark grown etiolated tissue or norflurazon treated tissue must be used. Hypocotyl hooks tend to have a relatively large concentration of phytochrome and therefore this tissue is generally used for measurements. To assess the status of the major phytochrome in light grown plants, phytochrome-B, mutants are often used that are phytochrome-A deficient and phytochrome-B over-expressers (Klose et al., 2015). The tissue is packed tightly into a cuvette for measurements.

This technique requires a spectrophotometer, which measures the absorbance (or optical density, OD) of two wavelengths simultaneously and calculates the difference between them, ΔOD. This instrument is called a dual wavelength spectrophotometer and is described in Butler et al. (1963) and Klose (2019). The two wavelengths used to calculate the ΔOD are 730 and 800 nm, such that $\Delta OD = OD_{730} - OD_{800}$. These wavelengths are chosen because the absorbance peak of P_{fr} is close to 730 nm and 800 nm is a stable reference wavelength that does not change upon irradiation. Chlorophyll can still affect the readings in this region. These measurements rely on the Beer-Lampert law that states that concentration is proportional to absorbance. Therefore, ΔOD is roughly a proxy for the concentration of P_{fr}.

First, samples in the cuvettes are exposed to the photon source of interest. Then they are placed in the dark, frozen and transported to the spectrophotometer where an initial ΔOD measurement is made, ΔOD_i. Then the sample is exposed to saturating actinic red irradiation

(about 660 nm) and the ΔOD is measured again, ΔOD_R. If only P_r absorbed at 660 nm, saturating red radiation would convert all the phytochrome to P_{fr}, and ΔOD_R would thus be a proxy for the total pool of phytochrome (P_{total}). However, that is not the case and both P_r and P_{fr} absorb at 660 nm, so ΔOD_R must be corrected to estimate P_{total} using an estimation of PPE under saturating red. Many publications have calculated this value, called $X^{fr}_{red\ eq}$, ϕ_{660} or PPE_R. Smith and Holmes (1977) use an estimation from Pratt (1975), but this appears to be a low estimate (see Lagarias et al., 1987; Mancinelli, 1994). A good estimate of ϕ_{660} is 0.89.

Finally, the sample is exposed to saturating actinic FR (about 730 nm) radiation, which converts all the phytochrome to P_r, reaching a P_{fr} minimum, ΔOD_{FR}. Unlike 660 nm which is absorbed significantly by both forms of phytochrome, 730 nm radiation is predominately absorbed by P_{fr}. P_r may cause less than 1% of the absorbance, but this error is small enough to be ignored. Therefore ΔOD_{FR} should be a proxy for a P_{fr} concentration of zero, and therefore it is treated as noise and is subtracted from both ΔOD_i and ΔOD_R as follows:

$$[P_{fr}] \propto \Delta OD_i - \Delta OD_{FR} \qquad [E.1]$$

$$[P_{total}] \propto \frac{\Delta OD_R - \Delta OD_{FR}}{\phi_{660}} \qquad [E.2]$$

Therefore, the final calculation of measured phytochrome photoequilibrium under a specific photon source is uses the following equations:

$$PPE = \frac{\phi_{660} \times (\Delta OD_i - \Delta OD_{FR})}{\Delta OD_R - \Delta OD_{FR}} \qquad [E.3]$$

This technique can only measure the relative ratio of all the phytochromes (5 in Arabidopsis and 3 in rice), unless the use of mutants is adopted. In the main text we say that only PPE can be measured with this technique, not [P_{fr}] or [P_{total}], but a semi-absolute measurement of P_{total} can be measured using Eq. [S1.2] if careful sample preparation is undertaken. With careful preparation in a single species the scattering of light within the tissue can be assumed to be the same, and thus an absolute value of P_{total} can be obtained with units of ΔΔOD/mg fresh mass (Klose, 2019). However, it seems unlikely that P_{total} can be compared among species and between young and old tissue due to differences in light-scattering. This would indicate that the careful measurement of P_{total} is only a semi-absolute value.

E.2 Literature Cited

Butler, W.L., H.C. Lane, and H.W. Siegelman. 1963. Nonphotochemical transformations of phytochrome in vivo. Plant Physiol. 38:514-519. https://doi.org/10.1104/pp.38.5.514

Kendrick, R.E., and B. Frankland. 1968. Kinetics of phytochrome decay in Amaranthus seedlings. Planta 82:317-320. https://doi.org/10.1007/BF00386434

Klein, W.H., J.L. Edwards, and W. Shropshire. 1967. Spectrophotometric measurements of phytochrome in vivo and their correlation with photomorphogenic responses of Phaseolus. Plant Physiol. 42:264-270. https://doi.org/10.1104/pp.42.2.264

Klose, C., F. Venezia, A. Hussong, S. Kircher, E. Schäfer, and C. Fleck. 2015. Systematic analysis of how phytochrome B dimerization determines its specificity. Nature Plants 1:1-9. https://doi.org/10.1038/nplants.2015.90

Klose, C. 2019. In vivo spectroscopy, p. 113-120. In: A. Hiltbrunner (ed.). Phytochromes. Humana Press, New York, NY. https://doi.org/10.1007/978-1-4939-9612-4_8

Lagarias, J.C., J.M. Kelly, K.L. Cyr, and W.O. Smith, Jr. 1987. Comparative photochemical analysis of highly purified 124 kilodalton oat and rye phytochromes in vitro. Photochemistry Photobiology 46:5-13. https://doi.org/10.1111/j.1751-1097.1987.tb04729.x

Mancinelli, A.L. 1994. The physiology of phytochrome action. In: R.E. Kendrick and G.H.M. Kronenberg (eds.). Photomorphogenesis in plants. Springer, Dordrecht, The Netherlands. https://doi.org/10.1007/978-94-011-1884-2_10

Pratt, L.H. 1975. Photochemistry of high molecular weight phytochrome in vitro. Photochemistry Photobiology 22:33-36. https://doi.org/10.1111/j.1751-1097.1975.tb06717.x

Smith, H., and M.G. Holmes. 1977. The function of phytochrome in the natural environment—III. Measurement and calculation of phytochrome photoequilibria. Photochemistry Photobiology 25:547-550. https://doi.org/10.1111/j.1751-1097.1977.tb09126.x

APPENDIX F

ENVIRONMENTAL FACTORS IMPACTING THE R:FR RATIO IN SUNLIGHT

F.1 R:FR Ratio in the Natural Environment

The R:FR ratio of sunlight varies widely and values have been reported as low as 0.7 to as high as 1.8 (Holmes and Smith, 1977; Kotilainen et al., 2020; Salisbury, 1981; Smith, 1982, 1994). In the natural environment, water vapor, location and the time of day also affect the R:FR ratio.

It is often thought that in full sunlight near solar noon, when the sun is at a low zenith angle (high elevation angle), the R:FR ratio is relatively constant around 1.15 (Franklin and Whitelam, 2005; Smith, 1982), but recent data by Kotilainen et al. (2020) demonstrates the influence of atmospheric water vapor, location and the time of day on the R:FR ratio. There is an atmospheric water vapor absorbance band with a peak at 723 nm and two oxygen absorbance bands in the R and FR region (Patadia et al., 2018; Smith, 1982; Fig. 1). The water absorbance band depends on the amount of moisture in the atmosphere; the oxygen absorbance band is affected by length of the atmospheric path. Furthermore, light scattering through the atmosphere at low sun angles near dawn and dusk has historically been thought to significantly reduce the R:FR ratio. This has led to many end-of-day far-red studies (Kasperbauer, 1971; Salisbury, 1981). More recent data indicates that low sun angles can significantly increase the R:FR ratio in some environmental conditions (Kotilainen et al., 2020). Collectively, these factors alter R:FR ratios in full sunlight in the natural environment.

F.2 Literature Cited

Franklin, K.A., and G.C. Whitelam. 2005. Phytochromes and shade-avoidance responses in plants. Ann. Bot. 96:169-175. https://doi.org/10.1093/aob/mci165

Holmes, M.G., and H. Smith. 1977a. The function of phytochrome in the natural environment—I. Characterization of daylight for studies in photomorphogenesis and photoperiodism. Photochemistry Photobiology 25:533-538. https://doi.org/10.1111/j.1751-1097.1977.tb09124.x

Kasperbauer, M.J. 1971. Spectral distribution of light in a tobacco canopy and effects of end-of-day light quality on growth and development. Plant Physiol. 47:775-778. https://doi.org/10.1104/pp.47.6.775

Kotilainen, T., P.J. Aphalo, C.C. Brelsford, H. Böök, S. Devraj, A. Heikkilä, R. Hernández, A. Kylling, A.V. Lindfors, and T.M. Robson. 2020. Patterns in the spectral composition of sunlight and biologically meaningful spectral photon ratios as affected by atmospheric factors. Agr. For. Meteorol. 291:108041. https://doi.org/10.1016/j.agrformet.2020.108041

Patadia, F., R.C. Levy, and S. Mattoo. 2018. Correcting for trace gas absorption when retrieving aerosol optical depth from satellite observations of reflected shortwave radiation. Atmospheric Measurement Tech. 11:3205-3219. https://doi.org/10.5194/amt-11-3205-2018

Salisbury, F.B. 1981. Twilight effect: initiating dark measurement in photoperiodism of Xanthium. Plant Physiol. 67:1230-1238. https://doi.org/10.1104/pp.67.6.1230

Smith, H. 1982. Light quality, photoperception, and plant strategy. Ann. Rev. Plant Physiol. 33:481-518. https://doi.org/10.1146/annurev.pp.33.060182.002405

Smith, H. 1994. Sensing the light environment: The functions of the phytochrome family, p. 377-416. In: R.E. Kendrick and G.H.M. Kronenberg (eds.). Photomorphogenesis in plants. Springer, Dordrecht, The Netherlands. https://doi.org/10.1007/978-94-011-1884-2_15

APPENDIX G

SUPPLEMENTAL DATA FOR CHAPTER 4

Table G.1: Percent far-red in each treatment. There were 7 trials in time, each with a higher and lower dose of FR.

	Trial #	FR Dose	HIGH BLUE	HIGH GREEN	HIGH RED
% FAR-RED $\frac{\sum 701-750\,nm}{\sum 400-750\,nm}$	Trial 1	LOW	1.5	3.4	1.3
		HIGH	9.1	12	8.6
	Trial 2	LOW	1.5	3.2	1.8
		HIGH	9.2	9.0	9.2
	Trial 3	LOW	1.6	5.5	1.3
		HIGH	25	24	23
	Trial 4	LOW	1.6	6.3	1.4
		HIGH	25	25	25
	Trial 5	LOW	13	13	13
		HIGH	19	20	18
	Trial 6	LOW	13	13	12
		HIGH	20	20	20
	Trial 7	LOW	18	17	16
		HIGH	41	44	39

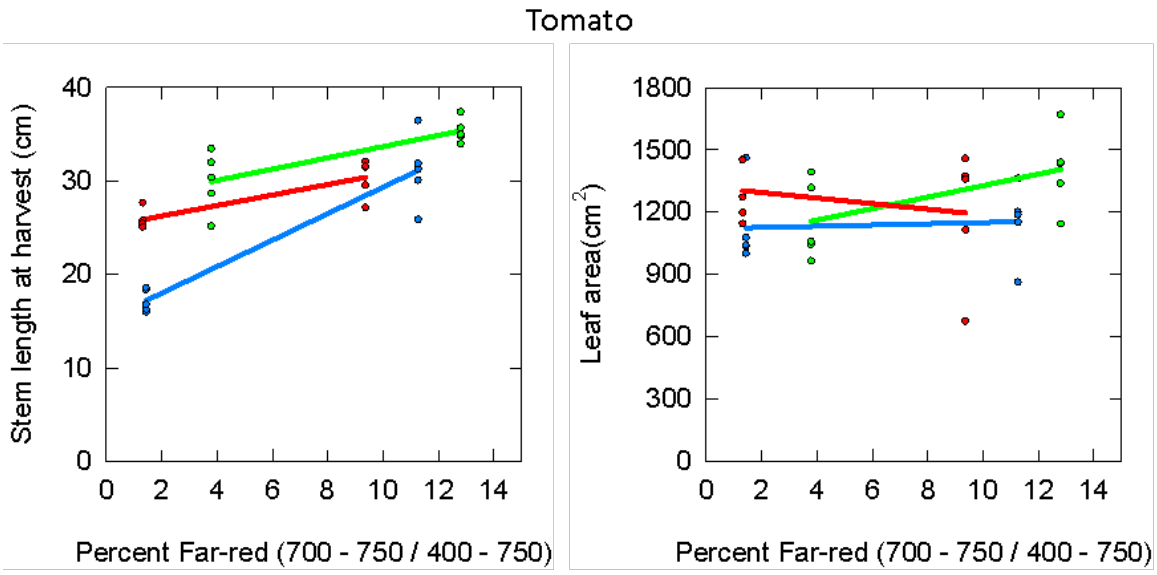

Fig. G-1: Effect of percent far-red on stem length and leaf area in tomato

Fig. G-2: Photo of the chambers used in the study.

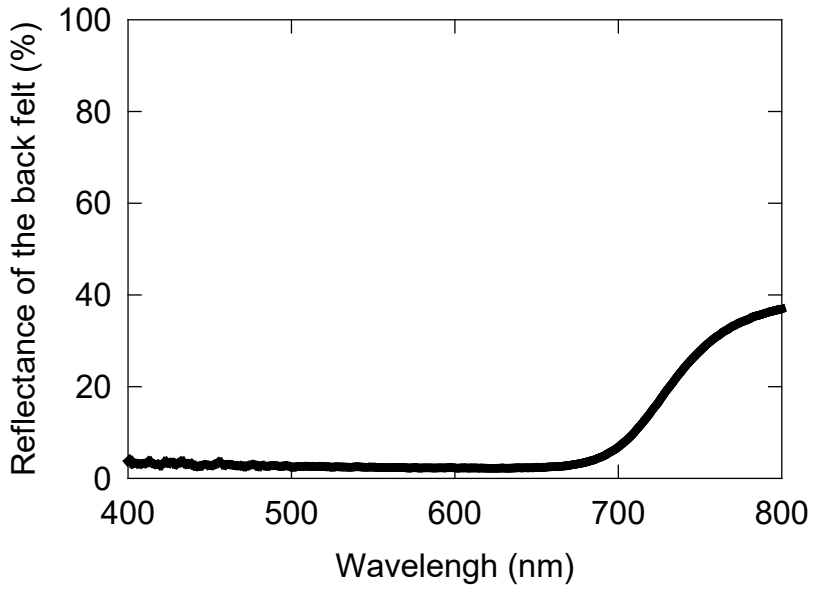

Fig. G-3: Reflectance of black felt used in short-term photobleaching study.

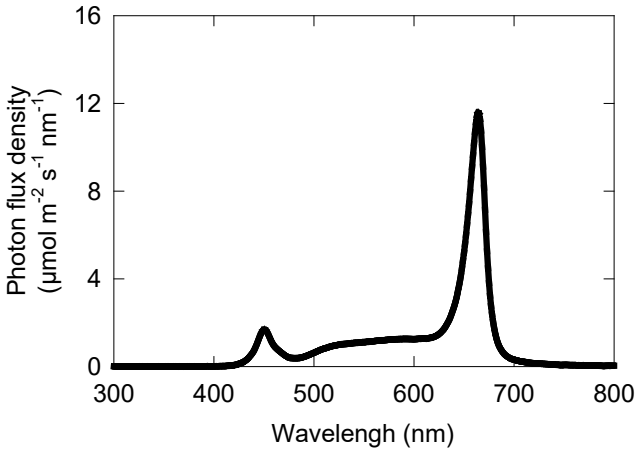

Fig. G-4: Spectrum of the pre-treatment for the short-term photobleached seedling study.

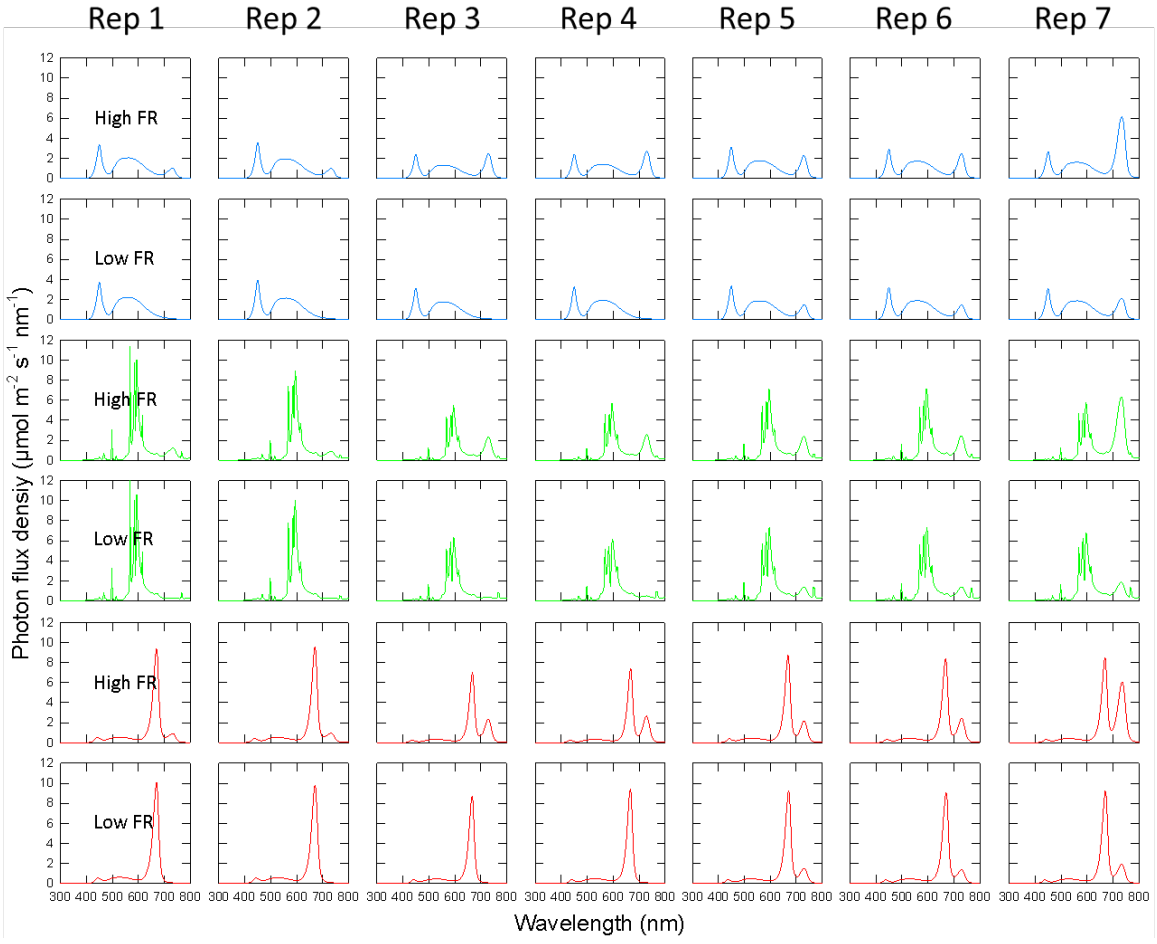

Fig. G-5: Average spectral photon distribution in each far-red (FR) dose treatment. Blue, green and red lines represent the high blue, green and red background treatments, respectively.

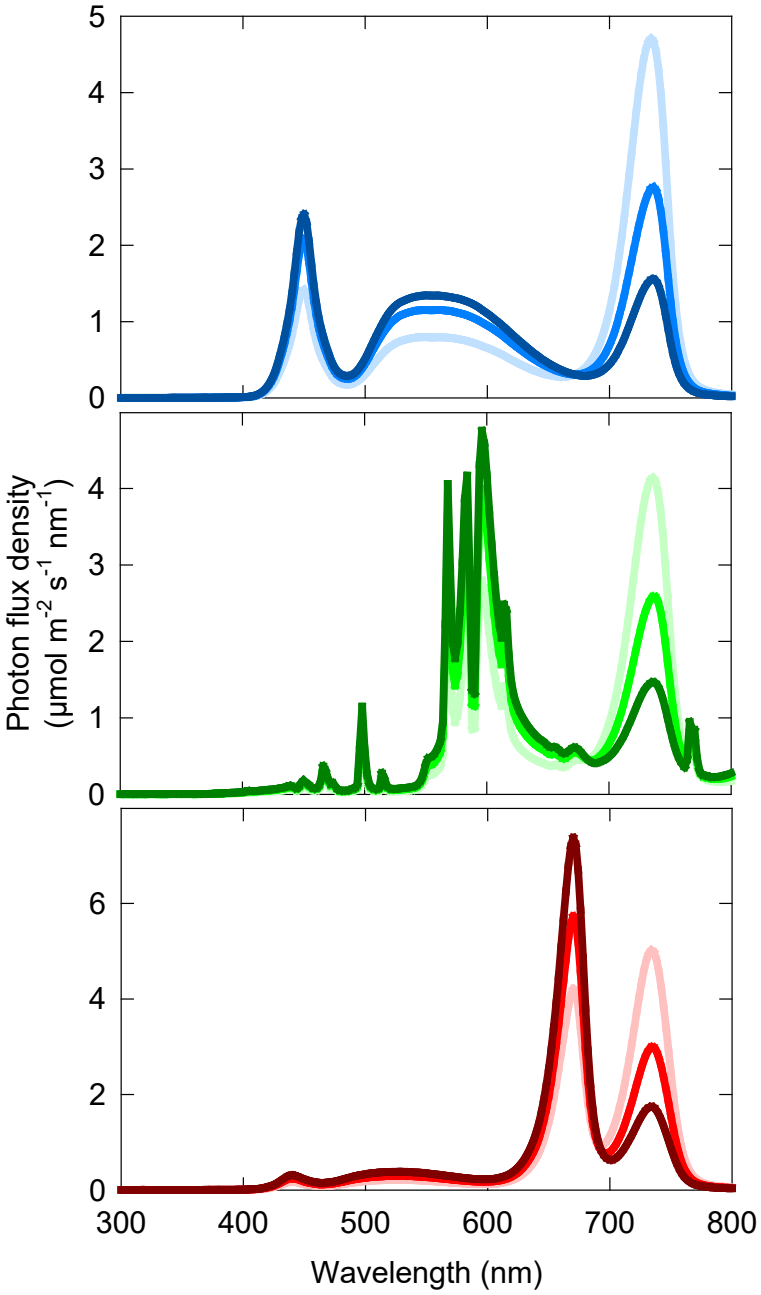

Fig. G-6: Spectral treatments from the short-term photobleaching study. These experiments used the same spectral backgrounds as the long-term study. These studies only contained three levels of FR. Measurements are averages from four replicate studies.

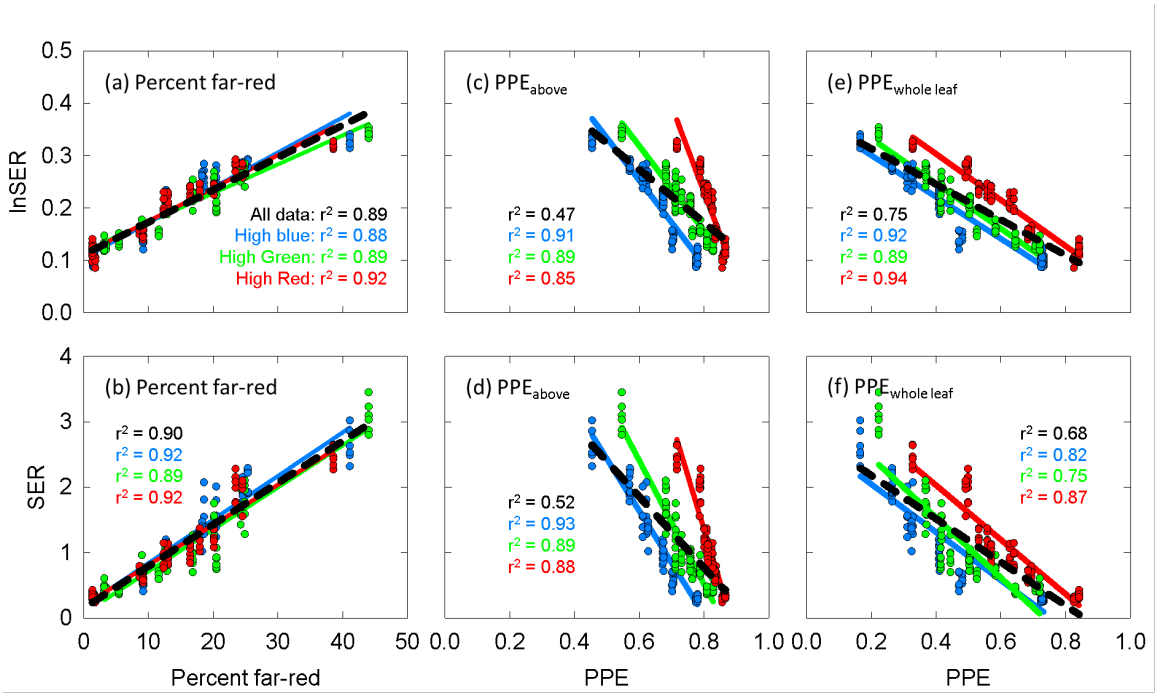

Fig. G-7: Comparing the assumption of log-linear stem elongation with linear elongation in the long-term study. Stems typically elongate following a sigmoidal curve (Fisher et al., 1996; Bjorkman, 1999) with exponential elongation in young plants (Morgan and Smith, 1978), followed by linear elongation, and finally, exponential rise to a maximum. This means that elongation is best described as a natural log function in the early stages of growth (Eq. 4.4 and 4.5). For this reason early studies regularly used log-linear stem elongation rates to predict elongation from phytochrome photoequilibrium (Morgan and Smith, 1976, 1978, 1979). Comparing exponential elongation (a,c,e) to linear elongation (b,d,f) resulted in minimal differences in the r^2 values. Importantly, comparing PPE estimated above the leaf compared to estimating PPE within the leaf result in the same conclusions regardless of assuming linear or log linear elongation. Additionally, percent far-red was a good metric regardless of linear or log-linear elongation.

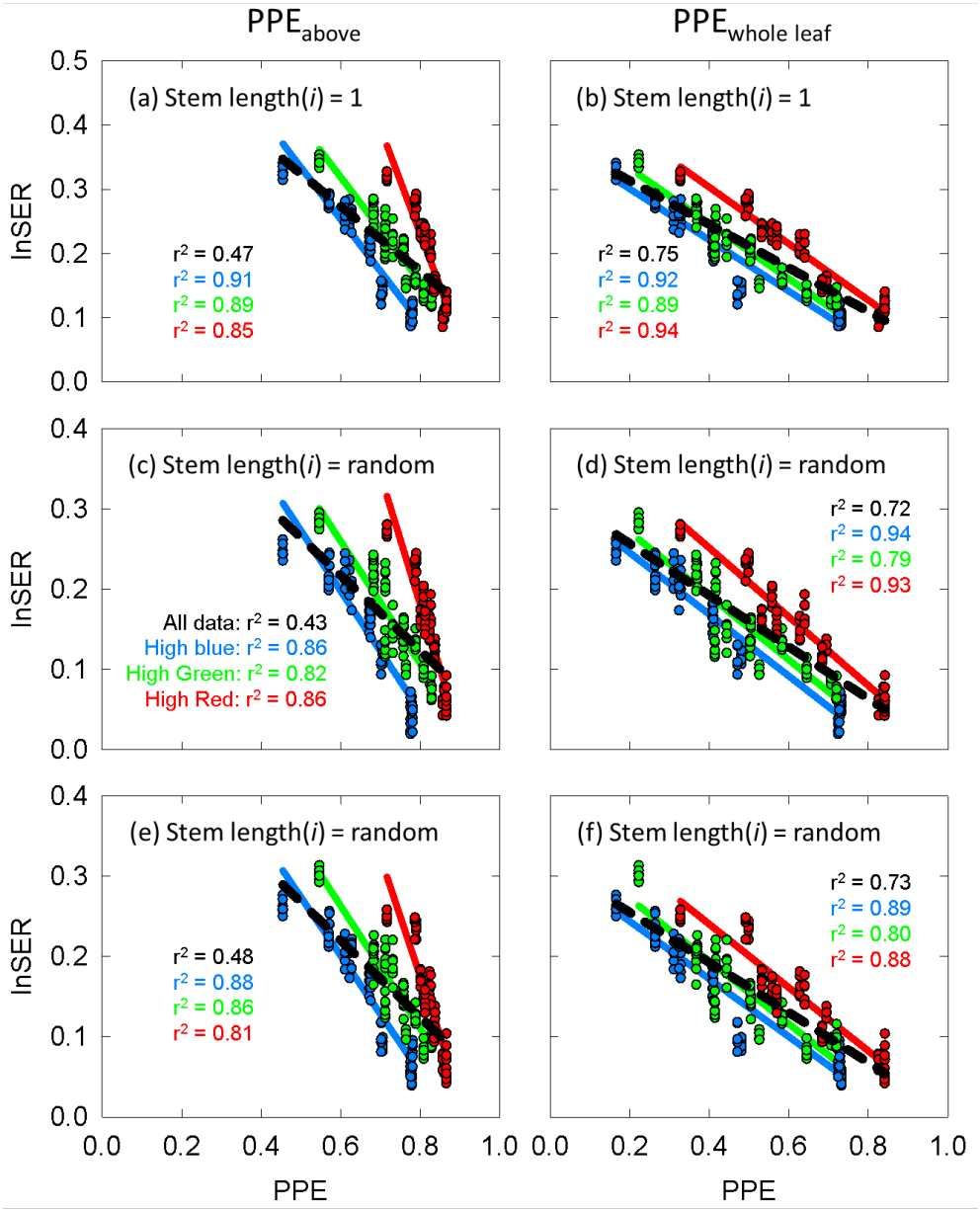

Fig. G-8: Changing the assumption in the initial plant height when calculating the natural log of the stem extension rate (lnSER). For the analysis used in the main text of this study, the initial stem length was assumed to be equal to one cm (a,b). (c) through (f) assume random initial values between 1.4 and 2.3 cm (measured initial cucumber heights in a separate study) for Stem length(*i*) in Eq. 4.4. Eq. 4.5 is then modified by dividing stem length at harvest by this random value for each data point. (c) and (d) assume the same set of random values for Stem length(*i*) and (e) and (f) assume a different set of random values. In both cases the r^2 values do change, but changes are minimal, and importantly, Estimating PPE within the leaf significantly improves the correlation through all the data in every case.

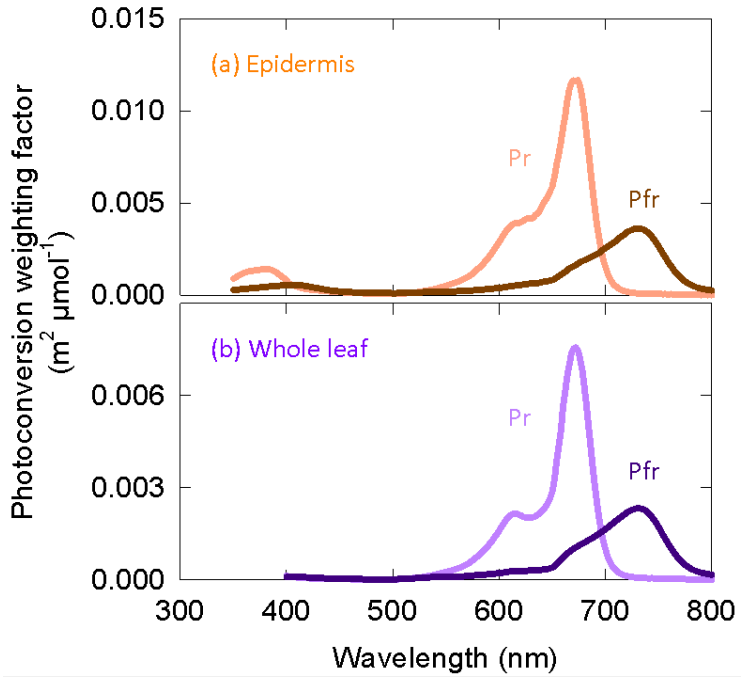

Fig. G-9: Photoconversion weighting factors for phytochrome conversion in etiolated tissue. Weighting factors are for (a) phytochrome in the epidermal tissue or (b) phytochrome homogeneously distributed through all cotyledon tissue.

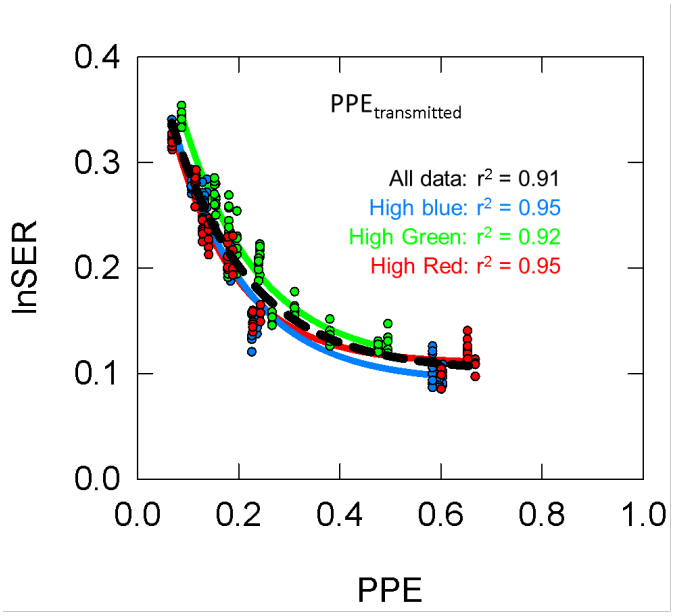

Fig. G-10: Relationship between lnSER in the long-term study and PPE estimated using the transmission spectrum as a distortion function. The relationship is non-linear.

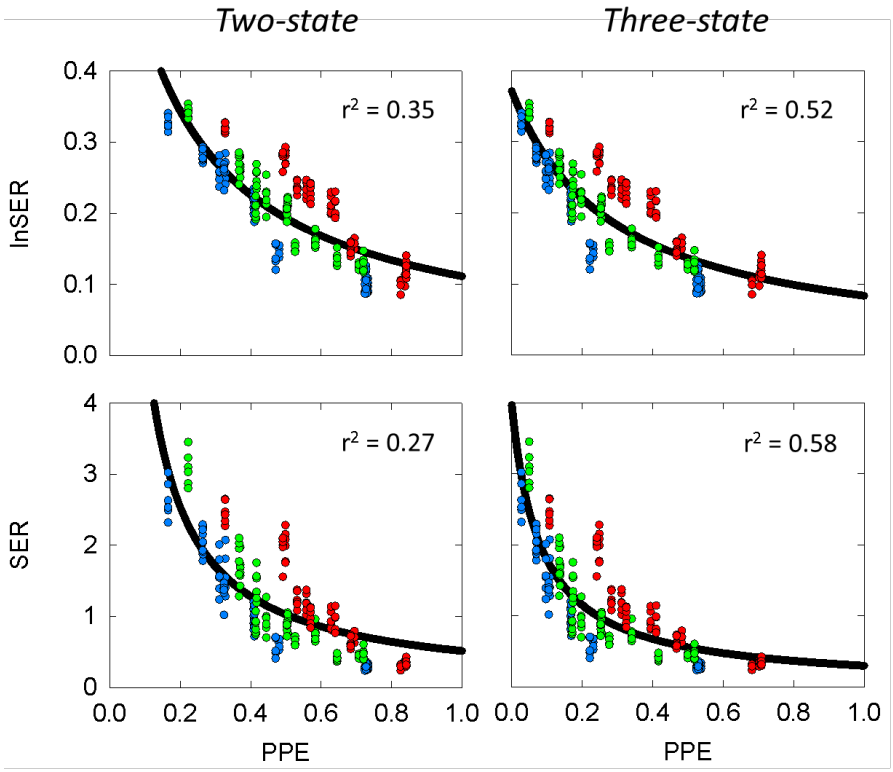

Fig. G-11: Alternative models to explain the stem elongation data in response to far-red using the modified Michaelis-Menten kinetic formula.

$$\text{Stem elongation (PIF activity)} = V_{max} - \frac{V_{max}\,[PPE]}{k_m + [PPE]}$$

Because the PIF transcription factors upregulate genes related to elongation, stem elongation is assumed to be correlated with PIF activity. In order to normalize this PIF activity, the normal Michaelis-Menten formula is subtracted from V_{max} (maximum PIF activity is assumes to be equal to the maximum elongation rate).Because Pfr inhibits the activity of PIFs, higher relative concentrations of Pfr concentrations would inhibit elongation. Pfr is normalized following the normal method of calculating PPE.

This model was fit to the log linear (a and b) and linear (c and d) stem elongation data using both the *two-state* (a and c) and *three-state* (b and d) *models* assuming PPE within the leaf in all cases. This model does follow the general non-linearity of the relationships between different estimates of active phytochrome and elongation rate, but the correlation coefficients are lower than the linear estimates used in chapter 4 (Fig. 4-7 and Fig. 4-8). In all cases, the model is significantly improved assuming the *three-state* over the *two-state model*. However, the assumption of this modified Michaelis-Menten formula, similar to general linear models, are questionable.

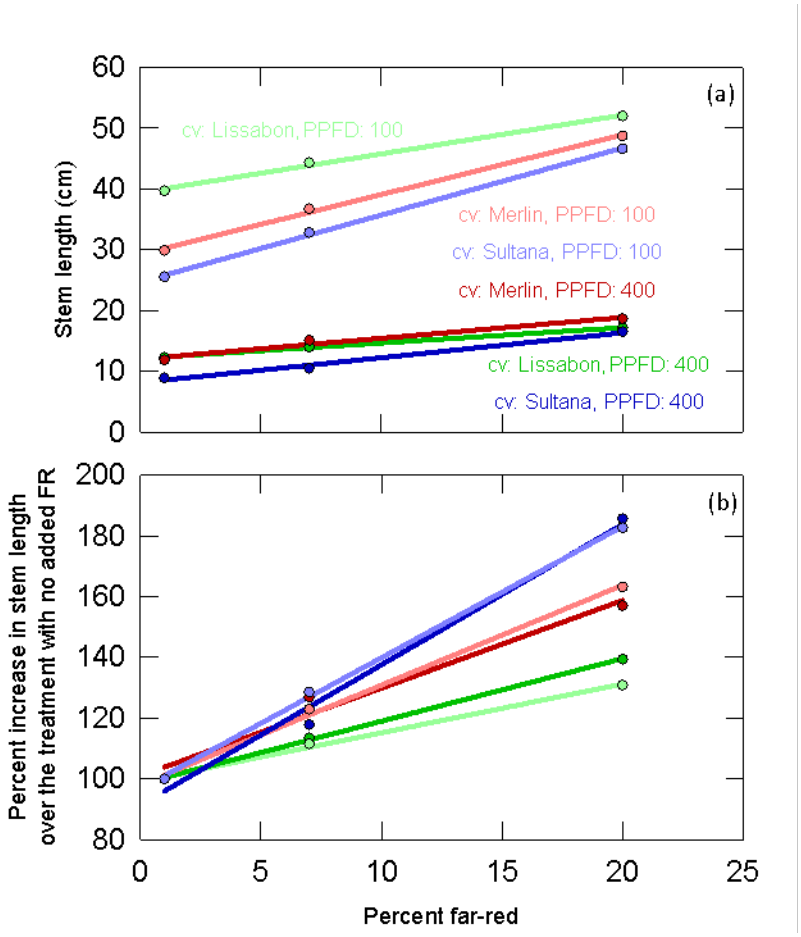

Fig. G-12: Data from Hitz et al. (2019) represented in graphs that use percent far-red (FR). Green data comes from the cv. Lissabon, red data comes from the cv. Merlin, and blue data comes from the cv. Sultana. Darker lines are were grown under a PPFD of 100 µmol m^{-2} s^{-1} and the dark lines were grown under 400 µmol m^{-2} s^{-1}. (a) The data graphed with absolute tem length. (b) The data re-graphed as percent increase compared to the treatment with no added FR.

G.1 Literature Cited

Björkman, T. (1999). Dose and timing of brushing to control excessive hypocotyl elongation in cucumber transplants. *HortTechnology* 9, 224–226. doi: 10.21273/HORTTECH.9.2.224

Fisher, P. R., Heins, R. D., and Lieth, J. H. (1996). Quantifying the relationship between

phases of stem elongation and flower initiation in poinsettia. *Journal of the American Society for Horticultural Science* 121, 686–693. doi: 10.21273/JASHS.121.4.686

Hitz, T., Hartung, J., Graeff-Hönninger, S., and Munz, S. (2019). Morphological response of soybean (*Glycine max* (L.) Merr.) cultivars to light intensity and red to far-red ratio. *Agronomy* 9, 428. doi: 10.3390/agronomy9080428

Morgan, D. C., and Smith, H. (1976). Linear relationship between phytochrome photo-equilibrium and growth in plants under simulated natural radiation. *Nature* 262, 210–212. doi: 10.1038/262210a0

Morgan, D., and Smith, H. (1978). The relationship between phytochrome-photoequilibrium and development in light grown *Chenopodium album* L. *Planta* 142, 187–193. doi: 10.1007/BF00388211

Morgan, D. C., and Smith, H. (1979). A systematic relationship between phytochrome controlled development and species habitat. *Planta* 145, 253–258. doi: 10.1007/BF00454449

APPENDIX H

SUPPLEMENTAL DATA FOR CHAPTER 5

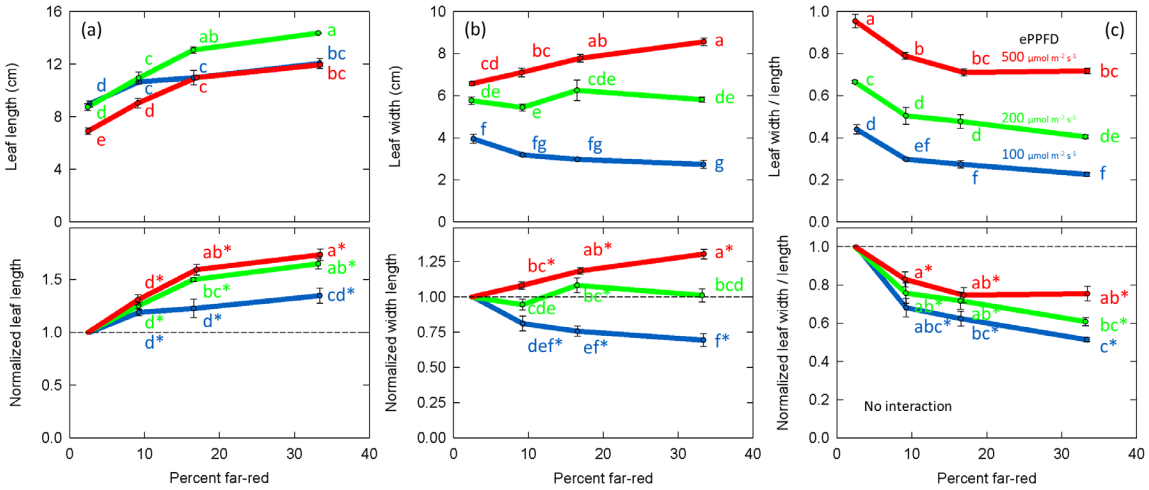

Fig. H-1: Effect of percent far-red (FR) and extended photosynthetic photon flux density (ePPFD) on leaf shape in lettuce. (a) Leaf length (b) leaf width and (c) leaf width divided by leaf length. Top graphs are absolute values while bottom graphs are the normalized response, where data from each replicate in time has been normalized to its respective 2% FR control treatment for each level of ePPFD. In the normalized graphs, * indicates that the treatment is statistically different from 1 (using a student's t-test), which represents the effect of the 2% FR control. Error bars represent standard error for n = 3 replicates.

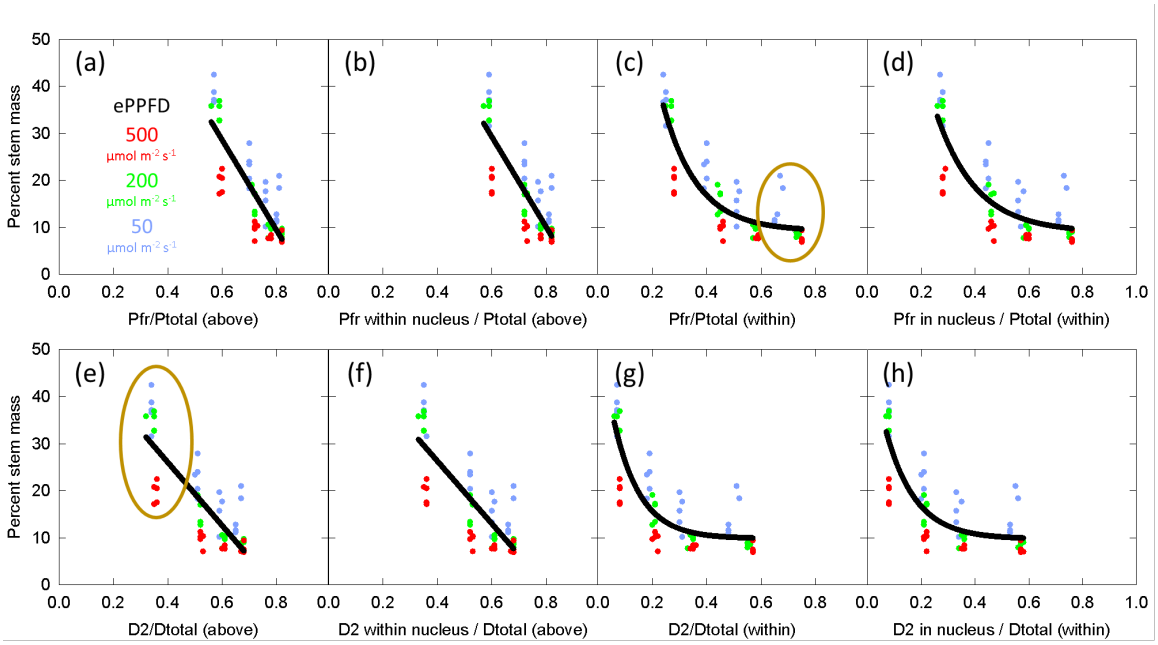

Fig. H-2: Model of the effect of percent far-red (FR) and extended photosynthetic photon flux density (ePPFD) on percent stem mass in cucumber using the *cellular model* developed by Rausenberger et al. (2010), Klose et al. (2015), Sellaro et al. (2019), and Smith and Fleck (2019). For each graph, the program provided by Smith and Fleck (2019) was used to calculate the size of different pools of phytochrome as a fraction of the total pool of phytochrome, given the average spectral photon distribution (SPD) of each replicate. Then, the average percent stem mass of the four plants in each treatment were plotted. Linear or exponential decay models were used to fit all the data.

In (a) through (d) Pfr is assumed to be the active form of phytochrome, while in (e) through (h), D2 (the fully active Pfr-Pfr homodimer) is assumed to be the active form. In (a), (b), (e) and (f) the SPD above the leaf is input into the model, while in (c), (d), (g) and (h), spectral distortion functions are first used to estimate the SPD within the leaf.

In (c), the dark yellow circle shows the relative decrease in Pfr at lower ePPFD compared to higher ePPFD. This is caused by a greater significance of thermal reversion at lower photon intensities. In (d) the dark yellow circle shows the spread of the data between different levels of ePPFD. This shows that thermal reversion did not shift the expected response at lower intensities enough make the data fall on a single line. This strongly indicates that some other factor (e.g. blue photons) were contributing to the response.

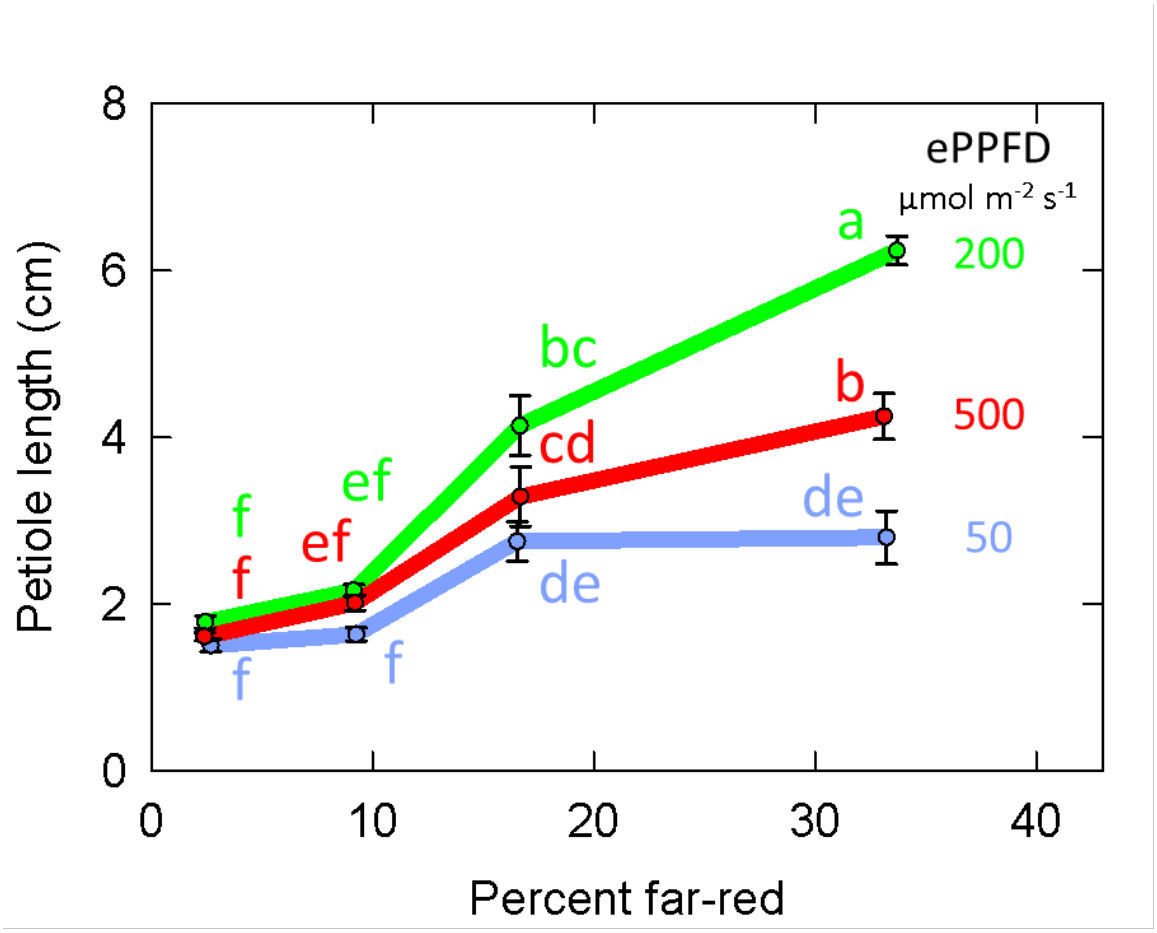

Fig. H-3: Effect of percent far-red (FR) and extended photosynthetic photon flux density (ePPFD) on petiole length in cucumber. Error bars represent standard error for n = 5 replicates in cucumber.

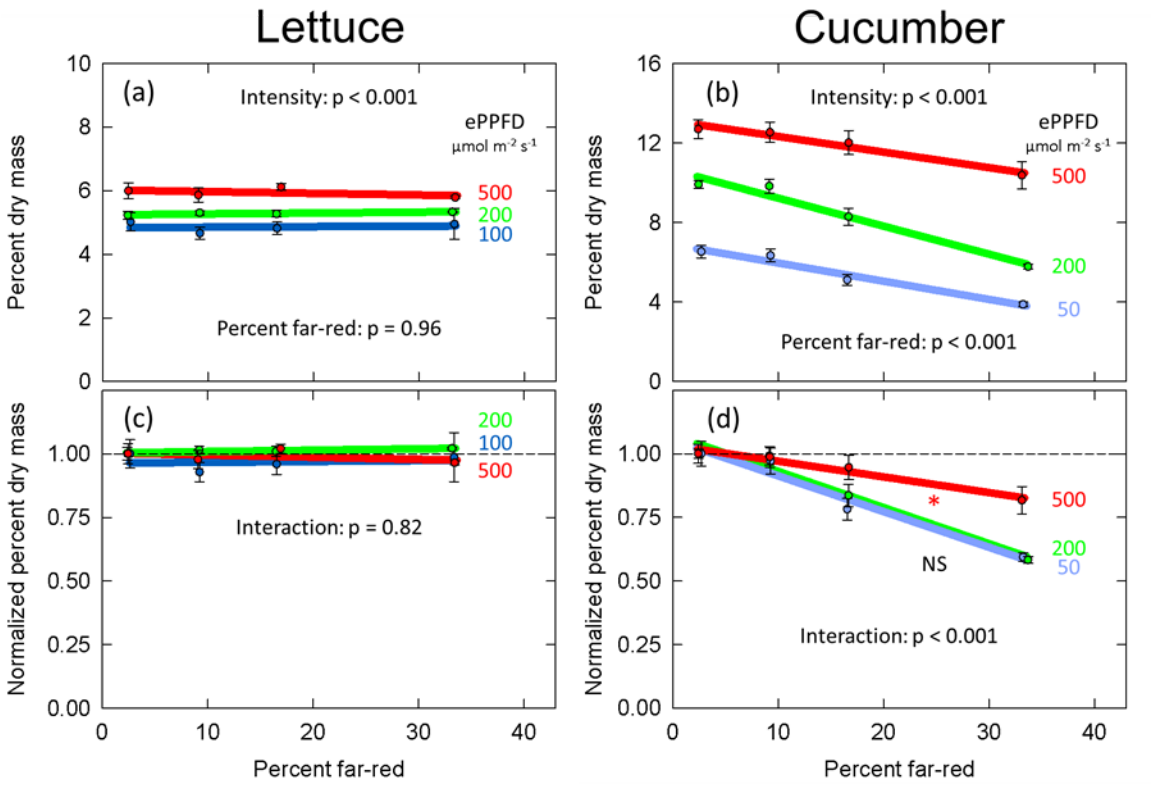

Fig. H-4 Effect of percent far-red (FR) at three levels of extended photosynthetic photon flux density (ePPFD) on percent dry mass in lettuce (a,c) and cucumber (b,d). Percent dry mass was calculated by dividing total shoot dry mass by total shoot fresh mass, and multiplying by 100. (a) and (b) represent absolute values of percent dry mass and (c) and (d) are the normalized response, where data has been normalized to the average response in the 2% FR control treatment for each ePPFD. Error bars represent standard error for n = 3 replicates in lettuce and n = 5 replicates in cucumber. In (d), the NS indicates that the slopes of the 50 and 200 µmol m^{-2} s^{-1} treatments are not statistically different, while the 500 µmol m^{-2} s^{-1} treatment (marked with an *) has a statistically different slope.

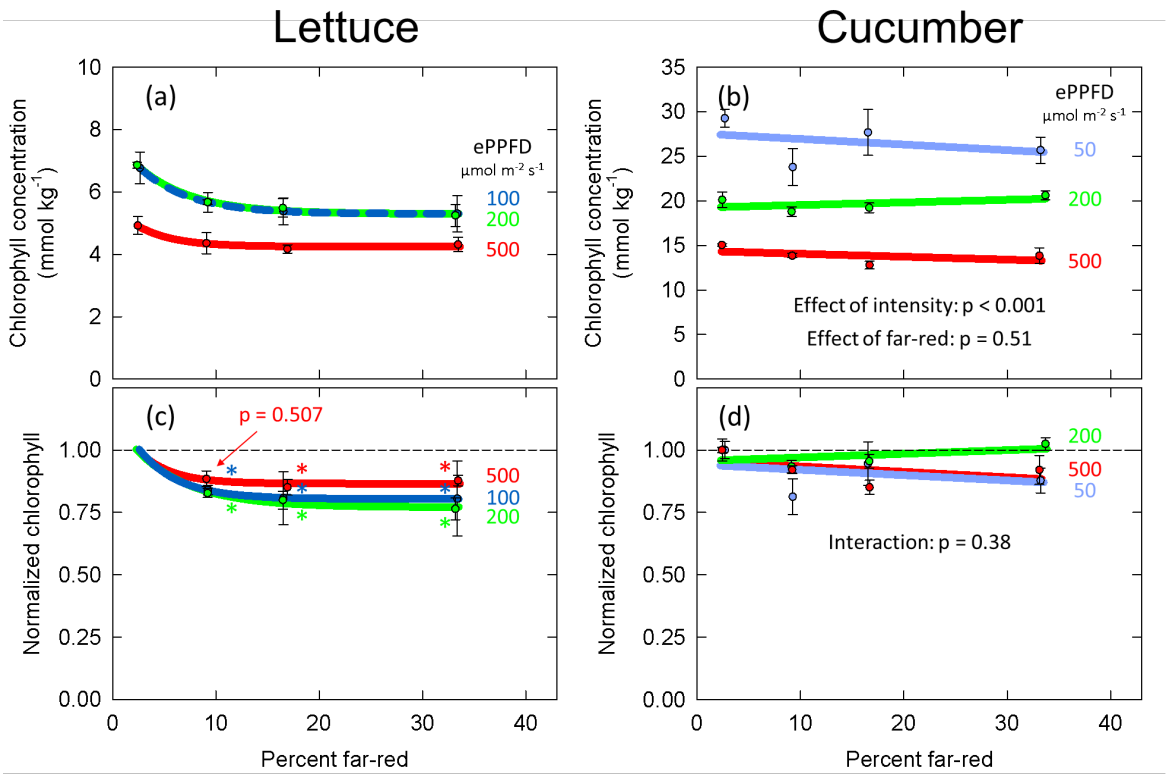

Fig. H-5 Effects of percent far-red (FR) and extended photosynthetic photon flux density (ePPFD) on chlorophyll concentration in lettuce (a,c) and cucumber (b,d). Chlorophyll concentration was measured with a chlorophyll concentration meter (MC-100, Apogee Instruments, Logan UT) using lettuce coefficients for the lettuce measurements and generic coefficients for the cucumber measurements**.** (a) and (b) the raw data and (c) and (d) are the normalized response. In (c) data from each replicate in time has been normalized to its respective 2% FR control treatment for each intensity, and * indicates that the treatment is statistically different from 1 (using a student's t-test), which represents the response of the 2% FR control. In (d) data has been normalized to the average response in the 2% FR control treatment for each ePPFD. In (a) and (c) trend lines are included to guide the eye, and not meant to be used as a statistical representation. Error bars represent standard error for n = 3 replicates in lettuce and n = 5 replicates in cucumber.

H.1 Literature Cited

Klose, C., Venezia, F., Hussong, A., Kircher, S., Schäfer, E. and Fleck, C., 2015. Systematic analysis of how phytochrome B dimerization determines its specificity. Nature plants, 1(7), 1-9.

Rausenberger, J., Hussong, A., Kircher, S., Kirchenbauer, D., Timmer, J., Nagy, F.,

Schäfer, E. and Fleck, C., 2010. An integrative model for phytochrome B mediated photomorphogenesis: from protein dynamics to physiology. PLoS One, 5(5),e10721.

Sellaro, R., Smith, R.W., Legris, M., Fleck, C. and Casal, J.J., 2019. Phytochrome B dynamics departs from photoequilibrium in the field. Plant, cell & environment, 42(2), 606-617.

Smith, R.W. and Fleck, C., 2019. Basic Phytochrome B Calculations. In Phytochromes (pp. 121-133). Humana, New York, NY.

CURRICULUM VITAE

PAUL KUSUMA

paul.kusuma@aggiemail.usu.edu • 407-929-2363
644 E 600 N #38, Logan, Utah, 84321

EDUCATION

Utah State University – Ph.D. Candidate	August 2016 – Present
University of Florida – B. S. in Horticulture	December 2015

RESEARCH EXPERIENCE

Ph.D. Candidate – Crop Physiology Laboratory – Utah State University	August 2016 – Present
Lab Assistant & Research – Folta Laboratory – University of Florida	May 2015 – July 2016
Lab Assistant – Darnell Laboratory – University of Florida	Summer 2015, 2016

FUNDING RECIEVED

Presidential Doctoral Research Fellowship	$10,000/year (2018-2021)
Utah NASA Space Grant Consortium Fellowship	$15,000/year (2018-2021)
The center for the utilization of biological engineering in space (CUBES)	$5,000/year (2017-2021)
Lighting approaches to maximize profits (LAMP)	$5,000/year (2017-2021)

AWARDS

Doctoral Student Researcher of the Year for the College of Agriculture and Applied Sciences	2020
Doctoral Student Researcher of the Year for the department of Plants, Soils & Climate	2020
Graduate Oral Presentation Award for Life Sciences – Student Research Symposium	2019, 2020
Graduate Student Poster Award, 2nd Place – PSC Showcase	2019
NCERA Graduate Student Travel Grant	2017, 2018, 2020
Bastian Family Graduate Fellowship	2018
Apogee Instruments – Campbell Scientific Graduate Fellowship	2017, 2018
Bertrand D. Tanner/Campbell Scientific Graduate Fellowship	2017, 2018, 2019, 2020

PUBLICATIONS

PEER-REVIEWED PUBLICATIONS

Kusuma, P. & B. Bugbee. (2021). Improving the predictive value of phytochrome photoequilibrium: Consideration of photon distortion within a leaf (*Accepted in Frontiers in Plant Science*)

Kusuma, P., B. Swan & B. Bugbee. (2021). Does green really mean go? Increasing the fraction of green photons promotes growth of tomato but not lettuce or cucumber. *Plants,* 10(4), 637

Westmoreland, F. M., P. Kusuma & B. Bugbee. (2021). Cannabis lighting: Efficacy is more important than spectra for yield and cannabinoids *PLoS ONE*, 16(3), e0248988.

Kusuma, P. & B. Bugbee. (2021). Far-red fraction: An improved metric for characterizing phytochrome effects on morphology. J*ournal of the American Society for Horticultural Science*, 146(1), 3-13.

Hardy, J. M., P. Kusuma, B. Bugbee, R. Wheeler & M. Ewert. (2020). Providing photons for food in regenerative life support: A comparative analysis of solar fiber optic and electrical light systems. *International Conference on Environmental Systems*. ICES-2020-523

Kusuma, P., P. M. Pattison & B. Bugbee. (2020). From physics to fixtures to food: Current and potential LED efficacy. *Horticulture Research,* 7(1), 1-9.

Song, S., P. Kusuma, S. D. Carvalho, Y. Li & K. M. Folta. (2019). Manipulation of seedling traits with pulsed light in closed controlled environments. *Environmental and Experimental Botany*, 166, 103803.

Soundararajan, M., R. Ledbetter, P. Kusuma, S. Zhen, P. Ludden, B. Bugbee, S. Ensign & L. Seefeldt. (2019). Phototrophic N_2 and CO_2 fixation using a *Rhodopseudomonas palustris*-H_2 mediated electrochemical system with infrared photons. *Frontiers in microbiology*, 10, 1817.

IN REVIEW

Kusuma, P., M. Westmoreland, S. Zhen & B. Bugbee. (2021). Far-red photons above 750 nm can delay flowering in short-day soybean and *Cannabis*: Implications for the activity of phytochrome (*In review in PLoS ONE*)

Berliner, A., J. Hilzinger, A. Abel, M. McNulty, G. Makrygiorgos, N. Averesch, S. Gupta, A. Benvenuti, D. Caddell, S. Cestellos-Blanco, A. Doloman, S. Friedline, D. Ho, W. Gu, A. Hill, P. Kusuma, I. Lipsky, M. Mirkovic, J. Meraz, V. Pane, K. Sander, F. Shi, J. Skerker, A. Styer, K. Valgardson, K. Wetmore, S. Woo, Y. Xiong, K. Yates, C. Zhang, S. Zhen, B. Bugbee, D. Coleman-Derr, A. Mesbah, S. Nandi, R. Waymouth, P. Yang, C. Criddle, K. McDonald, A. Menezes, L. Seefeldt, D. Clark & A. Arkin. (2021) Towards a Biomanufactory on Mars (*In review in Nature Communications*)

Langenfeld, N., P. Kusuma, T. Wallentine, C. Criddle, L. Seefeldt & B. Bugbee. (2021). Optimizing nitrogen fixation and recycling for food production in regenerative life support systems (*In review in Frontiers in Astronomy and Space Science*)

IN PREPARATION

Kusuma, P. & B. Bugbee. (2021). Photon capture in lettuce is increased in early shade, but decreased in sever shade: far-red interactions with intensity (*In Preparation*)

Kusuma, P. & B. Bugbee. (2021). An analysis of photoconversion coefficients and the prediction of phytochrome dynamics (*In Preparation*)

Berliner, A., K. Yates, M. McNulty, P. Kusuma, S. Zhen, S. Gupta, G. Makrygiorgos, A. Mesbah, A. Menezes, B. Bugbee, A. Arkin, S. Nandi & K. McDonald. (2021). Nitrogen dependence and systems-based extension of the modified energy cascade model for human Martian exploration (*In Preparation*)

BOOK CHAPTERS

Kusuma, P., P. M. Pattison & B. Bugbee. (2021). Photon efficacy in horticulture. Turning LEDs packages into LED luminaires for indoor farming. In: *Plant factory: basics, applications and advanced research*, Eds. T. Kozai, G. Niu & J. Masabni. Elsevier - *Invited*

Zhen, S., P. Kusuma & B. Bugbee. (2021). Spectral optimizations for indoor plant growth and development. In: *Plant factory: basics, applications and advanced research*, Eds. T. Kozai, G. Niu & J. Masabni. Elsevier - *Invited*

OTHER PUBLICATIONS

MAGAZINE ARTICLES

Kusuma, P. & B. Bugbee. (January 7, 2021). Shedding light on LED Tech for Cannabis production. *Greenhouse Grower*

NASA TECHNICAL MEMO

Kusuma, P., B. Fatzinger, W. Soer, R. Wheeler & B. Bugbee. (*In preparation*). High efficacy LEDs for extra-terrestrial agriculture

DIGITAL COMMONS

Kusuma, P. & B. Bugbee. (2021). Designing an optimal lighting fixture for extraterrestrial crop growth: Integrating efficacy and photobiology *Utah Space Grant Consortium*. Available online May 1, 2021.

Zhen, S. & P. Kusuma. (2020). Accuracy of the generic equation to convert CCI to chlorophyll concentration in the Apogee model MC-100 chlorophyll concentration meter. *Techniques and Instruments*. Paper 17. https://digitalcommons.usu.edu/cpl_techniquesinstruments/17/

Kusuma, P., M. Hardy & B. Bugbee. (2020). Growing food in Space: A comparison of LED and solar-fiber-optic technologies. *Utah Space Grant Consortium*. Paper 16. https://digitalcommons.usu.edu/spacegrant/2020/papers/16/

Kusuma, P. & B. Bugbee. (2020). An automated multi-chamber system for quantifying biological oxygen demand. *Techniques and Instruments*. Paper 16. https://digitalcommons.usu.edu/cpl_techniquesinstruments/16/

Kusuma, P. & B. Bugbee. (2019). Optimizing concentrating mirrors and fiber optics for food production on Mars. *Utah Space Grant Consortium*. Session 2. https://digitalcommons.usu.edu/spacegrant/2019/Session_two/6/

Johnson, J., P. Kusuma & B. Bugbee. (2017). Efficacy of two HORTILED fixtures. *Controlled Environments*. Paper 11. https://digitalcommons.usu.edu/cpl_env/11

PRESENTATIONS AT NATIONAL MEETINGS

ORAL PRESENTATIONS

Kusuma, P. & B. Bugbee. Lighting systems for Martian agriculture
Biannual Meeting – CUBES, Online (May 2021)

Kusuma, P. & B. Bugbee. Improving the predictive value of phytochrome photoequilibrium: Consideration of photon distortion within a leaf
Annual Meeting – LAMP, Online (February 2021)

Kusuma, P., N. Langenfeld, L. Seefeldt, C. Criddle & B. Bugbee. Optimization of nitrogen synthesis and recycling

for food and pharmaceutical production
Biannual Meeting – CUBES, Online (December 2020)
Kusuma, P., S. Zhen & B. Bugbee. The value of ultra-violet photons for food quality
Biannual Meeting – CUBES, Online (May 2020)
Kusuma, P., P. M. Pattison & B. Bugbee. From physics to fixtures to food: Potential LED efficacy
Annual Meeting – LAMP, Riverhead NY (March 2020)
Biannual Meeting – CUBES, Logan UT (September 2019)
Kusuma, P., M. Westmoreland, W. Wheeler, S. Zhen & B. Bugbee. Is there a limit?
Annual Meeting – PHOTOx, Austin TX (October 2019) - *Invited Speaker*
Kusuma, P. & B. Bugbee. An improved method for estimating phytochrome photo-equilibrium
Annual Meeting Lightning Talk – ASHS, Las Vegas NV (July 2019)
Annual Meeting Lightning Talk – NCERA-101, Montreal QC, Canada (April 2019)
Kusuma, P. & B. Bugbee. Phytochrome photo-conversion: From etiolated to green tissue
Annual Meeting Lightning Talk – NCERA-101, Raleigh NC (April 2018)
Kusuma, P. & B. Bugbee. On the challenge of iron nutrition in hydroponics
Annual Meeting Lightning Talk – NCERA-101, Pacific Grove CA (April 2017)

POSTER PRESENTATIONS

McNulty, M., P. Kusuma, K. Wetmore, A. Abel, A. Berliner, D. Clark, B. Bugbee, A. Arkin & K. McDonald. The center for the utilization of biological engineering in space (CUBES) – Using synthetic biology to support humans for deep space exploration
STRG Tech Day on the Hill – Washington D.C. (December 2019)
Kusuma, P., P. M. Pattison & B. Bugbee. From physics to fixtures to food: Potential LED efficacy
Biannual Meeting, CUBES – Utah State University (September 2019)
Kusuma, P., S. Zhen & B. Bugbee. Food production of Mars: Ultra-violet & Far-red
Biannual Meeting, CUBES – University of California, Davis (May 2019)
Zhen, S., P. Kusuma & B Bugbee. Far-red photons enhance photosynthesis and alter plant shape
Biannual Meeting, CUBES – University of California, Berkeley (October 2018)
Kusuma, P. & Bugbee, B. The FAR-PAR index is a better predictor of stem and leaf expansion than phytochrome photoequilibrium
Annual Meeting, NCERA-101 – Raleigh NC (April 2018)

PRESENTATIONS AT REGIONAL/LOCAL MEETINGS

ORAL PRESENTATIONS

Kusuma, P. & B. Bugbee. Designing an optimal lighting fixture for extraterrestrial crop growth: Integrating efficacy and photobiology
Utah NASA Space Grant Consortium Symposium – Online (May 2021)
Kusuma, P. & B. Bugbee. Environmental effects on flowering
Graduate Seminar – Utah State University (September 2020)
Doloman, A., P. Kusuma, N. Langenfeld, L. Banner, L. Seefeldt & B. Bugbee. Biological fertilizer for manned missions to deep space
Hansen Retreat – Utah State University (September 2020)
Kusuma, P. & B. Bugbee. The optimal light spectra: Food production on Mars
Student Research Symposium – Utah State University (April 2020) - *Graduate Oral Presentation Award for Life Sciences*
Kusuma, P., P. M. Pattison & B. Bugbee. From physics to fixtures to food: Potential LED efficacy
Graduate Seminar – Utah State University (October 2019)
Kusuma, P. & B. Bugbee. Food production on Mars: Optimizing sunlight
Utah NASA Space Grant Consortium Symposium – Brigham Young University (May 2019)
Student Research Symposium – Utah State University (April 2019) - *Graduate Oral Presentation Award for Life Sciences*
Kusuma, P. Far-red & ultra-violet radiation for plant growth
PSC Showcase – Utah State University (March 2019)
Kusuma, P. & B. Bugbee. Far-Red, phytochrome & physiology: A century of research and the rise of the LED age
Graduate Seminar – Utah State University (October 2018)
Kusuma, P. Color of light as a signal for plant development: Far-red and phytochrome
Student Research Symposium – Utah State University (April 2018)
Kusuma, P. Greenhouse lighting
Utah Green Industry Conference & Trade Show – UNLA, Sandy UT (January 2018) - *Invited Speaker*
Kusuma, P. & B. Bugbee. Far-Red: The forgotten photons
Graduate Seminar – Utah State University (October 2017)

POSTER PRESENTATIONS

Kusuma, P. Optimizing blue photons for efficient plant growth
Graduate Seminar Poster Session – Online (November 2020)

Kusuma, P., M. Pattison & B. Bugbee. From physics to fixtures to food: Potential LED efficacy
Student Research Symposium – Utah State University (April 2020)

Kusuma, P. & B. Bugbee. Optimizing concentrating mirrors and fiber optics for food production on Mars: Ultra-violet & Far-red
Student Research Symposium – Utah State University (April 2019)
PSC Showcase – Utah State University (March 2019) - *won 2nd place*

Kusuma, P. & Bugbee, B. The FAR-PAR index is a better predictor of stem and leaf expansion than phytochrome photoequilibrium
Student Research Symposium – Utah State University (April 2018)
PSC Showcase – Utah State University (March 2018)

Kusuma, P. & Bugbee, B. Reduced chelate strength increases iron bioavailability for monocots in hydroponic culture
Graduate Seminar Poster Session – Utah State University (October 2017)
PSC Showcase – Utah State University (March 2017)

TEACHING EXPERIENCE

Teaching Assistant – PSC 5270/6270 – Environmental Plant Physiology – USU	Spring 2018 – 2021
Guest Lecture – PSC 5430/6430 – Plant Nutrition – USU	Fall 2018, 2020
Teaching Assistant – PSC 5000/6000 – Environmental Instrumentation – USU	Fall 2017, 2019
Judge – SRS – USU	Spring 2020
Judge – FSRS – Poster Presentations – USU	Fall 2018
Reviewer – URCO – Proposals – USU	Spring 2018, 2019, 2020

UNDERGRADUATES MENTORED

Logan Banner - Expected Graduation: 2022
Kahlin Wacker - Expected Graduation: 2021
Wyatt Johnson - Graduated: 2019
Boston Swan - Graduated: 2018

PUBIC OUTREACH / INTERVIEWS

This scientist grows plants for Mars – Food & Farming Technology	February 2020
https://www.foodandfarmingtechnology.com/features/this-scientist-grows-plants-for-mars.html	
STRG Tech Day on the Hill – Met with congressional staffers	December 2019
Cultivate Magazine	Summer 2019